NOVEL DESIGNING OF CHITOSAN BASED NANOCOMPOSITES FOR TISSUE ENGINEERING AND DRUG DELIVERY APPLICATIONS

A THESIS SUBMITTED TO THE

UNIVERSITY OF PUNE

FOR THE DEGREE OF

DOCTOR OF PHILOSOPHY

IN

CHEMISTRY

BY

DILIP DEPAN

RESEARCH SUPERVISOR
DR. R.P. SINGH

POLYMER SCIENCE AND ENGINEERING DIVISION
NATIONAL CHEMICAL LABORATORY

PUNE 411 008

July 2008

CERTIFICATE

This is to certify that the work presented in the thesis entitled **"Novel Designing of Chitosan based Nanocomposites for Tissue Engineering and Drug-Delivery Applications"** submitted by ***Mr. Dilip Depan***, was carried out by the candidate at National Chemical Laboratory, Pune, under my supervision. Such materials as obtained from other sources have been duly acknowledged in the thesis.

Dr. R. P. Singh [F.R.S.C]

Research Supervisor,
Deputy Director,
Polymer Science and Engineering Division,
National Chemical Laboratory,
Pune 411 008 INDIA.

DECLARATION BY RESEARCH SCHOLAR

I, ***Mr. DILIP DEPAN***, hereby declare that the thesis entitled "**Novel Designing of Chitosan based Nanocomposites for Tissue Engineering and Drug Delivery Applications"** submitted for the degree of Doctor of Philosophy to the University of Pune, has been carried out by me at Polymer Science and Engineering Division, National Chemical Laboratory, Pune 411 008, India under the supervision of **Dr. R.P. Singh**.

The work is original and has not been submitted to in part or full by me for any other degree or diploma to this or any other university.

(**DILIP DEPAN**)

Research Scholar

Dedicated to My Family

Acknowledgements

I would like to express my gratitude to Dr. R.P. Singh for his invaluable guidance. I sincerely thank him for teaching me the skills of presenting and writing the technical matters. He has not just guided me in the scientific problems, but has always taken extra efforts to shape my approach towards research. He has always been a perfectionist and a good critic to bring this thesis in its present form. I learnt a great deal from interacting with him.

I would like to express my sincere gratitude towards Mrs. Durgesh Singh.

I am grateful to Dr. Sivaram, the Director, NCL, Pune, for providing the infrastructure and facilities for my research work. I am very much grateful to Dr. M. G. Kulkarni, Head, PSE division, for providing me access to the facilities in the division. I am also very thankful to other scientists in the division namely, Dr C. Ramesh, Dr. P. P. Wadgaonkar, Dr. C. V. Avadhani, Dr. B.M. Sarwade, Mr. K.G. Raut, Dr. K. Guruswamy, Dr. A.K. Lele, Dr. B. B Idage, Mr. S. K. Menon, Mrs. D. A. Dhoble, and Mrs. S. Poorvi, for their timely help, fruitful discussions and support.

I also acknowledge UGC, New Delhi for financial assistance for my research work and granting Senior Research Fellowship.

How can I forget my colleagues! Without their support, cooperation, discussions and timely help, my research work could not have matured enough. So I extend my gratitude to my earlier and present lab-mates Pratheep, Mukesh, Sravendra, Sunil, Amit, Bijandra and Rupali. I also express my sincere thanks to my divisional colleagues Malli, Mahesh, Ravi, Munirasu, Gnyaneshwar, Dhyaneshwar, Arun, Arvind, Asutosh, Vijay, Kedar, Vivek, Smitha, Rahul, Sudhir, Sachin, Dharma, and all others for maintaining a warm and friendly atmosphere. I also thank Mr. Mahesh, Mr Zine, Mr. U. Dhavale and Mr. Silas S. Kakade for their assistance.

I am again thankful to Dr. M. Patole (NCCS, Pune University), Dr. J.M. Khire, Dr. D. Srinivas, and Mr. Lakshi Saikia for being my collaborators.

I am also thankful to Mr. A.B. Gaikwad, Mr. Gholap (CMC) for SEM and TEM facilities. Thanks to Dr. Ajeeth, Ms. Rupali and Mr. Vinod for NMR experiments.

I would like to express thanks for the moral support and love to Mr. Kamendra Sharma-Trupti, Mr. Chandra Prakash-Sonu-Vindu, Mr. Tapeesh Bharti-Shipra, who came as friends and became more than friends for the life.

I would like to express my immense thanks to all of my NCL friends, Mr. Sunil-Sushma, Ms. Sampa, Mr. Sarvesh, and Mr. Arshad for their moral support and timely help. Apart from that the unforgettable time spent with our famous, forever fun-loving group. Just to recall the sweet memories, many thanks to Panna-Neetu, Arti-Vini, Suneel, Dr. Sharad, and Gayatri. Many thanks to my roommate Dr. Umashankar and Mr. Subrata Banik.

Apart from this I am thankful to the GJ Hostel Sports Lovers community, which consist of Bhaiya, Paaji, Tom, Poda, Rama, Arrey, Ganya, Sacchya, Ankya, Purds, Niks, Don, Atul, Shridhar, Shrikant, Sush, Sam, Softy, Thambi-1, Naga (Thambi-2), Patwa, Mandeep, Ambarish, Rameshu, Rahul, Soojeet and all time-umpire Baag. How can I forget the old guns like Captain, Sambhaji, Viji, Easwar, Prabhas, Soumitra, Subbu, Thakkar etc. for sportive moments.

Thanks to Chakru and other mess-workers to prepare yummy food. Thanks to my mess-group of the so-called Indians like Ambrish, Bhuban, Ashok, Taware, Abhilash, and Gyan prakash for giving company in mess and light moments.

I am indebted to my parents, my Bhai-Bhabhi (Mr. Praveen Depan and Mrs. Renu Depan), my sister Ms. Kalpana Depan and my sweet niece Mishu, for their unconditional love, support and encouragement which helped me reach this far. I do not think I can ever repay them. I am grateful to God, for giving me such loving family life.

I want to place on record my deep sense of gratitude to my father and mother-in-law. I consider myself lucky to have such understanding and encouraging in-laws. In the same period, I am fortunate to have Ms. Jagruti Asopiya as my life-partner, who is my-everything now and then, and I am in immense pleasure to express my gratitude for her love, encouragement and support.

I would like to express my thanks to my uncle Sri. Naveen Meghwal and his family for their inspiration and family support. I extend my thanks to my uncle Sri RamGopal, and his family for their love, inspiration, and encouragement.

Finally, I express my prayers and gratitude to the Almighty (Unified force) for the lead.

(DILIP DEPAN)

CONTENTS

Chapter 1: Introduction of Biomaterials and its applications in tissue engineering

Chapter 2: Scope, Objectives and Approaches

Chapter 3: A- Preparation and Characterization of Novel Nanohybrids of Chitosan-g-Lactic Acid and Montmorillonite

B: Cell-proliferation and controlled drug-release studies of nanohybrids based on CS-g-LA and Montmorillonite

Chapter 4: Preparation and Characterization of Novel Hybrids of Chitosan-g-PDMS and Montmorillonite

Chapter 5: Preparation and Characterization of Novel Nanohybrids of Biomineralized Zn-Al Layered Double Hydroxides using Chitosan as a Template

Chapter 6: Enzymatic Synthesis of Nano-sized Hydroxyapatite and its Polymorphs

Chapter 7: Ultrasound Triggered Smart Release of Ibuprofen from a CS-Mesoporous Silica Composite: A Novel Approach of Controlled Drug Release

Chapter 8: Conclusions

ABSTRACT

Title of the Thesis

Novel designing of Chitosan based nanocomposites for tissue engineering and drug-delivery applications

Chitosan (CS), a natural polymer obtained by alkaline deacetylation of chitin, is non-toxic, biocompatible, biodegradable, having multiple functional groups and soluble in aqueous system. These properties make CS a good candidate with unlimited potential in biomaterials science, food packaging, bone substitute and novel drug delivery systems. However, its mechanical properties and high surface energy limits its wide range of applications. Incorporation of various inorganic fillers is an effective approach for improving the physio/ chemical properties of CS. CS based nanocomposites have been prepared by incorporating various inorganic fillers like nano-clay, carbon nano-tubes, layered double hydroxides, gold-silver nanoparticles etc.

Thus, the present research work is aimed to refocus or revisit the possibilities of utilization of CS for various applications esp. as a drug carrier for sustained release and as a scaffold in tissue engineering and other biomedical applications. ***Chapter 1*** gives an **introduction** and literature background on this area. ***Chapter 2*** reveals the **scope, objectives, and approaches** of the present study. The present study has been divided into three parts. ***Chapter 3*** is focused on the **Preparation and characterization of novel hybrid of chitosan grafted lactic acid and montmorillonite: Physical property improvement of smooth films.** Preparation of nanocomposites of chitosan has also been performed by intercalating chitosan into Na^{+}-MMT (sodium montmorillonite) through cationic exchange and hydrogen boding processes, with interesting structural and functional properties. Nanocomposites were prepared by dissolving chitosan and dispersing Na^{+}-MMT in aqueous solution of L- lactic acid with subsequent heating and film casting. The films have shown enhanced hydrophilicity as compared to PLA. Issues on the interactions of polycationic chitosan with clay are also discussed. It is observed that nanocomposites are exhibiting better thermal and physical

properties than Chitosan-g-LA and PLA. The lamellar host, in this study is layered silicates, which are composed of thin lamellae that are combined with rather weak interaction such as Vander walls force and H- bond. They can accommodate various organic molecules in the interlayer space to form intercalated compounds. In addition, the drug is also cationic which facilitates easy drug loading into the lumen of layered silicates posing a very demanding challenge to achieve adequate sustained release property due to the anticipated high diffusion gradient produced.

Chapter 4 discusses the **Preparation and characterization of novel hybrid of chitosan grafted with PDMS and sodium montmorillonite: Sorption and protein adsorption studies.** Although the properties of CS seem favorable to use CS as a wound dressing material, its solubility only in aqueous acidic solutions, high crystallinity and rigid structure has limited its use for wide-range biomedical applications. Polydimethyl siloxane (PDMS) is a high performance polymer with unique physical and chemical properties. Another advantage of adding PDMS into CS is to improve their mechanical properties. Because hardness and brittleness are major drawbacks of CS which limit their use as wound healing material, incorporation of elastomeric PDMS should somewhat soften the material hydrogen boding processes, with interesting structural and functional properties. Therefore, in this chapter, studies were carried out to prepare CS-g-PDMS nanocomposites by introducing PDMS onto CS-montmorillonite nanocomposites via photo induced grafting. The grafting of PDMS imparts the hydrophilicity and swelling behavior to the CS. The incorporation of clay affects the preparation and physio-morphic properties of grafted copolymer.

Chapter 5 reveals the strategy to prepare **Biomineralized Zn-Al Layered Double Hydroxides (LDH) using Chitosan as a template: Preparation, drug release and Cell-viability studies of prepared nanohybrids.** Lamellar LDH commonly called as synthetic anionic clays, whose structure is commonly described as edge-sharing octahedral sheets in which, by comparison with the Brucite M $(OH)_2$, some of the divalent cations are replaced by trivalent cations to give positively charged sheets. LDH is biocompatible and has found pharmaceutical applications as an antacid, which makes them promissory hosts for immobilization of NSAIDs aiming to reduce gastric irritation side effects. CSI molecules have C=O, -OH and -NH groups on its backbone, which can coordinate strongly with the Lewis acidic sites. So, we choose to synthesize LDH/CSI hybrids by a co-precipitation route involving the *in-situ* formation of LDH layers. Intercalation of Ibu was done by Ion-Exchange method. Here CSI acts as a

templating molecule for LDH crystallization where it acts as a glue to consolidate nanosized LDH particles into larger scale aggregates.

***Chapter 6*: Biosynthesis of Hydroxyapatite (HAP): A novel enzymatic route**

Synthetic Calcium Hydroxyapatite is a bioactive material that is chemically similar to biological apatite, the mineral component of bone. In this chapter, we describe the rapid, single step synthesis of crystalline nano-particle HAP hollow nanospheres by a wet biological method. Briefly, aqueous solution of calcium chloride was mixed with water-solubilized phytase and Phytic acid.

Chapter 7 is the **Ultrasound triggered smart drug release from chitosan-mesoporous silica (MS) composite: Structural and cell adhesion studies.** Recently, there has been increased interest in Mesoporous silica (MS) materials for use as carriers in controlled drug release, to meet the need for prolonged and better control of drug administration. Release systems that are sensitive to external impulses such as oscillating magnetic fields, thermal, ultrasound, or electric fields have therefore been investigated to achieve on-demand drug regulation. Ultrasound is one of the most promising external triggers for pulsatile delivery in which the release rate of the incorporated drug can be altered by applying ultrasound irradiation from the external environment. In this study, we used Mesoporous silica (MS) as the drug reservoir.

***Chapter 8*: Summary:** This chapter summarizes the results and describes the salient conclusions of the study. Future perspectives for further research are also expressed.

Abbreviations

Å	Angstrom
θ	Contact Angle
λ	Wave length
nm	Nanometre
μm	Micrometre
cm^{-1}	Wavenumber
AFM	Atomic Force Microscopy
ATR-FTIR	Attenuated Total Reflectance Fourier Transform Infra-red
EDAX	Energy-Dispersive Absorption X-Ray
CS	Chitosan
CNT	Carbon Nanotubes
DSC	Differential Scanning Calorimetry
FTIR	Fourier Transform Infra Red
HAP	Hydroxy apatite
LDH	Layered double Hydroxides
MMT	Montmorillonite
NMR	Nuclear Magnetic Resonance
PC	Polycarbonate
PLA	Polylactic Acid
SAXS	Small Angle X-Ray Scattering
SEM	Scanning Electron Microscopy
Tg	Glass Transition Temperature
TEM	Transmission Electron Microscopy
TGA	Thermogravimetric Analysis
UV	Ultraviolet
WAXD	Wide Angle X-Ray Diffraction
XRD	X-Ray Diffraction
XPS	X-Ray Photo Electron Spectroscopy

List of Tables

List of Figures

List of Schemes

CHAPTER I

Introduction of Biomaterials and its Applications in Tissue-Engineering

A biomaterial is a man-made or man-modified viable or non-viable material intended to interface with biological systems to evaluate, treat, augment, or replace any tissue, organ, or function of the body.

1.1 INTRODUCTION

A biomaterial is essentially a material that is used and adapted for a medical application[1]. Biomaterials can have a benign function, such as being used for a heart valve, or may be bioactive and used for a more interactive purpose such as hydroxy-apatite coated hip implants[2-5]. Biomaterials are also used every day in dental applications, surgery and drug delivery (a construct with impregnated pharmaceutical products can be placed into the body, which permits the prolonged release of a drug over an extended period of time)[6-10].

The definition of a biomaterial does not just include man-made materials which are constructed of metals or ceramics. A biomaterial may also be an autograft or allograft or xenograft, used as a transplant material. **Table 1.1** shows the applications of biomaterials.

Table 1.1 Some applications of biomaterials and modified natural materials in medicine.

Application	**Types of Materials**
Skeletal system	
Joint replacements (hip, knee)	Titanium, Ti—Al—V alloy, stainless
Bone plate for fracture fixation	steel, steel, cobalt—chromium alloy
Bone cement	Poly(methyl methacrylate)
Bony defect repair	Hydroxyapatite
Artificial tendon and ligament	Teflon, Dacron
Dental implant for tooth fixation	Titanium, alumina, calcium phosphate
Cardiovascular system	
Blood vessel prosthesis	Dacron, Teflon, polyurethane
Heart valve Reprocessed tissue,	stainless steel, carbon
Catheter	Silicone rubber, Teflon, polyurethane
Organs	
Artificial heart	Polyurethane
Skin repair template	Silicone-collagen composite, Chitosan
Artificial kidney (hemodialyzer)	Cellulose, polyacrylonitrile
Heart—Lung machine	Silicone rubber

Due to the aging of world population, the market for engineered biomaterials is growing at a rapid rate. Each year, more than 600,000 joint replacements are performed in the USA alone with an estimated worldwide cost in excess of 3 billion dollars. **Table 1.2** depicts an overview of health-care market of USA.

Table 1.2 Health-care market and biomaterials usage in USA

Total US Health Expenditure (2003)[1]	$1,678.9 Billion
% of GDP[2]	15%
No. of employees[2]	10 Million
Total Medical Device Market (2006)[3]	$86 Billion
No. of employees[4]	441,400
Medical and device sales[5]	$44 Billion
Biocompatible Materials (2007)[6]	$22.2 Billion
Implantable medical devices (2006)[6]	$7.9 Billion
Tissue Replacements (2006)[6]	$11.7 Billion
Skin Repair (2007)[7]	$270 Million
Vascular Grafts (2007)[5]	$650,000 Million
No. of devices[8]	
Intraocular lenses	1,400,000
Contact Lenses	4,000,000
Heart Valves	45,000
Artificial Knees	816,000
Artificial Hips	521,000

1- Espicom-2006, 2-WHO-2006, 3-Advamed-2006, 4-Medical product outsourcing-2006, 5-McMaster University-2006, 6-BCC Research-2006-7, 7-International Access corporation-2002, 8-Ratner et al.

There are also functional or structural classifications, such as whether biomaterials are hydrogels, injectable, surface modified, capable of drug delivery, by specific applications and so on. The wideness of biomaterials used in tissue engineering arises from the multiplicity of anatomical locations, tissue-cell types, and specific applications that apply. For e.g. relatively strong mechanical properties may be

required in situations, where the device may be subjected to weight-loading or strain, or where maintenance of a specific cell-architecture is needed.

The type of material used is also dependent on the anticipated mode of applications (open implantation is injection or minimally invasive procedure), the nature of any bioactive molecules, that might be released, the need for surface functionalization, the need of the cell types of interest in terms of porosity, and other issues. To be successful the biomaterial implant should effectively repair the defect where it has been applied without causing any adverse tissue reaction while maintaining mechanical and biological integrity for a desired time-span, ranging from few weeks to several years.

1.2 EVOLUTIONS OF BIOMATERIALS

Recently, tissue-engineering strategies using engineered biomaterials that support and promote tissue growth have been proposed for reconstructive surgeries[11]. The purpose of a tissue engineering approach is to repair and regenerate damaged human tissue with biomaterials based devices[12]. To initiate the natural developmental events, it requires functional cells that constitute the target tissue, a matrix or scaffold supporting those cells, bioactive molecules regulating cellular behavior and the compatible integration of this composite in the damaged tissue[13]. Cells used in tissue engineering can be stem cells or tissue specific cells. Bioactive molecules can be growth factors, hormones, and other proteins. The matrix may be synthetic or natural, coming in the form of fibrils, foams, hydrogels, and capsules. An implant composed of a biocompatible and biodegradable scaffolds, the reservoir own cells and biomolecule that modulate the cells to form the neotissues would be the foundation for the future generation of bio medical engineering[14, 15].

Such an implant, not only creates a local environment for pre-loaded cell proliferation and differentiation in the targeted tissue, but also interacts with the hosts own tissue and integrates into it. Ideally, the only foreign part left, the scaffold, will be degraded and excreted from the human body. In this manner the implant eventually transforms itself into the patient's own body. The biomolecules and the cells together with the intrinsic properties of the chosen biomaterials determine the biocompatibility and longevity of the implants.

Though this strategy is still in its infancy, diverse knowledge has been accumulated toward addressing its key elements including cell sources, material properties, scaffold

structure and bimolecular recognition[16-20]. The success of the approach depends on the understanding of the impact of these key items.

1.3 PROPERTIES OF BIOMATERIALS

1.3.1 FOR TISSUE ENGINEERING:

The three, main functions of tissue engineering scaffolds are:

a) Providing temporary mechanical support.
b) Guiding tissue regeneration and organization.
c) Promoting tissue formation and subsequent regeneration.

As the building block of the scaffold or matrix for bone repair, bone-grafting material itself must be optimized for biocompatibility, biodegradability and biomedical properties.

1. **Biocompatibility**: A biomaterial must be immune acceptable. The host immune system should recognize the implant as part of the host and not reject it. Further, a biomaterial should minimize, if not be free, an inflammatory response[21]. Biocompatibility is not an intrinsic property of a material, but depends on the biological environment and the leeway that exists with respect to tissue reaction. For e.g. a formulation, that is biocompatible in subcutaneous tissue might not be so in nerve or in the peritoneum.
2. **Biodegradability**: The implanted foreign material should be degraded and expelled from the host's physiological system. In those cases the implants are required to provide mechanical support, the degradation rate must be engineered to comply with the growth rate of new tissue. Ideally, the entire scaffold would be degraded when the damaged tissue is totally regenerated[22].
3. **Biomechanical Properties**: Our primary purpose about biomaterials is that they exists to repair, correct, or improve a physiological defect or deformation by their implantation. In most cases, implanted biomaterials must have certain mechanical strength to maintain tissue growth and integration, or at least survive the hydrostatic pressure and other mechanical conditions at the damaged tissue site[23]. Repair of certain tissues, bone for instance, often demands a structural immobilization at an early stage. In a more complicated manner, mechanical properties of an implant may affect the growth and

integration of new tissue by influencing cell attachment and behavior through a process known as mechano-transduction[24]. A successfully designed device has to fir the mechanical requirements of the implant location. For e.g. tendon and soft tissue implants must be strong enough to withstand everyday forces applied to them by the patient.

4. **Surface Chemistry**: The surface chemistry is the main factor to cellular adhesion[25]. Cellular adhesion at the cell-material interface is mediated by proteins adsorbed from the surrounding medium onto the substratum[26, 27]. The material ions modify the adsorption and orientation of proteins on the surface, and thus also affect the subsequent cell binding. Cells are sensitive to the environment in which they exist. It is though that a poorly adhesive surface on which weak cell adhesion occurs, no traction and no net movement can be observed. However, a highly adhesive surface allowing for a strong cell adhesion may also result in cell immobilization[28]. Although the common synthetic polymeric scaffolds have great advantages in terms of their degradability and other properties, they lack desirable surface properties. One approach to providing them is by modifying their surfaces, by physical adsorption of compounds or by chemical modification. This approach can also be used to increase polymer hydrophilicity to repel proteins and perhaps reduce the tendency towards adhesion.

5. **Micro topography**:

   Surface texture or micro topography plays an important role in the cellular response and adhesion[29]. On smooth surfaces, the cells are able to spread, perhaps forming greater number of hemi-desmosomes as anchors to the substrate. In contrast, on rougher surfaces, the cells appear to form local contacts that allow the cells to span across the space between surfaces. Such modifications in attachment numbers and even distribution on a cell surface can result in new gene transcription, and new protein synthesis, ultimately affecting phenotypic expression.

6. **Porosity, pore size:**

   The microstructure of scaffolding material should be highly porous with interconnected pore network. In such scaffolds, the large void volume facilitates anchorage-dependent cell seeding; maximize attachment, migration and growth,

extracellular matrix production, fluid circulation, and vascularization within the pore space throughout the scaffold structure[30].

1.3.2 FOR DRUG DELIVERY:

There are two ways to give a patient a dose of drug: in a single dose or with a drug release system. When the patient takes one dose, the concentration of drug in his blood will increase fast but then it will also fast decrease (**Figure 1.1**). To maintain an effective concentration of drug in the blood, the patient must take other doses at interval. The aim of a controlled drug delivery system is to maintain the concentration of drug in the blood within several days with a single dose. If we consider the evolution of drug concentration in the blood according to time we have the following graph:

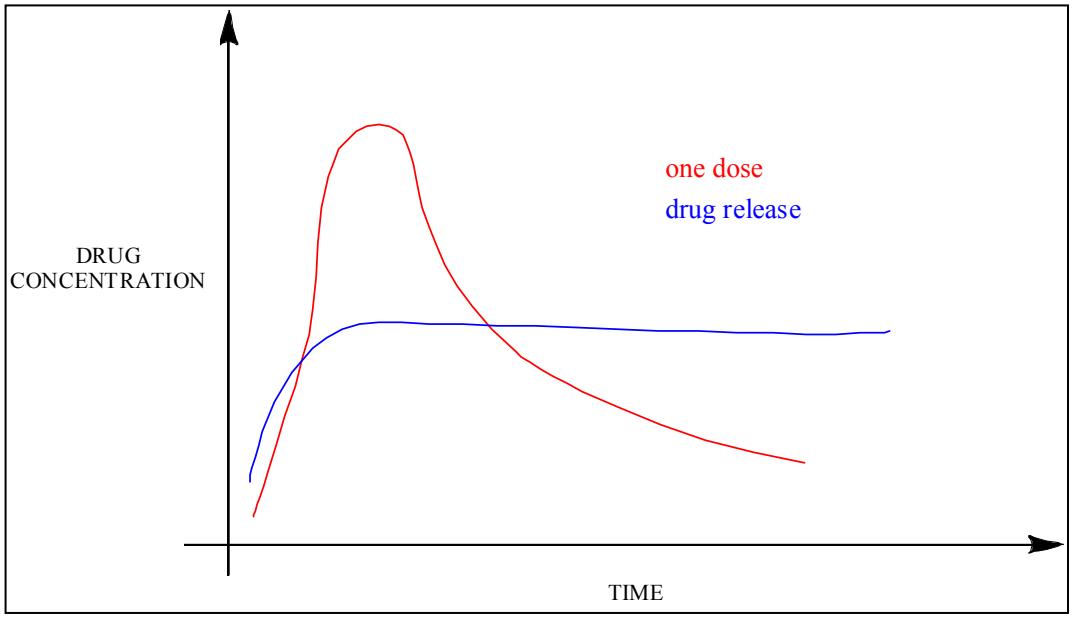

Figure 1.1: Plot of Drug concentration versus time of drug release.

We see that it is very interesting and safer for the patient to have a drug release system, which delivers drug on a long time. So the goal of the controlled drug release device is to maintain a constant amount of drug with just a single dose and this kind of delivery preserves medications that are rapidly destroyed by the body and improve patient comfort. One classification of drug delivery system is based on the mechanism that controls the release of the substance. The main mechanism is the diffusion, and two types of diffusion-controlled systems have been developed:

- The *reservoir device,* in which the drug forms a reservoir surrounded by a diffusion barrier, it consists of regroups membranes, capsules, and liposomes.
- The *monolithic device,* in which the drug is dispersed or dissolved (depending if its concentration is above or below its solubility limit), in a polymer.

In these two systems, the release is directly linked to the choice of polymer and its properties.

Another delivery system, is the chemically controlled system, where three types of release can occurs, as shown in **Figure 1.2**:

- With *Biodegradable polymer*, the drug is dispersed in a biodegradable polymer (like in monolithic device) and this polymer is degraded which allows drug to be released.
- With *pendant chains* where drug is bound to polymer by covalent bonds which are destroyed by a chemical mechanism.
- The *solvent controlled system* where drug is dispersed in a polymer that swell in the fluid where it is used, thus the glass transition of polymer is decreased and drug can diffuse in the polymer and be released.

The different types of drug delivery systems:

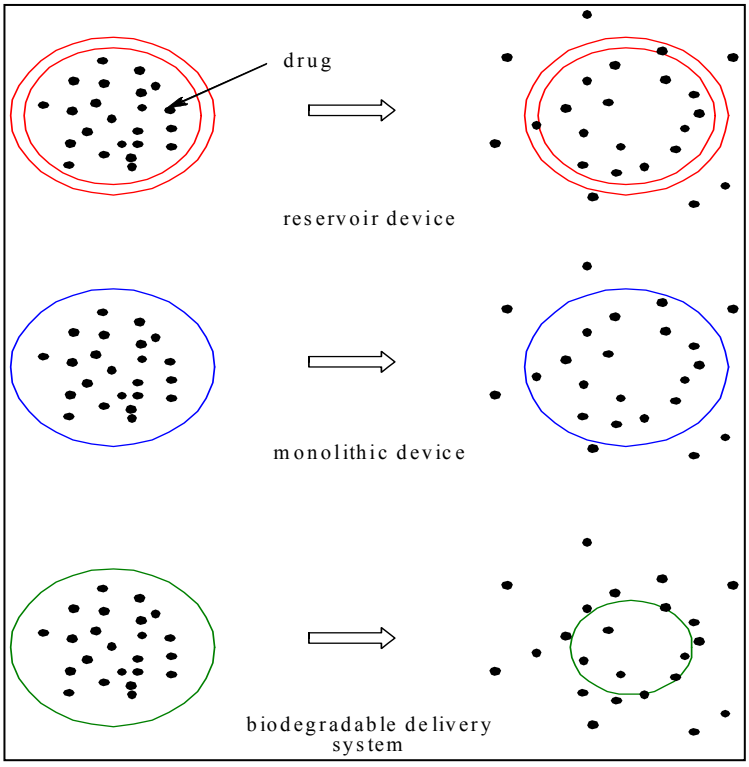

Figure 1.2: Various drug delivery systems.

In this context, “drug” means essentially any bioactive molecule, from small molecules to proteins and nucleic acids. There has been a natural emphasis on the delivery of growth factors. While the construct is incubated *in vitro*, it is often sufficient to add the drug to the ambient medium, provided that the compound is capable of diffusing throughout. However, it may be desirable to maintain exposure to that drug after the construct is implanted *in vivo*. Biomaterials play a key role in achieving this in tissue engineering, drawing on experiences in the broader field of drug delivery. Many of the examples below are drawn from that experience, rather than the narrower field of tissue engineering. A number of drug delivery approaches and polymers have been used. Many investigators have incorporated drugs into constructs; both polymeric and hydrogel-based systems have been used, although the former are often better at controlling drug release kinetics[36]. The drugs can be incorporated directly into the scaffolds, i.e., distributed throughout the polymeric matrix during casting, as is the case with many micro- and nanoparticulate drug delivery systems and hydrogels[37-39].

The goals of drug delivery are:

(1) To overcome the inherent limitations associated with biomacromolecular therapeutics, which include a short plasma half-life, poor stability and potential immunogenicity, and (2) to maximize the therapeutic activity while minimizing the toxic side effects of drugs. Current drug-delivery systems are effective at releasing drugs in a controlled fashion to produce a high local concentration; however, the scope is limited to targeting tissues rather than individual cells. At the expense of lower drug loading capacity, the nanometer size range enhances the ability of drug-delivery carriers to cross cell membranes, reduces the risk of undesired clearance from the body through the liver or spleen and minimizes their uptake by the endothelial system. Smaller particles have greater surface area-to-volume ratios, which increase the particles’ dissolution rate, enabling them to overcome solubility-limited bioavailability. Particle size is extremely important to the biological properties and, hence, functions, of nano-scale drug-delivery systems. Nano-scale drug-delivery systems take advantage of the fact that nano-scaled materials (10^{-9} to 10^{-7} m) can exhibit distinctive physical properties, electrical, mechanical and optical, that differ from those observed in the macroscopic and atomic realms. Through rational design, nano-scale drug-delivery systems can be manufactured to combine desirable modules, both biological and synthetic, for various applications, including implantable, inhalable, injectable, oral, topical, and transdermal drug delivery. Many properties of nano-scale drug-delivery

systems can be tailored for specific applications: solubility (inherent hydrophilicity of the material, addition of solubilizing moiety); biodistribution (molecular weight, addition of targeting group); biocompatibility (electrical charge, addition of bioinert functionality); biodegradability (backbone, spacer); drug release (physical interaction between drug and carrier, chemical cleavage of covalent spacer); drug encapsulation (physical interaction between drug and carrier); and shape (materials and chemistry employed).

Drugs can also be reversibly conjugated to the matrix covalently or by other means[40]. However, other methods of providing drug delivery to scaffold-type systems have arisen that might provide greater flexibility in the types and quantities of drugs that can be delivered. All these approaches have pros and cons, particularly in terms of the stability of the drug payload during and after device manufacture. In the case of growth factors, the rationale is particularly compelling in that most tissues are composed of more than one cell type, and sometimes, two factors work better than one. For example, polymeric scaffolds have been developed that simultaneously release vascular epithelial growth factor and platelet derived growth factor[41]. Many of the methodologies described above could be suitable for achieving multiple drug release (e.g., particles containing different drugs dispersed in a matrix). It is also possible to encapsulate many compounds within one particulate system[42]. Temporal control of drug release within constructs is important, either to deliver drugs in a pulsatile manner or different drugs at different times. This could be achieved in a number of ways. For example, drugs could be entrapped within or beneath polymer layers of differing thicknesses or with differing degradation rates. They could be entrapped within separate populations of particles with differing release kinetics. Drugs could be contained within chip-like implantable devices that are programmed to release defined payloads in response to electrical stimuli or polymer degradation[43-45]. There is also an increasing literature on polymeric drug-releasing systems that respond to externally applied energy or forces, such as ultrasound, pH, magnetism, and heat, or electricity[46-50].

Controlled-Release Drug Delivery Systems:

It covers a wide range of products, including “delayed release”; “extended release”, “site-specific targeting” and “receptor targeting” dosage forms. Delayed-release systems are those in which drug release is delayed for a finite “lag time”, after which release is unhindered (e.g. enteric coated oral tablets). Extended-release (or

prolonged-release) dosage forms include any system in which the drug is made available over an extended period of time after administration. Site-specific and receptor targeting systems are those that deliver the active substance at the desired biological site, e.g. the diseased organ or tissue (site-specific targeting), or the particular drug receptor within an organ or tissue (receptor targeting). Systems providing some actual therapeutic temporal and/or spatial controls of drug release are considered "controlled delivery" systems, so, "controlled release" cannot be considered equivalent to "extended release". Controlled-release drug delivery systems are summarized in **Table 1.3**, according to the classification proposed by Chien and Lin[51].

Table 1.3 Types of Controlled-Release Drug Delivery systems.

Group	**Drug Delivery System**	**Drug Release Control Mechanism**	**Example**
Rate-programmed systems	Polymer Membranes, Permeation systems, Polymer Matrix/Hybrid Systems. Micro-reservoir partition systems.	Diffusion	Ocusert, Transderm-Nitro, Norplant Nitrodisc, Syncromate-C.
Activation-Modulated Systems	Osmotic-Hydrodynamic Pressure, Vapor-pressure activated systems Mechanical-force activated systems Hydration-activated systems Magnetic, Sonophoresis, pH, Ion, Hydrolytic, Temperature, Enzyme.	Modulation of the activation input	Alzet osmotic pump, Acutrim tablet, Infusaid, Nasal metered dose nebulisers. Syncro-Male-B, Valrelease tablet, Lapron-Depot, Zoladex.
Feed-back regulated systems	Bio-erosion and Bio-responsive regulated systems, Self-Regulating systems.	Concentration of the activating substance in the body.	
Site-specific systems			

On the basis of the technological approach applied, four main groups have been distinguished: rate-pre-programmed- systems (those controlling molecular diffusion of drug molecules in and/or across a polymer barrier), activation-modulated systems (in which drug release is activated and then modulated by some physical, chemical or biochemical input), feedback-regulated systems (in which drug release is activated in the body via some feedback mechanisms) and site-targeting drug delivery systems. Most of these strategies assume a new concept of "excipient". Thus, excipients (and among them clay minerals) are not only "inert ingredients", but they can also be used by formulators to provide targets of a biopharmaceutical (decreasing or increasing dissolution rate, delaying and/or targeting drug release), pharmacological (prevention or reduction of side effects), technological (taste masking) or chemical (increasing stability) nature.

1.4 TYPES OF SCAFFOLD MATERIALS:

Four categories of biomaterials have been investigated by numerous groups, both *in vivo* and *in vitro* as candidates for tissue engineering scaffolds:

(i) Synthetic organic materials: mainly the polyester family poly (α-hydroxyl acids) such as polylactide (PLA), polyglycolide (PGA) and their co-polymer (PLGA).

(ii) Synthetic inorganic materials: mainly hydroxyapatite, tricalcium phosphate, glass ceramics;

(iii) Organic materials of natural origin: collagen, alginate, fibrin glue; and chitosan, and

(iv) Inorganic material of natural origin: hydroxyapatite.

1.4.1 Organic materials

Organic materials are widely used in several different applications, principally due to their availability in large variety of compositions and forms (solids, films, gels, etc.). They are also attractive because they can be fabricated readily into various shapes and structures with desired macro porous features[51]. All the polymers of natural and synthetic origin that have been investigated for use as scaffolds in tissue engineering are biodegradable, biocompatible and have their own distinctive characteristics[52]. However, both synthetic and natural biopolymers are mechanically weak, do not have good bioactivity, degrade too fast in physiological media loosing their mechanical

properties and sterilization processes (autoclave, ethylene oxide, and Co irradiation) may alter polymer properties[53].

1.4.2 Polymer biomaterials

1.4.2.1 Synthetic polymers

Synthetic polymers can be produced in large quantities, and their synthesis allows for direct control over chemical composition[54]. Therefore, depending on the application, a desired set of physical specifications can be obtained when modifying the chemical structure with specific functional groups[55]. Synthetic biomaterials are generally biologically inert, they have more predictable properties and batch-to-batch uniformity and they have the unique advantage having tailored property profiles for specific applications, devoid of many of the disadvantages of natural polymers. Hydrolytically degradable polymers are generally preferred as implants due to their minimal site-to-site and patient-to-patient variations compared to enzymatically degradable polymers. The successful performance of the first synthetic poly (glycolic acid) based suture system during the late 1960s led to the design and development of a new array of biodegradable polymers as transient implants for orthopaedic and related medical applications. Extensive research has gone since then to custom designing biodegradable polymer systems with predictable erosion kinetics as drug/gene delivery vehicles or as scaffolds for tissue engineering. For applications that need materials with a certain level of biological activity, strategies to incorporate biological motifs onto synthetic polymers in the form of hybrid materials have also been developed. A vast majority of the research has focus on the synthetic polymers that already have the advantage of Food and Drug Administration approval as sutures[56]. These belong to the aliphatic polyester family e.g. poly (α-hydroxyl acids), mainly PLA, PGA, and their copolymer, PLGA. They degrade by hydrolysis into non-toxic byproducts that can be metabolized and excreted. Also, since PLLA is less crystalline than PGA, and more hydrophobic with its additional methyl group, variable rates of hydration and hydrolysis can be obtained with different combinations of PLA and PGA[57]. Synthetic polymers, such as biodegradable polyesters, have succeeded to some degree in tissue engineering applications, but despite their attractive properties, they are limited by important drawbacks[58]. The general problems with these polymers are their low biocompatibility, the generation of acidic degradation by-products, processing difficulties and loss, that is too rapid of mechanical integrity while degrading[59].

1.4.2.2 Natural polymers:

The use of naturally occurring biomaterials is an alternate scaffold strategy offering distinct advantages[60]. These polymers may be much more similar to the native cellular milieu that has been optimized through evolution. Scaffolding applications requires such natural materials, which are expected to have a higher biocompatibility and have demonstrated a better and faster healing process[61]. Natural polymers can be considered as the first biodegradable biomaterials used clinically. The rate of in vivo degradation of enzymatically degradable polymers however, varies significantly with the site of implantation depending on the availability and concentration of the enzymes. Chemical modification of these polymers also can significantly affect their rate of degradation. Natural polymers possess several inherent advantages such as bioactivity, the ability to present receptor-binding ligands to cells, susceptibility to cell-triggered proteolytic degradation and natural remodelling.

Chitosan (CS) is a unique polysaccharide derived from partial de-acetylation of chitin, which is, after cellulose, the most abundant natural polysaccharide[62]. Found in arthropod exoskeletons, each year several million tons of chitin is harvested worldwide from the shell of shrimp, lobster, crab or krill[63]. With its chemical nature and biological properties, CS biomaterial is highly versatile (**Figure 1.3**)[64]. The polymer has reactive amino and hydroxyl groups that provide many possibilities for covalent and ionic modifications. They can be easily modified with a large variety of groups that can be chosen to modify specific functionality such as biological and physical properties[65]. Chitosan intrinsically possesses strong biological activity that has been extensively studied in the past 20 years. First, it is biocompatible, biodegradable, bioresorbable and has a hydrophilic surface, which facilitates cell adhesion, proliferation and differentiation[66]. Second, with its cationic nature in physiological pH, CS mediates non-specific binding interactions with various proteins. Soluble proteins, most of which are negatively charge, may also be expected to have varying binding affinities to CS-based material[67]. Third, CS is made of glucosamine and N-acetyl-D-glucosamine units linked by one to four glycosidic bonds (**Figure 1.4**).

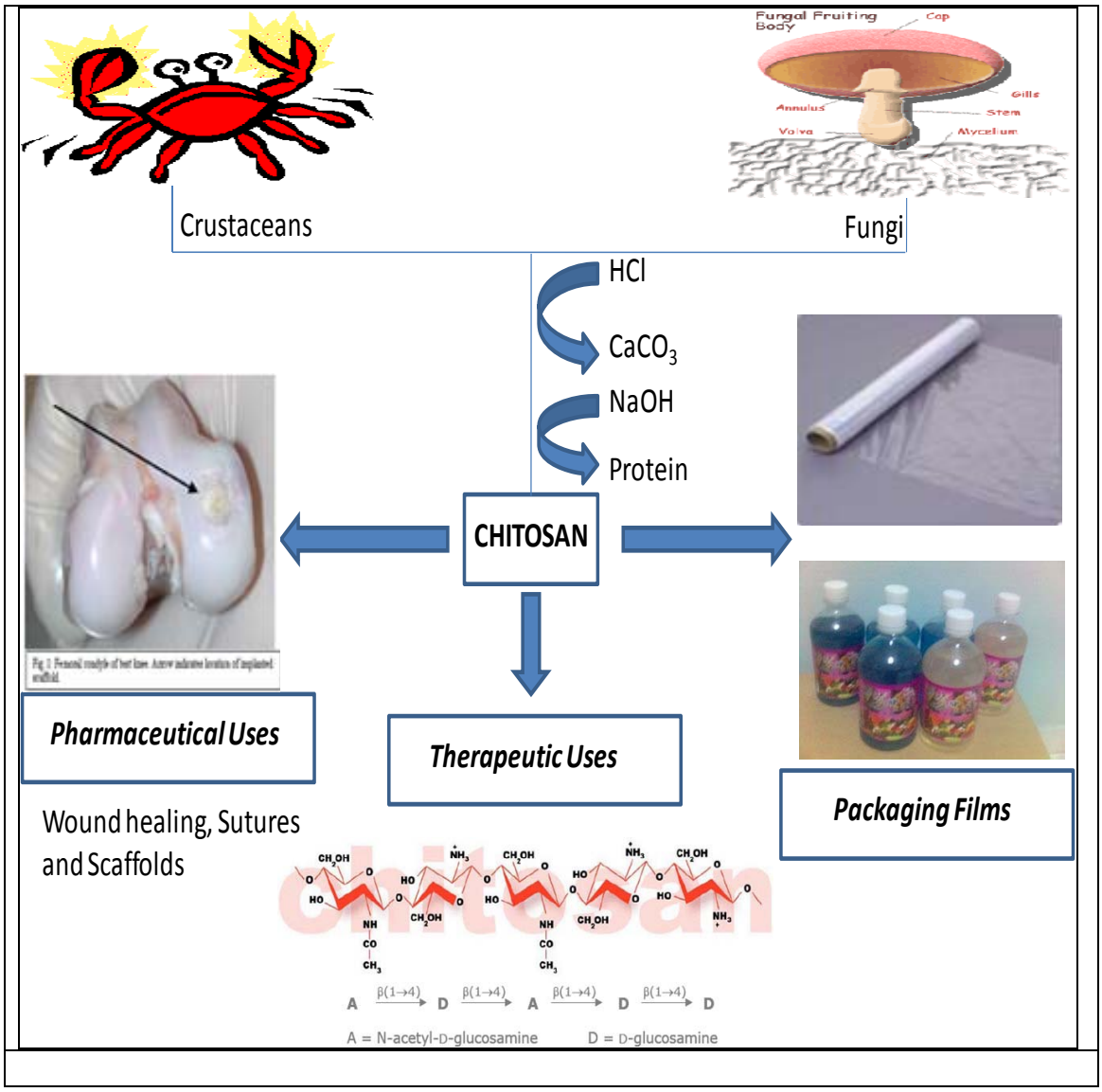

Figure 1.3 Production and various applications of CS

The latter moiety is a structural molecule found in glycosaminoglycans[68], which is a polysaccharide occurring ubiquitously within extra cellular matrix (ECM), including the one in bone and cartilage[69]. Glycosaminoglycans are known to be involved in several cell-cell/cell-matrix interactions, including specific bindings to growth factor receptors and adhesion proteins, and thus modulate cell morphology, motility, differentiation, synthesis, and function[70]. **Table 1.4** shows the various forms, applications and properties of CS.

Table 1.4 Various forms, applications, and properties of CS.

Form	**Application**	**Route of delivery/properties**
Beads	Drug Delivery	Oral
Microspheres	Enzyme Immobilization	Oral, Implantable, Injectable
Coatings	Surface Modification, Textile Finishes	CS increases mucoadhesiveness of Alginate capsules
Fibers	Medical Textiles, Sutures	Biodegradable
Nanofibers	Guided Bone Generation,	
Films	Wound Care, Dialysis Membranes	
Powder	Adsorbent for pharmaceutical and medical devices, Surgical glove powder,	
Sponge	Mucosomal Hemostatic dressing, Wound Dressing, Enzyme Entrapment	
Shaped Objects	Orthopedics, Contact Lenses	
Solutions	Cosmetics, Bacteriostaic Agents, Hemostatic agents, Anticoagulant, Anti-tumor agent.	Moisture Holding, Oral, Nasal Complex Formation-Gene Delivery
Gels	Delivery Vehicle, Implants, Coatings,	
Tablets	Compressed Diluents, Disintegrating Agents	Oral, Buccal
Capsules	Delivery Vehicle	

With its hydrophilic and cationic nature, and its structure analogous to glycosaminoglycans, CS is expected to be endowed with related biological activity[71-73]. In fact, CS exhibits interactions with ECM components, immune cells and growth

factors such as the fibroblasts growth factors[74]. Chitosan has a number of other desirable properties for a tissue scaffold: it has anticoagulant properties, antibacterial and antifungal action[75]. Moreover, CS has an excellent ability to be processed into porous structures and smooth films for use in cell transplantation and in tissue regeneration[76]. Chitosan properties have only been thoroughly studied in the last few decades[77], starting approximately when the scientific principles for use of the monomer N- acetylglucosamine in enhancing wound healing process were reported in 1960[78]. In the 1970s, the role of CS in potentiating wound healing was documented for various animal models[79]. Since then, CS material has been widely investigated in a number of biomedical applications[80-85], from wound dressings, drug or gene delivery systems, and nerve regeneration to space filling implant. The utility of CS as a scaffolding material to support cell growth and proliferation has also been reported[86-88]. As biomaterial, CS is an exceptional polysaccharide, the most promising of this class of materials. It has excellent potential for engineering numerous tissue systems, including bone tissue, by serving as a structural base material on which normal tissue architecture is organized. However, although pure CS has very attractive properties, it lacks bioactivity and is mechanically weak[89]. These drawbacks limit its biomedical applications. For these reasons, it is highly desirable to develop a hybrid material made of CS and appropriate inorganic filler, hoping that it can combine the favorable properties of the materials, and further enhance tissue regenerative efficacy. **Table 1.5** gives the general chemical and biological properties of CS, and **Figure 1.4** is the structure of CS.

Table 1.5 General characteristics of CS:

Chemical Properties	**Biological Properties**
Cationic Polyamine	Naturally Occurring Polymer
High charge density	Biodegradable
Adheres to negatively charged surfaces	Biocompatible
High Molecular weight polyelectrolyte	Safe and non-toxic
Reactive $-NH_2$ and –OH group	Anti-carcinogen

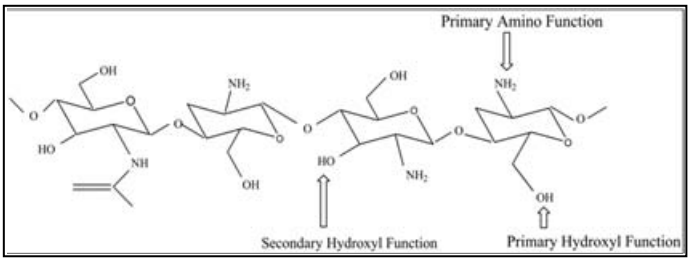

Figure 1.4 Structure of Chitosan

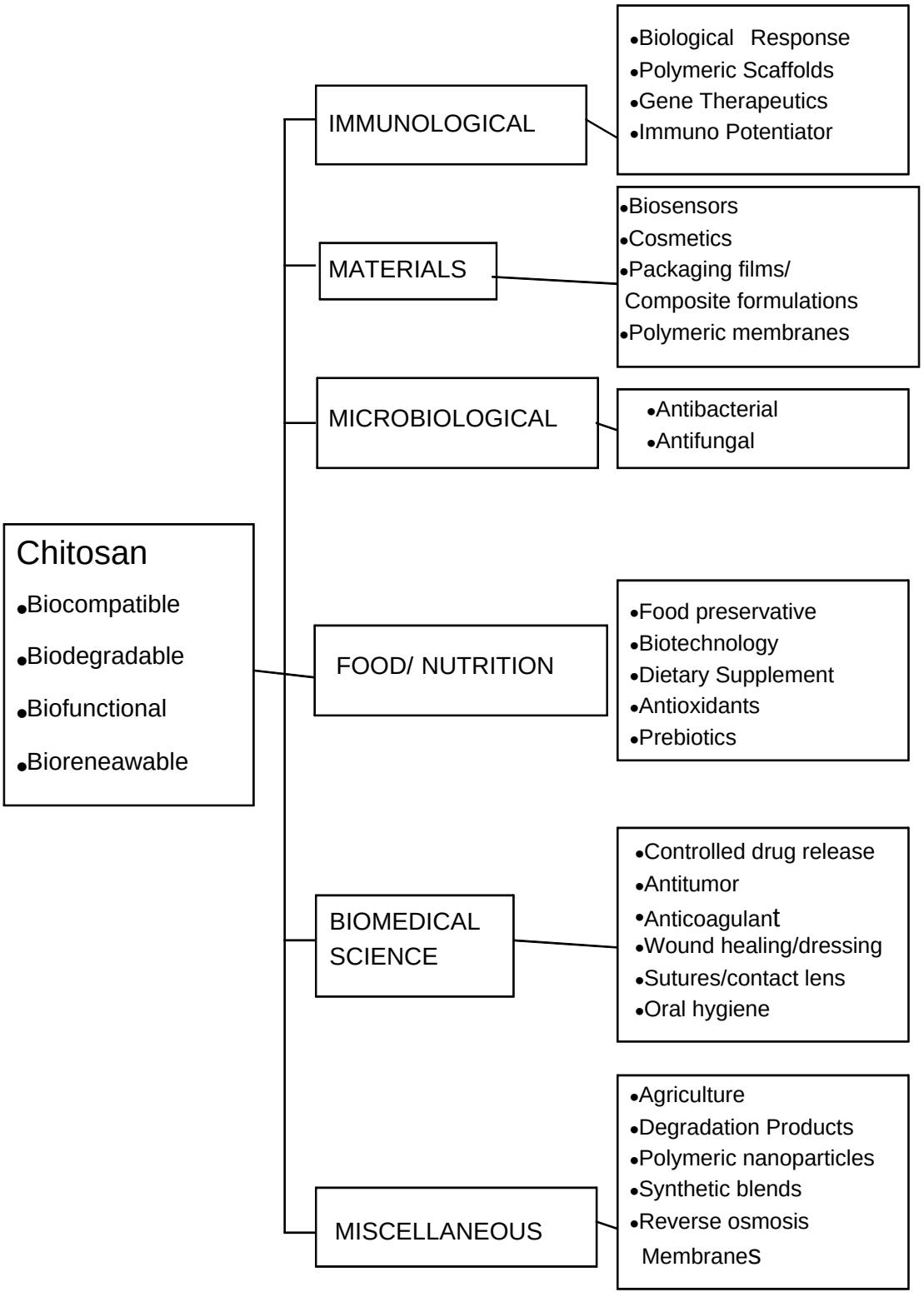

Figure 1.5 Various applications of CS

Figure 1.5 explains the various applications of CS. Chitosan is much easier to process than chitin, but the stability of CS materials is generally lower, owing to their more hydrophilic character and, especially, pH sensitivity. To control both their mechanical and chemical properties, various techniques are used. First, CS may be crosslinked by reagents such as epichlorohydrin[90], diisocyanate[91] or 1,4-butanediol diglycidyl ether[92]. Specific cross linking was performed on a blend of starch and CS: starch was oxidized to produce a polyaldehyde that reacts with the $–NH_2$ group of CS in the presence of a reducing agent[93]. Many CS hydrogels are obtained by treatment with multivalent anions: the case of glycerol phosphate is mentioned above[94], but oxalic acid has also been used[95] as well as tripolyphosphate[96]. Blends and composites have been prepared especially by Hirano, in the way mentioned previously for chitin[97]. Other systems are proposed in the literature: chitosan/polyamide 6[98], chitosan/cellulose fibers[99], chitosan/cellulose using a common solvent[100], chitosan/ polyelthylene glycol[101], chitosan/polyvinylpyrrolidone and chitosan/polyvinyl alcohol[102].

Recently, reinforcement of CS film with carbon nanotubes was tested; this composite exhibits a large increase of the tensile modulus with incorporation of only 0.8% of multiwalled carbon nanotubes[103]. The advantage of CS in such materials is not only its biodegradability and its antibacterial activity, but also the hydrophilicity introduced by addition of the polar groups able to form secondary interactions (–OH and $–NH_2$ groups involved in H bonds with other polymers). The most promising developments at present are in pharmaceutical and biological areas, and at a lower level in cosmetics.

1.5 CHEMICAL MODIFICATION OF CHITOSAN

Among the many mentions of CS derivatives in the literature[104-106], one can differentiate specific reactions involving the $–NH_2$ group at the C-2 position or nonspecific reactions of –OH groups at the C-3 and C-6 positions (especially esterification and etherification)[107]. The $–NH_2$ in the C-2 position is the important point of difference between CS and cellulose, where three –OH groups of nearly equal reactivity are available. The main reaction is easily performed involving the C-2 position is the quaternization of the amino group or a reaction in which an aldehydic function reacts with $–NH_2$ by reductive amination. This latter reaction can be performed in aqueous solution under very mild conditions to obtain randomly distributed substituents in a controlled amount along the CS chain. This method has

been proposed to introduce different functional groups on CS using acryl reagents in an aqueous medium; introduction of N-cyano-ethyl groups is said to produce some cross-linking through a reaction between the nitrile group and the amine group[108]. In addition, it is important to note that more regular and reproducible derivatives should be obtained from highly deacetylated chitin[109]—assuring control of the quality of the initial material that is essential before modification, especially when biological applications are to be explored. One of the most explored derivatives is poly (ethylene glycol) - grafted CS, which has the advantage of being water soluble, depending on the degree of grafting: higher molecular weight PEG at low degree of substitution (DS) gives higher solubility than low molecular weight PEG[110]. PEG can also be introduced by reductive amination of CS using PEG-aldehyde[111]. Polypeptides have been grafted by reaction with N-carboxyanhydrides of amino acids with the purpose of developing new biomaterials[112], but the degree of polymerization of the grafted chains cited in this work remains low (DP ¼ 5.9–6.6). **Figure 1.6** gives the various chemical modification reactions of CS.

1.5.1 Graft copolymerization

The possibility of grafting synthetic polymers to CS has attracted worldwide attention as a new and exciting way to modify and extend their use against the rapidly growing competition from synthetic polymers themselves. Research in this field has blossomed quickly and is still an extremely active subject of study. In spite of enormous efforts, there is still no large-scale commercial application of CS graft copolymers. Graft copolymerization onto CS has not yet been explored extensively; it is a rapidly advancing field in polymer modification[113]. Graft copolymerization reaction introduces side chains and makes various molecular designs possible, thus affording novel types of tailored hybrid materials composed of natural polysaccharides and synthetic polymers. The properties of the graft copolymers may be controlled by molecular structure, length and number of side chains attached. It is thus one of the most attractive approaches towards constructing versatile molecular environments. Grafting behavior is generally discussed in terms of grafting percentage, which is a ratio of the weight of introduced side chains to the weight of the main chain. Several types of CS-graft-copolymers with acrylic, vinyl, non-vinyl, etc. have been prepared for use as flocculants, paper binder-strengthener, slow-release drug carrier, etc. Conventionally, such graft co-polymerizations are being carried out using a variety of

redox systems, although simultaneous homopolymerization leading to low grafting yield is the major constraint.

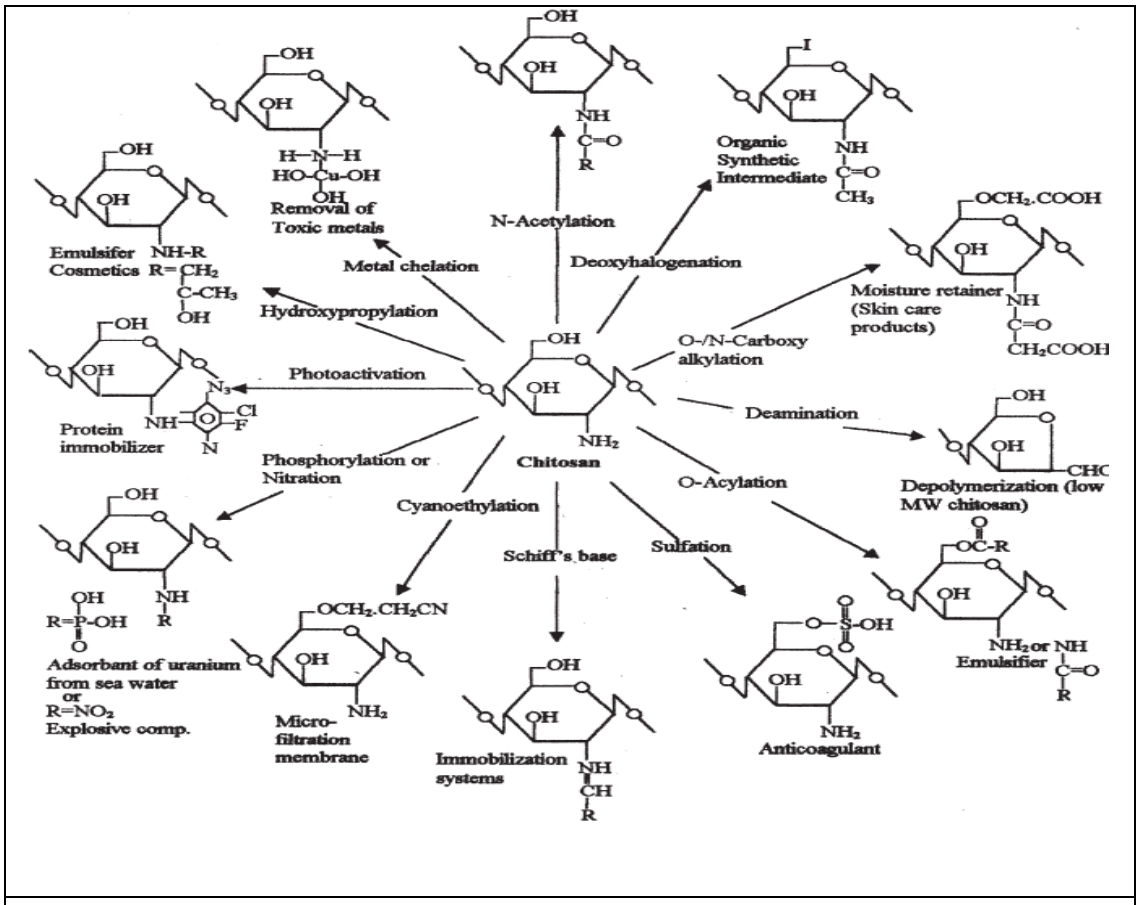

Figure 1.6 Chemical modification reactions of CS.

1.5.2 Grafting onto chitosan

Graft copolymerization onto CS has been attempted by various methods[114, 115], but it is performed typically with 2, 2-azo bisisobutyronitrile, Ce(IV), or a redox system. Vinyl monomers such as acrylonitrile, methylmethacrylate, methylacrylate and vinylacetate were graft copolymerized onto CS with 2, 2-azobisisobutyronitrile in aqueous acetic acid solution or in aqueous suspension. The grafting percentages were generally low. The CS-g-poly (vinylacetate) was converted into CS-g-poly(vinylalcohol) by hydrolysis[116]. Ce(IV) is also a suitable initiator, for graft copolymerization of polyacrylamide, poly(acrylic acid), and poly(4-vinylpyridine) with chitosan[117]. In addition to higher yield of grafting, the reaction takes place at much lower temperatures.

1.4.3 Inorganic materials

Inorganic bioceramics are known for their good biocompatibility, high compression resistance, and have also long been considered for a variety of medical applications[118]. Bioceramics with bioactive potential are of special interest as scaffolding materials to tissue engineers since they can form a continuous interface with surrounding bone tissue.

1.6 BIO-NANOCOMPOSITE SCAFFOLD

1.6.1 NANOHYBRIDS BASED ON CS AND INORGANIC FILLERS:

Bionanocomposites are an emerging class of hybrid materials derived from a naturally occurring biopolymer and inorganic solids interacting at the nanometric scale. In the last few years, the exploration on these biomaterials has received very important attention from researchers with expertise in diverse areas of nanotechnology, biomedical engineering and material science. As a combination product of biopolymers and inorganic solids at the nanometric level, bio-nanocomposites can be classified as a group of these materials. These organic-inorganic hybrids show extraordinary and versatile properties, as they could be formed from a large variety of biopolymers and also from different inorganic solid particles such as, layered silicates[119-125] (clay minerals), carbon nanotubes[126, 127] (CNT), hydroxyapatite (HAP[128]), gold-silver nanoparticles[129], silica and other metallic/non metallic oxides[130-132].

Nanocomposites have an increased number of atoms and crystal grains at their surfaces and possesses a higher surface area to volume ratio then conventional microscale biomaterials. These differences in surface topography alter the corresponding surface energy for protein adsorption. Other possible fields of applications are associated to their mechanical, thermal and barrier properties, making this class of materials attractive for potential uses in tissue engineering, controlled drug and pesticides delivery, membranes for food processing, biosensors, oxygen barrier films, food package, and as a non-viral gene delivery vectors. The importance of this field is apparent when one considers that for a single type of bio-medical material-drug eluting stents-over 2.5 million patients worldwide have benefited, while the market reports value of drug delivery systems in the USA alone is predicted to reach $85 billion by 2010. It should be noted that fundamental studies on the adsorption pathway of biopolymers on the surface of soil minerals, have been deeply developed in recent decades. Among these minerals the expanding 2:1 type layered silicates, of which

montmorillonite (MMT) is the best example, were of particular interest in view of their ability to intercalate a huge list of compounds. Nanocomposites are materials that are created by introducing nanoparticulates into a macroscopic sample material. Bionanocomposites are synthetic or natural material used to replace part of a living system or to function in intimate contact with living tissue. So we can say that it consists on filler dispersed in a matrix, one of the most used filler is the layered silicates. Montmorillonite (MMT) is a hydrated aluminium silicate with two-dimensional layered structure. Each layer is composed of one Al-octahedral sheet sandwiched between two Si-O-tetrahedral sheets with an interlayer space to form T-O-T unit cell. The space between the two layers is termed the "interlayer space", that is about 12 Å. The space is not enough to insert the Biopolymers due to their macromolecular size. We need to expand the interlayer space for Biopolymer accommodation. The negative charge of the inter-space resulting from isomorphic substitution is balanced by the sorption of exchangeable cations in interlayer sites (known as the cation exchange capacity (CEC), and is expressed in meq/100g). In order to render these hydrophilic phyllosilicates more organophilic, the hydrated cations of the interlayer should be exchanged with cationic surfactants such as alkylammonium. The modified clay (or organoclay) should be more organophilic and is more compatible with organic materials.

Layered solids have been extensively used to prepare a large variety of functional and structural nanocomposites by intercalation of organic molecules and polymers[133-135]. Belonging to this class of solids, clay minerals of the 2:1 charged phyllosilicates family (smectites) are excellent hosts to intercalate molecular and macromolecular species[136]. Moreover, Montmorillonite (MMT), smectite type clay, exhibit swelling properties, enhanced gel strength, mucoadhesive capability to cross the gastro-intestinal (GI) barrier and adsorb bacterial toxins and metabolic toxins such as steroidal metabolites. Considering these advantages in medical applications, it has taken the credit to be called as medical clay[137]. **Figure 1.7** is the structure of (**a**) MMT and (**b**) LDH.

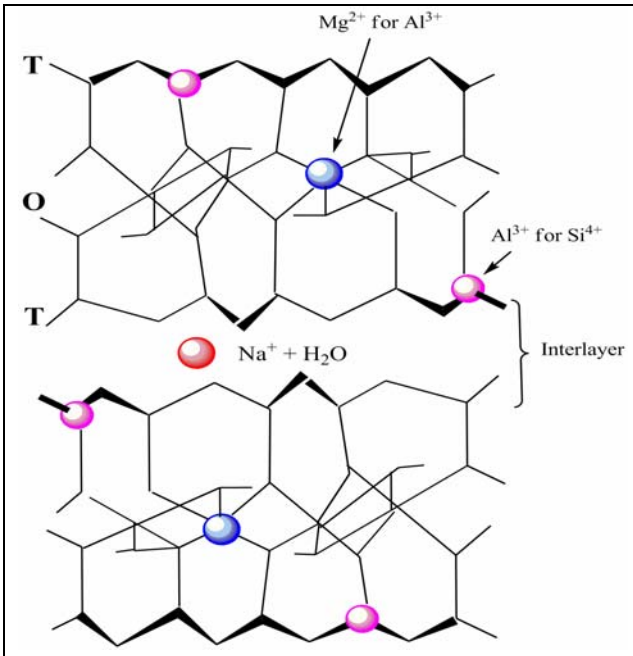

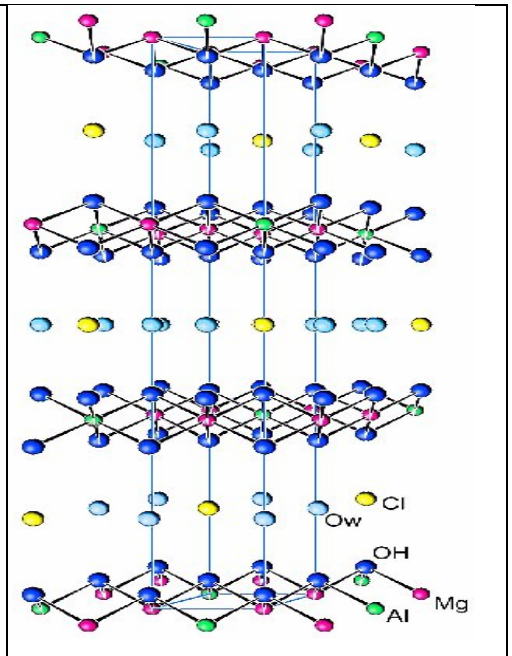

Figure 1.7 (a) Structure of MMT **(b)** Structure of LDH

In addition, of particular relevance to this study, the drug is also cationic which facilitates easy drug loading into the lumen of layered silicates posing a very demanding challenge to achieve adequate sustained release property due to the anticipated high diffusion gradient produced. Some of these resulting nanocomposites have functional properties with potential applications as advanced materials[138]. A representative example of these last compounds are the polymer–clay nanocomposites based on the intercalation of poly (ethylene oxide), PEO, which remains strongly adsorbed into the interlamellar space by coordination with the exchangeable cations of the silicate[139]. These polymer–clay nanocomposites are the first reported hybrid materials with ionic conductivity that can be useful for applications in electrical and electrochemical devices[140].

Layered double hydroxides (LDH) are 2-dimensional solids also able to act as hosts for intercalations of anionic species including negatively charged polymers such as polystyrene sulfonate and polyacrylates[141]. This is due to the positive electrical charge of the LDH layers that can be considered as brucite-like sheets, in which isomorphous substitutions of divalent by trivalent cations take place[142]. Smectites show a structural opposite behavior, because the isomorphous substitutions in both tetrahedral and octahedral layers deserve a negative charge, which is compensated in the interlayer space by extra framework of exchangeable cations[143].

More specifically, a bio-nanocomposite is developed for three main reasons highlighted in the following:

1. To enhance the mechanical properties of the scaffold.
2. To improved biological response at the implant site.
3. To overcome the various effect of undesirable characteristics of each constituents when taken separately.

The above-mentioned findings have shown that CS-based nanocomposites are promising candidates for tissue engineering and drug delivery applications. Therefore, in our work, by taking advantage of these findings, we have proposed to use inorganic clays as nanofillers to develop bionanocomposites with improved physical and biological properties.

Our hypotheses are based on two reasons: The physical properties of the scaffold may be enhanced: By being incorporated into CS, clay is expected to act simultaneously as particulate reinforcing phase to result in a reinforced structure. Also, the toughness and plasticity of the CS phase could be combined to the strength of the inorganic phase and enhance its relatively weak mechanical properties[144]. Moreover, the strong biological activity of CS, combined with the excellent biocompatibility and the bioactive potential of clays, might promote tissue regeneration and allow for potentially better cells delivery and control over their differentiation[145].

1.6.2 HYDROXYAPATITE [HAP]

Hydroxyapatite (HAP) is a class of calcium phosphate-based bioceramics, frequently used as a bone graft substitute owing to its chemical and structural similarity with natural bone mineral[146]. The stoichiometric HAP has a chemical composition of $Ca_{10}(PO_4)_6(OH)_2$ with Ca/P ratio of 1.67. HAP is not only bioactive but also osteoconductive, non-toxic, non-immunogenic, and its structure is similar to that of bone mineral. On the other hand, it has also been used in dental surgery, bio-molecular delivery and drug delivery. HAP has a long history of use as a biomaterial. **Table 1.6** gives the various methods of synthesis of HAP. Daubree[147] carried out the first synthesis of apatite in 1851 by a process in which phosphorous trichloride vapor was passed over the red-hot lime. In 1951, a synthetic HAP was prepared by Ray and Ward[148], suitable for bone defects. They implanted HAP into surgically created defects in the long bones and iliac wings of dogs and the skulls of cats and monkeys and obtained affirmative results.

Table 1.6 Methods involve in the synthesis of Nano-HAP

Method	Particle size (nm)	Remarks
Solid State	500	In-homogenous, large grain size, irregular shape, reaction condition 900-1300 °C
Wet Chemical	20-200	Nanograin size, irregular crystallinity, homogenous, reaction condition: 37-100 °C
Precipitation/hydrothermal	10-25	Homogenous, ultra-fine particles, low crystallinity, reaction condition: 37-100 °C
Hydrothermal	10-80	Homogenous, Fine crystals, high temperature and high pressure atmosphere
Mechanochemical	<20	Easy production, semi-crystallinity, ultra-fine crystals, room temperature process
pH Shock-Wave	20-100	High-energy dispersing, non-porous monocrystalline particles, Ca/P ratio 1.43-1.66
Microwave	100-300	Uniformity, nanosize particles, time and energy saving

Hydroxyapatite (HAP) is the most stable calcium phosphate salt at normal temperatures and pH between 4 and 12. It is a compound of great interest in catalysis, the industry of fertilizers and pharmaceutical products, protein chromatography applications; water treatment processes, preparation of biocompatible materials, and mostly because it is the main inorganic component in calcified hard tissues (e.g., bone and teeth) of vertebrates. HAP is also formed pathologically as a result of functional irregularities resulting in cartilage arthritis, formation of renal, bladder, and bile stones, and calcification of transplanted cardiac valves. In this context, HAP is considered as a model compound to study biomineralization phenomena. For this reason there is a strong interest for synthetic, extra pure, well-defined HAP crystals for use in detailed physicochemical in vitro and in vivo studies, and bio-medical applications. In literature, several methods to prepare HAP crystals have been reported, including solid state reactions, plasma techniques, crystal growth under hydrothermal conditions, layer hydrolysis of other calcium phosphate salts, and sol-gel crystallization[149-152]. Essentially, the synthesis of HAP crystals from supersaturated aqueous solutions is advantageous due to low cost and simplicity, but most of the synthetic procedures followed until now led to the formation of nonstoichiometric products. Deviation from the stoichiometry of HAP is due to the presence in the crystal lattice of vacancies and

ion substitutes such as carbonates, hydrogen phosphates, potassium, sodium, nitrates, and chloride, which are usually introduced into the precipitating system with the reactants.

Contamination of HAP with these ions or formation of deficient HAP suffer from significant changes in their crystallographic characteristics and have different crystal morphology as compared to the stoichiometric. Difficulties encountered in preparing synthetic HAP crystals from aqueous solutions are mainly caused by the high chemical affinity of the material to some ions, the complex nature of the calcium phosphates system, and the role of kinetic parameters, which, depending on the experimental conditions, prevail over the thermodynamics. Recently, nanoscale HAP (10–100 nm) has received much attention owing to its superior functional properties over its microscale counterpart, particularly surface reactivity and ultra-fine structure, which are the most imperative properties for tissue–graft interaction upon implantation. It has also been proven that the nano- HAP, compared to conventional micro HAP, promotes osteoblast adhesion, differentiation and proliferation, osteointegration, and deposition of calcium-containing minerals on its surface, which leads to enhanced formation of new bone tissue within a short period[153]. HAP has a unique capability of binding to the natural bone through biochemical bonding, which promotes the interaction between host bone and grafted material. Although nano-HAP is an excellent bone graft material, its inherent low fracture toughness has limited its use in certain orthopedic applications, in particular heavy load-bearing implantation[154].

1.7 CHARACTERIZATION TECHNIQUES OF NANOHYBRIDS

1.7.1 X-ray Diffraction (XRD)

X-ray diffraction (XRD) is a non-destructive analytical technique for identification and quantitative determination of long-range order in various crystalline compounds. XRD uses the "fingerprint" of crystalline material to allow identification and quantification of unknown phases in a mixture. X-rays are electromagnetic radiation generated when an electron beam accelerated through a high voltage field hits a metal, which acts as an anode. The wavelength of x-ray is comparable to the size of atoms; therefore they can be effectively used to measure the structural arrangement of atoms in materials. When x-rays collide with electrons, some x-rays from the incident beam are deflected away from the incident direction. If the wavelengths of these scattered x-rays remain unchanged, the process is called an elastic scattering

(Thompson Scattering) in that only momentum is transferred during collision. These are the x-rays that are measured in diffraction experiments. They carry information about the electron distribution in materials. On the other hand, during inelastic collision (Compton Scattering), x-rays transfer some of their energy to the electrons and so the scattered x-rays will have different wavelength than the incident x-rays. X-rays diffracted from different atoms interfere with each other. If the atoms are arranged in a periodic fashion, as in the case of crystals, the peaks in the interference pattern will correspond to the distribution of atoms. The peaks in an x-ray diffraction pattern are directly related to the atomic distances by Bragg's law:

$$n \lambda = 2d \sin \theta$$

where, λ is the wavelength of x-ray, is the inter-planar distance, $d\theta$ is the scattering angle and n an integer representing the order of the diffraction peak.

1.7.2 Transmission Electron Microscopy (TEM)

A transmission electron microscope (TEM) is used to observe the fine scale structure. A TEM functions exactly as its optical counterpart except that it uses a focused beam of electrons instead of visible light to "image" the specimen and gain insight about the structure and composition. The four basic operations involved are: 1) A stream of electrons is formed and accelerated towards the specimen using a positive electrical potential, 2) This stream is confined and focused using a metal aperture and magnetic lenses into a thin, monochromatic beam, (magnetic lenses are circular electro-magnets capable of projecting a precise circular magnetic field in a specified region) 3) The focused beam is impinged on the sample by a magnetic lens, 4) The energetic electrons then interact with the irradiated sample. These interactions and effects are detected and transformed into an image.

1.7.3 Fourier Transform Infra-Red (FT-IR) Spectroscopy

In FT-IR spectroscopy, IR radiation is passed through the sample. Some of the IR radiations are absorbed by the sample and some of it passed through it (transmitted). The resulting spectrum represents the molecular absorption and transmission, creating the molecular fingerprint of the sample (**Figure 1.8**).

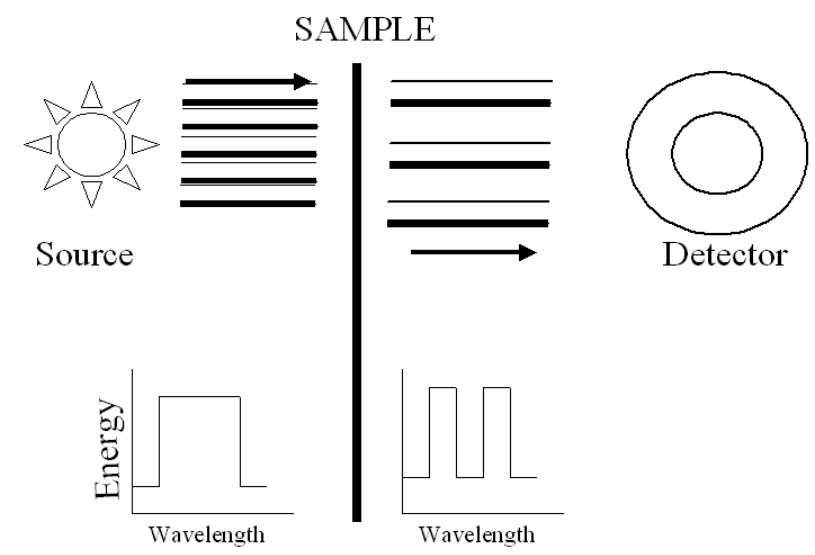

Figure 1.8 Experimental set-up of FT-IR.

1.7.4 Atomic Force Microscopy [AFM]

The AFM works by measuring a local property-such as height, with a probe or tip placed very close to the sample. The small probe-sample separation makes it possible to take measurements over a small area. To acquire an image the microscope scans the probe over the sample while measuring the local property in question. The resulting image resembles an image that both consist of many rows or lines of information placed one above the other.

AFM operates by measuring attractive or repulsive forces between a tip and the sample. In its repulsive contact mode, the instrument lightly touches a tip at the end of a leaf spring or cantilever to the sample. As a raster-scan drags the tip over the sample, some sort of the detection apparatus measure the vertical deflection of the cantilever, which indicates the local sample height. Thus in contact mode the AFM measures hard-sphere repulsion forces between the tip and sample. In non contact mode, the AFM devices topographic images from measurements of attractive forces; the tip does not touch the sample.

1.7.5 Scanning Electron Microscopy [SEM]

This technique is essentially employed when high resolution three- dimensional images of the surface morphology are desired. When an electron beam impinges on a sample, back scattered electrons and X-rays are produced**.** A scintillation detector detects secondary electron**s,** which are emitted from a surface with low energy 50 eV.

They are primarily produced within the top few nanometers of the sample. Back scattered electrons are high energy and come from the depth of μm or more.
If the system is equipped with an X-ray detector, which measures either the wavelength or the energy of the X-rays, elemental analysis can also be performed. The primary electron beam can be focused down to nanometer scale. High energy electrons are used to increase surface details. To attain a conducting surface and to minimize the beam damage, polymer samples are usually coated with metal such as gold.

1.8 CONCLUSION

Any biomaterial implanted into the body has to interface well with the existing tissue while performing its function. The obvious implication of that statement is that the body receiving the implant should not reject it physiologically. The more subtle, but equally significant implication is that the mechanical properties of the implant should be appropriate for the location in which it is implanted. This entails insuring the correct anisotropy is maintained and the material responds appropriately to mechanical stimuli. Sometimes empirical evidence through simple burst or biaxial tests is all that is needed for confirmation. Other times, it is necessary and convenient to find the natural biomaterial's properties and model using finite element analysis**,** expanding the limits of what experiments and conditions can be tested. Just as a structural engineer is able to determine if a high rise building will withstand the forces of strong winds when it is full erected before construction ever begins, a biomedical engineer can use these data to determine if an implant will fail mechanically when subjected to the wear and tear of daily living inside a person.

Further understanding of the natural tissues and advancement of the composite science are necessary in order to achieve this goal. Experimental and clinical studies are needed to test new candidate materials or composites having the required qualities for biomaterial. We have come a long way from the beginnings of natural biomaterial implantation and we are at a point when the available technology intersects with the desire for knowledge. All of today's available tools can yield valuable and accurate information. It only depends on the researcher to choose how much information they need and how best to use it.

The work underlying this thesis is to answer the fundamental questions:

1. CS can be modified to obtain better thermal and mechanical properties and the formulation with montmorillonite could be useful for a controlled drug release carrier. (***Chapter 3***).
2. Can modified CS with PDMS films prove as a better alternate in selective surface protein adsorption (***Chapter 4***)?
3. CS can be used to mineralize layered double hydroxide (LDH) on its surface and the resulting nanohybrids can be used as a sustained release carrier and as an effective antacid (***Chapter 5***).
4. Can CS act as a biocompatible matrix for preparation of CS-Mesoporous silica composite for stimulated drug release (**Chapter 7**)?

Following the proof-of-concept answer to each question, conclusion on the feasibility of using CS as a biomaterial for tissue engineering and drug delivery application will be drawn for the future outlook of the biomaterials in this regard will be discussed.

1.9 REFERENCES

1. B.D. Ratner, A.S. Hoffman, F.J. Schoen, and J.E. Lemons, *Biomaterials Science, Academic Press*, 1996.
2. J. Karp, and R. Langer, *Curr. Opin. Biotech*., **18**, 454 (2007).
3. G. Balssundaram, and T.J. Webster, *Nanomed*., **1**, 169 (2006).
4. L.S. Nair, and C.T. Laurencin, *Adv. In Biochem. Eng*., **102**, 47 (2006).
5. R. Langer, *MRS Bull*., **31**, 477 (2006).
6. C. Du, and J. Moradian-Oldak, *Biomed. Mater*., **1**, R10 (2006).
7. B. Baroli, *J. Chem. Technol. Biotechnol*., **81**, 491 (2005).
8. T. Hadlock, and C. Sundback, *Exp. Opi. Biol. Therap*., **6**, 1105 (2006).
9. E. Anitua, M. Sanchez, G. Orive, and I. Andia, *Trends Pharmacolog. Sci*., **29**, 37 (2008).
10. L. De-Laporte, and L.D. Shea, *Adv. Drug Del. Rev*., **59**, 292 (2007).
11. D.F. Williams, *Trends in Biotechnol*., **24**, 4 (2006).
12. R. Vasita, and D.S. Katti, *Exp. Rev. Med. Dev*., **3**, 29 (2006).
13. V. M. Goldberg, and A. J. Caplan, Orhopedic tissue engineering, Eds Goldberg and Caplan, Marcell Dekker, *Inc., New York*, **1**, (2004).
14. S. MacNeil, *Mater. Today*, **11**, 26 (2008).
15. P.X. Ma, *Adv. Drug. Del. Rev*., **60**, 184 (2008).

16. K.J.C. Burg, S. Porter, and J.F. Kellan, *Biomater*., **21**, 2347 (2000).
17. A.J. Salgado, O.P. Coutinho, and R.L. Reis, *Macromol. Biosci*., **4**, 743 (2004).
18. M. C. Kruyt et al, *Biomater*., **25**, 1463 (2004).
19. J. Sun, S.Y. Wu, and F. Lin, *Biomater*., **26**, 3953 (2005).
20. H. Hu, C. Lin, P.P. Lui, and Y. Leng. *J. Biomed. Mater. Res., A*, **65**, 24 (2003).
21. D.W. Hutmacher, *Biomater.*, **21**, 2529 (2000).
22. T. Tateishi, G. Chen, and T. Ushida, *J. Art. Organs*, **5**, 77 (2002).
23. A.J. Salgado, O.P. Cautinho, and R.L. Reis, *Macromol. Biosci*., **4**, 743 (2004).
24. L.J. Gibson, *J. Biomechanics*, **38**, 377 (2005).
25. A.J. Gracia, *Adv. Polym. Sci*., **203**, 171 (2006).
26. Y.P. Jiao, and F.Z. Cui, *Biomed. Mater*., **2**, R24 (2007).
27. C.J. Wilson, R.E. Clegg, D.I. Leavesley, and M.J. Pearcy, *Tissue Eng*., **11**, 1 (2005).
28. M.C. Durrieu, *ITBM-RBM*, **26**, 229 (2006).
29. E.K.F. Yim, K.W. Leong, *Nanomed. Nanotechnol. Biol. Med*., **1**, 10 (2005).
30. J.W. Wang, and M.H. Hon, *J. Biomed. Mater. Res*., **64**, 262 (2003).
31. J.K. Oh, R. Drumright, D.J. Siegwart, and K. Matyjaszewski, *Prog. Polym Sci*., **33**, 448 (2008).
32. D. Schmaljohann, *Adv. Drug Del. Rev*. **58**, 1665 (2006).
33. G. Acharya, and K. Park, *Adv. Drug Del. Rev*., **58**, 401 (2006).
34. H. Aliabadi, and A. Lavasanifar, *Exp. Opi. Drug Del*., **3**, 139 (2006).
35. I.S. Fraser, and D. Mansour, *Exp. Opi. Drug Del*., **3**, 191 (2006).
36. H.T. Ta, C.R. Dass, and D.E. Dunstan, *J. Control. Rel*., **126**, 205 (2008).
37. J.L. Drury, and D.J. Mooney, *Biomater*., **24**, 4337 (2003).
38. M. Biondi, F. Ungaro, F. Quaglia, and P.A. Netti, *Adv. Drug Del. Rev*., **60**, 229 (2008).
39. S.R. Von Tomme, and W.E. Hennink, *Exp. Rev. Med. Dev*., **4**, 147 (2007).
40. Y. Cheng, J. Wang, T. Rao, X. He, and T. Xu, *Front. Biosci*., **13**, 1447 (2008).
41. L. Moroni, J.R. De-Wijn, and C.A. Van Blittereswijk, *J. Biomater. Sci.: Polym. Edn*., **19**, 543 (2008).
42. C.P. Reis, R.J. Wenfeld, A.J. Ribeiro, and F. Veiga, *Nanomed. Nanotechnol. Biol. Med*., **2**, 53 (2006).
43. R.V. Kulkarni, and S. Biswanath, *J. Appl. Biomater. Biomech*., **5**, 125 (2007).
44. S. Murdan, *J. Control. Rel*., **92**, 1 (2003).

45. Y. Tang, and J. Singh, *Int. J. Pharma*., **357**, 119 (2008).
46. J.L. Bull, *Exp. Opi. Drug Del*., **5**, 475 (2007).
47. C. He, S.W. Kim, and D.S. Lee, *J. Control. Rel*., **127**, 189 (2008).
48. S. Giri, B.G. Trewyn, M.P. Stellmaker, and VSY Lin, *Angew. Chem*., **44**, 5038 (2005).
49. G. Jiang, W. Chen, and W. Xia, *Design. Monom. Polym*., **11**, 105 (2008).
50. C. Brus, P. Santi, P. Colombo, and T. Kissel, *J. Control. Rel*., **84**, 171 (2002).
51. Y.W. Chien, and S. Lin, II Edn., *Encyclp. Pharma. Technol.,* Vol I, Marcel-Dekker Inc, Basel (CH), 811 (2002).
52. P.A. Gunatillake, and R. Adhikari, *Eur. Cell Mater*., **5**, 1 (2003).
53. Y. Zhang, and M. Zhang, *J. Biomed. Mater. Res*., **61**, 1 (2002).
54. S. Ramakrishna, J. Mayer, E. Wintermantel, and K.W. Leong, *Compost. Sci. Technol*., **61**, 1189 (2001).
55. L.T. Laurencin, A.M. Ambrosio, M.D. Borden, and J.A. Cooper, *Ann. Rev. Biomed. Eng*., **1**, 19 (1999).
56. J.L. Ifkovits, and J.A. Burdick, *Tissue Eng*., **13**, 2369 (2007)
57. F.R. Rose, and R.O. Oreffo, *Biochem. Biophys. Res. Commun*., **292**, 1 (2002).
58. D.W. Hutmacher, J.C. Goh, and S.H. Teoh, *Ann. Acad. Med. Singapore*, **30**, 183 (2001).
59. M. Jobmann, and G. Rafler, *Internat. J. Pharmaceut*., **242**, 213 (2002).
60. W. Linhart, F. Peters, W. Lehmann, K. Schwarz, A.F. Schlling, M. Amling, J.M. Rueger, and M. Epple, *J. Biomed. Mater. Res*., **54**, 162 (2001).
61. J.P. Vacanti, R. Langer, J. Upton, and J.J. Marler, *Adv. Drug Del. Rev*., **3**, 165 (1998).
62. E. Khor, and L.Y. Lim, *Biomater*., **24**, 2339 (2003).
63. R. Hejazi, and M. Amizi, *In Polymeric Biomaterials, Marcel Dekker, NY*, **213** (2001).
64. (a) M.N.V. Ravi Kumar, *Reac. Funct. Polym*., **46**, 1 (2000), (b) K.V. Harish Prashanth, and R.N. Tharantharan, *Trends Food Sci. Technol.,* **18,** 117 (2007).
65. P.R. Periodontal, L. Vandemark, E.B. Kenney, and G.W. Bernard, *J. Periodontal*, **67**, 1170 (1996).
66. J.K. Suh, and H.W. Matthew, *Biomater*., **24**, 2589 (2000).
67. A. Domard, and M. Domard, *In Polymeric Biomaterials, Marcel Dekker, NY*, **187** (2001).

68. D.K. Malik, S. Baboota, A. Ahuja, S. Hasan, J. Ali, *Curr. Drug. Del*., **4**, 141 (2007).
69. W. Tan, R. Krishnaraj, and T.A. Desai, *Tissue Eng*., **7**, 203 (2001).
70. A. Lahizi, A. Sohrabi, D.S. Hungerford, and C.G. Frondoza, *J. Biomed. Mater. Res*., **15**, 586 (2000).
71. E. Dawson, G. Mapili, K. Erickson, S. Taqvi, and K. Roy, *Adv. Drug Del. Rev*., **60**, 215 (2008).
72. P.J. VandeVord, H.W. Matthew, S.P. DeSilva, L. Mayton, B. Wu, P.H. Wooley, *J. Biomed. Mater. Res*., **5**, 585 (2002).
73. I.Y. Kim, S.J. Seo, H.S. Moon, M.K. Yoo, I.Y. Park, B.C. Kim, and C.S. Cho, *Biotechnol. Adv*., **26**, 1 (2008).
74. M. Rinaudo, *Polym. Int*., **57**, 397 (2008).
75. Y. Hamilton, Y. Yuan, D.A. Rigney, B.M. Chesnutt, A.D. Puckett, J.L. Ong, Y. Yang, and J.D. Bumgardner, *Polym. Int*., **56**, 641 (2007).
76. M. Ishihara, K. Obara, S. Nakamura, M. Fujita, K. Masuoka, Y. Kanatani, B. Takase, and M. Kikuchi, *J. Artif. Org*., **9**, 8 (2006).
77. Z. Liu, Y. Jiao, Z. Zhang, and C. Zhou, *J. Biomed. Mater. Res*., **83 A**, 1110 (2007).
78. K. Song, P. Wen, and T. Liu, *Key Eng. Mater*., **373**, 722 (2008).
79. P.R. Klokkevold, L. Vandemark, E.B. Kenney, and G.W. Bernard, *J. Periodontol*., **67**, 1170 (1996).
80. (a) B.L. Reynolds, *Am. J. Surg*., **26**, 113 (1960), (b) R.N. Tharantharan, and F.S. Kittur, *Critical Rev. Food Sci. Nutri.,* **43,** 61 (2003).
81. J.F. Prudden, P. Migel, P. Hanson, L. Friedrich, and L. Balassa, *Am. J. Surg*., **119**, 560 (1970).
82. (a) W. Liu, S.J. Sun, X. Zhang, and D. Yao, *J. Biomater. Sci. Polym. Edn.,* **14**, 851 (2003), (b) M. Rinaudo, *Polym. Int.,* **57,** 397 (2008).
83. H. Yi, L-Q. Wu, W.E. Bentley, R. Ghadssi, G.W. Rubloff, and J.N. Culver, *Biomacromol.*, **6**, 2881 (2005).
84. Z. Li, H.R. Ramay, K.D. Hauch, D. Xiao, and M. Zhang, *Biomater*., **26**, 3919 (2005).
85. L. Wang, E. Khor, A. Wee, and L.Y. Lim, *J. Biomed. Mater. Res*., **63**, 610 (2002).

86. T.H. Kim, J.W. Nah, M.H. Cho, T.G. Park, and C.S. Cho, *J. Nanosci. Nanotechnol*., **6**, 2796 (2006).
87. Z. Ding, J. Chen, S. Gao, J. Chang, and E.T. Kang, *Biomater*., **25**, 1059 (2004).
88. I. Adekogbe, and A. Ghanem, *Biomater*., **26**, 7241 (2005).
89. A.D. Metcalfe, and M.W. Ferguson, *J.R. Soc. Interface*, **4**, 413 (2007).
90. K. Mizuno, K. Yamamura, K. Yano, T. Osada, S. Saeki, and N. Takimoto, *J. Biomed. Mater. Res.*, **64**, 177 (2003).
91. W.S. WanNgah, M.A.K.M. Hafiah, and S.S. Yong, *Coll. Surf. B Biointerface*., (in press).
92. Y.C. Wei, S.M. Hudson, J.M. Mayer, and D.L. Kaplan, *J. Polym. Sci. A. Polym. Chem*., **30**, 2187 (1992).
93. E.R. Welsh, and R.R. Price, *Biomacromol*., **4**, 1357 (2003).
94. S.K. Ray, J.G. Todd, and W.G. Glasser, *US Patent*, **5770**, 712 (1998).
95. E.T. Baran, J.F. Mano, and R.L. Reis, *J. Mater. Sci. Mater. Med*., **15**, 759 (2004).
96. A. Chenite, C. Chaput, D. Wang, C. Combes, M.D. Buschmann, and C.D. Hoemann, *Biomater*., **21**, 2155 (2000).
97. S. Hirano, R. Yamaguchi, N. Fukui, and M. Iwata, *Carbohydr. Res*., **20**, 145 (1990).
98. KGH Desai, and H.J. Park, *J. Microencapsulation*, **22**, 179 (2005).
99. S. Hirano, In Natural and Synthetic Polymers: Challenges and Perspectives, *Macromol. Symp., Weinheim, Wiley VCH*, **168**, 21 (2001).
100. M.J. Ko, W.H. Jo, H.C. Kim, and S.C. Lee, *Polym. J*., **29**, 997 (1997).
101. J. Hosokawa, M. Nishiyama, K. Yoshihaara, and T. Kubo, *Ind. Eng. Chem. Res*., **29**, 800 (1990).
102. M. Hasegawa, A. Isogai, S. Kuga, and F. Onabe, *Polym*., **35**, 983 (1994).
103. M. Mucha, J. Piekielna, and A. Wieczorek, *Macrmol. Symp*., **144**, 391 (1999).
104. T.H.M. Abou-Aiad, K.N. Abd-El-Nour, I.K. Hakim, and M.Z. Elsabee, *Polym*., **47**, 379 (2005).
105. S.F. Wang, L. Shen, W.D. Zhang, and Y.J. Tong, *Biomacromol.*, **6**, 3067 (2005).

106. M. Morimoto, H. Saimoto, and Y. Shigemasa, *Trends Glycosci. Glycotech*., **14**, 205 (2002).
107. B. Liao, R. Liu, and Y. Huang, *Polym. J*., **39**, 1071 (2007).
108. B. Liao, R. Liu, and Y. Huang, *Polym. J*. **39**, 1071 (2007).
109. Y. Dong, K. Sakurai, Y. Wu, and Y. Kondo, *Polym. Bull*., **49**, 189 (2002).
110. E.I. Rabea, MET Badawy, C.V. Stevens, G. Smaggle, and W. Steurbaut, *Biomacromol*., **4**, 1457, (2003).
111. M. Rutnakornpituk, and P. Ngamdee, *Polym*., **47**, 7909 (2006).
112. L. Deng, H. Qi, C. Yao, M. Feng, and A. Dong, *J. Biomater. Sci. Polym. Edn*., **18**, 1575 (2007).
113. H. Yu, X. hen, T. Lu, J. Sun, H. Tian, J. Hu, Y. Wang, and X. Jing, *Biomacromol*., **8**, 1425 (2007).
114. N. Ma, Q. Wang, S. Sun, and A. Wang, *Prog. Chem*., **16**, 643 (2004).
115. K. Kurita, *Prog. Polym. Sci*., **26**, 1921 (2001).
116. K. Kurita, M. Kawata, Y. Koyama, and S. Nishimura, *J. Appl. Polym. Sci*., **42**, 2885, (1991).
117. M.J.Z. Mehr, *Iranian Polym*. J., **14**, 235 (2005).
118. Z.G. Wang, L.S. Wan, and Z.K. Xu, *J. Mem. Sci*., **304**, 8 (2007).
119. Hertz, J.J. Bruce, *Nanomed*., **2**, 899 (2007).
120. J.C. Lin, *Composite Str*., **84,** 125 (2008).
121. G. Wang, Y. Chen, and Q. Wang, *J. Polym. Sci. B: Polym. Phy*., **46**, 807 (2008).
122. A.R. McLauchlin, and N.L. Thomas, *J. Col. Inter. Sci*., **321**, 39 (2008).
123. A. Ammala, C. Bell, and K. Dean, *Composite Science Technol*., **68**, 1328 (2008).
124. W.S. Chow, and S.K. Lok, *J. Thermoplastic Comp. Mater*., **21**, 265 (2008).
125. M.S. Kim, J.K. Jun, and H.M. Jeong, *Compos. Sci. Technol*., **68**, 1919 (2008).
126. J.C. Lin, *Compos. Str*., **84**, 125 (2008).
127. W. Yang, P. Thordarson, J.J. Gooding, S.P. Ringer, and F. Braet, *Nanotechnol*., **18**, art. No. 412001, (2007).
128. B.S. Harrison, and A. Atala, *Biomater*., **28**, 344 (2007).
129. K. Koutsopoulos, *J. Biomed. Mater. Res*, **62** A, 600 (2002).
130. S.J. Son, X. Bai, and S.B. Lee, *Drug Discovery Today*, **12**, 657 (2007).

131. F. Schuth, *Chem. Mater*., **13**, 3184 (2001).
132. R.B. Laughin, *Adv. Phy*., **47**, 943 (1998).
133. D. Keller, and I. Mangelsdorf, *Env. Health*, **226**, X (2002).
134. M. Darder, A.I. Ruiz-Hitzky, P. Aranda, H. Van Damme, E. Ruiz-Hitzky, *Curr. Nanosci*., **2**, 231, (2006).
135. O. Becker, G.P. Simon, *Adv. Polym. Sci*., **179**, 29 (2005).
136. S.S. Ray, and M. Bousmina, *Prog. Mater. Sci*., **50**, 962 (2005).
137. E. Ruiz Hitzky, P. Aranda, J.M. Serratosa, in Handbook of layered materials, ed. S.M. Auerbach, K.A. Carrado and P.K. Dutta, *Marcel Dekker, Inc. New York*, **91** (2004).
138. Y. Dong, and S.S. Feng, *Biomater*., **26,** 6068 (2005).
139. P.A. Monnard, M.S. DeClue, and H.J. Ziock, *Curr. Nanosci.*, **4**, 71 (2008).
140. P. Aranda, Y. Mosqueda, E. Perez-Cappe and E. Ruiz Hitzky. *J. Polym. Sci, Part B; Polym. Phys*., **41**, 3249 (2003).
141. E. Ruiz-Hitzky and P. Aranda, in Polymer-clay nanocomposites, ed. T.J. Pinnavaia and G.W. Beall, *John Wiley & Sons, Chichester*, **19** (2000).
142. P. Ding, M. Zhang, J. Gai, and B. Qu, *J. Mater. Chem*., **17**, 1117 (2007).
143. F.R. Costa, A. Leuteritz, U. Wagenknecht, D. Jehnichen, L. Haubler, and G. Heinrich, *Appl. Clay Sci*., **38**, 154 (2008).
144. Y. Wang, and H. Gao, *J. Coll. Interf., Sci*., **301**, 19 (2006).
145. H.H. Jin, C.H. Lee, W.K. Lee, J.K. Lee, H.C. Park, and S.Y. Yoon, *Mater. Lett*., **62**, 1630 (2008).
146. H. Zhuang, J.P. Zheng, H. Gao, and K. De Yao, *J. Mater. Sci.: Mater. Med*., **18**, 951 (2007).
147. P. Liu-Snyder, and T.J. Webster, *Curr. Nanosci*., **4**, 111, (2008).
148. A Daubree, Comp. Rend. *Acad. Sci*., **32**, 625 (1851).
149. R.D. Ray, and A.A. Ward, *Surg. Forum*, **2**, 429 (1951).
150. E.P. Paschalis, Q. Zhao, B.E. Tucker, S. Mukhopahayay, J.A. Bearcroft, N.B. Beals, M. Spector, and G.H. Nancollas, *J. Biomed. Mater. Res*., **29,** 1499 (1995).
151. N. Yamasaki, T. Kai, M. Nishioka, K. Yanagisawa, and K. Ioku, *J. Mater. Sci*., **9,** 1150 **(**1990).
152. R.Z. LeGeros, G. Daculsi, I. Orly, T. Abergas, and W. Torres. *Scan. Microsc*., **3,** 129 **(**1989).

153. M. Tanahashi, K. Kamiya, T. Suzuki, H. Nasu, *J. Mater. Sci. Mater. Med*., **3,** 48 **(**1992).
154. H. Ozawa, K. Hoshi, and N. Amizuka, *J. Oral Biosci*., **50**, 1 (2008).
155. Z. Hong, P. Zhang, C. He, X. Qiu, A. Liu, L. Chen, X. Chen, and X. Jing, *Biomater*., **26**, 6296 (2005).

CHAPTER II

Scope, Objectives and Approaches

2.1 INTRODUCTION AND OBJECTIVES

Bionanocomposites are an emerging class of hybrid materials derived from a naturally occurring biopolymer and inorganic solids interacting at the nanometric scale[1, 2]. In the last few years the exploration on these bio-materials has received very important attention from researchers with expertise in diverse areas of nanotechnology[3-4], biomedical engineering[5] and material science. As a combination product of biopolymers and inorganic solids at the nanometric level, bio-nanocomposites can be classified as a group of these materials. These organic-inorganic hybrids show extraordinary and versatile properties, as they could be formed from a large variety of biopolymers and also from different inorganic solid particles such as, layered silicates (clay minerals)[6], carbon nanotubes (CNT)[7], hydroxyapatite (HAP)[8], gold-silver nanoparticles[9], silica and other metallic/non metallic oxides[10]. Of particular relevance from applications point of view of bionanocomposites, it should be taken into consideration that biopolymers are biocompatible and biodegradable compounds and, therefore, their composites are of interest for advanced biomaterials, as for instance tissue engineering, artificial bones or gene therapy, for better healthcare products and bio-medical materials.

Chitosan (CS), a biopolymer, is the deacetylated product of chitin. Due to its biodegradability, biocompatibility and avirulence, CS has been used in many biomedical applications. The high mechanical strength, hydrophilicity, good adhesion and non-toxicity of CS, offer it as food additive, anticoagulant and wound healing accelerator. Though CS has the ability to form films, yet the tensile properties of pristine CS film are poor (due to its crystallinity). Thus, the modification (chemical modification, blending and graft copolymerization) of CS has gained its importance for tailoring the desired mechanical properties[11-13]. Since CS is alkaline in nature, by combining it (as graft copolymer or blend) with the biodegradable polymers like polylactic acid, which generate acidic by-products, the local toxicity at the implant site can be reduced[14-18]. So, the primary objective of the present study is to design novel nanohybrids based on CS and layered clays like montmorillonite and layered double hydroxides. In this study, CS has been grafted with lactic acid and PDMS to improve its surface properties.

CS has been widely used in tissue engineering as a scaffold[19], orthopedic implants[20] and in drug delivery applications[21]. Generally, drug release kinetics of polymeric drug delivery systems is usually characterized by membrane permeability

and diffusion coefficient, which are employed to describe the release behavior of the membrane reservoir system and the diffusion mechanism of the release system[22]. Furthermore, both indexes in polymer-based materials are strongly dependent on crystallinity, plasticization, and swelling behavior of the biopolymer drug delivery vehicle, which are also affected by the type and presence of the nanofillers[23-25]. So, the secondary objective of the proposed work is to evaluate the effect of the nanofillers on the controlled drug release from the nanohybrids.

2.2 APPROACHES

2.2.1 CS intercalated with Montmorillonite (MMT) and grafted with lactic acid

2.2.1.1 Intercalation of CS into MMT**.**

2.2.1.2 Grafting of lactic acid onto CS.

2.2.1.3 Structural analysis by XRD, TEM, SEM, POM, and AFM techniques.

2.2.1.4 Swelling-deswelling properties of smooth films and porous scaffolds.

2.2.1.5 Loading of Ibu drug and controlled release studies.

2.2.1.6 Biocompatibility studies by *in-vitro* cell-culture testing.

2.2.2 CS intercalated with MMT and grafted with poly dimethyl Siloxane (PDMS)

2.2.2.1 Grafting of PDMS onto CS intercalated into MMT.

2.2.2.2 Structural change analysis by using XRD, FT-IR, and AFM.

2.2.2.3 Surface properties testing by Protein Adsorption and in-vitro cell-growth studies.

2.2.3 Role of CS in Biomineralization of Layered Double Hydroxides (LDH).

2.2.3.1 Preparation of Biomineralized LDH onto CS.

2.2.3.2 Structural studies by XRD, TEM, AFM, and SEM.

2.2.3.4 In-vitro buffer capability studies of the prepared nanohybrids.

2.2.4 Biomimetic synthesis of Hydroxyapatite (HAP) and its polymorphs

2.2.4.1 Biosynthesis of HAP and its polymorphs by Phytase Enzyme.

2.2.4.2 Structural analysis by XRD, HR-TEM, SAED, FT-IR, and NMR.

2.2.4.3 Reaction conditions like enzyme concentration, temperature, and time.

2.2.4.4 Physiological stability evaluation of HAP.

2.2.4.5 Osteoblasts culture studies on HAP.

2.2.5 Effect of Ultrasound (US) on smart drug release from a CS-Mesoporous silica (MS) composite

2.2.5.1 Preparation of MS and drug- loaded MS and CS-MS system.

2.2.5.2 Structural analysis by XRD, TEM, FT-IR, and NMR.

2.2.5.3 Temperature and pH-stimulated drug release studies.

2.2.5.4 Effect of US on smart release of Ibuprofen.

2.2.5.6 In-vitro cell-culture studies.

2.3 REFERENCES

1. M. Darder, P. Aranda, and E. Ruiz-Hitzky, *Adv. Mater*., **19**, 1309 (2007).
2. M.A.S. Azizi-Samir, F. Alloin, and A. Defresne, *Biomacromol*., **6**, 612 (2005).
3. R.A. Hule, and D.J. Pochan, *MRS Bull*., **32**, 354 (2007).
4. I.K. Tonle, T. Diaco, E. Ngameni, and C. Detellier, *Chem. Mater*., **19**, 6629 (2007).
5. V. Hasirci, E. Vrana, P. Zorlutana, A. Ndreau, P. Yilgor, F.B. Basmanan, and E. Aydin, *J. Biomater. Sci. Polym. Ed.,* **17**, 1241 (2006).
6. D. Depan, A.P. Kumar, and R.P. Singh, *J. Biomed. Mater. Res. A,* **72**, 372 (2006).
7. C. Tang, L. Xiang, J. Su, K. Wang, C. Yang, Q. Zhang, and Q. Fu, *J. Phys. Chem. B,* **112**, 3876 (2008).
8. K. Rezwan, Q.Z. Chen, J.J. Blaker, and A.R. Boccaccini, *Biomater.,***27**, 3413 (2006).
9. B. Wang, K. Chen, S. Jiang, F. Reincke, W. Tong, D. Wang, and C. Gao, *Biomacromol.,* **7,** 1203 (2006).
10. G.L. Kenausis, J. Voros, D.L. Elbert, N. Huang, R. Hofer, L. Ruiz-Taylor, M. Textor, J.A. Hubbell, and N.D. Spencer, *J. Phys. Chem., B,* **104,** 3298 (2000).
11. N.A. Peppas, and S.R. Lustig. *Annals of the New York Academy of Sciences*, **446**, 26 (1985).
12. M.R. Griffin. *The Am J Med*, **104**, 23S (1998).
13. Y. Dong, and S.S. Feng, *Biomater*, **26,** 6068 (2005).
14. J.P. Zheng, L. Luan, H.Y. Wang, L.F. Xi, and K.D. Yao, *Appl. Clay Sci*. **36,** 297 (2007).
15. N. Kubota, and K. Ogha, *J. Appl. Polym. Sci*., **42,** 495 (1991).
16. S.V. Madihally, and H.W. Matthew, *Biomater*., **20** 1133 (1999).
17. D. Depan, B. Kumar, R.P. Singh, *J. Biomed. Mater. Res.* **84B,** 184 (2008).
18. Q. Xin, and A. Anders Wirsen, *J. Appl. Polym. Sci.* **74,** 3193 (1999).
19. H. Liu, H. Fan, Y. Cui, Y. Chen, K. Yao, and J.C.H. Goh, *Biomacromol*., **8**, 1446 (2007).
20. A. Di-Martino, M. Sittinger, and M.V. Risbud, *Biomater*., **26**, 5983 (2005).

21. X. Wang, Y. Du, J. Luo, B. Lin, and J.F. Kennedy, *Carbohyd. Polym*., **69**, 41 (2007).
22. R. Langer, *Chem. Eng. Commun*., **6**, 1 (1980).
23. L.H. Sperling, Intro. to Phys. Polym. Sci., *John Wiley and Sons*, *New York*, **148** (1992).
24. K. Kesenci, L. Fambri, C. Migliaresi, and E. Piskin, *J. Biomater. Sci. Polym. Ed.*, **11**, 617 (2000).
25. V. Arrighi, J.J. McEwen, H. Qian, and M.B. Serrano Prieto, *Polym*, **44**, 6259 (2003).

CHAPTER III

A: Preparation and Characterization of Novel Hybrid of Chitosan-g-Lactic acid and Montmorillonite[*]

3.1 INTRODUCTION

Polylactic acid (PLA) is biocompatible polymer and undergoes scission in the body to monomeric units of lactic acid, which is a natural intermediate in carbohydrate metabolism. Owing to their biodegradability, homopolymers and copolymers of lactic acid, have been widely used in biomedical applications like, resorbable sutures, as a carrier for controlled release of drugs and as implants for orthopedic surgery or blood vessels which will be eventually replaced by tissues in the body[1,2]. Recently research efforts have been made on using this polymer as screws in the femur of sheep and rabbits and as disposable products (syringes, blood bag), adhesive, and sealant, prostheses for tissue engineering and artificial organs for temporary or permanent assist[3,4]. However, it was also found that as scaffold materials, PLA exhibits few drawbacks such as (1) The inherent hydrophilicity, (2) generation of acidic species, resulting in decrease in local pH which potentially may cause tissue inflammation surrounding implant and initiate enzyme hydrolysis, and (3) Self acceleration of degradation. A decrease in local pH (acidic environment) catalyzes the hydrolytic degradation of ester bonds of the polymer. Copolymerization of PLA with poly (glycolic acid) (PGA) is a possible approach to enhance the fast degradation rate by destroying the crystalline domains of PLA backbone, but the hydrophobic nature of PLGA limits its applicability in drug delivery and biomedical applications. Moreover, the accumulation of acidic degradation products formed by PLA degradation results in poorer soft-tissue compatibility.

Another biopolymer, Chitosan (CS), [poly-β(1, 4)-2-amino-2-deoxy-D-glucose], is the deacetylated product of chitin, poly (N-acetyl-D-glucoseamine), a natural polymer found in the cell wall of fungi and microorganisms. Due to its biocompatibility, biodegradability and avirulence, CS has been used in many biomedical applications[5-10]. According to recent studies, combining (as copolymer, blends) CS with biodegradable polymer whose degradation products are acidic, may reduce the local toxicity due to the acid by-products can be alleviated[11]. Because of its properties, such as high mechanical strength, hydrophilicity, good adhesion and non-toxicity, it is usually applied as food additive and as anticoagulant or wound healing accelerator[12]. It is well known that wound-dressing materials should be durable, stress resistant, flexible, pliable and elastic with reasonable tensile properties, which could bear the stresses exerted by different parts of the body having varying contours. The

increase in flexibility could improve the contact between the film and the tissue, hence promoting penetration of the polymeric chains into the tissue to form a strong bonding, leading to an increase in the adhesion strength. The dressing must be an absolute barrier to bacteria ingress and could prevent egress of wound organisms to the surface of dressing. Furthermore, the dressing is preferably permeable to water vapor to some extent that moist exudates under the dressing are maintained without pooling[13]. The ability of CS to form films may permit its extensive use in the formulation of film dosage forms[14] or as drug delivery systems[15]. Furthermore, CS has antimicrobial activities, so it can be used as antimicrobial packaging, which is a promising form of active food packaging. Interests on tailoring the CS for desired properties has also being grown in different ways e.g. graft copolymerization. The development of organic-inorganic hybrids has also been another field of research in preparing biocomposite / biomimetic materials. In most of the cases, the synthesis involves either melt-direct polymer intercalation by using a conventional polymer extrusion process or intercalation by a suitable monomer and then exfoliating the layered host into their nanoscale elements. It has been found that the reinforcement of layered silicates improves the optical, physical, thermal, rheological and mechanical properties of the obtained composites with very low amount of loading of nano-clay because of their nanoscale distribution with high aspect ratio[16-17]. Recently Nanocomposites of polylactic acid with layered silicates have also been prepared by different methods[18].

Asira[19] had a preliminary study about chitosan-clay nanocomposites and reported a markedly improved tensile property but inferior thermal property of composites to that of pure chitosan. Ruiz-Hitzky[20] and his co-workers synthesized functional CS/ montmorillonite nanocomposites, which can effectively act as active phase for an electrochemical sensor in the detection of different anions. All of them prepared nanocomposites by exfoliation-adsorption method, which used diluted acetic acid solvent for dispersing and dissolving clay and CS. However, there are few reports about the effect of grafting with Poly-lactic acid onto CS, and the effect of hydrogen bond between CS and MMT, which may be the key driving force to make the MMT layers assemble to form flocculated structure in CS matrix. Thus, it will be worthwhile to develop a new biocomposite materials based on lactic acid grafted onto CS with improved mechanical, thermal, optical properties. So far, very limited work has been reported on the approach of copolymerization of LA onto CS. In connection to this,

Yao et al.[12], reported the *in-vitro* fibroblast static cultivation on a biocompatible poly (chitosan-g-L-lactic acid) film and the cell growth rate on the copolymer film was found to be much faster than that of the pristine CS film. In another interesting work, Liu et. al[21], have reported the synthesis of a brush like copolymer of polylactide grafted onto CS. Later, Wu et al.[10] studied the amphiphilic properties of a graft copolymer of water soluble CS and polylactide prepared by using triethyl amine as catalyst. The first attempt to synthesize a pH-sensitive physically cross linked hydrogel by grafting D, L-lactic acid onto amino groups in chitosan without using a catalyst was reported by Albertsson et al[22].

We have been interested to prepare macromolecular organic-inorganic hybrids of layered silicates and CS-g-LA. It involves grafting of lactic acid on CS in the presence of layered silicates without using any catalyst and using lactic acid itself as solvent. It is also expected that grafted poly-(lactic acid) chains may act as internal plasticizers to reduce the brittleness of CS films / to obtain more soft and elastic film and this will introduce side chains and thus make various molecular designs possible, affording novel types of tailored hybrid materials composed of natural polysaccharide and grafted polymer. Apart from that, controlled salvation and degradation could be achieved by controlling the ration of CS: LA in the graft copolymers to obtain an optimum hydrophilic: hydrophobic balance.

3.2 EXPERIMENTAL

3.2.1 Materials

CS of low molecular weight (M_v $1.5x10^5$, degree of deacetylation was 85%) was obtained from Aldrich. L-Lactic acid (purity 92%) was purchased from Spectrochem and was used as such for graft copolymerization. Montmorrilonite Na^+-MMT, with Cation Exchange Capacity of 76.4-meqv/100 g was received from M/s. Southern Clay Inc.USA.

3.2.2 Preparation of nanocomposites and graft copolymerization

Preparation involves aqueous dispersion of clay, suspension of CS in L-lactic acid, mixing them, drying and dehydration. The nanocomposites were prepared keeping CS: clay (Na^+-MMT) ratios as 100:0, 95:5, 90:10 and 80:20. First CS was dispersed in L-lactic acid and clay was dispersed in deionized water (30ml) overnight at room

temperature. They were mixed and mixture was again dissolved in L- lactic acid and the resulting solution was heated up to 100°C with continuous degassing for 30 –45 minutes. They were casted on a glass plate and dried at 60°C for 8 hrs. Then, the films were again dried at 60°C in vacuum oven for 8 hrs to promote dehydration of the CS copolymer with formation of the corresponding amide linkages. To remove the unreacted L-Lactic Acid, and oligomers of L-Lactic acid, the samples were extracted with methanol in a soxhlet apparatus for 48 hrs. The thickness of the resulting films were measured and found to be about ≈0.10mm. The composition of the prepared nanocomposites is compiled in **Table 3.1.**

Table 3.1 The composition of the prepared nanohybrids.

S. No	Chitosan (g)	Lactic acid (ml)	Na^+-MMT (g)	Sample code
1.	1	1	0.0	CLA-1
2.	1	1	0.05	CLA-2
3.	1	1	0.10	CLA-3
4.	1	1	0.20	CLA-4
5.	2	1	0.05	CLA-5

3.3 Characterization of Nanocomposites

3.3.1 X-Ray Diffraction

The Wide Angle X-ray Diffractometer patterns of the samples were obtained by Rigaku (Japan) X-Ray diffractometer with Cu-Kα radiation at 50kV between the scan ranges of 2θ from 2-30 degree by the scan rate of 2 degree/min. The system consists of a rotating anode generator with a Cu target and a wide angle powder goniometer having a diffracted beam graphite monochromator. The generator was operated at 40 kV and 150 mA. All the experiments were performed in the reflection mode. The d- spacing was calculated by Bragg's formula where the λ was 0.154nm.

3.3.2 Microscopic measurements

The supermolecular structure was examined by means of Polar Optical Microscopy (Olympus B201). All optical micrographs presented in this paper were taken under cross-polarized light. To clarify the nanoscale structure, TEM image was obtained by TEM 2000 EX-II instrument (JEOL, Tokyo, Japan) operated at an

accelerating voltage of 100 kV to observe the nanoscale morphology. All the ultrathin sections were microtomed using a Super NOVA instrument (M/s. Leica, Switerzerland) with a diamond knife and then subjected to TEM without staining.

3.3.3 Thermo gravimetric analysis

The thermal gravimetric analysis (TGA) was conducted on a Perkin-Elmer TGA 7 – thermal analyzer from 50°C to 900°C with a heating rate of 10°C min^{-1} under nitrogen with flow rate 20ml min^{-1}.

3.3.4 FTIR- Spectroscopy

The Fourier-transform infrared (FTIR) spectra were obtained from the sample under ATR mode on a Perkin-Elmer Spectrum GX.

3.3.5 Water Absorption measurements

According to ASTM D570 the clean, dried film samples of known weights were immersed in distilled water at 25°C for one day (24 h). The films were removed, blotted quickly with absorbent paper and then weighed. The absorption percentage of these samples was calculated using the equation X (%) = $(W_1-W_0) / W_0$, Where W_0 and W_1 are the weight of dry and swollen samples, respectively.

3.4 RESULTS AND DISCUSSION

3.4.1 Graft copolymerization of CS and L-lactic acid.

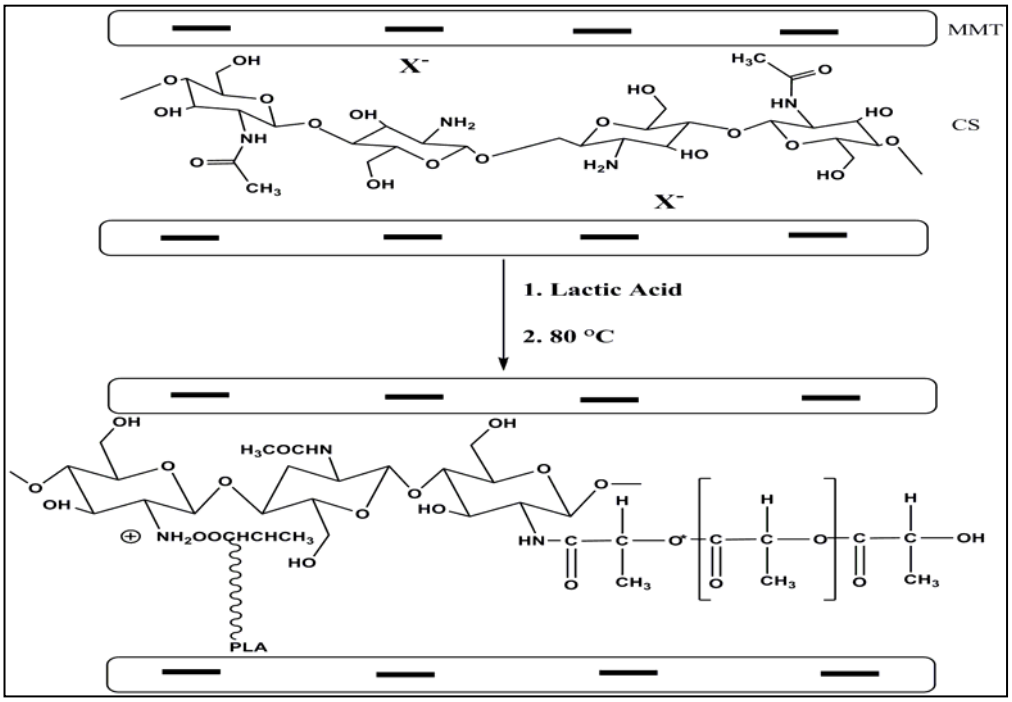

Scheme 3.1 Schematic illustration of the intercalation of CS into MMT and grafting of LA onto CS.

Scheme 3.1 shows the expected reaction mechanism for the preparation of nanocomposites of CS-*g*-LA and montmorillonite. CS was dissolved in aqueous lactic acid solution to give a homogenous viscous polyelectrolyte solution. The protonation of amino groups of CS will result in CS amino lactate salt. It is expected that the dehydration of the salt will occur to form amide groups between the chitosan and L-lactic acid by heating the solution and simultaneously L-lactic acid will undergo polycondensation. The polyesterification of LA follows the well-known acid catalyzed reaction involving protonation of the carboxylic group, followed by reaction of the protonated species with the hydroxyl functional group to yield the ester linkage.

The freshly prepared semitransparent films are brittle, but upon exposure to air, they easily absorb moisture and become sticky and soft. This may be due to the presence of unreacted LA, oligomeric LA, amide and ammonium salt in the 'as-prepared' product during the removal of water from the solid state in the amide forming dehydration step. Chloroform or methanol could dissolve the unreacted monomers and oligomers. So these copolymer films were extracted with methanol in soxhlet apparatus. During the heating process, the formation of amide links and the polycondensation reaction of LA took place at the same time. So the content of the oligomer and the unreacted LA in the crude product enhanced when raising the amount of LA added. The results of the yield values and Degree of polymerization (DP) of side chains are given in **Table 3.2**.

Table 3.2: Yield (%) and Degree of polymerization (DP) of the grafted samples

CS (g)	LA (g)	LA/NH_2 (mol/mol)	Yield (g)	DP* of side chains
1.0	0.5	1.2	1.44	1.39
1.0	1.0	2.5	1.86	1.77
1.0	2.0	4.38	3.91	3.78
1.0	3.0	6.86	4.68	4.81
1.0	4.0	7.6	5.27	5.31

*- DP_{PLA} determined by ^{1}H-NMR from the integration ratio of the $-CH_3$ groups within PLA blocks versus those of the hydroxylated lactyl end units.

Both the amidation and polycondensation reactions occurred in solid state i.e. during the film casting, so the specific surface area or the film thickness would have an impact on the extent of reaction. The prepared nanocomposites were purified by soxhlet

extraction using methanol as solvent. The results of elemental analysis of the samples are shown in **Table 3.3.**

Table 3.3 Results from the elemental analysis of the nanohybrids.

Sample	Elemental Analysis		
	C	H	N
CLA-1	38.20	6.18	7.59
CLA-2	37.14	6.51	6.91
CLA-3	36.52	6.30	6.54
CLA-4	38.19	6.06	6.33
CLA-5	39.91	6.20	6.35

3.4.2 CHARACTERIZATION

3.4.2.1 Morphology and Structure.

The bright field TEM image of the CS-g-L.A./ Na^+-MMT is given in **Figure 3.1 (a)**. It shows the characteristic platelets of the montmorillonite tactoids, in which the dark entities are the cross section of intercalated Na^+-MMT layers and bright areas are the biopolymer matrix. For nanocomposite preparation, aqueous suspension of Na^+-MMT was treated with CS dispersed in L-lactic acid, adjusting the pH ≈ 5.0 to avoid any structural alteration of the phyllosilicate. On the other hand, acidic pH is necessary for the formation of $–NH_3^+$ groups in the CS structure. In such conditions, the adsorption process is mainly controlled by a cationic exchange mechanism due to the columbic interactions between the positive $–NH_3^+$ groups of the biopolymer and the negative sites in the clay structure.

The WAXD patterns of neat Na^+ -MMT and its nanocomposites with CS-g-LA are shown in **Figure 3.1 (b).** It was reported[23, 24] that CS has an orthorhombic unit cell with a = 8.24 *Å*, b = 10.39 *Å*, and c = 16.48 *Å*. The peaks appearing at around 2θ = 10° are assigned to (001) and (100), while the peaks around 2 θ = 20° are assigned to (020) and (200). The reflection at (020) is associated with the highly ordered domains formed through intra-molecular hydrogen bonding between acetamido groups, which further facilitates the incorporation of water molecules forming a hydrated crystal. The measured d_{001}- spacing of Na^+-MMT was 12.26 A° (2θ = 7.2°). It can be observed that d_{001}-spacing of the nanocomposite (CLA-2) was increased to 15.88 A° (2θ = 5.56°).

This decrease in 2θ value or increase in d-spacing confirms the intercalation of biopolymer in the clay interlayer.

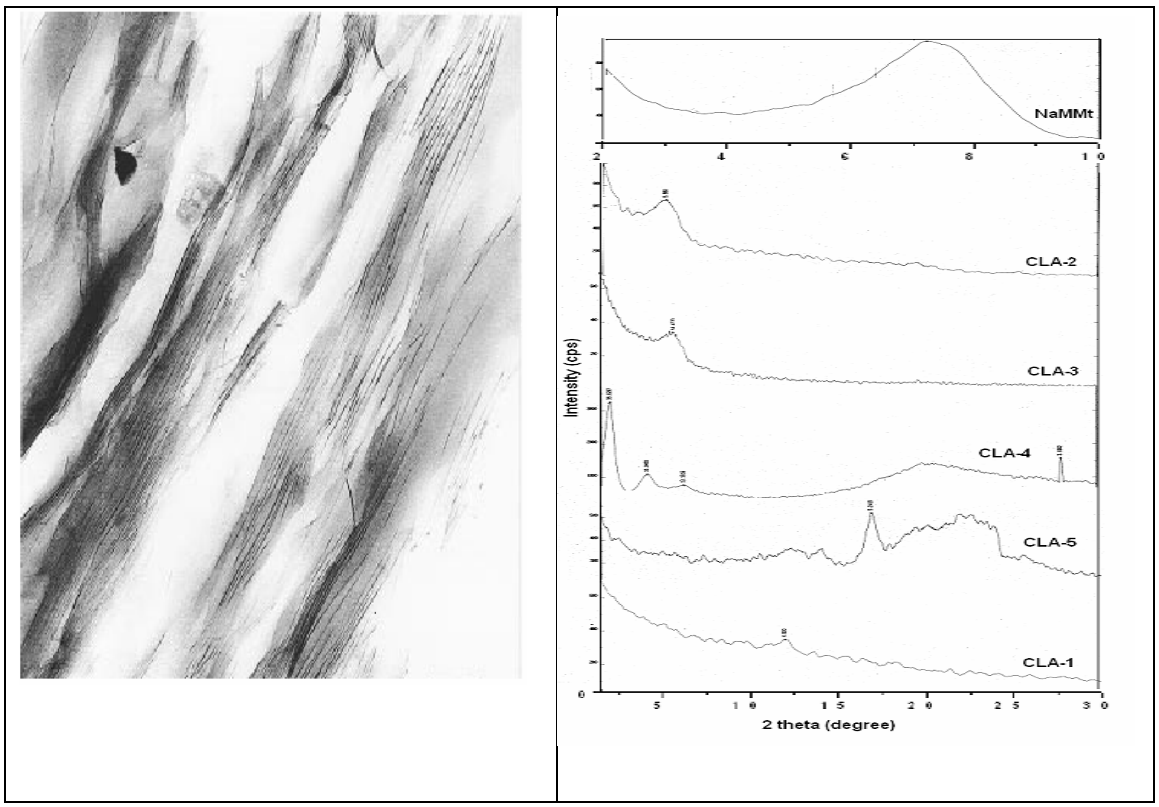

Figure 3.1 (a) TEM image of CLA-2, and **(b)** WAXD of the prepared nanohybrids.

This may be attributed to the cation exchange between the Na^+ of clay layers and $–NH_3^+$ groups of CS. This is in agreement with the d_{001} value of 3.8 A° measured from the XRD pattern of a CS film, which represents the thickness of a sheet of polysaccharide chains. The d-spacing of other nanocomposites were also observed to increase depending on the composition while CLA-5 was observed to be exfoliated nanocomposite.

The higher d_{001} value obtained for the nanocomposites with the highest amount of CS is attributed to the intercalation of the CS i.e. corresponding to the thickness of layers of CS together with thickness of the acetate anion. The second layer of chitosan may be adsorbed by means of a hydrogen bonding mechanism, since the $–NH_3^+$ groups of the first layer have already balanced the cation exchange capacity of the clay.

Thus, the $–NH_3^+$ groups of the second layer interact electrostatically with the acetate anions which are available from the starting CS solution for anionic exchange as shown in scheme 1. This was supported by Darder et.al.[20] that when CS amount relative to clay exceeds 75%, a second layer of chitosan would get adsorbed onto the

first layer of the already adsorbed CS onto clay. In addition, the grafted polymer chains may further increase the d_{001}-spacing of clay to give exfoliated nanocomposites where CS amount was higher (CLA-5). The peak around 2θ = 20° which is assigned for orthorhombic cell unit of CS was not observed for CLA-1 and nanocomposites CLA-2, CLA-3 and CLA-4 where the CS amount was same. This peak was observed for CLA-5 where the CS amount was higher. It is inferred that the graft-polymerized samples whose ratio of LA/CS was same, became almost amorphous (2θ = 20°). Since LA reacts with CS in a homogeneous solution, the grafting by PLA will take place at random along the chain, giving rise to a random copolymer. This will efficiently destroy the regularity of the packing of the original CS chains, which results in the formation of almost amorphous copolymers. On the other hand, in CLA-5 where the CS amount was higher thought the availability of reaction centers is more; some crystalline domains of CS were not completely destroyed. The adsorption of CS on the montmorillonite (MMT) via cationic exchange mechanism is also supported by EDX results. The electrostatic interaction of $–NH_3^+$ groups of CS with the negatively charged sites of the clay substrate exchange the existing Na^+ ions in the MMT. It can be observed in **Figure 3.2 (a)**, which represents the Na/Si ratio as a function of the adsorbed CS amount that the Na^+ ions decrease significantly with the increase of CS amount. The successful incorporation of CS onto the nanoscale silicate layers was also demonstrated by with energy-dispersive spectroscopy (EDX). As shown in **Figure 3.2 (b)**, the incorporation of CS moieties was directly observed from the presence of the carbon absorption peak. Moreover, peaks assignable to oxygen and nitrogen also appeared in the EDX spectrum of CS-g-LA nanocomposite. In acidic solutions, CS shows an extended structure that may facilitate the biopolymer intercalation in the clay interlayer space in opposition to analogous polysaccharide with coiled or helicoidal structures that are only adsorbed in the external surface of clays[20]. The good stability of this material towards CS desorption is inferred from NaCl salt solution treatment. The treatment of the CS-g-LA/ Na^+-MMT nanocomposite (CLA-2) with 1.0 M NaCl for a period of 30 days treatment did not release any component of the adsorbed biopolymer from the clay interface, as confirmed by TG analysis and further confirmed from XRD, as there was no difference in d-spacing was found.

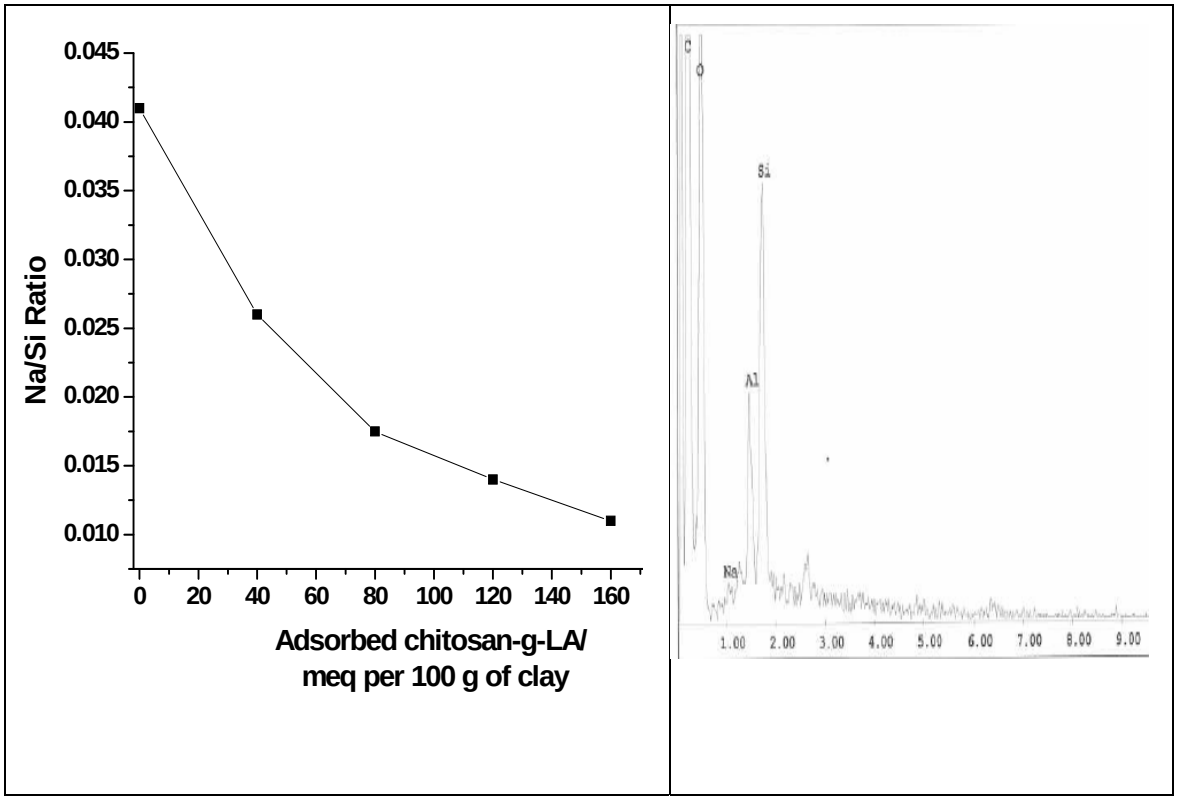

Figure 3.2 (a) Na/Si ratio of CLA-1, and **(b)** EDAX analysis of CLA-1.

3.4.2.1 FTIR Spectroscopy.

Figure 3.3 (a) shows the IR spectra of samples where peak at 1560 cm^{-1} which is attributed to the deformation vibration (δNH_3^+) of the protonated amine group, is shifted towards lower frequency, confirming the interaction i.e. grafting of LA onto NH_3^+ group.

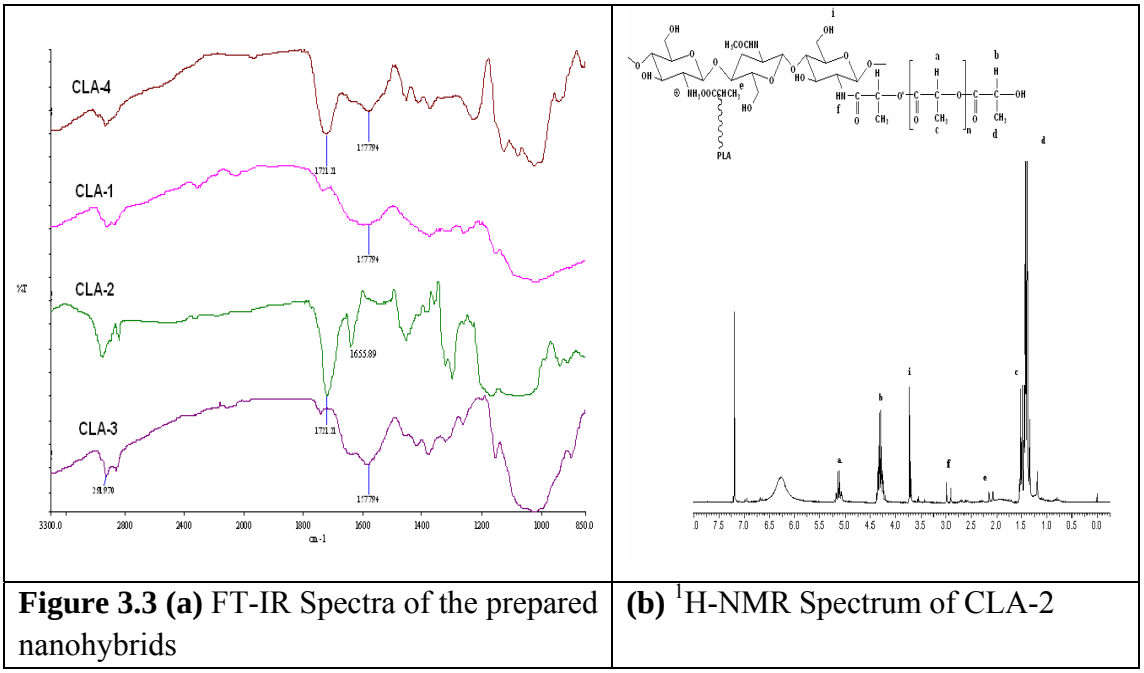

Figure 3.3 (a) FT-IR Spectra of the prepared nanohybrids	**(b)** ^{1}H-NMR Spectrum of CLA-2

In addition to CS, the peak at 1652 cm^{-1} of $–NH_2$, a new peak assigned to amide group at 1578 cm^{-1} appears which confirms the conversion of $–NH_2$ to –NH-CO. The band at 1721 cm^{-1} may be attributed to the ν_{CO} stretching band of acetate ions associated with the second layer of CS. The peak at 1655 cm^{-1} indicates the amide formation by reaction of CS with lactic acid. No peak corresponding to ether group (if -OH groups of CS and of L.A. undergo cross-linking) was found, so it can be supposed that chemical cross-linking does not occur. Besides the vibrational band characteristics of the silicate (ν_{OH} of Al, Mg (OH) ~ 3635 cm^{-1}; ν_{OH} of H_2O~ 3430 and 3250 cm^{-1} is diminished due to the electrostatic interaction of polycationic CS, the bands attributed to the intercalated CS and grafted copolymers are also observed. The peaks at 897 and 1152 cm^{-1} in CS are assigned to the saccharine structures and a strong peak at 1597 cm^{-1} due to strong amino group characteristic. In rest of the samples this peak is diminished. It means that –NH group is protonated and it lost its integrity.

The peaks at 2920, 2880, 1430, 1320 and 1215 cm^{-1} attributed to the symmetric/asymmetric CH stretching vibrations of pyranose rings. The peak at 1730 cm^{-1} is due to carbonyl group vibration. A new peak is arising at 1743, and 1733 $cm^{-1,}$ corresponding to the carboxylic group of OLLA existing as freedom of side chains. An obvious shift to a lower wave number in comparison with PLLA can be observed and is attributed to the formation of H- bonds between the ester groups of OLLA and amino or –OH groups of CS. The peak at 3440 cm^{-1} appeared in CLA-5, so we may predict that in this case the biopolymer was not sufficient to cover the entire clay surface. Methanol-extracted samples could not dissolve in water, while chloroform-extracted samples free of oligomers but containing salt-bound side chains could swell in water after several days of continuous stirring.

Figure 3.3 (b) is the ^{1}H-NMR spectrum of methanol-extracted sample. The graft copolymers showed the characteristic peak of CS at δ 7.2 (s, 2H, $-NH_2$). Along with this, two peaks at δ 4.2 and 5.4 were also observed, which can be ascribed to the terminal methine protons of the branched PLA and its repeat units in the chain, respectively. The resonance of methyl protons in lactyl units arising from amide and salt linked main chains units (1.4-1.3 ppm) can be seen. The existence of peak at 1.3-1.2 ppm is due to hydroxylated lactyl units. These results indicate that the CS-g-LA copolymers contained PLA side chains.

3.4.2.2 Thermal Properties

The thermal decomposition profile exhibit two main decomposition stages, with one starting at around 100°C and another at 230°C as shown in **Figure 3.4**. The first stage may be attributed to the water evaporation. The amount of weight loss at this temperature range decreased with increasing clay content of the samples. This implies that the formation of a CS-silica complex would decrease the water absorbability of the films, i.e., decrease the hydrophilicity of the films.

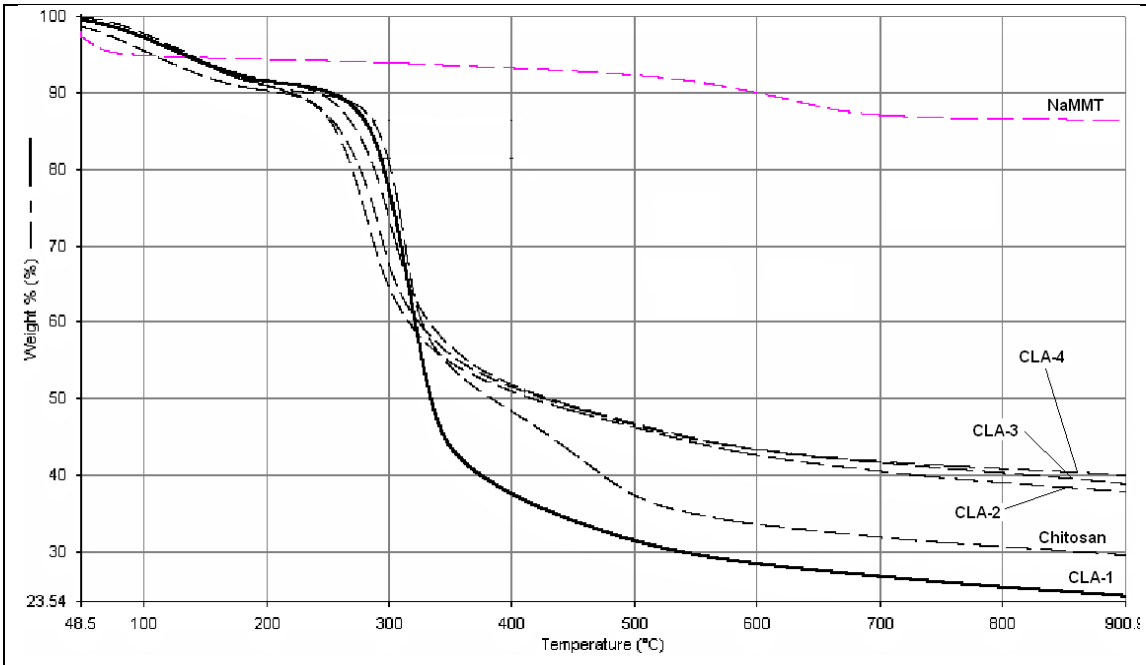

Figure 3.4 Thermograms of the prepared nanohybrids

This was also confirmed by swelling behavior in section 3.5. The second stage, where the maximum weight loss was observed at around 280-300 ˚C, can be attributed to the decomposition of the copolymers. It can be been that weight loss at higher temperature was slow / low. It may be attributed to the presence of crosslinked structure, which is formed by thermal crosslinking at first stage of decomposition. It appears that at higher temperature, the thermal degradation may result into a new cross-linked material, which occurs in the first stage of degradation. The maximum decomposition temperature was observed to be higher for nanocomposites with clay loading of 5 % and 10 % than that with 20 %. The weight loss at> 400 ˚C was not significant in the case of nanocomposites and it was attributed to the incorporation of silicate layers with high aspect ratio decomposed / charred material on the clay surface act as a carbonaceous insulators.

The silicate has an excellent barrier property that prevents permeation of various degraded gaseous products. The addition of clay enhanced the performance by acting as a superior insulator and mass transport barrier to the volatile products generated during decomposition. The clay acts as a heat barrier, which could enhance the overall thermal stability of the system, as well as assisting in the formation of char during thermal decomposition. It is important to mention here that the values of char yields were almost coincident with the amounts of the clay in nanocomposites. Therefore, the increased char ratios mainly resulted from the nonvolatile silica, and the char formation from organic part (grafted chains and CS). Similar results were also reported for other polymer-silica hybrid materials[25]. On the basis of the above result, we may conclude that silica in CS might not alter the thermal degradation mechanism of CS. In case of 20 %clay loaded composite, the incorporation of silicate layers gets more and more hindered because of geometrical constraints within the limited space remaining available in the polymer matrix and much increased thermal stability was not observed.

3.4.2.3 Water Swelling behavior.

The behavior of water absorption of CS-*g*-LA/ Na^+-MMT composites was investigated, and results were shown in **Table 3.3.** The water absorption of composite films decreases with an increase of clay with CS matrix. This is probably due to the formation of a barrier in the form of cross-linking points, which prevents water permeation into CS. Pure CS is hydrophilic, but it doesn't absorb much water. There are many –OH and –NH groups in CS, which cause strong intermolecular and intramolecular hydrogen bonds; thus the infiltration and diffusion of water, are restrained. The water absorption of lactic acid grafted CS is higher than neat CS. It can be attributed to the fact that the integrity of molecular structure is broken in grafted CS, which can expose more functional groups for water absorption. This swelling extent will depend on the osmotic pressure and charge repulsion, the degree of ionization and grafting extent also[26] which have already been demonstrated by the dependence of lactic acid grafted CS on the temperature and pH of solution. In comparison of grafted CS, samples of nanocomposites have shown lower water absorption and it decreases with increasing content of clay. It can be attributed to the interaction between layered silicates and copolymers in which intercalated polymer chains, which are more responsible for hydrophilicity, were confined into silicate galleries. Since sodium montmorillonite is hydrophilic clay, resulting composites were expected to be

hydrophilic. The reduction in water absorption may be due to the fact that the formation of nanocomposites occurred through the cation exchange between $-NH_3^+$ and Na^+ ions. Thus, water absorption to the silicate layers appears to be reduced. In other words, in a particular space (size) of composite, cationically modified silicate layers will be as immobilized phases. The increasing content of layered silicate increases the immobilized phase throughout the matrix. The interaction between the mobilized and immobilized phases has shown to reduce the water absorption[27] and have already been demonstrated by Eisenberg et. al[28] in favor of reduction of water absorption.

In addition, the composites were allowed to swell upto their equilibrium, which was reached after 25 hrs. After complete swelling, we dried the films under vacuum oven at 65°C to investigate the moisture retention capacity of the composite films. We observed that the films could hold the moisture for a long time. It shows the high water retention capacity of CS. The increasing clay loading decreases the water absorption and increases the time for drying upto constant weight i.e. they hold the moisture for longer time. It may be due to clay, which may act as a physical barrier for the moisture to exude out from the films.

3.4.2.4 Morphological Investigation

Figure 3.5 a-e shows the polar optical micrographs of the samples.

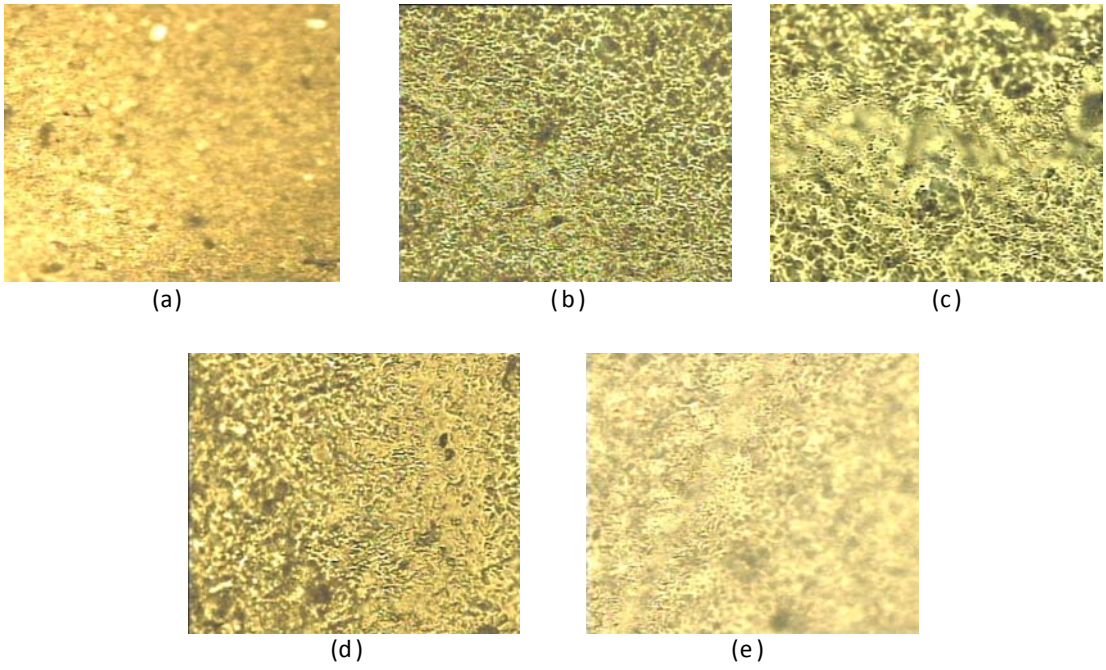

Figure 3.5 POM images of the prepared nanohybrids.

For the nanocomposites, the small bright regions were seen in the patterns which may be due to depolarization and scattering of the polarized light by the nanoclay inclusion. These bright regions were not observed in CLA-1. The micrographs of nanocomposites have shown the branched crystallite structures. As the films were casted, the solvent evaporation may impart this kind of branched structures, which were not observed in CLA-1. This might be due to that silicate layers may act as nucleating agents in cooling and during drying, solvent may evaporate slowly from inner structure. The exact mechanism of formation of branched like structures is not clear, but we can speculate that clay nanoparticles, which were homogenously dispersed, may act as nuclei in the formation of those branched like crystal structure.

3.4.2.5 Contact angle measurements

Contact angle measurement of liquid droplets on substrate surfaces are used to characterize surface wettability, surface cleanliness and the hydrophilic/ hydrophobic nature of the surface. The contact angle is defined as the angle between the substrate support surface and the tangent line at the point of contact of the liquid droplet with the substrate. The average value out of eight contact angle measurements of same specimen was calculated. The values of various samples are given in **Table 3.3,** where it can be observed that the contact angle value decreases with increasing content of clay. The standard deviation reveals the heterogeneity of the film surfaces. The water absorption and contact angle measurements have shown the hydrophilicity of the prepared nanocomposites.

Table 3.4 Results from water absorption studies and contact angle values of nanohybrids.

Sample	Water absorption (%)	Contact angle
PLA	-	75
CLA-1	486	59± 0.9
CLA-2	250	62± 1
CLA-3	225	65± 1
CLA-4	219	66± 1
CLA-5	255	66± 1
Neat Chitosan	54	58

3.5 CONCLUSION

The novel inorganic-organic hybrids were prepared from biopolymer and natural clay. The intercalation of cationic biopolymer CS into Na^+- MMT by a cationic exchange process results into nanocomposites with both interesting structural and functional properties. The grafting of lactic acid imparts the hydrophilicity and optimum swelling behavior to pristine CS. The incorporation of MMT clay affects the preparation and properties of grafted copolymers. The grafted lactic acid chains were acting as a plasticizer to give flexible films. The increasing content of clay decreases the value of water absorption and contact angle, and imparts little branched crystallite structure in the film. The swelling behavior and longer water retention properties were discussed, which could be applied in biomedical field.

3.6 REFERENCES

1. L. Lihua, and D. Shan, *J. Appl. Polym. Sci*., **91,** 274 (2004).
2. P. Jukkala, and O. Laitenin, *Arch. Orthop. Trauma. Surg*., **122,** 360 (2002).
3. O. Laitinen, and A. Sukura, *J. Biomed. Mater. Res*., **61,** 33 (2002).
4. I. Yoshido, and T. Hideto, *Macromol. Rapid Comm*., **21,** 117 (2000).
5. Y. J. Shin, H.I. Lee, M. K. Kim, W. R. Wee, J. H. Lee, J. K. Koh, and H. Y. Kim, *Curr. Eye Res*., **32,** 1 (2007).
6. L. Ding, C. Hao, Y. Xue, and H. Ju, *Biomacromol*., **8,** 1341 (2007).
7. H. Zhuang, J. P. Zheng, H. Gao, and K. De-Yao, *J. Mater. Sci. Mater. Med*., **18,** 951 (2007).
8. S. J. Ding, *Dental Mater*., (Tokyo) **25,** 706 (2006).
9. F. Lianes, C. Diaz, H. Ryan, and R. H. Marchessault, *Inter. J. Polym. Mater*., **51**, 537 (2002).
10. Y. Wu, and W. Yang, *Intern. J. Pharm*., **295,** 235 (2005).
11. Q, Xin, and A. Anders Wirsen, *J. Appl. Polym. Sci*., **74,** 3193 (1999).
12. Y. Fanglian, C. Wei, and W. Hao, *Polym*., **44,** 6435 (2003).

13. K. Tanveer, and P. Kok, *J. Pharm. Pharm. Sci*., **3,** 303 (2000).

14. F. Cui, C. He, L. Yin, F. Qian, M. He, C. Tang, and C. Yin, *Biomacromol*., **8,** 2845 (2007).

15. S. Aoyagi, H. Onishi, and Y. Machida, *Inter. J. Pharm*., **330,** 138 (2007).

16. W. Fernando and S. Kestur, *J. Colloid. Intern. Sci*., **2,** 532 (2005).

17. S. C. Tjong, *Mater. Sci Eng R: Reports*., **53,** 73 (2006).

18. R. Suprakas Sinha, and O. Masami, *Macro. Rapid. Comm*., **24,** 815 (2003).

19. F. Asira, *Adv. Chitin. Sci.,* **46,** 1 (2000).

20. M. Darder, M. Colilla, and E. Ruiz-Hitzky, *Chem. Mater*., **15,** 3774 (2003).

21. Y. Liu, L.K. Guo, L. Huang, and X.M.O. Deng, *J. Appl. Polym. Sci.,* **90,** 3150 (2003).

22. X. Qu, A. Wirsen, and A.C. Albertsson, *Polym.,* **41,** 4841 (2000).

23. I. Yamaguchi, K. Tokuchi, H. Fukuzaki, Y. Koyama, K. Takakuda, H. Monma, and J. Tanaka, *J. Biomed. Mater. Res*., **55,** 20 (2001).

24. T. Yui, K. Imada, and K. Okuyama, *Macromol*., **27,** 7601 (1994).

25. K. Takashi, and M. Alexandre, *J. Appl. Polym. Sci*., **89,** 2072 (2003).

26. P. Seong, Y. Jin, and P. Ham, *Biomater*., **22,** 323 (2000).

27. A.P. Kumar, and R.P. Singh, *J. Appl. Polym. Sci.*, **104,** 2672 (2007).

28. G. Tsagaroulos, and A. Eisenberg, *Macromol*., **28,** 6067 (1995).

B: Cell Proliferation and Controlled Drug Release Studies of Nanohybrids Based on CS-g-LA and Montmorillonite

3.2.1 INTRODUCTION

The properties such as inherent biodegradability, biocompatibility and tunable mechanical properties are essential for the scaffolds in tissue engineering applications. The scaffolds should also be durable, stress resistant, flexible, pliable and elastic with reasonable tensile properties, which could bear the stresses exerted by different parts of the body having varying contours. According to Peppas et. al.[1], the increase in flexibility of the scaffolds could improve the contact between the scaffold material and the tissue; hence it promotes the penetration of the polymeric chains into the tissue to form strong adhesion. The surface morphology and structural integrity of the scaffolds should also allow the cells to attach and proliferate. In therapeutic applications, the efficiency of a drug lies in targeting specific body parts and maintaining a desired concentration level for longer period of time. For example, Ibuprofen (Ibu), α-methyl-4-(2-methyl propyl)-benzene acetic acid, which is a non-steroidal anti-inflammatory drug (NSAID), is used for relief of rheumatoid arthritis, osteoarthritis and moderate pain. However, its use is limited due to side effects of gastrointestinal tract, central nervous system, and other ulcerogenic effects, which are often consequences of high plasma levels following the administration of conventional formulations[2].

By designing controlled delivery systems, the desired concentration of the drug can be maintained without reaching a higher toxic level or dropping below the minimum effective level. For this purpose, the interaction between drug and lamellar host has been considered. The idea is to store the drug in the interlayer region of the lamellar host and allow the drug release as a consequence of diffusion and / or de-intercalation process. The montmorillonite (MMT), clay is composed of thin silicate-layers, which are parallelly stacked by rather weak interactions such as van der Walls force and H-bonding. MMT exhibits enhanced gel strength, mucoadhesive capability to cross the gastrointestinal (GI) barrier; adsorb bacterial toxins, and metabolic toxins such as steroidal metabolites. Because of these advantages in bio-medical applications, it has taken the credit to be called as medical clay[3]. In addition, of particular relevance, the drug (Ibu), which is cationic in nature, can also facilitate drug loading into interlayer region of MMT and assist to achieve adequate sustained release property[4].

Though CS has the ability to form films, the tensile properties of pristine CS film are poor (due to its crystallinity). Thus, the modification (chemical modification, blending and graft copolymerization) of CS has gained its importance for tailoring the desired mechanical properties[5-7]. Since CS is alkaline in nature, by combining it (as

graft copolymer or blend) with the biodegradable polymers like polylactic acid, which generate acidic by-products, the local toxicity at the implant site can be reduced[8-10]. In the present study, we investigate the effect of MMT on physical properties, such as the microstructures, swelling behavior, cell growth, and drug-release behavior of the prepared CS-g-LA/MMT hybrids.

When the low concentration of the drug solution is added to the CSI-MMT suspension, the pH of the clay surface would be relatively low (~5.5) and hence the strongly electronegative surface has a high binding affinity for the cationic drug. As more added drug locates in proximity to the phyllosilicate surface, the accumulation of the acidic drug causes the microenvironment around the mineral to become increasingly acidic, altering the ionization of the siloxane groups, thereby reducing the overall negative charge and hence sites available for drug binding. A second phase could arise due to a build-up of a second adsorbed layer due to hydrophilic adsorption of unionized drug (approximately 50%, as the pKa of drug is 5.5) to itself or to hydrophobic binding sites on the phyllosilicate surface. Greater protonation of free amino groups at low pH causes CS molecules in films to uncoil, elongate and become more permeable.

3.2.2 EXPERIMENTAL

3.2.2.1 Materials

CS of low molecular weight (M_v $1.5x10^5$, degree of deacetylation: 85%) was obtained from Aldrich. L-Lactic acid (purity 92%) was purchased from M/s Spectrochem and used as such for graft copolymerization. Ibuprofen (Ibu) was purchased from Aldrich. Sodium montmorillonite, with cation exchange capacity (CEC) of 76.4-meqv/100 g was received from M/s. Southern Clay Inc. USA.

3.2.2.2 Preparation of nanohybrids and drug loading

It involves aqueous dispersion of clay, suspension of CS in L-lactic acid, mixing them, drying and dehydration. First, the suspension of CS was added into aqueous dispersion of clay, heated up to 60 °C with continuous degassing for 40–45 minutes.

This solution was casted and dried for 8 h at 60 °C under air and subsequently at 60 °C in vacuum oven for 8 h to obtain films. For obtaining porous scaffolds, the solution of

CS-g-LA/MMT was freeze-dried at -56 °C using 9 well tissue culture plates. The dimensions of obtained cylindrical scaffolds are about 20 x 20 mm. The drug-loaded CS and CS-g-LA/MMT nanohybrid films and porous scaffolds were prepared by following above-mentioned procedure. The dispersion of Ibuprofen (0.1 g), in the reaction mixture was done just after degassing and cooling.

Table 3.2.1: Formulations of ibuprofen loaded nanohybrids of chitosan-g-lactic acid and sodium montmorillonite.

S. No.	Chitosan (g)	Lactic acid (ml)	MMT (g)	Ibu (%)	Drying process	Sample code
1.	1	1	-	-	Vacuum	NTCS *
2.	1	1	-	-	Vacuum	CL
3.	1	1	0.05	-	Vacuum	CLM
4.	1	1	-	10	Vacuum	CLI
5.	1	1	0.05	10	Vacuum	CLMI-1
6.	1	1	0.10	10	Vacuum	CLMI-2
7.	1	1	0.05	-	Freeze	FCLM
8.	1	1	-	10	Freeze	FCLI
9.	1	1	0.05	10	Freeze	FCLMI-1
10.	1	1	0.10	10	Freeze	FCLMI-2

* NTCS is neat CS without grafting.

After 24 h of stirring, the Ibu-loaded solution was casted to obtain films and freeze dried to obtain porous scaffolds. The formulations are given in **Table 3.2.1.**

3.2.3 CHARACTERIZATION

3.2.3.1 X-Ray Diffraction

The Wide Angle X-ray Diffractometer patterns of the samples were obtained by Rigaku (Japan) X-Ray diffractometer with Cu-Kα radiation at 50 kV between the scan ranges of 2θ from 2-30 degree by the scan rate of 2 degree/min. The d- spacing was calculated by Bragg's formula where the λ was 0.154nm.

3.2.3.2 FT-IR Spectroscopy

The Fourier-transform infrared (FTIR) spectra were obtained from the sample under attenuated total reflectance (ATR) mode on a Perkin-Elmer Spectrum GX.

3.2.3.4 Microscopic Analysis

Surface morphology was investigated by scanning electron microscopy (SEM) (Model: JEOL Stereoscan 440, Cambridge). AFM of pristine CS film and drug loaded nanohybrid film samples were done on a Nanoscope IV AFM instrument under contact mode.

3.2.4 Swelling behavior

3.2.4.1 Water Absorption behavior (films)

The water absorption behavior of the film samples were followed according to ASTM D570. The clean, dried film samples of known weights were immersed in distilled water at 25°C for one day (24 h). The films were removed, blotted quickly with absorbent paper and then weighed. The absorption percentage of these samples was calculated using the equation $X\ (\%) = (W_1-W_0) / W_0$, where W_0 and W_1 are the weight of dry and swollen samples, respectively.

3.2.4.2 Shape retention study (scaffolds)

The swelling behavior of the porous scaffolds was investigated by exposing them to media of different pH: 1N HCl, 1N NaOH, and simulated body fluid (SBF) (pH 7.4) solutions. The shape retention was quantified by measuring the changes in diameter as a function of immersion time in the media. Three specimens were measured for each sample and the values are averaged.

3.2.5 Tensile properties

For tensile properties measurement, the nanocomposites were cut in the size of 1 cm x 6cm specimens. Both ends of tensile specimens were clipped with a special gripper. The tensile strength and modulus of the scaffolds were measured by a Universal Testing Machine (Instron 4204) with a load cell of 1kN and the crosshead speed was 5 mm min^{-1} at room temperature. Average value out of five measurements is reported for each sample.

3.2.6 Cell growth study

The cell growth study was performed on HL-60 Leukemia Cell Line as a direct contact test. The relative cell growth compared to control cells containing cell culture medium without CS was calculated by $[A]_{test}/[A]_{control}$. For this, after every 24 h, 100 μl of the cell culture was incubated for MTT assay and the absorbance was measured at 490 nm wavelength in Spectrophotometer Plate Reader. Pristine CS was used as a positive control of the method. All the in-vitro tests were done in triplicate and the results were reported as an average value.

3.2.7 In-Vitro drug–release

The drug-loaded films and scaffolds were immersed in 40 ml aliquots of 0.1 M sodium phosphate buffer (pH 7.4) and incubated on a constant temperature shaking bed at 37 ˚C with continuous stirring. After specific intervals 3 ml aliquot of samples were withdrawn and immediately replaced with the same amount of fresh medium. The '*Ibu*' content in the aliquot was quantitatively analyzed by UV-VIS spectrophotometer at 292 nm. The aliquot from the pristine CS film was taken as the control (100%). All the experiments were done in triplicate and mean values were reported.

3.2.8 Thermal Studies

Differential scanning Calorimetry (DSC) curves of the pristine CS and drug loaded nanohybrid samples were recorded using a DSC Q10 (TA Instrument). The analysis was performed by heating the samples in a temperature range of -60 °C to 400 °C at the rate of 10 °C per minute under inert atmosphere.

3.3 RESULTS AND DISCUSSION

3.3.1 CHARACTERIZATION

Figure 3.2.1 (a) shows the WAXD pattern of MMT and CS-g-LA/MMT confirming the formation of nanocomposites. The increase in d-spacing (001 plane) of MMT implies the intercalation of grafted chitosan biopolymer chains into silicate galleries. **Figure 3.2.1 (b)** shows the FT-IR spectra of CS-g-LA/MMT and Ibu-loaded nanohybrids. With respect to pristine CS, the characteristics absorption band at 3420 cm^{-1} was attributed to the stretching vibration of the N-H group bonded to the O-H

groups; bands at 1599 cm^{-1} and 1260 cm^{-1} were attributed to the bending vibrations of the N-H and the O-H groups, respectively.

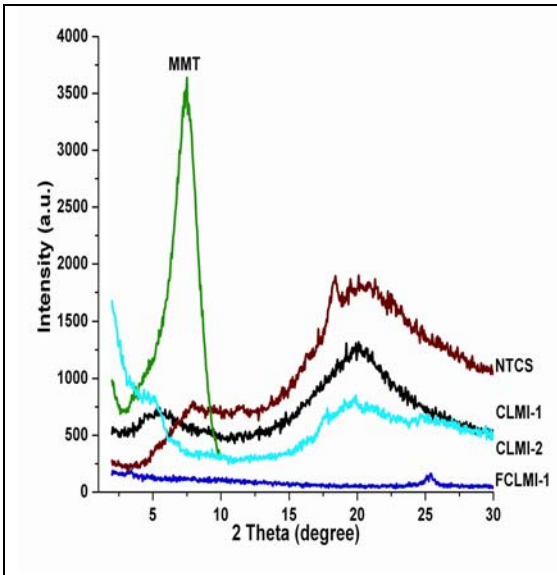

Figure 3.2.1 (a) WAXD pattern of prepared nanohybrid samples

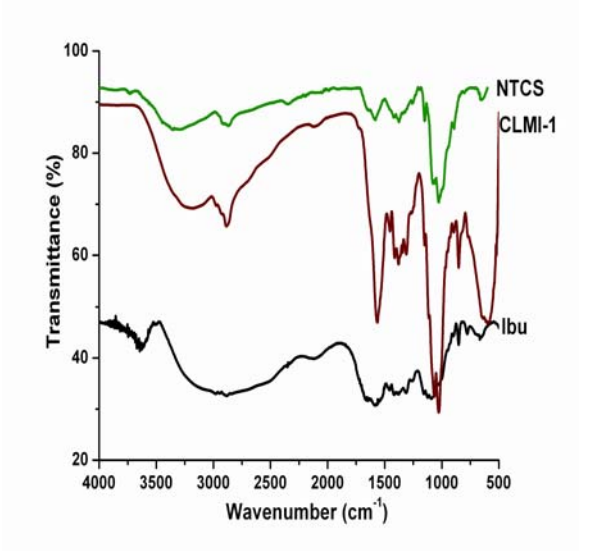

(b) FTIR spectra of CS, Ibuprofen, and Ibuprofen loaded nanohybrids

It can be observed that for the drug-loaded sample, the absorption band at 3420 cm^{-1} become wider indicating the enhanced H bonding. The bands 1098 cm^{-1} and 665 cm^{-1} of NTCS are responsible for crystalline CS. The disappearance of these peaks in neat and drug-loaded nanohybrids demonstrated the disturbed crystallization of CS after grafting and incorporation of clay and ibuprofen. This observation was further confirmed by XRD analysis. The IR spectra of the CLMI-1 show most of the characteristic bands of Ibu. The appearance of new bands at 1588 cm^{-1} (asymmetric stretch of COO-) and 1398 cm^{-1} (symmetric stretch of COO-) clearly indicate the presence of Ibu within the galleries. The band at 1690 cm^{-1} in the spectra of Ibu, due to the asymmetric stretch of the undissociated –COOH, is absent in the intercalated material. The methyl symmetric and asymmetric stretching modes at 2954 cm^{-1} and 2886 cm^{-1} in the CLMI-1 are well resolved, and their positions show no significant difference from those of pristine Ibu, other than the shifting of $–CH_3$ bending mode from 1462 cm^{-1} to 1466 cm^{-1} upon intercalation. The characteristic M-OH layer stretching bands at around 427 cm^{-1} and 620 cm^{-1} are distinct in the intercalated hybrid indicating that the interlayer structure of MMT is unaffected upon intercalation of Ibu. The FT-IR spectra confirm that the integrity of the Ibu anion is preserved upon intercalation with the MMT interlayer

galleries with a structure and geometry similar to that of the molecule outside the layers.

3.3.2 MORPHOLOGICAL ASPECTS

As shown in the AFM image, the drug loaded CS-g-LA/MMT film samples was found to be spherical in shape and their size was around 300 nm (**Figure 3.2.2 a-b**).

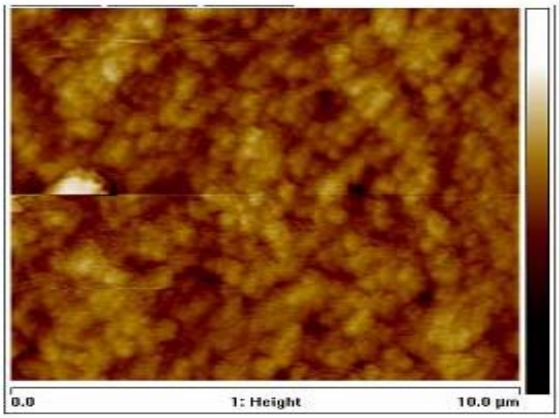

Figure 3.2.2 (a) AFM image of pristine CS

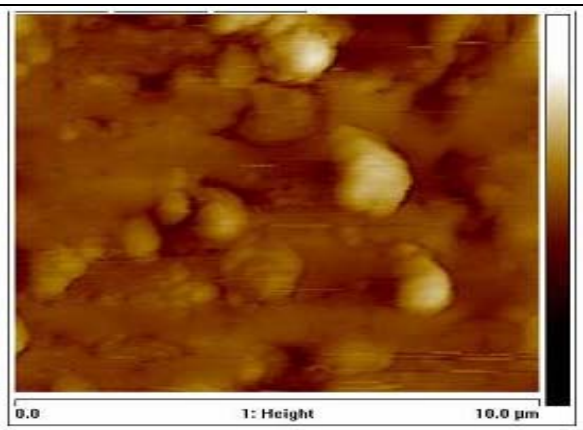

(b) AFM image of CSD-1

Figure 3.2.3 shows the typical surface morphology of the top, middle and bottom portions of the scaffolds of drug-loaded and pristine CS-g-lactic acid. The interconnected porous morphology resulted from phase separation between *polymer-poor* and *polymer-rich* phases. The *polymer-poor* phase is of mostly solvent i.e. water. The water molecules were removed by freezing and subsequent sublimation of ice crystals, which leads to the formation of pores. On the other hand, the polymer-rich phase consists of mostly the polymer solution and forms the cell walls around the pores[11]. The dimensions of cylindrical well in tissue culture plates used are about ~20 mm thick and 20 mm in diameter.

When a polymeric solution was exposed in such dimension (cylindrical & thick) to a quenching medium, a temperature gradient along the solution could be induced resulting in the difference in quenching rate. For instance, during quenching, the bottom layer was exposed to the interface of solution and freezer where the cooling rate is relatively fast. At such a rapid rate of cooling, many ice-crystal nuclei could be formed and they might not have enough time to grow because of extracted heat of crystallization. As a result, the surface of bottom portion of the scaffolds has the small

and interconnected pores. The top surface of solution, on the other hand, was exposed to the interface of the solution and vacuum where rate of quenching is comparatively slow because of temperature gradient. In such a slow rate, *ice-crystal nuclei* may have enough time to grow resulting in large and well-interconnected pores.

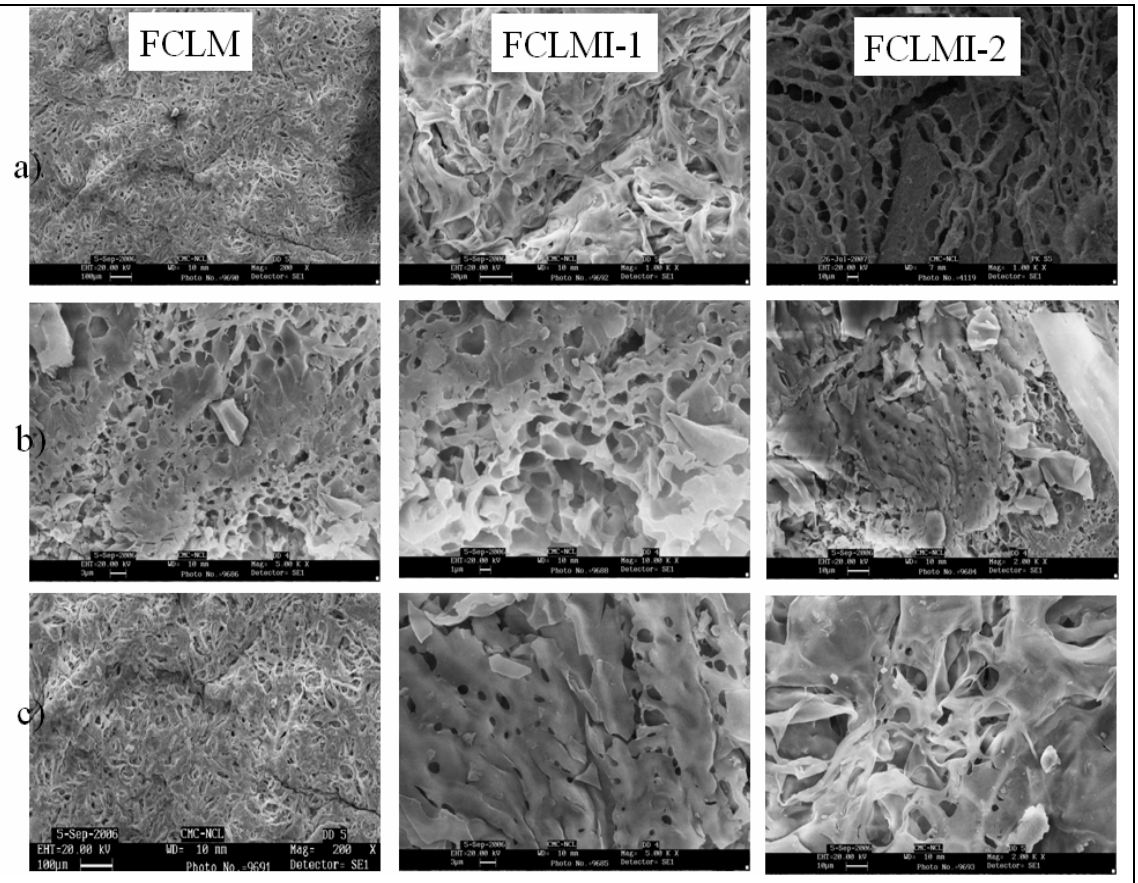

Figure 3.2.3: Scanning electron micrographs of a) top, b) middle and c) bottom portions of freeze dried porous scaffolds.

However, the quenching rate at the middle part of the solution will be different from both top and bottom portion. Thus, the *ice-crystal nuclei* can have relatively enough time to grow and the crystal growth would be directed by temperature gradient. This is confirmed by elongated pore morphology in midsection of the obtained scaffolds. In addition, the ratio between CS matrix and lactic acid monomer kept constant with varied clay content and drug. According to Prabaharan et al[12], by varying ratio of CS / PLA - blend, the pore interconnectivity of the scaffolds was not apparently affected and the framework structure of the obtained scaffolds was typically maintained. However, CS concentration has a significant effect on the pore structure. With increasing CS

concentration, the volume of the PLA pores is occupied by a low density and highly hydrated CS. This results in highly porous CS network, which facilitates the diffusion of nutrients for cells and release of wastes. Hence, we infer that pore structure can be manipulated by varying the ratio of lactic acid and chitosan without affecting the interconnectivity.

3.3.3 SWELLING BEHAVIOR

3.3.3.1 WATER ABSORPTION BEHAVIOR (FILMS)

The water absorption values of the prepared samples have shown that the grafting of lactic acid onto CS increased the water absorption significantly. It was attributed to the fact that the integrity of molecular structure is broken in grafted CS, which can expose more functional groups for water absorption. The MMT incorporated nanohybrids have shown lower water absorption and it decreases with increasing content of clay. In nanohybrids, the polymer chains, which are more responsible for hydrophilicity, are confined into silicate galleries. Though the sodium montmorillonite is hydrophilic, the resulted nanocomposites have exhibited resistance towards water absorption. It was explained that in nanolayers incorporated system, the cationically modified silicate layer will be as immobilized phase, which reduces the inclusion of water. The increasing content of layered silicate increases the immobilized phase throughout the matrix[13]. It was also observed that the drying of swollen nanohybrid films taken longer time for drying upto a constant weight indicating that the films can hold the moisture for longer time.

It may be due to clay, which may act as a physical barrier for the moisture to exude out from the films. This water retention behavior is favorable for cell adhesion. In tissue engineering applications, during the course of cell proliferation, the retained hydrophilicity of the scaffold would enhance cell attachment and proliferation on its surface. It is purported that the hydrophilicity can be varied by playing with grafting extent (*which renders hydrophilicity*) and clay incorporation (*which reduces water absorption and rate of desorption*).

3.3.3.2 SHAPE RETENTION BEHAVIOR (SCAFFOLDS)

Swelling behavior and structural stability of scaffolds, which strongly depend on the pH of the implantation site, are critical for their practical use in tissue engineering. Most natural polymers, including CS, swell readily in biological fluids. The *in-vitro* cell culture studies[14] indicate that initial swelling is desirable and the increase in pore size facilitates cell attachment and growth in a three-dimensional fashion. However, continuous swelling would lead to loss of mechanical integrity and generation of compressive stress to surrounding tissue. The scaffolds were subjected to various pH solutions such as SBF (pH: 7.4), HCl (pH: 1.2) and NaOH (pH: 14) for 2 weeks. **Figure 3.2.4** shows the shape retention in terms of diameter (mm) of scaffold versus time (h).

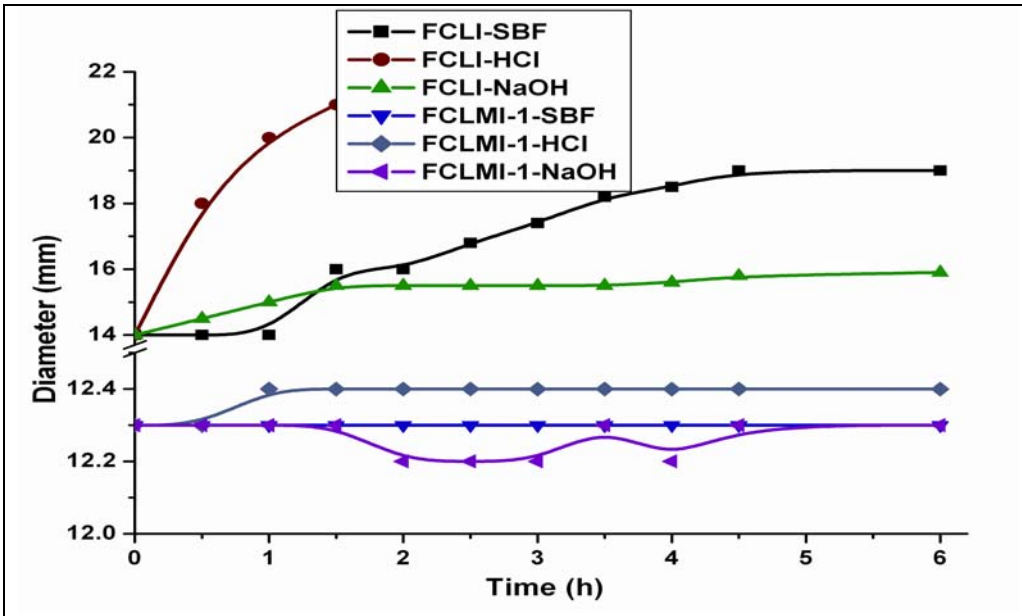

Figure 3.2.4: Shape retention of scaffolds prepared from chitosan and nanohybrids of CS-g-LA/MMT

It can be observed that the shape of the scaffolds of 'FCLI' is disturbed by fluids with increasing time of immersion. It is a general observation that in an acidic pH, the swelling of the scaffolds is higher than that in SBF and alkaline solution. The scaffold 'FCLI' was found to dissolve completely in HCl solution within 2 hours of immersion, whereas, in SBF solution, FCLI was swollen over time with its diameter increasing by ~20% within 2 h and thereafter underwent a minor swelling at a significantly reduced rate reaching the plateau level at 5 h. The rate of swelling in NaOH was very low (diameter increase <5%) and reached the plateau level around 1.5 h of immersion but retained its overall size thereafter for several weeks. Thus, the CS scaffold was stable

only in solutions of physiological and / or higher pH. On the other hand, MMT incorporated scaffold appeared to retain its overall size and cylindrical shape. The swelling behavior was almost same in all three solutions. Even in acidic solution, a slight swelling was observed initially (within 1 hour) and the scaffold retained its overall size through the period of study. This suggests that the CS-*g*-LA/MMT scaffold is stable regardless of the pH value of the solution over the time. The swelling of pristine CS generally involve the protonation of amino/imine groups and the mechanical relaxation of coiled CS chains[15, 16]. In case of CS-*g*-LA, some amino groups might be converted as graft-point and remaining amino groups could interact with carboxyl groups of PLA side chains, preventing the protonation. Further, in nanohybrids, these biopolymeric chains are intercalated in between silicate layers. As mentioned earlier, absorption and desorption of fluids will be slower in system which contains immobilized phases (MMT). Owing to their mucoadhesive properties[3], the MMT incorporated nanohybrids can retain the stability of the scaffolds.

3.4 TENSILE PROPERTIES

The scaffolds / implants based on polymeric materials should be resistant towards the stresses exerted by different parts of the body. The tensile properties of film specimen of nanohybrids were measured and their results were represented in **Figure 3.2.5 a-b**. Figure-a shows the tensile modulus and ultimate tensile strength of the film specimen of nanohybrids. The tensile modulus, which denotes the stiffness of the material, was observed to increase drastically in clay loaded samples.

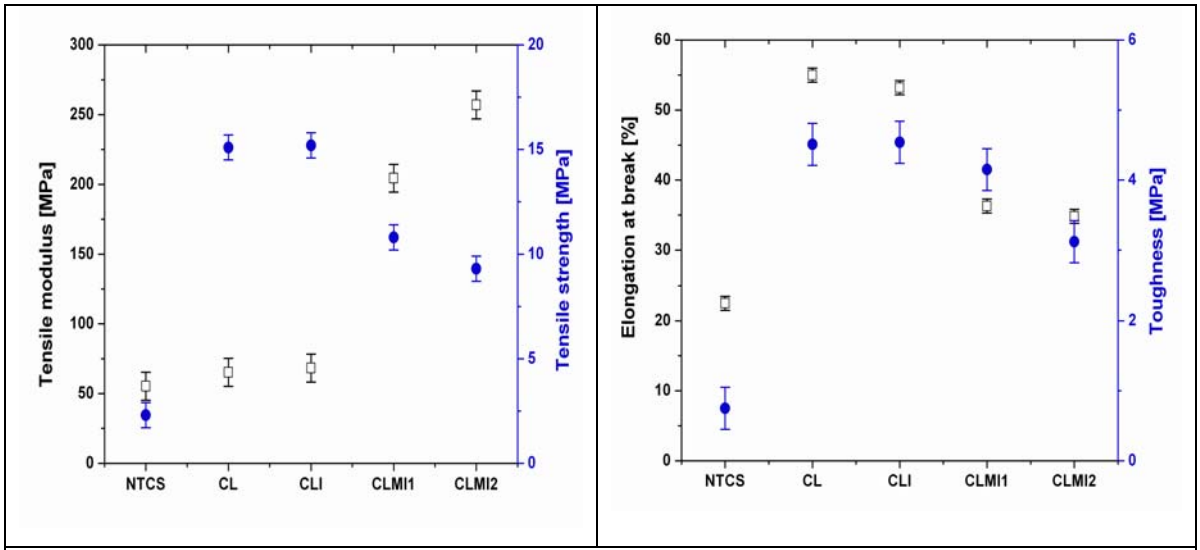

Figure 3.2.5: Tensile properties a) tensile modulus (□), tensile strength (●), b) elongation at break (□) and toughness (●) of prepared samples

It is found that the grafting of lactic acid and incorporation of 5 % MMT have exhibited 269 % improvement in tensile modulus. The 364 % increase was observed for 10% MMT incorporated nanohybrids. The effect of grafting can also be seen in tensile strength, which is stress value noted at break point. About 556 % increase in tensile strength was observed after lactic acid grafting. This may be due to the fact that the molecular integrity of CS matrix has been lost during grafting of lactic acid. Since PLA grafted copolymers consisted of hydrophilic CS main chains and hydrophobic PLA side chains, it is reasonable to believe that PLA side chains could turn inward and aggregate together while the CS chains stretched outward during the film formation by virtue of acidic aqueous solution. As a result, many hydrophobic domains constructed by the PLA side chains would exist inside the films, and possibly act as physically cross-linked sites, which would enhance the tensile strength and modulus of grafted copolymer films. The grafted polylactic acid chains can absorb the applied energy, so as to improve the tensile strength with deformation. The MMT reinforcement has shown slight decrease in tensile strength from the grafted CS. **Figure 3.2.5 b** shows the elongation at break and toughness of the corresponding specimen. The significant effect (144% improvement) of grafting can be found in Figure-b as an increase in elongation (%) values at break, which is directly related to flexibility and toughness of the materials.

The lower value for NTCS is observed due to the restricted mobility of macromolecular chains. On the other hand, in the grafted CS, the linear / low molecular weight polylactic acid chains can act as plasticizer which can improve the mobility of polymer chains. It is also known that during tensile test[17, 18], linear polymers undergo craze failure mechanism and composites/cross linked polymers undergo the crack failure mechanism. Thus we assume that the grafted chains merely act as linear chains to undergo craze mechanism, which involves uncoiling, stretching and slippage of polymeric chains. By this failure mechanism, the applied energy will be utilized for deformation. This phenomenon is confirmed by an increase (about 500%) in toughness of the grafted CS (CL). The effect of reinforcement of clay has resulted in decrease in both elongation and toughness values. The prepared nanocomposites are intercalated ones. In such a system, the polymeric chains are uncoiled and sandwiched in between the silicate layers and are restricted to undergo / follow the craze failure mechanism[19]. However, the prepared materials have shown overall improvement in tensile properties after grafting and nanoscale reinforcement. The porous scaffolds may also exhibit the

same trend in properties. However, the modulus may be adjusted by changing the pore morphology, the extent of porosity, and intercalation / exfoliation of nanoclay.

3.5 CELL GROWTH

The cell-viability, which was measured by MTT assay of fibroblasts cultures on the CLMI-1 specimen, is shown in **Figure 3.2.6**. The growth of fibroblasts cultured on films (at 250μg/ml) is higher on first day, while, it decreases with increasing time. It may be due to that during proliferation, cells may have occupied all the available spaces on the films. Earlier, Yao et.al[20] reported that the fibroblasts growth rate on the film of CS-*g*-LA graft copolymer was faster than on CS. The results in the present study imply that the cell proliferation is not affected by the incorporation of MMT into lactic acid grafted chitosan.

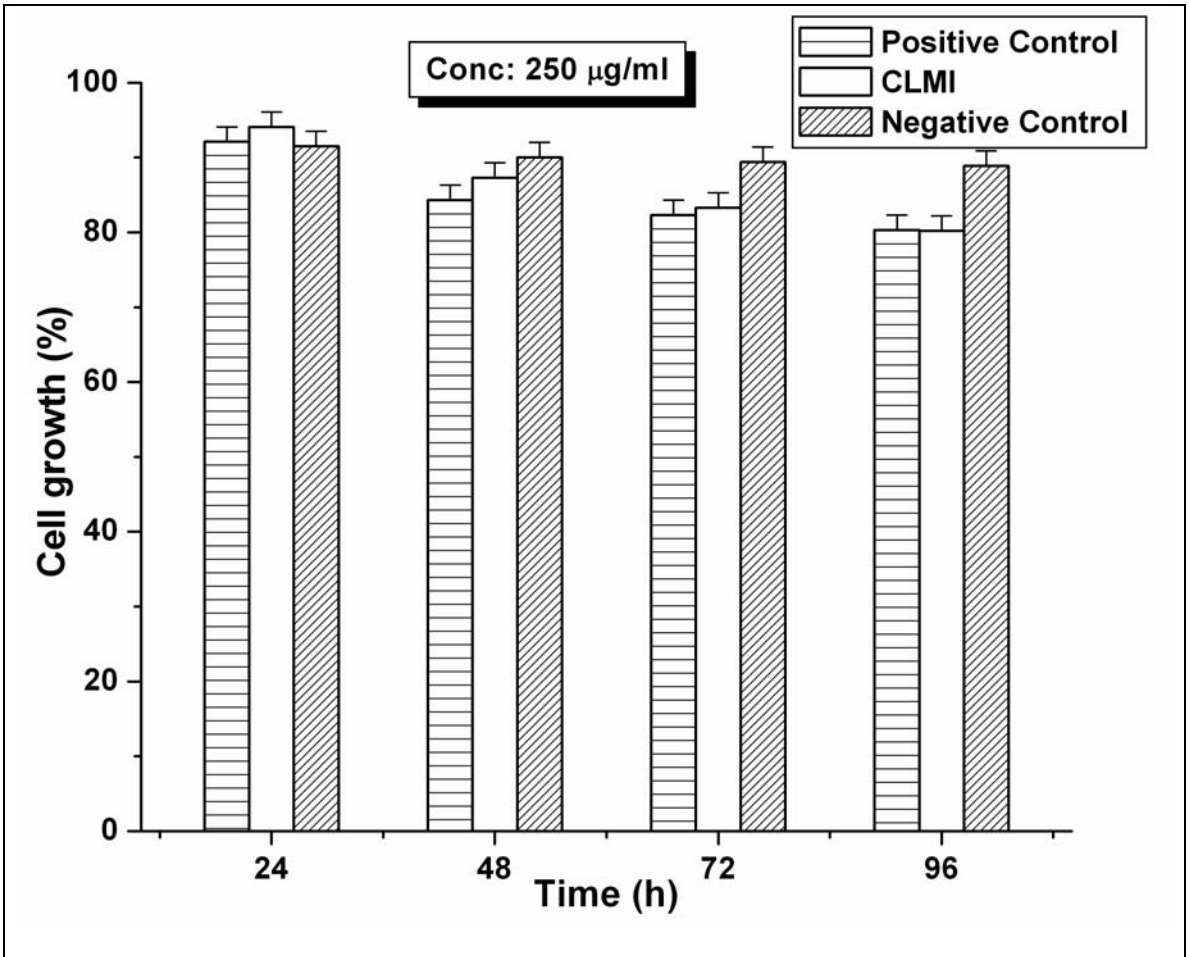

Figure 3.2.6: Cell proliferation (%) of CLMI-1

This may be due to the enhanced interactions between MMT and growing cells on the biopolymer matrix. According to Lavie et.al.[21], MMT may develop London-van der Walls forces and hydrogen bonding with cells. In nanohybrids, the grafted (CS-*g*-LA) copolymer would be surrounded and / or adsorbed onto MMT layers. These layers can act as adhesive between the biopolymer and the cells through hydrogen bonding between the hydroxyl groups of CS and the water of hydration on MMT.

3.6. IN-VITRO DRUG RELEASE

In-vitro drug release was studied under simulated body fluid (SBF, pH 7.4), and release media was quantified by UV-VIS spectral absorbance values. **Figure 3.2.7** shows the release (%) of Ibu versus immersion time from both film and porous scaffolds of nanohybrids. The release of drug from freeze-dried scaffolds can be observed to be faster and higher than that from the smooth films over the time.

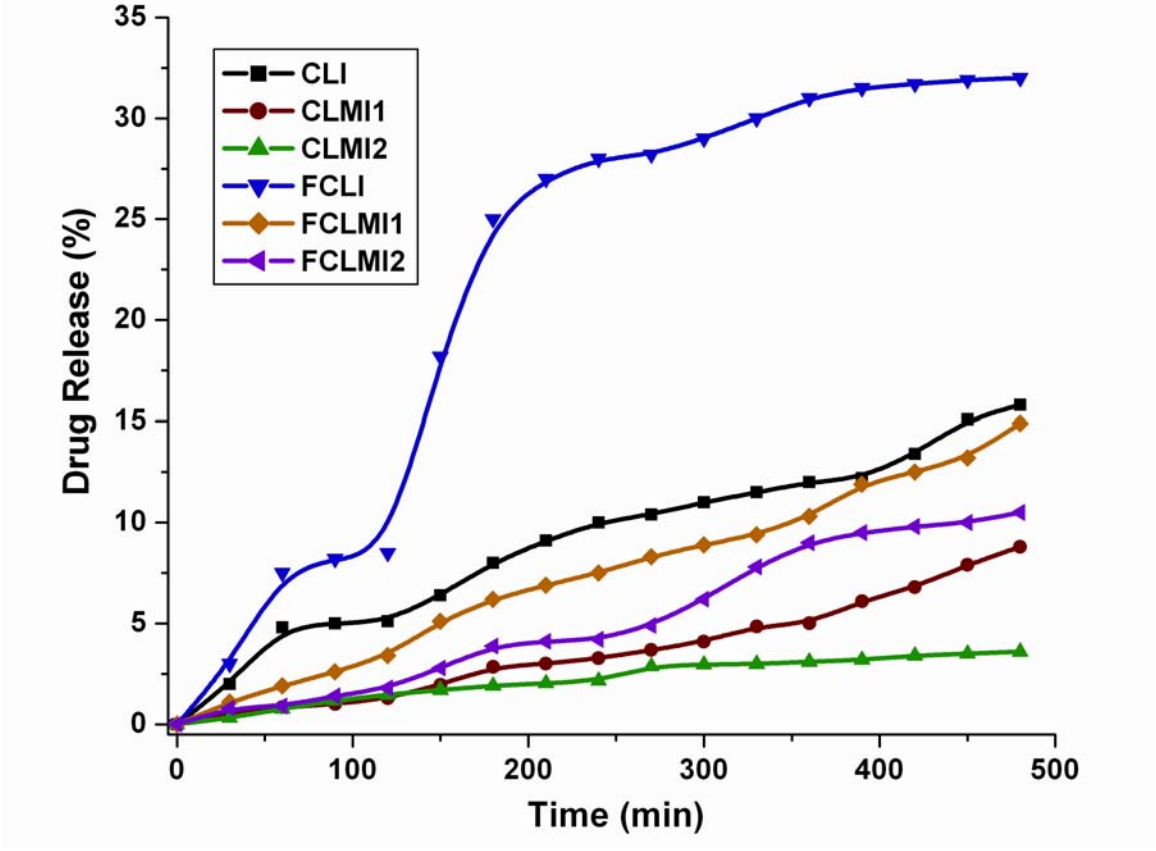

Figure 3.2.7: Ibuprofen release profile from the prepared samples

Among all the samples, FCLI has shown higher drug release rate. The higher release rate of porous scaffolds can be attributed to the fact that the inclusion of solvent and

diffusion of drug molecules will be rapid in porous scaffolds than in film samples. This result is consistent with the swelling behavior (Figure 3.2.8). The effect of incorporation of MMT layers can be significantly observed as reduced rate of release at initial stage of immersion (up to 150 min). Initially, the specimen is solvated, which facilitates the lateral diffusion of drugs[22]. After 200 min, the rate of release is moderate and sustained over the time. This may be due to the interactions of MMT layers and grafted PLA chains with the drug loaded as shown in Scheme 3.2.1. Clay minerals have a large surface area and the ability to incorporate various substances in nano-pores based on their organized structures to form organo-clay composites. This structure undergoes interactions having guest compounds with various types of bindings, such as electrostatic interactions and H-bonding [26]. When Ibu is dispersed in water with MT, although the individual silicate layers are separated from each other, Ibu is still in contact with the clay surface in an amorphous state, due to the high affinity between Ibu molecules and the MMT adsorption sites. The interaction between the sodium salt of Ibuprofen (*because of its cationic nature*) and MMT surface is stable enough to exhibit the sustained release profile.

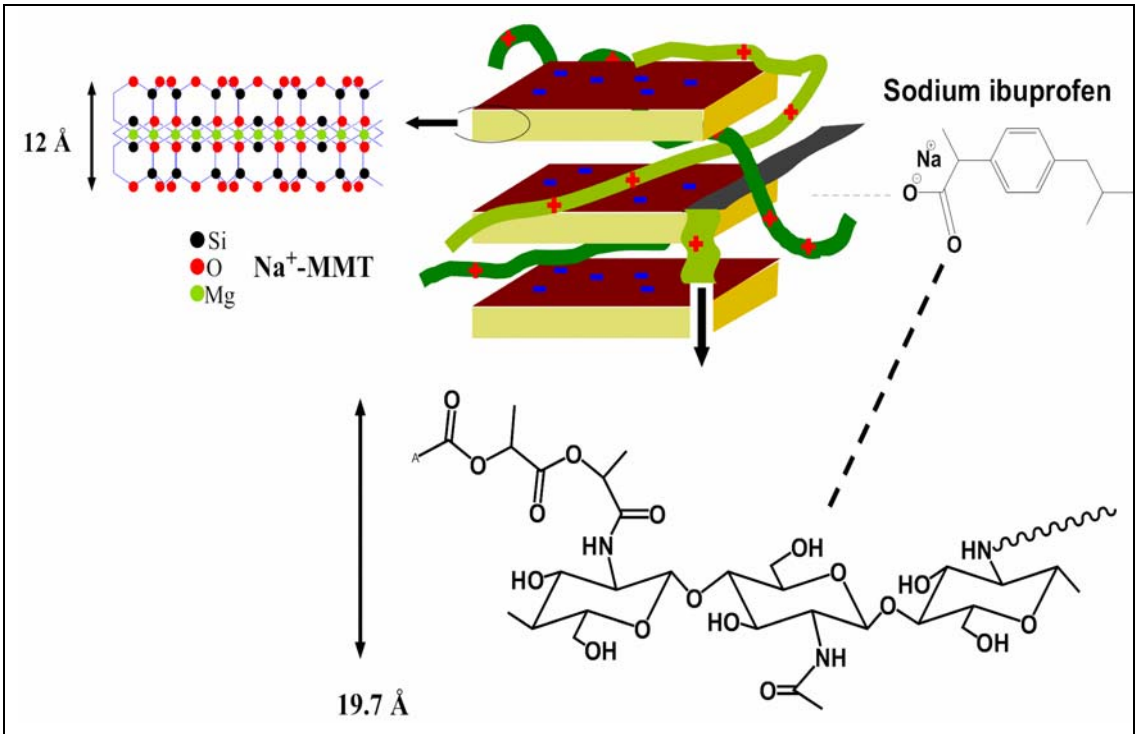

Scheme 3.2.1: Schematic illustration of interactions between, chitosan-g-lactic acid, Ibu and layered silicates

These results showed that CS-g-LA/MMT scaffold could be suitable for sustained drug release in tissue engineering applications. From the present study, we observed that by grafting biodegradable polymeric chains on CS and incorporating layered nanostructures, the desired properties such as physical, mechanical and swelling behavior can be tailored. In addition, the inclusion of nanolayers like MMT into biopolymers may be used for the sustained delivery of drug and other bioactive molecules such as vitamins, proteins and DNA, in tissue engineering applications[23].

3.7 Thermal Studies:

Thermal analysis was used to examine whether the nature of materials changed during the quenching process. The second DSC scan was used to report the glass transition temperature (Tg) of the CS powder and CS-g-LA/ Na^+-MMT. **Figure 3.2.8** shows that the glass transition temperatures of pristine CS film and various CS/MMT samples were all about the same, which demonstrated that the CS/MMT structure was not changed during the fabrication process.

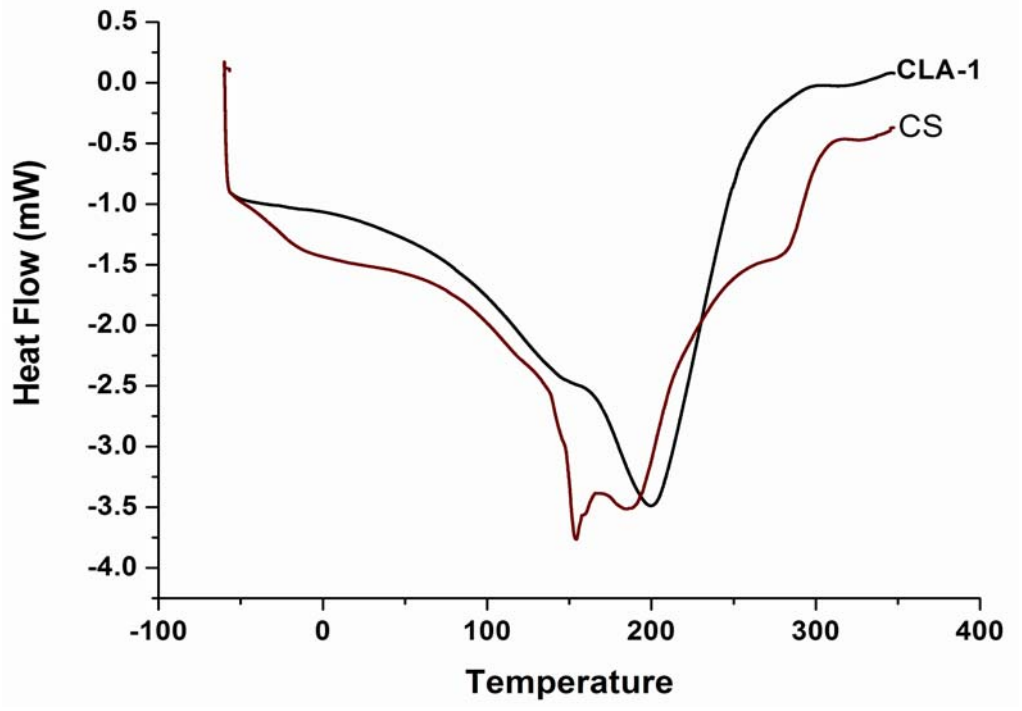

Figure 3.2.8 DSC results of CS and drug loaded nanohybrid sample.

The fabrication technique described here has some advantages over other techniques. One advantage is that it uses water only to dissolve CS; therefore, there is no residual organic solvent to be concerned about. A second advantage is that unlike in the particulate leaching technique[24, 25], which exposes the scaffold materials to high temperatures; here the porous structure was developed simply by removing the ice crystals through sublimation. These advantages protect the transplanted cells and nearby tissue from damage and any biologically active factors incorporated into the scaffold that may remain active[26-28]. Thus the present process might be a promising approach for fabricating scaffolds suitable for tissue engineering applications.

This quenching process begins with a container of CS solution either placed inside a freezer at a desired setting temperature or dipped directly into liquid nitrogen. When the temperature of the solution is lowered, the water is super-cooled to well below its freezing point, and ice-crystals start to from, which releases the heat of crystallization and warms the water above its melting point. As a result, a mixture of water and ice-crystals is formed. At the final stage of sample preparation, the frozen material is dried under vacuum at low temperature by sublimation of the ice-crystals to develop the pore structure. Therefore, the pore size of the scaffolds is controlled by the size of crystals formed in the freezing process.

3.8 CONCLUSION

The present study was to examine the potential uses of nanohybrids based on CS-g-lactic acid and montmorillonite as biomaterial. The nanohybrids, which are successfully prepared by vacuum drying and freeze-drying, have exhibited different morphologies such as smooth films and porous scaffolds, respectively. The porous morphology was obtained by phase separation. The water absorption was found to increase by grafting of lactic acid and to decrease with increasing content of clay. The scaffolds of nanohybrids are stable regardless of the pH value of the solution over the time. The reinforcing effect of clay and grafting were found to increase the tensile modulus, flexibility and strength. The significant difference in drug release from the smooth films and porous scaffolds was observed. The porous scaffolds have shown higher and faster drug release. The incorporation of MMT layers was observed to control the initial release of drug. We summarize that a combination of grafting of

biodegradable polymeric chains and clay reinforcement can be applied to achieve desired combination of properties (mechanical, swelling and controlled release) of materials used for biomedical applications.

3.9 REFERENCES

1. N.A. Peppas, and S.R. Lustig, *Ann. of the New York Acad. of Sci.*, **446,** 26 (1985).
2. H. Suleyman, B. Demircan, and Y. Karagoz, *Pharmocol. Res*., **59,** 247 (2007).
3. Y. Dong, and S.S. Feng, *Biomater*., **26,** 6068 (2005).
4. J.P. Zheng, L. Luan, H.Y. Wang, L.F. Xi, and K.D. Yao, *Appl. Clay Sci*., **36,** 297 (2007).
5. Y. Nakano, Y. Bin, M. Bando, T. Nakashima, T. Okuno, H. kurosu, and M. Matsuo, *Macromol. Symp*., **258,** 63 (2007).
6. A. S. Rowlands, J. E. Hudson, and J. J. Cooper-White, *Expert Rev. of Med. Dev*., **4,** 709 (2007).
7. P. Kolhe, and R. M. Kannan, *Biomacromol.,* **4,** 173 (2003).
8. Q. Xin, and A. Anders Wirsen, *J. Appl. Polym. Sci*., **74,** 3193 (1999).
9. K.Y. Lee, W.S. Ha, and W.H. Park, *Biomater*., **16,** 1211 (1995).
10. S. Miyazaki and H. Yamaguchi, *Acta. Pharm. Nord*., **2,** 401 (1990).
11. R.L. Hong, and J.Y. Yu *J. Biomed. Mater: Appl. Biomater*., **71B,** 52 (2004).
12. M. Prabaharan, M.A. Rodriguez-Perez, J.A. De Saja, and J.F. Mano,. *J. Biomed. Mater. Res. Appl. Biomater.*, **81,** 427 (2007).
13. G. Tsagaroulos, and A. Eisenberg, *Macromol*., **28,** 6067 (1995).
14. N. Shanmugasundram, P. Ravichandaran, P.N. Reddy, N. Ramamurthy, S. Pal, and K.P. Rao, *Biomater*., **22,** 1943 (2001).
15. L. Vachoud, N. Zydowicz, and A. Domard, *Carbohy. Res*., **326,** 295 (2000).
16. H. Park, K. Park, and D. Kim, *J. Biomed. Mater. Res*., **76A,** 144 (2006).
17. K. C. Gupta, and F. H. Jabrail, *Carbo. Polym*., **66,** 43 (2006).
18. J. Bicerano, Marcel Dekker, III edition. 2002.
19. A.P. Kumar, and R.P. Singh, *J. Appl. Polym. Sci*., **104,** 2672 (2007).
20. F. Yao, W. Chen, H. Wang, H. Liu, K. Yao, P. Sun, and H. Lin, *Polym*., **44,** 6435 (2003).
21. S. Lavie, and G. Stotzky, *Appl. Environ. Microbiol*., **51,** 65 (1986).

22. T. Takahashi, and M. Yamaguchi, *J. Colloid. Interface. Sci*., **146,** 556 (1991).
23. L.G. Griffith, and G. Naughton, *Science*, **295,** 1009 (2002).
24. H.R. Lin, C.J. Kuo, C.Y. Yang, S.Y. Shaw, and Y.J. Wu, *J. Biomed. Mater. Res*. **63,** 271 (2002).
25. Y.S. Nam, J.J. Yoon, and T.G. Park, *J. Biomed. Mater. Res*., **53,** 1 (2000).
26. L.D. Harris, B.S. Kim, and D.J. Mooney, *J. Biomed. Mater. Res*., **42,** 396 (1998).
27. D.J. Mooney, D.F. Baldwin, N.P. Suh, J.P. Vacanti, and R. Langer, Biomater., **17,** 1417 (1996).
28. Y. Tabata, *Tissue Engineering*, **9**, S5 (2003).

CHAPTER IV

Preparation and Characterization of Novel Hybrid of Chitosan-g-PDMS and Montmorillonite

4.1 INTRODUCTION

Graft copolymerization is one of the best methods to bring together synthetic and natural polymers to retain the good properties of natural polymers such as biodegradation, bioactivity and biocompatibility. In this work, CS and Poly Dimethyl Siloxane (PDMS) were used to synthesize the graft copolymer with hydrophobic, synthetic side chains and hydrophilic, natural main chains by direct polycondensation reaction without using catalyst. Chitosan (CS), which is cationic in nature, is biologically renewable, biodegradable, biocompatible, non-antigenic, non-toxic and biofunctional material[1]. As opposed to synthetic polymers, CS displays a hydrophilic surface promoting cell adhesion, proliferation, differentiation and evokes a minimal foreign body reaction the on implantation[2-3]. In spite of its general acceptance as a tissue compatible material, CS is mechanically weak and unstable and therefore, unable to maintain a predefined shape for transplantation as a result of swelling[4]. In addition to that, CS enhances plasma protein adsorption, platelet adhesion and activation, and thrombus development, in other words, CS is an effective hemostatic agent, possibly due to electrostatic attraction. Therefore, CS cannot be applied for direct blood contacting unless it is modified.

Thrombus development takes place when polymeric biomaterial possessing high surface energy comes in direct contact with blood, followed by adsorption of blood cells and serum proteins onto the surfaces. Incorporation of low surface energy polymers into CS films has been proposed to minimize these disadvantages. Among polymers frequently employed as biomaterial, hydrogels have demonstrated relatively low thrmogenecity. Hydrogels, defined as a polymer network capable of imbibing a large volume of water but retaining their three-dimensional structures after swelling, have received increasing attention for biomedical applications such as drug delivery systems, contact lenses, catheters and wound dressings. In addition, their surface hydrophilicity is responsible for less protein adsorption and less cellular adhesion, resulting in improved biocompatibility. A natural polymer-based, hybrid scaffold with better mechanical strength and biological property equivalent to or better than CS has yet to be developed. On the other hand, Siloxane derivative such as PDMS (**Figure 4.1**) is a high performance polymer with unique physical and chemical properties such as 1) it is transparent down to 280 nm, which makes it suitable for detection at a wide range of wave-lengths, 2) it is biologically inert and non-toxic, which is good for cell-

patterning on various substrates, 3) it is permeable to gases, a property which is useful when supplying oxygen to cell cultures in closed systems, 4) it seals readily with other materials such as glass, polystyrene, and PMMA for making hybrid chips, which makes PDMS probably the most versatile material in micro-chip technology[5, 6]. Rutnakornpituk[7] has reported the grafting of PDMS homopolymer onto CS by chemical modification. Slight decrease in its critical surface energy and increase in tensile strength and elongation was observed. PDMS has been used in the preparation of nanocomposites[8] and in drug delivery applications[9]. It has been found that PDMS can be used with poly (ethylene oxide) (PEO) with a significant decrease in macrophage density[10].

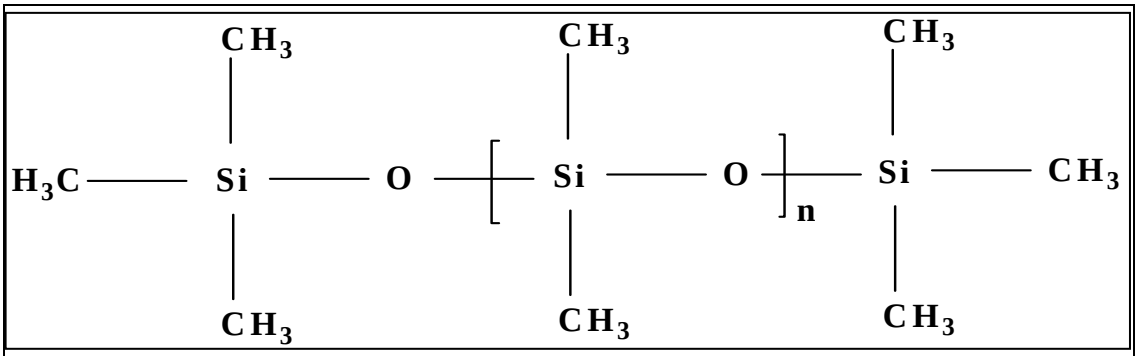

Figure 4.1 The structure of a linear PDMS.

Medical devices made of Polyurethane (PU) containing PDMS soft segment has been reported to exhibit better blood contact properties relative to commercially available PU[11]. Another advantage of adding PDMS into CS is to improve their mechanical properties. Because hardness and brittleness are major drawbacks of CS which limit their use as wound healing material, incorporation of elastomeric PDMS should somewhat soften the material. The development of organic-inorganic hybrids has also been another field of research in preparing biocomposite/ biomimetic materials. Since last few decades, it has been found that the reinforcement of layered silicates improves the optical, physical, thermal and mechanical properties of the obtained composites with very low amount of loading of nano-clay because of their nanoscale distribution with high aspect ratio filler[12, 13]. Montmorillonite (MMT) can provide swelling properties, enhanced gel strength, mucoadhesive capability to cross the gastro-intestinal (GI) barrier, adsorbs bacterial toxins and metabolic toxins such as steroidal metabolites. MMT not only cures minor problems such as diarrhea and constipation through local

application, but also acts on all organs as well. Considering these advantages in medical applications, it has taken the credit to be called as medical clay[14]. Recently nanocomposites of polylactic acid with layered silicates have also been prepared by different methods[15]. Preparation of nanocomposites of CS has also been performed by intercalating CS into Na^{+}-MMT through cationic exchange and hydrogen boding processes, with interesting structural and functional properties[16]. Thus, it will be worthwhile to fabricate a new nanohybrid based on PDMS grafted onto CS with improved mechanical, thermal and surface properties. We have intended to prepare macromolecular organic-inorganic hybrids of layered silicates and CS-g-PDMS. It involves grafting of PDMS onto CS in the presence of layered silicates under UV irradiation. It is also anticipated that grafted PDMS chains may act as internal plasticizers to lessen the brittleness of CS films to obtain softer and flexible films and this will introduce side chains and thus make various molecular designs possible, affording novel types of tailored hybrid materials composed of natural polysaccharide and grafted synthetic polymer. Moreover, it is reported that PDMS has an affinity with organoclay for making an exfoliated nanocomposite[17]. Later on Ishida et al[18] used PDMS as a swelling agent to enhance the diffusion of polymer chains into a gallery of nanoclay. For a wound dressing material, the dressing is preferably permeable to water vapor to some extent so that the moist exudates under the dressing are maintained without pooling during the recovery period.

This property can be assessed by measuring the water vapor permeability of the films and its swelling behavior, which are directly associated to membrane capability of draining wound exudates. The ability of CS to form films may permit its extensive use in the formulation of film dosage forms[19] or as drug delivery systems[20]. Interests on tailoring the CS for desired properties has also being grown in different ways e.g. graft copolymerization. Therefore, in this paper, studies were carried out to prepare CS-g-PDMS nano composites by introducing PDMS onto CS-montmorillonite nanocomposites via photo induced grafting. Here CS will act as a hydrophilic block while PDMS was introduced as a hydrophobic block, since both of them have been constituents of biomedical devices such as artificial hearts, blood vessels and various catheters. When biomolecules, such as proteins approach the surface, the CS chains will create a hydrophilic wall and keep biomolecules at a sufficient distance from the PDMS, thus, preventing biofouling. To the best of our knowledge, this is the first

example of the preparation of CS-g-PDMS nanohybrids via intercalation into clay interlayer galleries.

4.2 EXPERIMENTAL

4.2.1 Materials

Chitosan of low molecular weight (M_v 1.5x10^5, degree of deacetylation was 85%) was obtained from Aldrich. Sodium Montmorillonite Na^+-MMT, with Cation Exchange Capacity of 76.4-meqv/100 g was received from M/s. Southern Clay Inc. USA and was used as such. Hydroxyl terminated Poly dimethyl siloxane of (PDMS) of high molecular weight was purchased from Aldrich. It was used as obtained.

4.2.2 Preparation of nanocomposites:

First CS was dissolved in an aqueous solution of L-lactic acid and clay was dispersed in deionized water (30ml) overnight at room temperature. On the other hand, clay (MMT) was dispersed in distilled water overnight. Preparation involves aqueous dispersion of clay, aqueous solution of CS in L-lactic acid, followed by mixing. The nanocomposites were prepared keeping CS: clay (Na^+-MMT) ratios as 100:0, 95:5, 90:10 and 80:20. All the reaction mixtures were applied for sonication for 2 hrs to remove air bubbles.

4.2.3 Grafting of PDMS:

The synthesis of CS–g– PDMS nano composites was carried out by photo grafting of PDMS onto CS in the absence of catalyst, according to the method reported by Kim et al[21]. PDMS was dissolved in the aqueous solution of CS and this solution was heated up to 80 °C for three hrs with constant stirring. UV irradiation was conducted using a 450 W UV lamp for three hrs at a distance of 15 cm and at room temperature under inert conditions for 6 hrs. The resulting solution was then poured onto glass Petri-plates to obtain sample films by solvent casting method by drying the films at 60 °C for 24 hrs. The films were neutralized in a 0.5 M NaOH solution and dried at 50 °C for 24 hrs under vacuum. The CS-g-PDMS films were somewhat opaque as compared to the pristine CS. The composition of the prepared nanocomposites can be seen in **Table 4.1**.

Table 4.1 Recipe of the prepared chitosan-g-PDMS Na^+-MMT nanocomposites

S. No.	Chitosan (%)	PDMS (%)	Na^+-MMT (%)	Sample code
1.	85	5	10	CS-PD-A
2.	80	10	10	CS-PD-B
3.	70	20	10	CS-PD-C
4.	85	10	5	CS-PD-D
5.	70	10	20	CS-PD-E

4.3 CHARACTERIZATION OF NANOCOMPOSITES

4.3.1 X-Ray Diffraction:

The WAXD patterns of the film samples were obtained using a Rigaku (Japan) Dmax 2500 X-ray diffractometer with Cu-Kα radiation. The system consists of a rotating anode generator with a Cu target and a wide angle powder goniometer having a diffracted beam graphite monochromator. The generator was operated at 40 kV and 150 mA. All the experiments were performed in the reflection mode. The samples were scanned between 2θ= 2° to 30 ° at a scan rate of 2°/minute. The d-spacing was calculated by Bragg's formula, where the λ was 0.154 nm.

4.3.2 FTIR- Spectroscopy:

The Fourier-transform infrared (FTIR) spectra were obtained from the sample under ATR mode on a Perkin-Elmer Spectrum GX. The sample films were scanned in the range of 4000 cm-1 to 400 cm-1 at a resolution of 4 cm-1. A total of 10 scans were used for signal averaging.

4.3.3 Atomic Force Microscopy (AFM) analysis:

AFM images of pristine CS film and PDMS grafted CS nanohybrid film samples were taken on a Nanoscope IV AFM instrument under contact mode.

4.3.4 ^{13}C-NMR:

The proton-decoupled solid state ^{13}C-NMR (I = 1/2) CP-MAS NMR spectra were obtained in a Bruker Avance 300 spectrometer, using a standard cross-

polarization pulse sequence. Samples were spun at 10 kHz. Spectrometer frequencies were set to 100.62 for ^{13}C. The numbers of scans were of 800. The cross polarization time was 0.5 ms. Chemical shift values were referenced to tetra methyl silane (TMS).

4.3.5 Elemental Analysis (EA) and Percentage of grafting:

The content of C, H, and N was determined for pristine and grafted CS samples. The total nitrogen content was determined according Dumas with a Carlo Erba NA 1500 instrument. The percentage of grafting of the CS amino groups was determined by the method given by Kweon[22] for grafted samples, according to the equation:

$$\textbf{Grafting \%} = \frac{\text{Weight of CS-g-PDMS-Weight of CS}}{\text{Weight of CS}} \times 100$$

4.3.6 Thermal Methods:

The thermal gravimetric analysis (TGA) was conducted on a Perkin-Elmer TGA 7- thermal analyzer from 50°C to 900°C with a heating rate of 10°C min^{-1} under nitrogen with flow rate 20ml min^{-1}, in a platinum crucible.

4.3.7 Water Absorption measurements:

According to ASTM D570 the clean, dried film samples of known weights were immersed in simulated body fluid (SBF) at 25°C for one day (24 h). The films were removed, blotted quickly with absorbent paper and then weighed. The absorption percentage of these samples was calculated using the equation X (%) = $(W_1-W_0) / W_0$, Where W_0 and W_1 are the weight of dry and swollen samples, respectively. Three independent measurements were performed for each sample and the average values were taken for swelling behavior studies.

4.3.8 Protein adsorption studies:

In vitro single protein adsorption experiments were performed in phosphate-buffered saline (PBS, pH ¼ 7.4, 0.15 mol/L), according to the reported procedure[23]. Samples were immersed in 4.5 mg/mL of BAF-5 and lysozyme. Clean, modified and unmodified PDMS membranes were first immersed in PBS filled 24-well plate for 24 h in order to be full hydrated. The specimens were moved into wells containing protein

solution and adsorption was allowed to proceed at 37 °C for 2 hrs under gentle shaking. Each sample was then rinsed in the fresh PBS by 50 dippings. The samples were subsequently transferred into a well-plate filled in 1mL of PBS solution containing 1wt% of sodium dodecyl sulfate (SDS), and the surface adsorbed protein was completely desorbed by sonication for 20 min. A protein analysis kit (Micro BCATM protein assay reagent kit, #23235, Pierece, Rockford, IL, USA) based on the bicinchoninic acid (BCA) method was used to determine the concentration of the protein in the 1wt% SDS solution. The amount of protein on the sample films was calculated from the concentration in the SDS solution. The concentration of the protein was measured by an absorptiometer (Wallac 1420 ARVO SX, Perkin-Elmer, Japan) at 560 nm.

4.4 RESULTS AND DISCUSSION

4.4.1 XRD: Structure Analysis

Scheme 4.1 shows the expected reaction mechanism for the preparation of nanocomposites of CS-*g*-PDMS and montmorillonite.

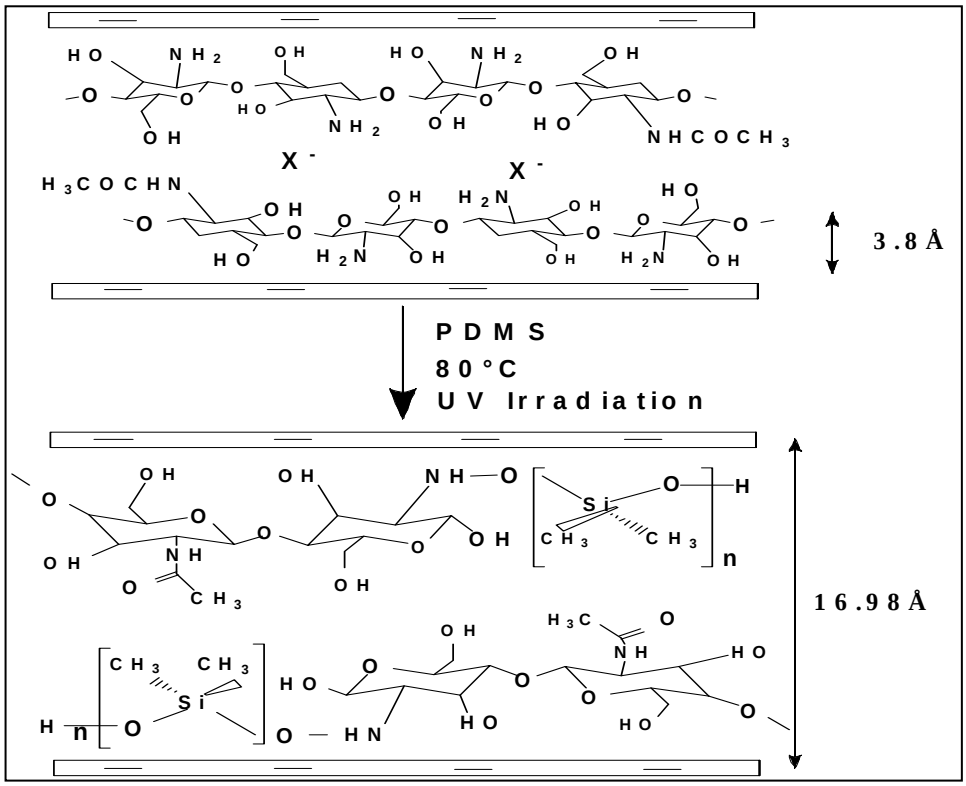

Scheme 4.1 Schematic illustration of preparation of grafted nanohybrids

For nanocomposite preparation, aqueous suspension of Na^+-MMT was treated with aqueous CS solution, by controlling the pH ~ 5.0 to avoid any structural change of the silicate layers. On the other hand, acidic pH is necessary for the protonation of -NH_2 groups of CS. In such conditions, the adsorption process is mainly controlled by a cationic exchange mechanism due to the columbic interactions between the positive –NH_3^+ groups of the biopolymer and the negative sites in the MMT clay structure. Because of the hydrophilic and polycationic nature of CS in acidic media, this biopolymer solution has good miscibility with Na^+-MMT and can easily intercalate into the clay interlayer by means of cationic exchange process. Since one CS unit possesses one –NH_2 and two –OH groups, these functional groups can form strong intermolecular hydrogen bonds with the silanol (Si-OH) edges, which lead to the strong affinity between the matrix and silicate layers. The WAXD patterns of pristine Na^+ -MMT and its nanocomposites with CS-g-PDMS are shown in **Figure 4.2**.

It was reported[24, 25], that CS has an orthorhombic unit cell of crystal plane 001 with *a* = 8.24 Å, *b* = 10.39 Å, and *c* = 16.48 Å, and is larger than that of crystal plane 002 with a = 4.5 Å, b = 10.1 Å, and c = 0.35 Å. The peaks appearing at around 2θ = 5.2° are assigned to (001) and (100), while the peaks around 2θ = 21° are assigned to (020) and (200), according to ICDD No. 39-1894, which can be identified as semi-crystalline chitosan. The measured d_{001}-spacing of Na^+-MMT was 12.26 Å (2θ =7.4°). This peak in CS-g-PDMS nanocomposites is substituted by a new weakened broad peak at around 2θ = 4.9°. It can be observed that d_{001}- spacing of the nanocomposite (CS-PD-A) was increased to 16.98 Å (2θ = 5.2°). This decrease in 2θ value or increase in d-spacing confirms the formation of intercalated nanostructure of CS in the clay interlayer, while the peak broadening and decrease in intensity is likely to assign as disordered intercalated or exfoliated structure (CS-PD-B). This may be attributed to the cation exchange between the Na^+ ions of clay layers and –NH_3^+ groups of CS. This is in agreement with the d_{001} value of 3.8 Å measured from the XRD pattern of a CS film, which represents the thickness of a sheet of polysaccharide chains.

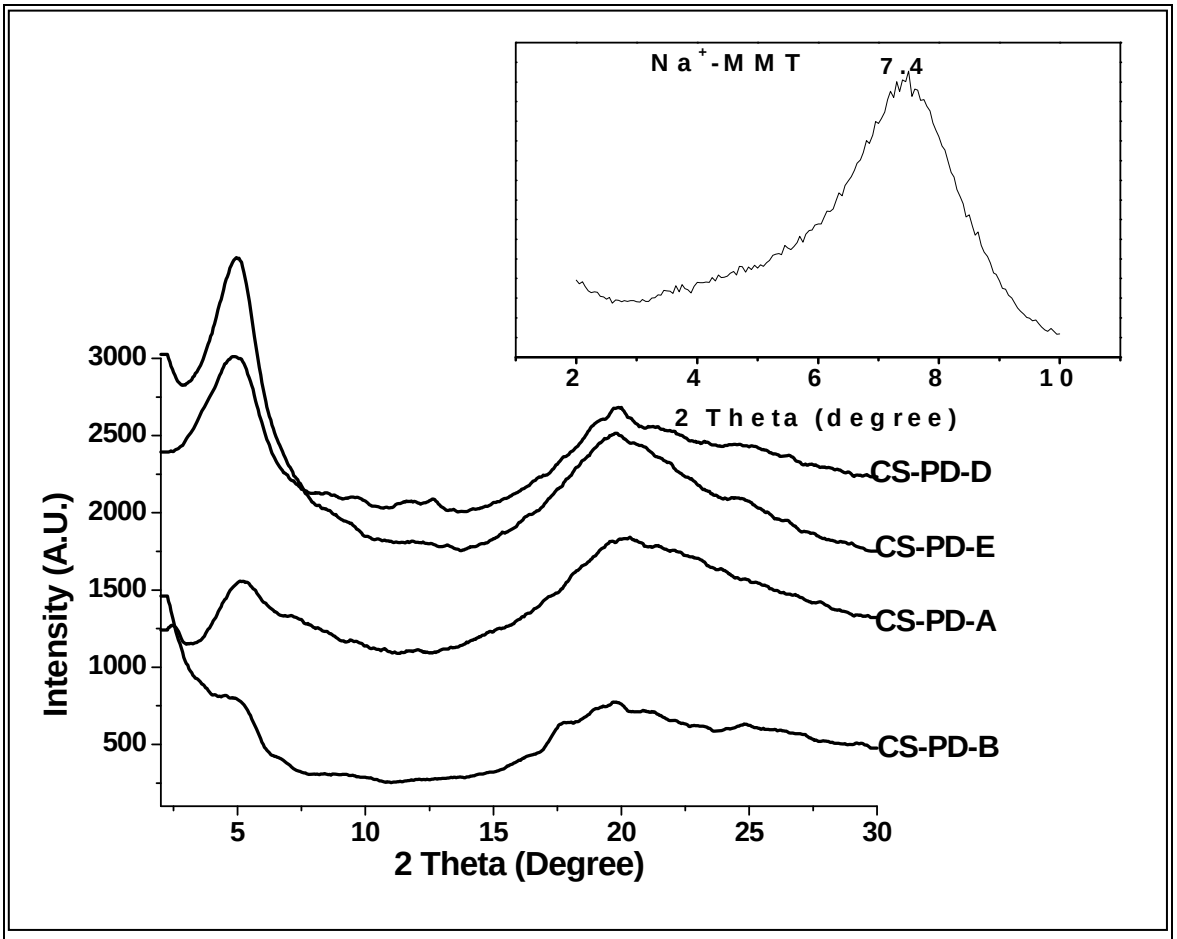

Figure 4.2 WXRD patterns of the prepared nanohybrids.

Since PDMS reacts with CS in a homogeneous solution of aqueous lactic acid, the grafting will take place at random along the chain, giving rise to a random copolymer. This will efficiently destroy the regularity of the packing of the original CS chains, which results in the formation of almost amorphous copolymers as most of the crystalline domains of CS were destroyed, as shown by the broad peaks in the XRD patterns of the prepared nanocomposites, and further confirmed by TGA and DTG curves.

Furthermore, it was found that the crystallinity of CS was decreased with increasing clay content, which is probably caused by the well-dispersed clay nano-crystals which acts as point defects in the CS matrix. In addition Strawhecker et al[26] also reported that strong polymer-filler interaction could change the molecular conformation of polymer chain in the vicinity of filler and simultaneously gave rise to the formation of localized amorphous regions.

4.4.2 FT-IR Spectral Analysis

Figure 4.3 shows the IR spectra of pristine PDMS and CS-g-PDMS nanohybrid film sample. As shown in the spectra of CS-PD-A, the at 1560 cm^{-1}, which is attributed to the deformation vibration (δ NH_3^+) of the protonated amine groups of CS , is shifted towards lower frequency, confirming the interaction between clay and NH_3^+ group.

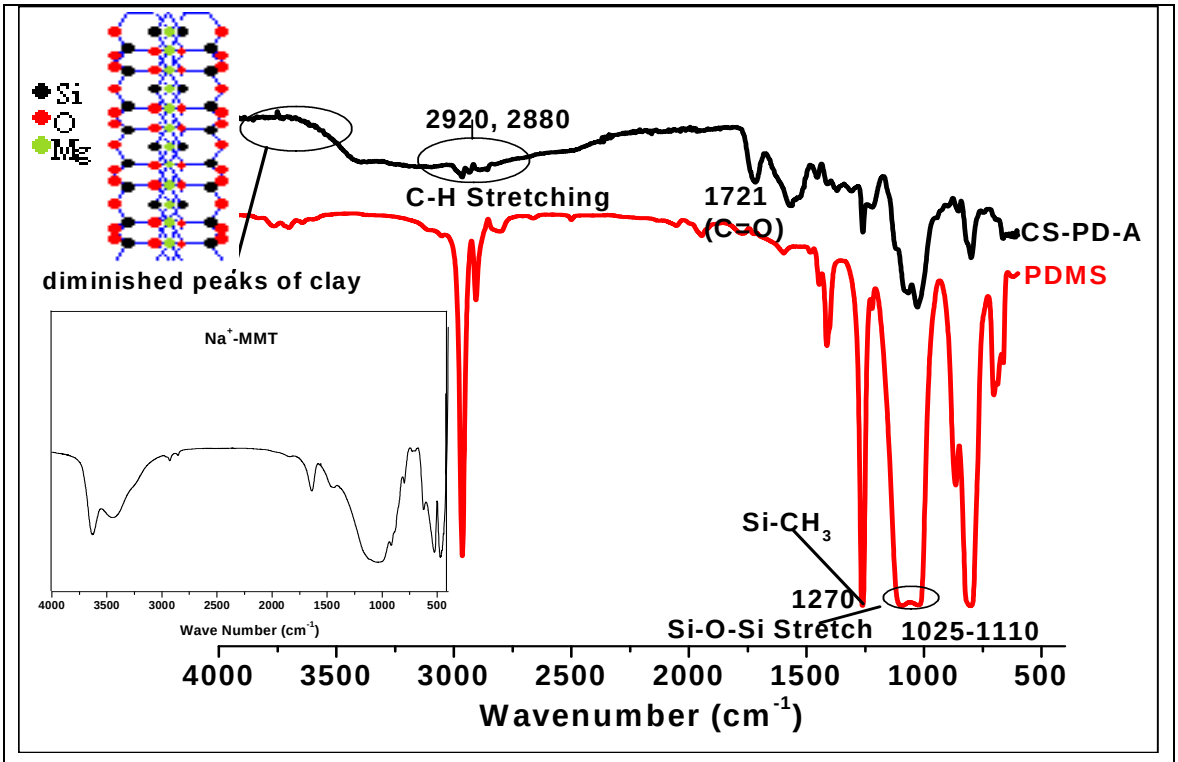

Figure 4.3 Spectral analysis results of the prepared nanohybrids.

These observations are in good agreement with the results obtained from XRD, which depicts that the interaction between MMT clay and CS is crucial for the intercalation of biopolymer chains into MMT. The characteristic peaks of amine –NH vibration deformation appeared at 1595 cm^{-1} for CS. It is noteworthy here that this peak is diminished in CS-PD-A, caused by the grafting of PDMS onto CS. The band at 1721 cm^{-1} may be attributed to the ν_{CO} stretching band of acetate ions associated with the CS moieties.

The results of elemental analysis (EA) and percentage of grafting, for the PDMS grafted samples were shown in **Table 4.2**.

Table 4.2 Sorption behavior, EA results and percentage of grafting of the prepared composites

Sample	Water absorption	EA (%)			Grafting
	(%)	C	H	N	(%)
CS-PD-A	370	44.92	13.9	8.11	14
CS-PD-B	465	45.43	7.13	7.87	16
CS-PD-C	832	45.89	6.11	6.12	19
CS-PD-D	553	47.11	8.17	7.93	15
CS-PD-E	312	47.48	13.6	5.19	14
Neat Chitosan	54	43.22	6.11	7.71	-

The results show that C wt % increases and N wt % decreases after grafting PDMS. Besides the vibrational band characteristics of the silicate (ν_{OH} of Al, Mg (OH) at ~ 3635 cm^{-1}; ν_{OH} of H_2O~ 3430 and 3250 cm^{-1} are diminished due to the electrostatic interaction of polycationic CS (as shown in the INSET **Figure 4.3**), the bands attributed to the intercalated CS and grafted copolymers are also observed. The peaks at 2920, 2880, 1430, 1320 and 1215 cm^{-1} attributed to the symmetric/asymmetric CH stretching vibrations of pyranose rings. A new peak in CS-PD-A, arising at 1025-1110 cm^{-1} is attributed to Si-O-Si stretch and 1270 cm^{-1} is due to Si-CH_3, a finding consistent with the presence of PDMS chains onto CS.

4.4.3 AFM Analysis

Because of its high spatial and vertical resolution, atomic force microscopy (AFM) has been applied to determine morphology of nanohybrids and considered as a powerful tol for imaging the topography of surfaces.

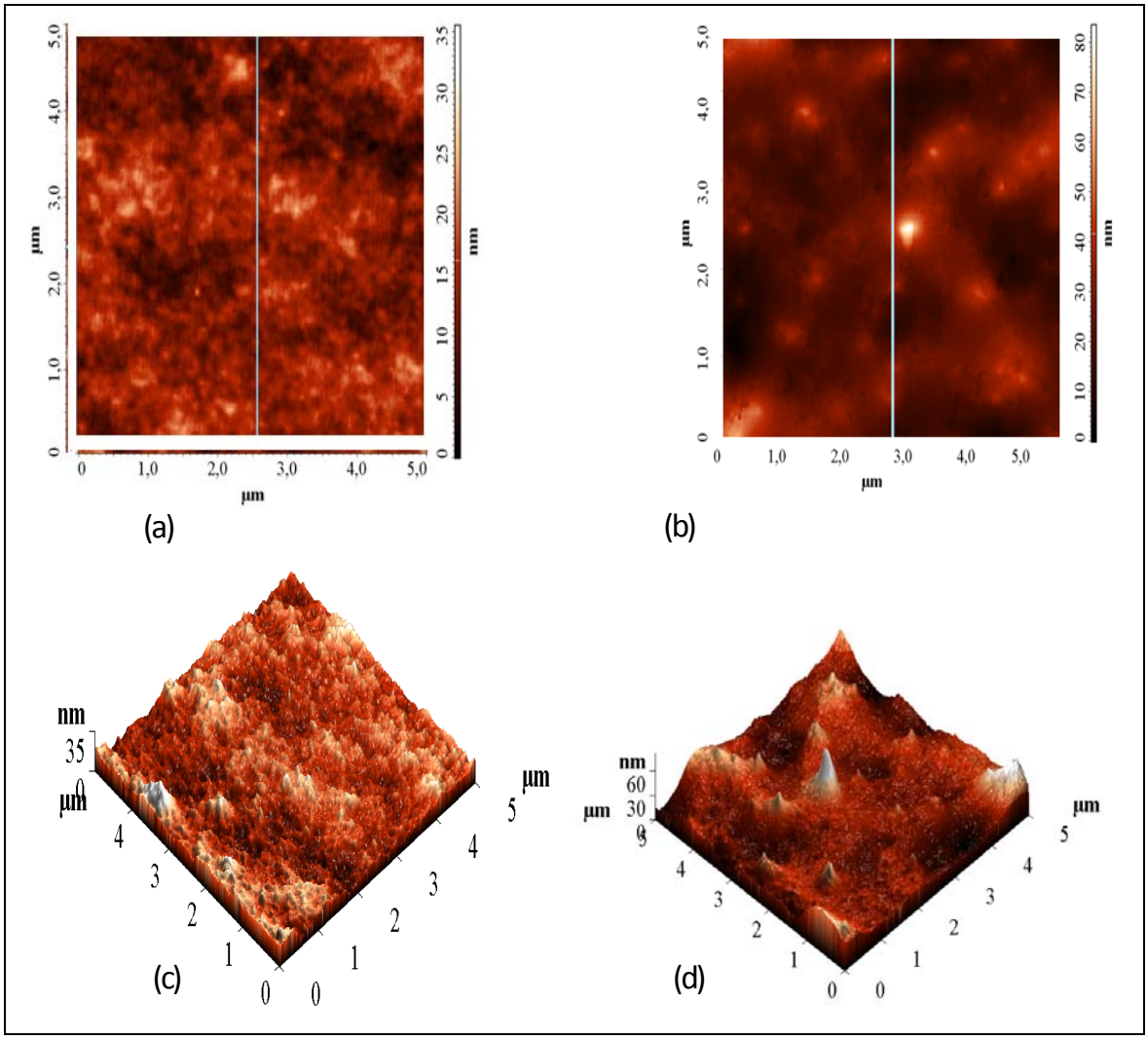

Figure 4.4 AFM Images of the prepared grafted CS nanohybrids.

Figures 4.4 (**a, b**) shows the morphology of the pristine CS and CS-g-PDMS hybrid films, respectively, analyzed by atomic force microscopy. Pure CS film presents quite homogeneous surface while the PDMS grafted film reveals a predominantly hill-valley-structured surface with irregular pores of nanoscale topography, in accordance with other reports[27]. The surface roughness, measured on scanning areas of 5.00 x 5.00 μm^2 indicated values of 2.99 and 6.24 nm for pure CS film and grafted sample film, respectively. The differences between CS and CS-g-PDMS can also be seen in 3D images (**Figures 4.4** c, d). The highest majority of height population is situated around 14 and 25 nm for CS and grafted films, respectively. The obtained results support the evidence of grafting of PDMS molecular chains onto CS and the images clearly shows the variations in the morphology of the pristine CS films and PDMS grafted films.

4.4.4 ^{13}C-NMR Spectral Analysis

Solid-state high-resolution NMR spectroscopy was also applied to characterize the CS-g-PDMS nanocomposites.

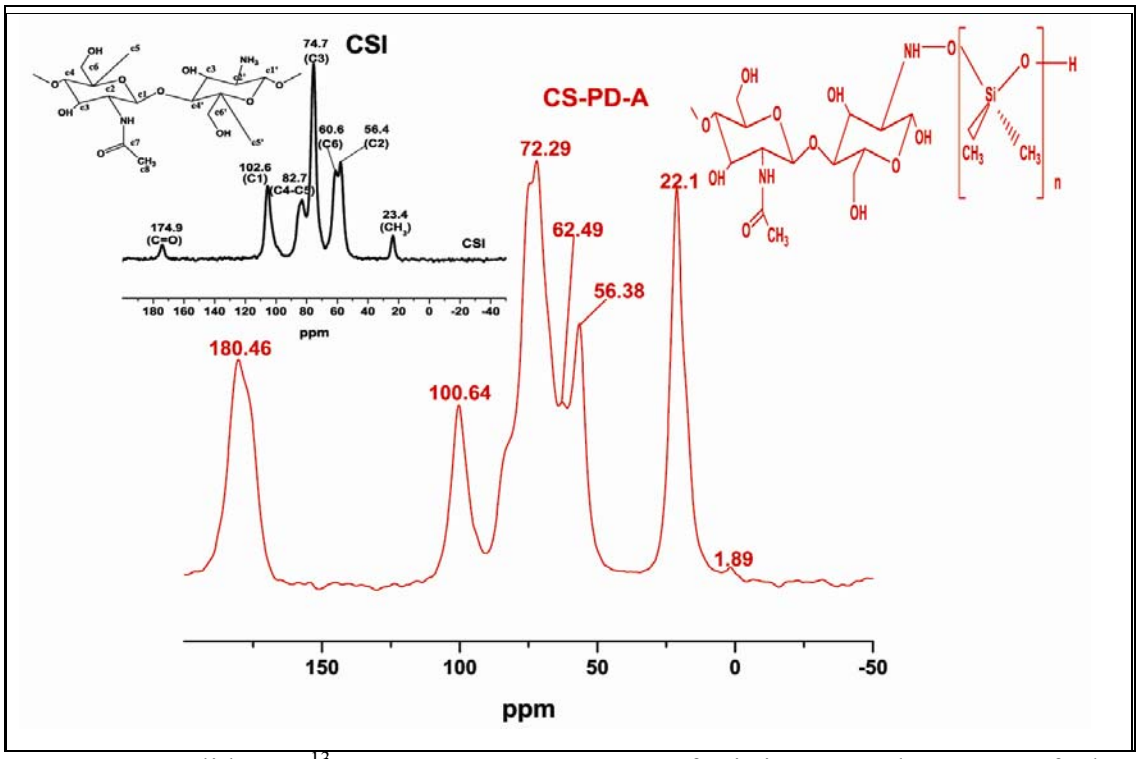

Figure 4.5 Solid state ^{13}C-NMR CP-MAS spectra of pristine CS and PDMS grafted CS nanohybrids.

Solid state CP-MAS ^{13}-C-NMR is known to be very sensitive to changes in the local structure and the chemical shifts of C-1 and C-4 carbon in 1, 4-linked carbohydrate are believed to be highly sensitive to any conformational change at the glycosidic linkage[28]. The resonance peaks for CS are assigned according to the reported literature[29]. The signals observed on the spectra at 23.4 and 174.9 ppm, were attributed to the signals of $-CH_3$ and carbonyl (–C=O) of the glucosamine ring, respectively, are given in **Figure 4.5**. Apart from this a new peak around 1.89 ppm, which is attributed to Si-CH_3[30, 31], appeared which confirms the grafting of PDMS onto CS which is in good agreement with the results obtained from FT-IR.

4.4.5 Elemental analysis and % Grafting

The percentage of grafting increases with the feed ratio of PDMS to CS, approaching a saturation level of 19 % for CS-PD-C. The percentage of grafting increases as the feed ratio increases but only at a constant amount of clay. As the

amount of clay increases i.e. for CS-PD-E, the percentage of grafting decreases. This is attributed to the fact that the diffusion of PDMS chains into CS matrix was inhibited under higher clay content. The results show that the light transmittance of the materials does not change significantly in the presence of the clay (at low clay content), i.e. the nanocomposite films preserve the polymer transparency, but at higher clay content, the matrix will loosen its optical transparency resulting into lower extent of grafting. The high value of light transmitted through the nanocomposites is due to the fine dispersion of the filler into the polymer matrixes; however polymer micro-composites show a drastic decrease of the light transmittance in the presence of solid transparency[24]. Apart from this, CS will not only effectively enlarge the inter-lamellar spacing of Na-$^{+}$MMT, but also form a uniform structure in clay. The size of clay inter-lamellae is smaller than the wavelength of visible light so that the composites might retain satisfactory transparency during UV irradiation.

4.4.6 Thermal Methods

TGA (the residual weight percentage versus temperature) and DTG (derivative of the differential weight percentage versus temperature) traces for prepared nanocomposites are shown in **Figure 4.6**. The shape of the curves reflects the amorphous nature of the copolymers as evidenced by a curve with two well differentiated regions. The thermal decomposition profile exhibit two main decomposition stages, with one starting at around 100 °C and another at 220 °C, as shown in the thermograms. The first stage may be attributed to the elimination of both, non-gallery surface adsorbed water and interlayer water molecules. The amount of weight loss at this temperature range decreased with increasing clay content of the samples, which implies to the formation of a CS-silicate complex, which decreases the water absorbability of the films, i.e., decrease the hydrophilicity of the films. The second stage, observation of a maximum weight loss at around 290-300 ˚C, can be attributed to the scission of the grafted copolymer chains. The weight loss at higher temperature was observed to be low. It reveals the presence of cross linked structure, which is formed by thermal cross linking at first stage of decomposition[32]. The maximum decomposition temperature was observed to be higher for nanocomposites CS-PD-A and CS-PD-B than that for CS-PD-E. The presence of nano-sized silicate layers plays a leading role in enhancing the thermal stabilities of the grafted copolymers, by obstructing the out-diffusion of the volatile decomposition products. It

is important to mention here that the values of char yields were almost coincident with the amounts of the clay in nanocomposites.

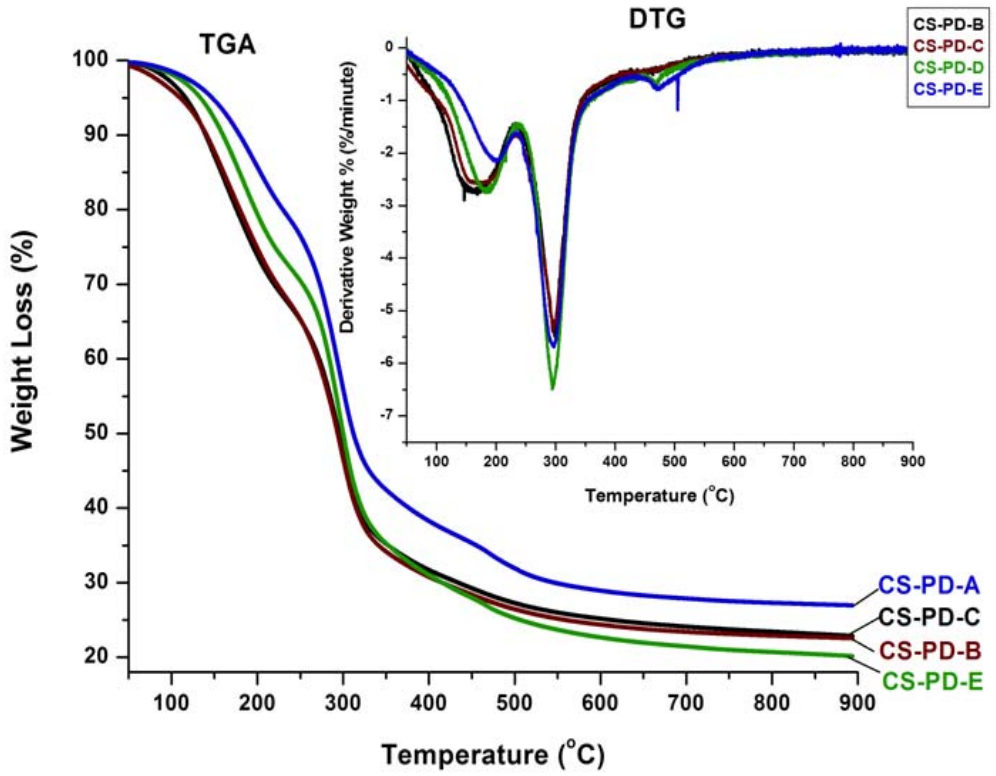

Figure 4.6 TGA and DTG Thermograms of CS-g-PDMS nanocomposites

Therefore, the increased char ratios mainly resulted from the nonvolatile silicate layers and the char formation from organic part (grafted PDMS chains and CS). This was also supported for other polymer-silica hybrid materials[33]. In case of CS-PD-E (20 %wt. Clay), the incorporation of silicate layers gets more and more hindered because of geometrical constraints within the limited space remaining available in the polymer matrix. In other words, the polymer chain confinement into silicate galleries (in CS-PD-E) is reduced in a limited space. The DTG curves corresponding to the prepared nanocomposites show an endothermic process at 160 ˚C which is associated with a weight loss of physically adsorbed water molecules and two endothermic processes at 294 ˚C and 470 ˚C endothermic processes i.e. pyrolytic decomposition (weight loss of 41%) followed by the combustion (weight loss of 33%) of the biopolymer.

4.4.7 Water Absorption Studies:

The behavior of water absorption of CS-*g*-PDMS/ Na^+-MMT composites was investigated, and results were shown in **Table 4.2**. The water absorption of composite films decreases with an increase of clay with CS matrix. This is probably due to the formation of a barrier in the form of cross-linking points, which prevent water permeation into CS. Pure CS is hydrophilic, but it does not absorb much water. CS displays many –OH and –NH groups, which cause strong intermolecular and intramolecular hydrogen bonds; thus, the infiltration and diffusion of water, is restrained. The water absorption of PDMS grafted CS is higher than the pristine CS. It can be attributed to the fact that the presence of microphase separation of PDMS amphiphile in CS matrix will effectively break the integrity of molecular structure in grafted CS, which can expose more functional groups for water absorption. Along with this the grafted hydrophobic PDMS backbone might microphasically aggregate and renders hydrophilic parts exposed due to hydroxyl end groups hydrogen bonding with CS. This swelling extent will depend on the osmotic pressure and charge repulsion, the degree of ionization and also on grafting extent[34] which have already been demonstrated by the dependence of lactic acid grafted CS on the temperature and pH of solution. In comparison of grafted CS, samples of nanocomposites have shown lower water absorption and it decreases with increasing content of clay. It can be attributed to the interaction between layered silicates and copolymers in which intercalated polymer chains, which are more responsible for hydrophilicity, were confined into silicate galleries. Since sodium montmorillonite is hydrophilic clay, resulting composites were expected to be hydrophilic. The reduction in water absorption may be due to the fact that the formation of nanocomposites occurred through the cation exchange between $-NH_3^+$ and Na^+ ions. Thus, water absorption to the silicate layers appears to be reduced. In other words, in a particular space (size) of composite, cationically modified silicate layers will be as immobilized phases. The increasing content of layered silicate increases the immobilized phase throughout the matrix.

The interaction between the mobilized and immobilized phases has shown to reduce the water absorption[35] and have already been demonstrated by Xu et al[36] in favor of reduction of water absorption. In addition, the composites were allowed to swell up to their equilibrium, which was reached after 25 hrs. After complete swelling, we dried the films under vacuum oven at 65°C to investigate the moisture retention

capacity of the composite films. We observed that the films could hold the moisture for a long time. It shows the high water retention capacity of CS. The increasing clay loading decreases the water absorption and increases the time for drying up to constant weight i.e. they hold the moisture for longer time. It may be due to clay, which may act as a physical barrier for the moisture to exude out from the films.

4.4.8 Protein Adsorption Studies:

Table 4.3 shows the amount of BAF-5 and lysozyme adsorption on the membranes from the PBS buffer with 10% *in vivo* concentrations. There were little differences in the amount of adsorptions among the grafted PDMS membranes, which strongly agree with the results of the surface characterization. The average amount of BAF-5 adsorption on the PDMS grafted film (CSPD-1) was 7.65μg/ml, which is around 70% less as compared to the unmodified PDMS film sample, which is 12.1μg/ml. These results also agree with a previous report on the poly (MPC)-grafted surface[37].

Table 4.3 Protein adsorption values of the pristine CS and PDMS grafted nanohybrids.

Sample	Adsorption of BAF-5 (%)	Adsorption of Lysozyme (%)
PDMS	2.41	5.83
CSPD-1	1.70	4.02
CSPD-2	1.99	4.20
CSPD-3	1.78	3.94

The mechanism of protein adsorption resistivity on the PDMS grafted samples is thought to be based on the interactions between water and the PDMS side chains. The large amount of free water around the grafted PDMS is thought to repel proteins and even prevent conformational changes in the adsorbed proteins[38]. The reduction in protein adsorption is also thought to be due to the presence of a thick hydrated layer around the hydrophobic PDMS side chains[39]. The determining factors for the protein adsorption behavior of the end-tethered polymer chains have been identified as the graft density, chain length, and chain conformation on the surface.

The large portion of proteins, reversibly adsorbed on the film samples was eluted by rinsing with the SDS solution, while there were no considerable changes in the proportion of proteins adsorbed before the SDS treatments. The hydrophobic characteristics of PDMS have appeared to attract most proteins, originating from the hydrophobic interaction with proteins, which motivated surface modification to endow hydrophilicity. This suggests that a certain amount of PDMS in CS-g-PDMS remains on the surface to be exposed on human plasma although the high flexibility of PDMS has a high tendency to bury itself in the interior of the hydrogel. Although there exists a general concept that hydrogels tend to adsorb less proteins than hydrophobic materials which is mainly ascribed to the hydrophilicity and low interfacial energy in an aqueous environment, but the studies to find a correlation between hydrophilicity and protein adsorption have often failed. For example, Lee[40] investigated the relationship between serum protein adsorption and the surface hydrophilicity of polymeric materials by using wettability gradient surfaces prepared by treating polyurethane in air with corona. Their study showed that the serum proteins were adsorbed more onto the positions with moderate hydrophilicity than those with extremely hydrophilic or hydrophobic characteristics. Our results also suggest that the hydrophilicity of polymers is not necessarily responsible for protein adsorption, which is definitely influenced by the surface chemistry and type of proteins.

4.5 CONCLUSIONS

We have demonstrated a novel way to prepare inorganic-organic hybrids from biopolymer and montmorillonite. The intercalation of cationic biopolymer CS into Na^+-MMT by a cationic exchange process results into nanohybrids with both interesting structural and functional properties. The grafting of PDMS imparts the hydrophilicity and swelling behavior to the CS. The incorporation of clay affects the preparation and physio-morphic properties of grafted copolymer. The grafted PDMS chains were acting as a plasticizer to give flexible films. The increasing content of clay decreases water absorption and imparts little branched crystallite structure in the film. The swelling behavior and longer water retention properties were discussed, which could be applied in biomedical field. Reductions of the adsorbed single proteins on the CS-g-PDMS films were about 40-50 %. The presence of highly hydrated thick water layer around the grafted samples is seem to reduce the protein adsorption. Our study reveals that the PDMS grafted CS nanohybrid film is a potential candidate in biomedical applications.

4.6 REFERENCES

1. D-A, Wang J. Ji, Y-H, Sun, G-H. Yu, and L-X. Feng, *J Biomed. Mater. Res.* **58**, 372, (2001)
2. J.K. Suh and H.W. Matthew, *Biomaterials,* **21**, 2589(2000)
3. D.W. Hutmacher J.C. Goh and S.H. Teoh *Ann Acad Med Singapore,* **30,** 183, (2001)
4. N. Shanmugasundram, P. Ravichandran, P.N. Reddy, N. Ramamurthy, S. Pal K.P. Rao*, Biomaterials* **22**, 1943(2001)
5. H. Shikhu, T. Saito C.-C, Wu, T. Yasukawa, M. Yokoo, H. Abe, T. Matsue, H. Yamada, *Chem. Lett*. **35**, 234 (2006)
6. (a) K.U. Senthil, R. Rajini, B.S.R. Reddy, *J. Memb. Sci,* **254**, 169 (2005), (b) H. Makamba, J.H. Kim, K. Lim, N. Park, and J.H. Hahn, *Electrophoresis*, **24,** 3607 (2003).
7. M. Rutnakornpituk, P. Ngamdee, and P. Phinyocheep, *Carbo. Polym.,* **63,** 229 (2006).
8. H.M. Jeong, J.S. Choi, Y.T. Ahn, and K.H. Kwon, *J. Appl. Polym Sci.,* **99**, 2841 (2006)
9. Z. Gao, J.S. Nahrup, J.E. Mark, and A. Sakr, *J. Appl. Polym Sci.,* **96**, 494(2005)
10. J.H. Park and Y.H. Bae. *J Biomed Mater Res Part: A*. **64,** 309, (2003)
11. F. Lim, C.Z. Yang, and S.L. Cooper, *Biomaterials* **15,** 408(1994)
12. W. Fernando, and S. Kestur*, J Colloid Intern Sci.,* **2,** 532(2005)
13. G. Emmanuel *Appl Organomet Chem* **12,** 675, (1999)
14. Y. Dong, and S.S. Feng **26**, 6068 (2005)
15. S.R. Suprakas, and O Masami Macro Rapid Comm 2003;24(14):815-840.
16. D. Depan, R.P. Singh *J Biomed Mater Res Part A*, **78,** 372(2006).
17. S.D. Burnside, and E.P. Giannelis, *Chem. Mater*., **7**, 1597 (1995).
18. H. Ishida, S. Cambell, and J. Blackwell, *J. Chem. Mater*., **12**, 1250 (2000).
19. K.K. Ofori and J.T. Fell, *Int. J. Pharm.* 26, 139(2001)
20. A.W. Basit, *Drugs* **65**, 1991 (2005)
21. I.Y. Kim, S.J. Kim, M.S. Shin, Y.M. Lee, D.I. Shin and S.I. Kim, J. Appl. Polym. Sci. **85,** 2661(2002)
22. D.K. Kweon, *Polym. Bull*., **41,** 645 (1998).

23. Y. Inoue, J. Watanabe, and K. Ishihara, *J. Colloid. Interface. Sci*., **274,** 465 (2004).
24. K. Ogawa, S. Hirano, and T. Miyanishi, *Macromolecules,* **17,** 973 (1984)
25. T. Yui, K. Imada, and K. Okuyama, *Macromolecules.,* **27**, 7601 (1994).
26. K.E. Strawhecker, and E.Manias E. *Chem. Mater.* **15**, 844 (2003).
27. R.Y.M. Huang, G.Y. Moon, and R. Pal, *J. Membr. Sci*., **184**, 1 (2001)
28. Y. Peneva, E. Tashev, and L. Minkova, *Euro. Polym. J*. **42**, 2228 (2006)
29. S. Tanner, H. Chanzy, M. Vicendon, J.-C, Roux, and F. Gaill, *Macromol.,* **23**, 3576, (1990)
30. M.F. Cervera, J. Heinamaki, M. Rasanen, S.L. Maunu M. Karjalainen, O.M.N. Acosta, A.I. Colarte, and J. Yliruusi. *Carbohyd. Polym*., **58**, 401 (2004)
31. D.J.T. Hill, C.M.L. Preston, and A.K. Whittaker, *Polymer*. **43**, 1051(2001)
32. X. Qu, A. Wirsen, and A.-C. Albertsson, *Polymer*. **41**, 4841 (2000)
33. K. Takashi, and M. Alexandre, *J. Appl. Polym. Sci.* **89**, 2072(2003).
34. G. Fundueanu, M. Constantin, and P. Ascenzi, *Biomater.,* **29,** 2767 (2008).
35. A.P. Kumar and R.P. Singh *J. Appl. Polym. Sci.* **104**, 2672 (2007).
36. Z.-K. Xu, F.-Q. Nie, C. Qu, L.-S. Wan, J. Wu, and K. Yao, *Biomaterials* **26,** 589(2005).
37. Y, Iwasaki, and N. Saito, *Colloid. Surf B: Biointerf*., **32,** 77 (2003).
38. T. Goda, J. Watanabe, M. Takai, and K. Ishihara, *Polym.*, 2006;**47**:1390–6.
39. H. Kitano, A. Kawasaki, H. Kawasaki, and S. Morokoshi, *J. Coll. Inter. Sci*., **282,** 340 (2005).
40. J.H. Lee, G. Khang, J.W. Lee, and H.B. Lee, *J. Coll. Inter. Sci*., **205**, 323 (1998).

CHAPTER V

Preparation and Characterization of Novel Nanohybrid of Biomineralized Zn-Al Layered Double Hydroxides using Chitosan as a Template

5.1 INTRODUCTION

Biomineralization is the process leading to the formation of a variety of solid inorganic structures by living organisms, such as intracellular bone, teeth, egg-shells, algae and invertebrate exoskeletons, and also pathological biominerals such as gall- and kidney stones. Molecular biomimetics or biomineralization is the marriage of physical and biological fields that lead to the formation of a variety of solid inorganic structures by living organisms, such as sea-shells, intracellular bone, teeth, algae and also pathological biominerals such as gall and kidney stones[1]. Material scientists have shown ample interest for biomineralization process because the produced inorganic-organic hybrid biocomposites by natures self assembled processes show interesting properties with a controlled morphological structure and well defined. In biominerals, the organic component exerts a reinforcing effect on the mechanical properties and expels the mineralization process, to the formation of particles of well-defined size, novel crystal morphology, specific crystallographic orientation and superb properties[2].

In biomimetic mineralization, commonly designed experiments involve the combination of insoluble templates/matrixes and soluble macromolecules in an aqueous medium. A frequently used template is Chitosan (CSI) film/fiber, which is present in all mollusks shells and is believed to play an important role during the biomineralization process *in-vivo*. The matrix exerts a control through supramolecular architecture with soluble macromolecules, while soluble additives act as the enriching agency of metallic ions via electrostatic/coordinative interaction to form nucleation points for the crystallization. There are few reports of biomineralization and duplication of living bio-assembly by associating a biopolymer and a mineral, such as polylactide/layered silicate nanocomposites[3]. Alginate-silica biocomposite was used for enzyme and cell immobilization[4]. Polymers have been used to control the nucleation and growth of calcium carbonate crystals. In many cases, the field of biomineralization has motivated these studies. Many polysaccharides are natural block copolymers and consist of two or more different glycosidic monomer units. Alginates, which, are extracted from seaweed, are composed of mannuronic and glucoronic acid residues. Their importance in the field of biomineralization, where anionic polysaccharides provide the template for the intricate hierarchical assemblies of calcium carbonate in cocoliths[5], relatively little work has been done on the systematic study of the influence of simple polysaccharides on calcium carbonate crystallization. Chitosan, is a partially

deacetylated derivative of chitin, which is a natural polymer found in the cell wall of fungi, microorganisms and in all mollusk shells, is believed to play an important role in controlling the biomineralization process, *in vivo*[6].

The biomineralization process mainly occurs through the following steps: (1) the matrix forms a mineralization framework, where metal ions are entrapped and associated through electrostatic interaction with soluble proteins/polysaccharides and adopts its shape; (2) subsequently an oriented nuclei form across the intracellular sites and the crystallization front propagates from the surface of the matrix, resulting in the formation of a single crystal with controlled orientation and predetermined microstructure. The biomolecules control crystal habit, morphology, as well as the size and shape of crystal complexed with organic substances. If we could even partly mimic such biomineralization processes, new high-performance and/or functional materials that are environmentally benign could be obtained with energy consumption.

Ibuprofen (Ibu) is a non-steroidal anti-inflammatory (NSAID) drug used for the relief of rheumatoid arthritis and osteoarthritis. Due to frequent side effects, its use is often limited[7]. These problems could be reduced by a formulation able to control the drug release. As matrices to prepare a controlled release formulation, we have taken into account lamellar compounds. The idea was to store the drug in the interlayer region of the lamellar host and allow the drug release as a consequence of a de-intercalation process.

Lamellar LDH structure is commonly described as edge-sharing octahedral sheets in which, by comparison with the Brucite M $(OH)_2$, some of the divalent cations are replaced by trivalent cations. The excess of charge, i.e. Al^{+3} content, is counter balanced by interlayer anions, leading to an anionic exchange capacity. The latter may be as high as 2.46 mq/g and associated with a layer charge density of 25.4Å^2 per e^- for a ratio of 2 Zn to Al of 2. The general formula for LDH is $M^{+2}_{1-x}M^{+3}(OH)_2$. $(A^{n-})_{x/n}$. mH_2O, where M^{+2} is the divalent cation, M^{+3} is the trivalent cation, A^{n-} is the interlayer anion, and mH_2O refers to the water in the interlayer space.

For biological applications, the use of LDH was limited as an antacid agent[8], where dissolved LDH was used as a buffer and acids were neutralized in the presence of its basic components (carbonate and hydroxyl ions). Other uses of LDH were also reported[9, 10], however, none of them focused on utilizing the intercalating properties as a drug delivery/carrier agent, until Ambrogi and coworkers[11]. The authors investigated the intercalating properties and sustained drug release properties of LDH by using Ibu

as a model drug. This study was followed by other reports of successful intercalation of drug molecules into LDH[12-14]. In continuation to this Kwak[15] et al proposed LDH as the gene delivery agent where DNA can be intercalated for gene therapy applications. Later on, Tyner[16] et al reported the successful expression of gene, following a LDH facilitated transfection. This study has its importance which lies in the fact that biological macromolecules can be intercalated in LDH, delivered as a LDH bionanohybrids, and can be de-intercalated within the cell without loss of its functionality. Based on these studies, it may be concluded that the LDH can be classified as a bio-ceramic and has tremendous potential in drug delivery system (DDS). The primary objective of the current study is to contribute to the eventual development of a new generation biomaterial based on LDH for applications as a drug carrier. Therefore, a couple of issues, namely, biomineralization, bio-interaction and in-vitro release studies, including buffer properties and cell-proliferation studies to be addressed. Bio-interaction is a central issue in DDS, which involves not only biocompatibility but also the behavior of the LDH system *in-vitro*. The study of bio-interaction was initiated by performing an extensive literature survey to assimilate and evaluate existing data on LDH from a drug delivery perspective. Following this, two specific objectives were set. Firstly, to identify the parameters involved in the synthesis of LDH, with compositions suitable for DDS. It is noteworthy here that the composition/formulation of DDS would include elements which are prevalent in the physiological system and, therefore, would offer the highest biocompatibility. Second objective is to formulate a robust methodology to produce LDH with Zn and Al ions. Unlike the Brucite like layers, the interlayer region of LDH is not a rigid structure. It primarily consists of ionic bonds between the anions and the Brucite like layers. The structure is further stabilized through Hydrogen-bonding between the interlayer water molecules with the hydroxyls, as well as between the –OH on adjacent sides. The interlayer anions and water molecules are free to move since these bonds can form and reform much like in water. Thus the anions can be exchanged with other negatively charged species such as drugs and genes, thereby varying the interlayer spacing. The inherent structural flexibility of LDH allows many different types of anions to be intercalated; the list includes both organic and inorganic anions, ranging from simple amino acids to proteins and DNA, as well as drugs[17] genes[18], adenosine monophosphate[19] and biopolymer such as poly (α, β-aspartate)[20].

CSI molecules have C=O, -OH and -NH groups on its backbone, which can coordinate strongly with the Lewis acidic sites. This interaction is supposed to occur during the growth of LDH crystals, which can lead to specific size, control and morphology[21]. We have intended to know how the biopolymer could direct an ordered structure with specific morphology and could orientate the assembly of inorganic intricate lamellae. Their biological importance is due to the fact that inorganic/polymer compositions can be designed to imitate and/or simulate various biomineralization processes. Moreover, CSI can provide the necessary controlled release and buffering property for the prepared nanohybrids to be used as an effective antacid. So, we choose to synthesize LDH/CSI hybrids by a co-precipitation route involving the *in-situ* formation of LDH layers. Intercalation of Ibu was done by a well-known Ion-Exchange method. Here CSI acts as a templating molecule for LDH crystallization where it acts as a glue to consolidate nanosized LDH particles into larger scale aggregates. Generally, the macromolecule first formed a framework at the solution interface, and then Zn ions were bound to the polymer chain by the $–COO^-$ group, resulting in a local high concentration of the Zn ions inside the framework, consequently inducing the nucleation occurrence.

To the best of our knowledge, this is the first example of documentation of the preparation and physio-morphic investigation of Zn/Al layered double hydroxide using CSI as a template. The neutralizing and buffering capabilities of the nanohybrids in HCl aqueous solutions were also evaluated, followed by *in-vitro* cell-proliferation studies.

5.2 EXPERIMENTAL

5.2.1 Materials

Chitosan of low molecular weight (Mv $1.5x10^5$, degree of deacetylation was 85%) were obtained from Sigma-Aldrich. Aqueous solutions were prepared from chemicals of analytical grades: $AlCl_3.6H_2O$ (purity>99%, Merck), $ZnCl_2$ (98%, Merck), NaOH (98%, S.D. Fine Chemicals). Deionized water (resistivity of 18.2MΩ.cm) was obtained with a Millipore ultra pure water system, which was previously distilled and decarbonated by boiling and bubbling inert gas (N_2).

5.2.2 Synthesis procedure by Co-precipitation method:

First CSI is dissolved in 300ml of bidistilled water. Chitosan was dissolved in an aqueous solution of lactic acid, then NaOH was added to the biopolymer solution to reach a pH value of 9 to ensure complete deprotonation of carboxylic groups of CSI. Such a pH value is compatible with the standard co-precipitation of Zn-Al LDH as reported by de Roy[22]. $AlCl_3.6H_2O$ (0.68g) and 0.603g of $ZnCl_2$ were dissolved in 500ml of decarbonated bidistilled water. This solution was added drop-wise with an addition funnel to the biopolymer solution while kept under nitrogen atmosphere, to avoid the CO_3 contamination. [Zn^{2+} + Al^{3+} = 1 mol l^{-1}, Zn/Al = 3, were continuously added 12ml h^{-1}. Zn^{2+} + Al^{3+} concentration was about 0.14 mol l^{-1}.]

Simultaneously, a solution of 1M NaOH was also added drop wise to the biopolymer solution through an additional funnel by keeping a constant pH of 9 during the synthesis. The precipitate was aged in the mother liquid for 24h, and the white solid products were isolated by repeated centrifuging and washing with decarbonated water and finally dried at 40°C. The $[Zn_2Al\ (OH)_6]Cl.\ nH_2O$ LDH without intercalated biopolymer, denoted as LDH was synthesized following the same procedure but replacing the biopolymer solution with bi-distilled water.

Precipitation of LDH occurs at pH values of 8.5-9.0, where the solubility of Zn chloride is much higher than that of Al chloride. Therefore, almost all the Al is co-precipitated with the Zn ions to obtain a solid with the stoichiometry of two Zn for each Al. This corresponds to an ideal disposition in the Brucite-like sheet of each Al atom surrounded by six Zn atoms. During the centrifuging, sealed containers were used to avoid contact with air, and the deionized-distilled water used for synthesis and washing, was decarbonated prior to use by boiling and subsequent cooling in the absence of CO_2 by means of a gas-washing bottle filled with KOH solution. During the washing process, some of the LDH particles that remained suspended in the supernatant after centrifuging were discarded.

5.2.2 CHARACTERIZATION METHODS

5.2.2.1 X-Ray Diffraction:

The WAXD patterns of the sample powder were obtained using a Rigaku (Japan) Dmax 2500 X-ray diffractometer with Cu-Kα radiation. The system consists of a rotating anode generator with a Cu target and a wide angle powder goniometer having

a diffracted beam graphite monochromator. The generator was operated at 40 kV and 150 mA. All the experiments were performed in the reflection mode. The samples were scanned between 2θ= 2° to 70 ° at a scan rate of 5°/minute. The d-spacing was calculated by Bragg's formula, where the λ was 0.154 nm.

5.2.2.2 Transmission Electron Microscopy:

Transmission electron microscopy (TEM) was carried with a JEOL 2000 EX-II instrument (JEOL, Tokyo, Japan) operated at an accelerating voltage of 100 kV. TEM samples were prepared by dipping carbon coated copper TEM grids into dilute suspensions of the sample powder in ethanol, followed by sonication in a probe sonicator for 30 minutes.

5.2.2.3 FTIR- Spectroscopy:

The Fourier-transform infrared (FTIR) spectra were obtained from the sample on a Perkin-Elmer Spectrum GX. The samples were mixed with dry KBr, pelletized and then scanned in the range of 4000 cm-1 to 400 cm^{-1} at a resolution of 4 cm^{-1}. A total of 10 scans were used for signal averaging.

5.2.2.4 Atomic Force Microscopy (AFM) analysis:

AFM images of pristine CS film and biomineralized CS samples were taken on a Nanoscope IV AFM instrument under contact mode. The height (topography) and phase images were performed with a tapping silicon tip with specified resonance frequency of ~ 280 kHz and nominal tip radius of curvature smaller than 10 nm. Typical scan rate for image acquisition was ~1.00 lines/sec.

5.2.2.5 Scanning Electron Microscopy:

The internal structure and surface morphology was investigated by SEM (JEOL Stereoscan 440, Cambridge).

5.2.2.6 ^{13}C and ^{27}Al NMR:

The proton-decoupled solid state ^{13}C-NMR (I = 1/2) CP-MAS NMR spectra were obtained in a Bruker Avance 300 spectrometer, using a standard cross-polarization pulse sequence. Samples were spun at 10 kHz. Spectrometer frequencies were set to 100.62 for ^{13}C. The numbers of scans were of 800. The cross polarization

time was 0.5 ms. Chemical shift values were referenced to tetra methyl silane (TMS). ^{27}Al (I = 5/2) CP MAS NMR spectra were obtained in a Bruker Avance 300 spectrometer, using a standard cross-polarization pulse sequence. Samples were spun at 10 kHz.

5.2.2.7 Thermal Methods:

Thermal gravimetric analysis (TGA) was conducted on a Perkin-Elmer TGA 7- thermal analyzer from 50°C to 900°C with a heating rate of 10°C min^{-1} under nitrogen with flow rate 20ml min^{-1}, in a platinum crucible.

5.2.3 IN-VITRO STUDIES

5.2.3.1 Buffering Capability:

Buffering or neutralizing capability of the prepared nanohybrids was evaluated by monitoring the change in the pH value of the sample suspension with addition of 0.1 mol/L HCl aqueous solution at 37 ˚C. In a typical experiment, 100 mg of the powdered sample was suspended in a 10 ml of deionized water and kept stirring at 37 °C. At a regular interval of time, aliquots of 0.1-0.5 mL of the HCl aqueous solution were added to the suspensions until the pH reached the value of ca. 1. This procedure was repeated until the entire solid was dissolved.

5.2.3.2 In-Vitro Drug Release:

For in-vitro drug release studies, Ibuprofen (Ibu) was taken as model drug. For this study, 1g of LDH and CSI-LDH was added to 80 ml of a 5 mM aqueous Ibu drug solution at 60 °C and stirred for three days. The resulting Ibu loaded samples were dried under vacuum and washed thrice with hexane to remove unadsorbed Ibu. Release studies were performed by dispersing Ibu-LDH and CSI-Ibu-LDH in 200 ml Phosphate Buffer Saline (PBS, pH 6.8) at 37 °C in the USP XX paddle type apparatus and the Ibuprofen content (mass/volume ratio) was selected in order to simulate sink conditions, according to the Ibu solubility at this pH value[23]. Aliquots of 4 ml of dissolution medium were taken at different time interval, filtered with a 15 mm micro filter unit, and their Ibu content was determined by UV absorption at 264 nm.

5.2.3.3 Cell-Viability Studies:

Cell viability studies were performed on HL-60 Leukemia Cell Line and the procedure was followed in accordance with the procedure suggested by Jae[24]. After allowing 24 hours for cell adhesion, the cells were analyzed everyday (3 flasks per day) for 6 days. The relative cell-growth compared to control cells containing cell culture medium without CS was calculated by $[A]_{test}/[A]_{control}$. For this, after every 24 h, 100 µl of the cell culture was incubated for MTT assay and the absorbance was taken at 490 nm wavelength in Spectrophotometer Plate Reader.For this, after every 24 h, 100 µl of the cell culture was incubated for MTT assay and the absorbance was taken at 490 nm wavelength in Spectrophotometer Plate Reader. All the in-vitro tests were made in triplicate and the results were recorded as an average.

5.3 RESULTS AND DISCUSSION

5.3.1 Biomineralization Process

The process of biomineralization is usually related to the inorganic-organic interface reaction governed by hierarchical series of forces, such as hydrogen bonding, dipolar forces, van-der Walls forces, hydrophilic-hydrophobic interactions, structural and stereo-chemistry, and so on. In this process, the mineral nuclei will continue to grow within the confines of their supramolecular host. The most important principle understood from biomineralization processes is that nucleation and growth of the biomineral phase are almost carefully and exquisitely controlled by complex organic matrix biopolymer pre-organized supramolecular templates. Macromolecules play an important role in the amorphous-crystal transformation; these macromolecules act as conduits for the removal of water, stress, and impurities during the transformation from an amorphous structure to a crystal, implying a multi-step crystallization process in biomineralization.

Air must be carefully excluded prior to the nanohybrid synthesis in order to avoid incorporation of carbonate ions into the product. The preferential accommodation of carbonate is readily explained as a result of the favorable lattice stabilization enthalpy associated with the small, highly charged CO_3^{2-} anions, and is well known to cause difficulties in preparing LDHs with singly charged anions such as hydroxide and nitrate. Attempted synthesis of the polymer-LDH nanocomposites in air always resulted in the carbonate form with no evidence of polymer incorporation. Once prepared under

N_2, however, the polymer-containing nanocomposites are air stable. As a test, some nanocomposites were stirred in an aqueous solution of sodium carbonate for one week, with no evidence of exchange of polymeric anion for carbonate, as confirmed by XRD and chemical analysis. Here, CSI acts as template for LDH synthesis. The above results suggest that CSI has been successfully used as a kind of bio-mineralization template to modify LDH particle aggregation. CSI molecule dissolved in water can form regular self-assembled organic superstructure, and the hydroxyl and amino groups in CSI can coordinate strongly with Zn^{2+} and Al^{3+}. The growth of the LDH crystallites, which occurs at the inorganic-organic interface, is therefore, templated by CSI because of its coordination with Zn^{2+} and Al^{3+} located on the surface of LDH sheets. It is expected that a kind of organic template, which has stronger interaction with metal ions on the layers, can change the morphology of LDHs particles more significantly.

5.3.2 XRD Analysis

Figure 5.1 shows the powder XRD patterns of LDH and CSI-LDH. The d_{001} spacings are obtained by the first rational orders corresponding to the *00l* reflections. The XRD pattern of LDH exhibits strong basal sharp set of (*001*) reflections, indicative of a long-range ordering in the stacking dimension. Samples have not been contaminated by atmospheric carbon dioxide, as no peak corresponding to a secondary carbonate-intercalated hydrotalcite-like phase is recorded. The first peak occurring at a low 2θ angle was attributed to the reflections from the (*003*) family of crystallographic planes, which equals the thickness of one brucite-like layers (approximately 4.8 Å) plus one interlayer repeat distance d (where $d=\lambda/2\sin\theta$). All the peaks were indexed in a hexagonal unit cell with R_3m rhombohedral symmetry, where C_0= 23.19 Å, which corresponds to three times the distance between adjacent layers of interlayer distance of 7.73 Å, confirming the hydrotalcite-like material[25]. In addition, the sharp and symmetric features of the diffraction peaks reveal the high crystallinity, three-dimensional stacking order of the prepared LDH. The analogues peaks for the CSI-LDH are calculated from the d_{00l} spacing and the thickness of the inorganic layers. LDHs crystallites grow faster in (*110*) than in (*003*), because of closer crystal plane distance of (*110*)[26].

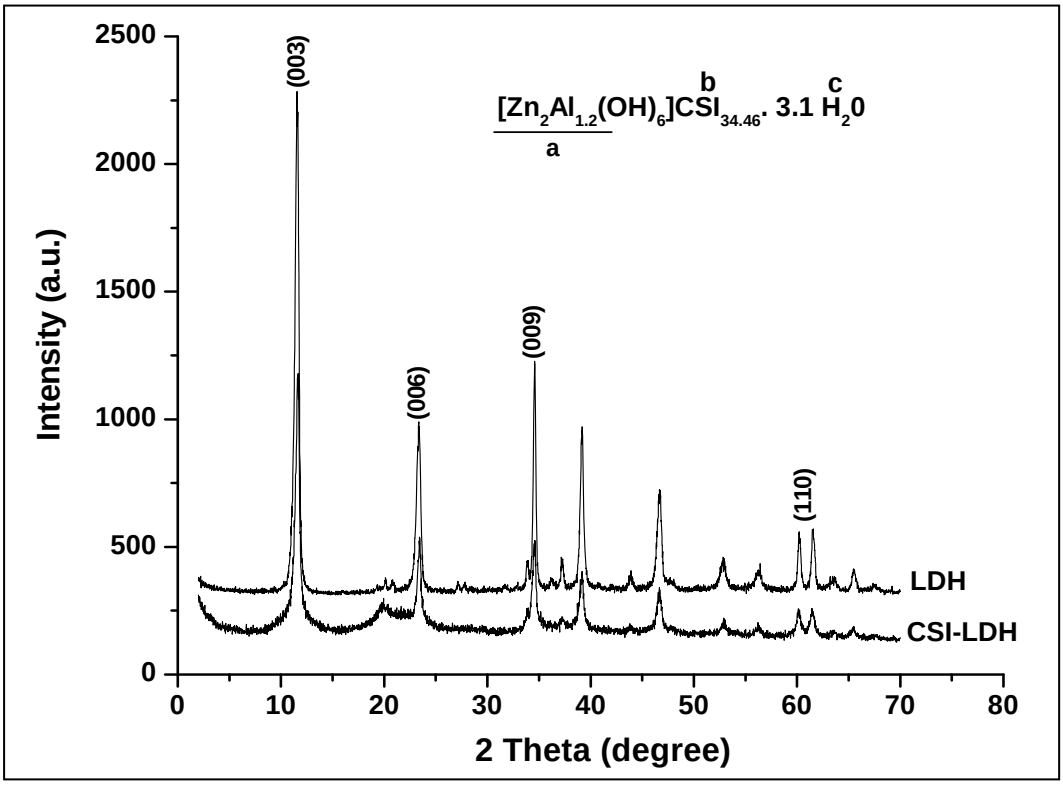

Figure 5.1 XRD patterns of the prepared nanohybrids.

The average value of d_{003} for CSI-LDH is 13.96 Å. If the width of the brucite like-layer (4.8 Å)[27] is subtracted, the gallery height is 9.16 Å for the CSI- (the size of the CSI is 7.23Å), somewhat smaller than the gallery height. This means that there is space enough to accommodate the biopolymer with its polysaccharide chain perpendicular to the layers in the interlayer, along with water molecules, even at high layer charge densities. The dimension of the interlamellar gap (~8 Å) is consistent with the presence of the biopolymer lying more or less perpendicularly to the sheets. As a more thorough investigation of the structure and properties of LDH using chitosan as template, the N_2 adsorption experiments were carried out to feature the surface area and the pore volume. Specific surface area of Zn-Al LDH decreases from 47.96 to 1.03 m^2/g and pore volume decreases from 0.29 to 0.01 cm^3/g, upon adding 2 g/l of CS, indicating the strong agglomeration of LDH primary particles onto CS.

5.3.3 FT-IR Spectra

FT-IR spectra of LDH and CSI-LDH, in the range of 4000-400 cm^{-1}, as shown in **Figure 5.2**, which shows vibration bands at 1622 cm^{-1} (δ_{HOH}), 787 and 621 cm^{-1} (ν_{M-}

$_O$), and a peak around 420 cm^{-1}, which is attributed to the $\delta_{O\text{-}M\text{-}O}$ deformation vibrations in the LDH sheets[28] indicating that the LDH structure is truly formed when CSI is used as a template, as confirmed previously by XRD.

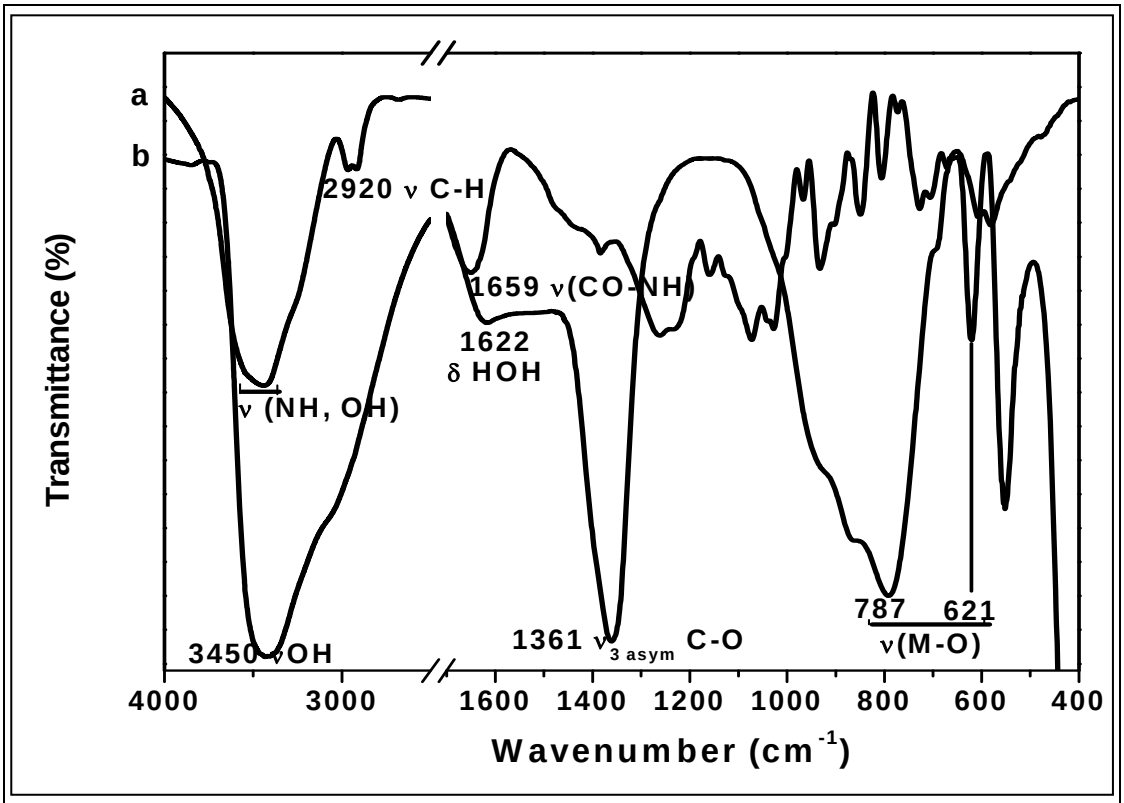

Figure 5.2 FT-IR spectral analysis of the prepared nanohybrids.

A strong vibration band around 3450 cm^{-1} is observed in both the spectra and is attributed to the stretching vibration (ν_{OH}) of water molecules and hydroxyl groups belonging to brucite layers[29]. For CSI-LDH, the bands arising from various functionalities of CSI are located at their characteristic wave number bearing amino and acetyl groups ($\nu_{N\text{-}H}$ at ~ 3450 cm^{-1}; $\nu_{O\text{-}H}$ ~3362 cm^{-1}, $\nu_{C\text{-}H}$ ~ 2920 cm^{-1}; amide II ~ 1659 cm^{-1}; δ_{NH_3} ~ 1597 cm^{-1}; δ_{CH}- 1320 cm^{-1}; $\nu_{C\text{-}O}$ of C-O-C ~1152 cm^{-1}), characteristics of the pyranose ring[30]. The amide I band at 1650 cm^{-1} is overlapped with δ_{HOH} bending vibrations at 1640 cm^{-1} of the water molecules associated to the nanohybrids, as expected for a biopolymer with high water retention capacity. A downshift in frequency corresponding to a weakening of the C=O (1361 cm^{-1}) bond strength is also observed. The disappearance of the C=O bond in CSI-LDH indicates the presence of an electrostatic binding with the anionic clay surface through a

hydrogen bond via the path C=O…H-O-M (M=Zn or Al). It has been accepted that the coordination of the O atom in the CSI decreases the electron density in the C-O bond and thus also decreases the force constant in the vibration resulting the downward shift of the C-O vibration band to the lower wave number side, which has been observed in the FT-IR spectra of CSI-LDH.

5.3.4 Microscopic Measurement

TEM micrographs of LDH and CSI-LDH is given in **Figure 5.3**, which clearly shows the thin plate-like morphology of LDH (**Figure 5.3 a**) having thickness of 30-40 nm and lateral dimension from 200 nm to 2 μm, while TEM of CSI-LDH (**Figure 5.3 b**) showed interesting curved tactoids with multiple layer agglomerates.

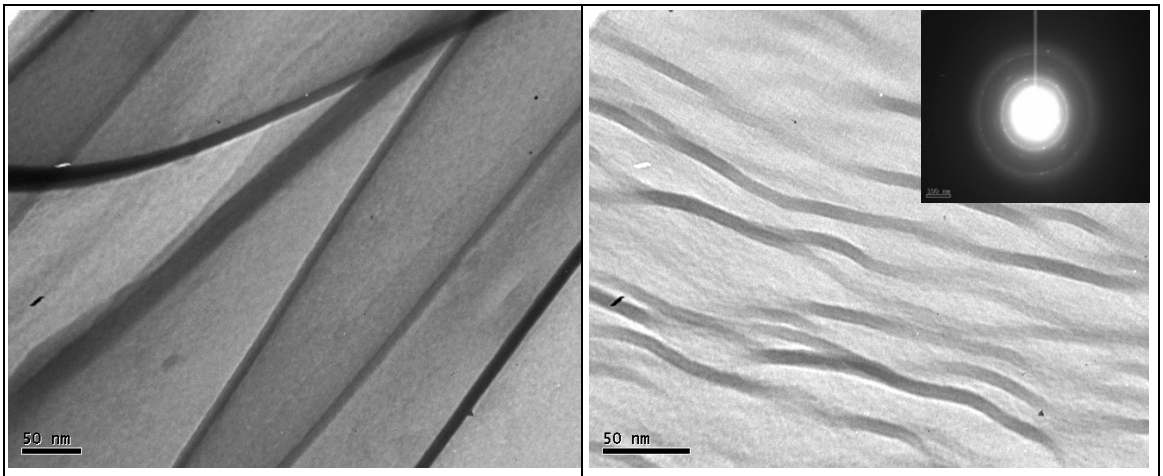

Figure 5.3 TEM images of (a) LDH (b) CSI-LDH and (c) Selected Area Electron Diffraction (SAED) of CSI-LDH.

He[31] and coworkers also observed similar morphology, and showed that it could be due to the strong agglomeration of the LDH primary particles on the biopolymer matrix. **Figure 5.3 c**, shows the corresponding selected area electron diffraction (SAED) of CSI-LDH, which displays a ring-pattern in agreement with the hexagonal plate like crystal structure with a crystallographic parameter a of 0.310 nm. These images are in good agreement with the results obtained from XRD and SEM.

The SEM image of LDH (**Figure 5.4**) shows the usual "sand rose" morphology of the LDH, which is quite different from that, observed in the SEM image of CSI-LDH. The micro crystals of the CSI-LDH differ from LDH with the presence of large hexagonal chunks. The biopolymer seems to provide compactness, which results in the aggregation of the LDH particles. This is due to the strong edge-surface platelet

interactions. Moreover, once the aggregates are formed they are very stable and resistant to de-cohesion even under powerful ultrasonic treatments. The size of the platelets is substantially reduced for the intercalation compound. The morphology of the LDH-biopolymer nanohybrids differs with the presence of large chunks. It is related to the synthesis pathway, with the LDH crystal being self-assembled on the biopolymer. Such arrangement of LDH layers and biopolymer slabs suggests the enhancement of mechanical and barrier properties of these nanocomposites. Their corresponding elemental analysis followed by Energy Dipersive X-ray analysis (EDAX) results (**Figure 5.4 c-d**) confirms the presence of particular constituent elements.

Because of its high spatial and vertical resolution, atomic force microscopy (AFM) has been previously applied to determine morphology of nano-sized objects. AFM has also proven very powerful in the study of smectite clay chemistry to determine the size distribution, the morphology of individual sheets and the structure of clay-polymers and even to track the crystallization process[32, 33]. **Figure 5.5** shows a typical AFM topographical image of CSI-LDH with LDH particles deposited onto the surface of CSI, by the biomineralization process. Isolated oval objects found in the AFM image, can be discerned on the CSI substrate. It is evident that all these particles have a uniform height distribution around 2.0 nm and a diameter distribution centered around 45 nm.

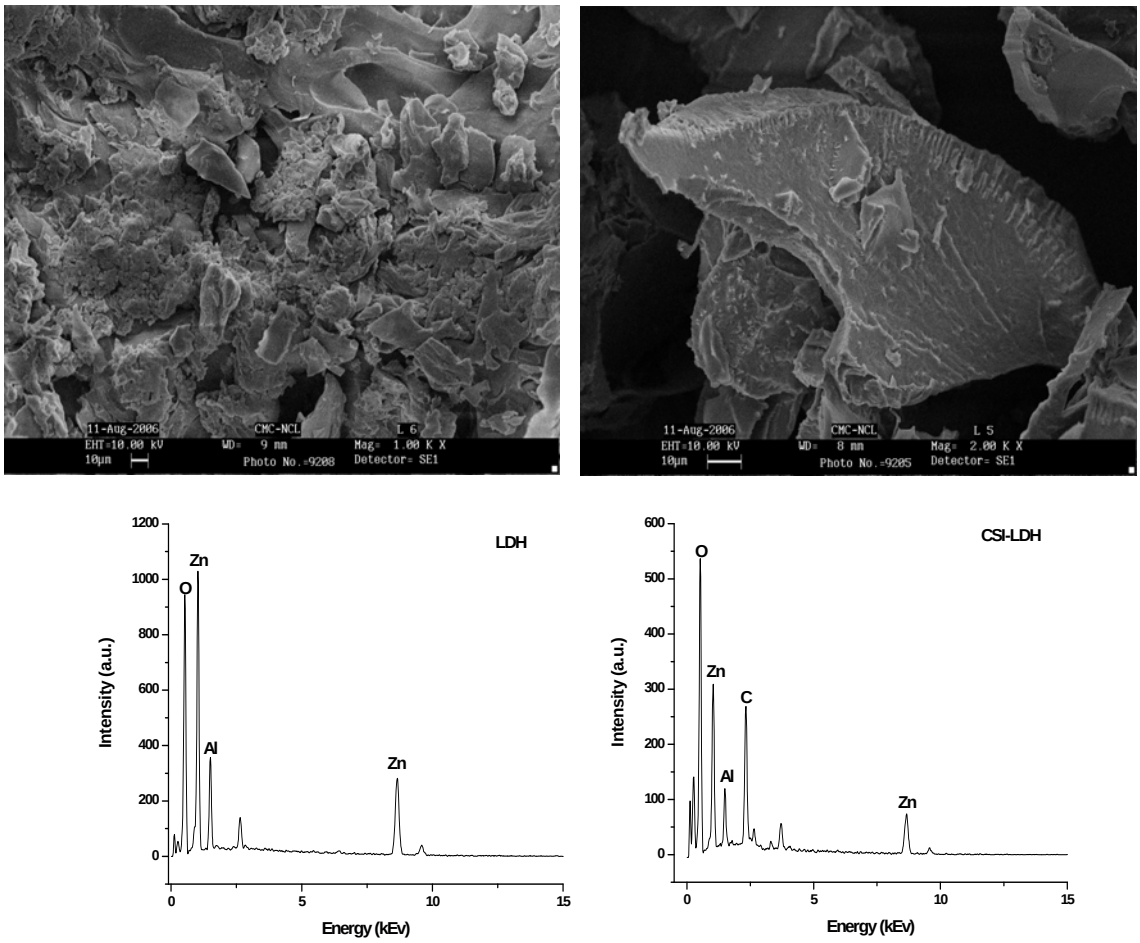

Figure 5.4 SEM images and their corresponding EDAX analysis results for (a) LDH and (b) CSI-LDH.

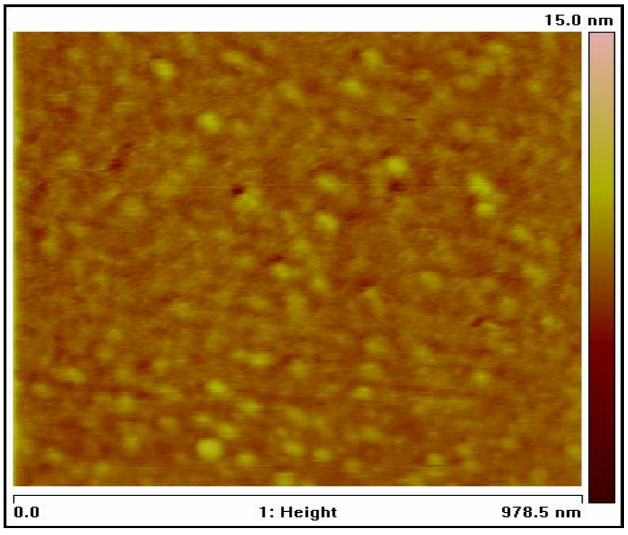

Figure 5.5 AFM image of CSI-LDH.

5.3.5 Solid State NMR Studies

Solid state CP-MAS ^{13}C-NMR is known to be very sensitive to changes in the local structure and the chemical shifts of C-1 and C-4 carbon in 1, 4-linked carbohydrate are believed to be highly sensitive to any conformational change at the glycosidic linkage[34]. The resonance peaks for CSI are assigned according to the literature[35]. The signals observed at 23.4 and 174.1 ppm, were attributed to the signals of $-CH_3$ and –C=O of the glucosamine ring, respectively (**Figure 5.6**). These peaks in CSI-LDH showed a slight shift, which is attributed to the electrostatic interaction between the biopolymer and positively charged Brucite layers, which is in qualitative agreement with the results obtained from TEM and FT-IR. Similar results were also observed when other macromolecular guest species is intercalated into LDH[36]. We have unsuccessfully tried to confirm the nature of the components related to Al species from ^{27}-Al-NMR spectra but only a single signal around 13.2 ppm (**INSET-5.6**), which corresponds to Al (III) in octahedral environment, appears in all the studied samples. The same type of signal is also observed in the LDH without CSI. EDAX analysis, along with ICP-AES, confirms the Zn/Al ratio for LDH and CSI-LDH as 1.87 and 2.1, respectively.

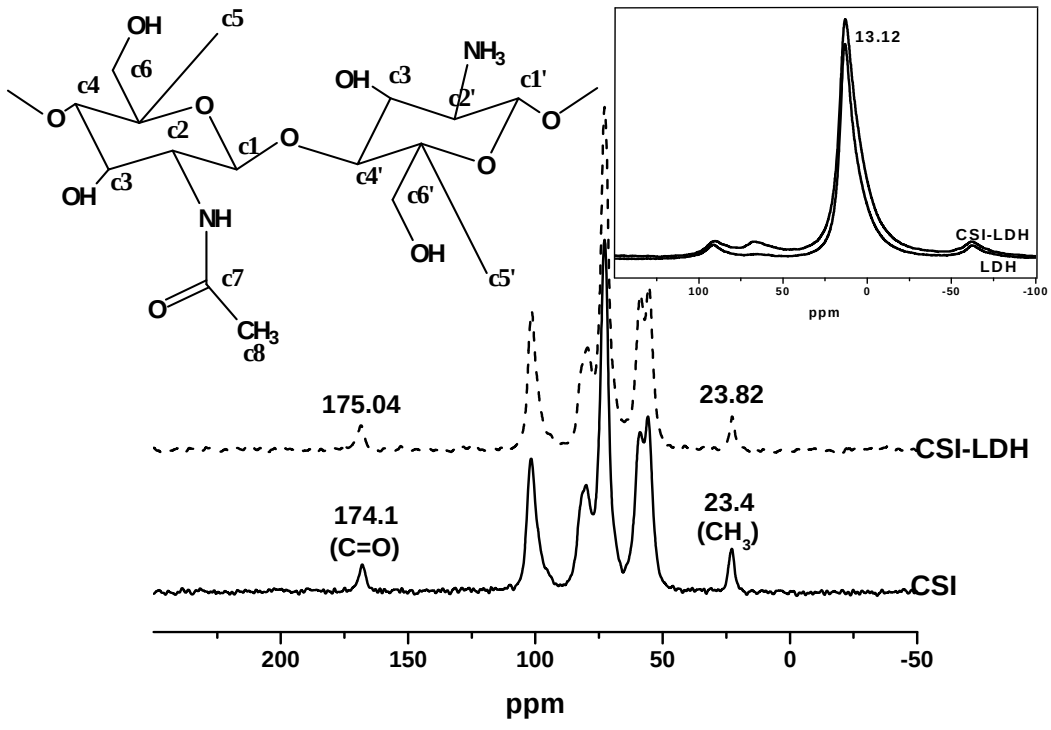

Figure 5.6 ^{13}-C NMR spectra of LDH and CSI-LDH. INSET figure shows the ^{27}-Al NMR of the prepared nanohybrids.

5.3.6 Thermal Analysis

TG and DTG traces for CSI-LDH and LDH are shown in **Figure 5.7** (a-b), respectively. The shape of the curves reflects good crystallinity degree of the samples. LDH shows two mass loss events as evidenced by a curve with two well differentiated regions. The first, corresponding to 15.5% loss between 50 °C and 210 °C, has been attributed to elimination of both non gallery surface adsorbed water and interlayer water molecules. The second event, approximately 28% loss from 300-450 °C, corresponds to the dehydroxylation and de-carbonation reactions of the Brucite layers[37]. The total mass loss, 43.5%, provides a water content of n=2.8 based on complete conversion to the metal oxides, which agrees well with previous estimates of n=2-4 for air-dried samples[11]. In contrast, three events are observed in the thermal trace obtained on the CSI-LDH. The first event, a 15% loss around 100 °C, correspond to the elimination of adsorbed water at the surface and between LDH layers. A second loss from 300 to 500 °C (23%) is ascribed to the dehydroxylation of the LDH layers and partial decomposition of the biopolymer.

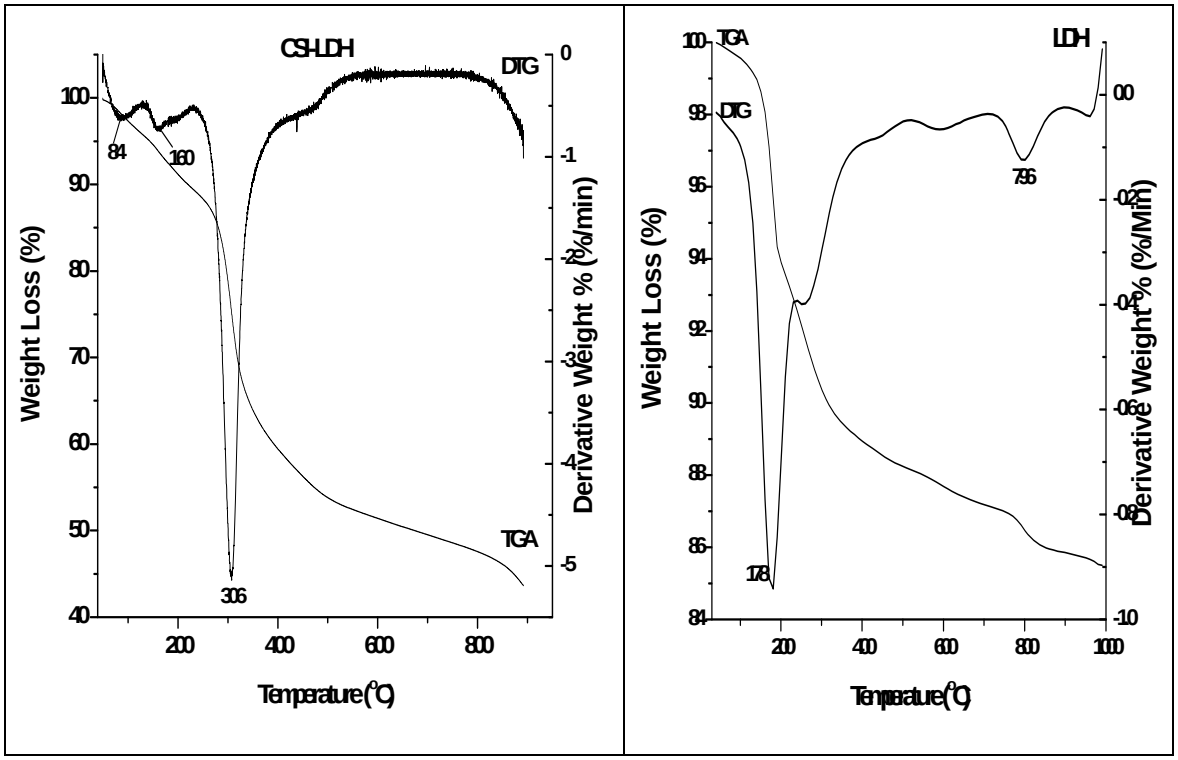

Figure 5.7 TGA and DTG Curves for (a) CSI-LDH and (b) LDH.

When the biopolymer is present between Zn_2Al-LDH sheets, the first process is delayed, and is concomitant with the dehydration and dehydroxylation of the inorganic layers. In contrary, the second process occurs at lower temperature for the

nanocomposites than for the polymer, and may be explained by the combustion of the organic residues favored by the presence of the oxide by-products arising from the degradation of the LDH moiety at this temperature. The final mass loss is observed at approximately 800 °C (22%) and is ascribed to complete oxidative elimination of the carbonaceous residue derived from the initial biopolymer degradation. It is important to mention here that the values of char yields were almost coincident with the amounts of the LDH in nanocomposites. Therefore, the increased char ratios mainly resulted from the nonvolatile LDH, and the char formation from organic part (biopolymers). Similar results were also reported for other polymer-silica hybrid materials[29]. On the basis of the above result, we may conclude that LDH in LDH-bionanocomposites might not alter the thermal degradation mechanism.

5.4 In-Vitro Studies

5.4.1 Buffer Capability

Buffering effects of the prepared materials were evaluated by monitoring the changes on the pH values due to the HCl addition into the perspective aqueous solutions.

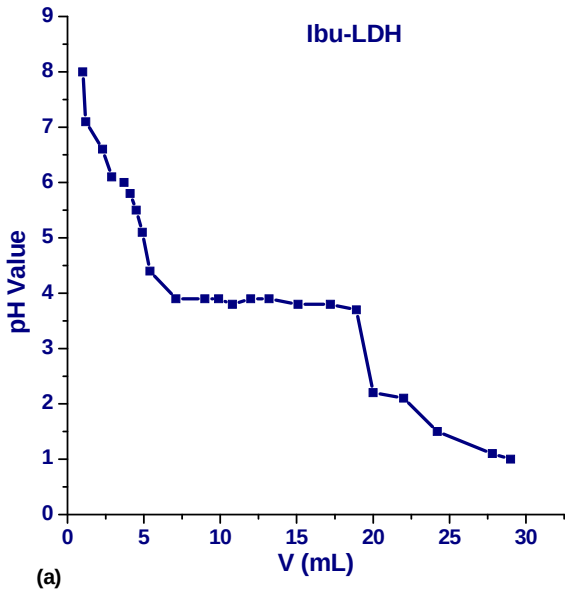

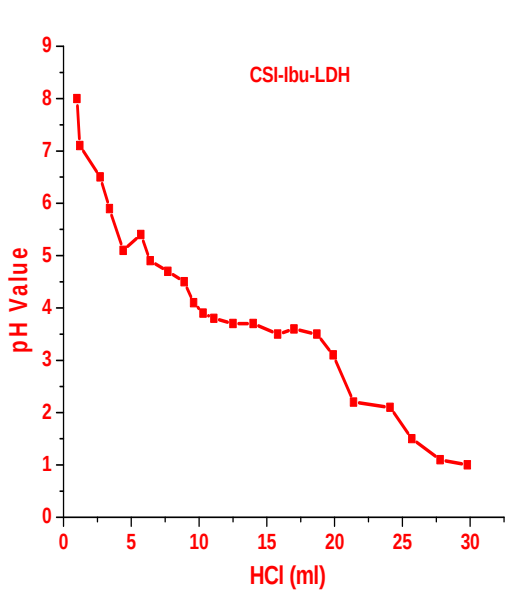

Figure 5.8 (a) Amount of HCl required for LDH. **(b)** Amount of HCl required for CSI-LDH.

The correspondent calibration graphs for the evaluation of buffer capability of the prepared nanohybrids are given in **Figure 5.8** (a-b). Ibu-LDH shows buffering effect by keeping the pH constant at 3.9 after an addition of 19 ml of HCl, while CSI-Ibu-LDH shows slightly more buffering activity due to the alkaline nature of CSI, which can effectively neutralize HCl. The neutralizing and buffering capabilities are due to the –OH and CO_3^{2-} located in the interlayer and on external surface of the LDH. The comparative results confirm that chloride anions adsorbed on the LDH external surfaces were exchanged by Ibu. In fact, the ion-exchange process on the external surfaces of the LDH contributes to decrease the amount of Cl anions, reducing the buffering capability of the material. In our study we have shown that, although gastric toxicity caused by the NSAID can occur due to their acidic nature or cytotoxic effects in the induction of gastric lesions, but these side effects could be reduced by the immobilization of the drugs on an antacid host.

5.4.2 Cell-viability

LDH and CSI-LDH were found to be non-toxic (the maximum concentration at 500 µg/ml) as evidenced by cell-viability studies as shown in **Figure 5.9**. The cell-viability was measured by MTT assay of fibroblasts cultures on the prepared nanohybrids. The viability of fibroblasts cultured is higher on the first day, while, it decreases with increasing time duration. It may be that during proliferation, cells may have occupied all the available spaces on the specimens. LDH and CSI-LDH did not show significant difference in the cell-viability. The lamellar host, in this study, is layered double hydroxides, which are composed of thin stacked lamellae of Zn and Al hydroxides that are combined with rather weak interaction such as Vander walls force and H-bonding. The interaction between the host (stacked lamellae) and guest (biopolymer and drug) compounds can offer an opportunity to develop various new hybrid compounds for pharmaceutical use. LDH may develop London-van der Walls forces and hydrogen bonding with the cells. As the biopolymer matrix is incorporated with LDH, the biopolymer would be surrounded and / or adsorbed onto LDH layers which can act as an adhesive between the polymer and the cells through hydrogen bonding between the hydroxyl groups of glycol proteins and the water of hydration on LDH.

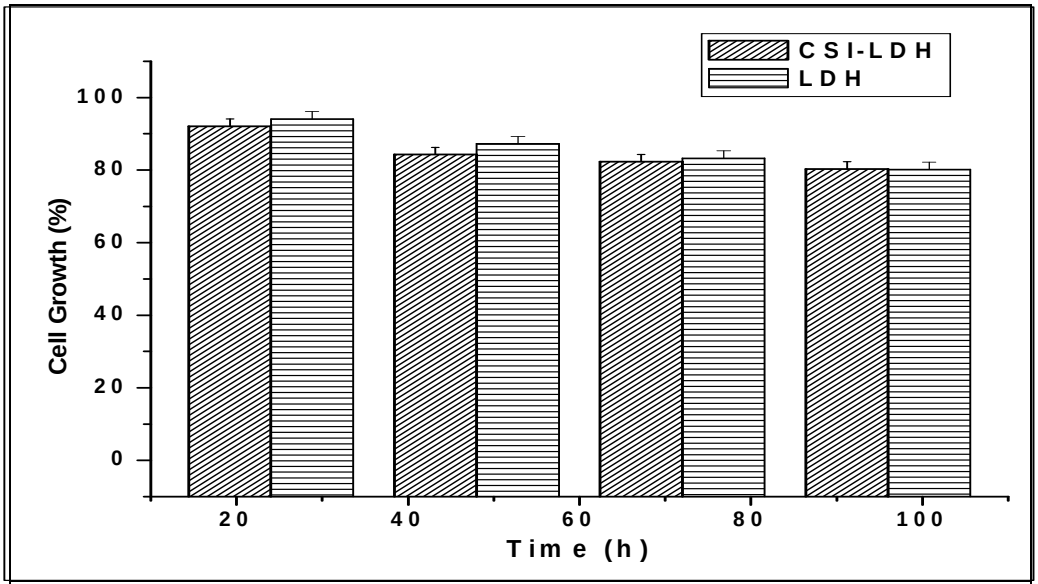

Figure 5.9 Cell-growth studies of the prepared nanohybrids.

Moreover, under acidic environment (pH 4-5) of cytoplasm, LDH disintegrates into Zn and Al ions that are cell-friendly and do not impart any toxic effects, even at a higher concentration, as proposed in the present study. Similar results were also observed by Kriven et al[38].

5.4.3 In-vitro release studies

Figure 5.10 shows the in-vitro drug release profile. For Ibu-LDH, 60 % of the drug was released after 20 minutes and 100 % after 120 minutes while for CSI-Ibu-LDH, it was 30 % drug release after 20 minutes and 100 % after 100 minutes. The interlayer region of this matrix acts like a micro vessel in which the loaded drug molecules can be released by a deintercalation process triggered by an ion exchange process, due to the ions already present in the phosphate buffer saline. This fluid is having the same pH and ionic concentration of small intestine. When LDH is dispersed in PBS solution, phosphate ions (small anionic species) will be in the proximity of stacked lamellae of LDH, and are more prone for an ion exchange process with the already present ions (drug molecules) of LDH. In the case of LDH, $H_2PO_4^-$ anions, once exchanged, react with the interlayer –OH of LDH to form layered hydroxyphosphates by a grafting reaction, where phosphates are no longer exchangeable and can obstruct the exit of intercalated Ibu, as suggested by Ambrogi et al[39]. As Ibu anions do not pass through the matrix directly, neither can pass over the grafted anions, they have to find the right pathway with consequent increase of the tortuosity and the length of the diffusion pathway in the limited and confined space. The effect of incorporation of

LDH layers can be significantly found as reduced rate of release at initial stage of immersion for both Ibu-LDH and CSI-Ibu-LDH.

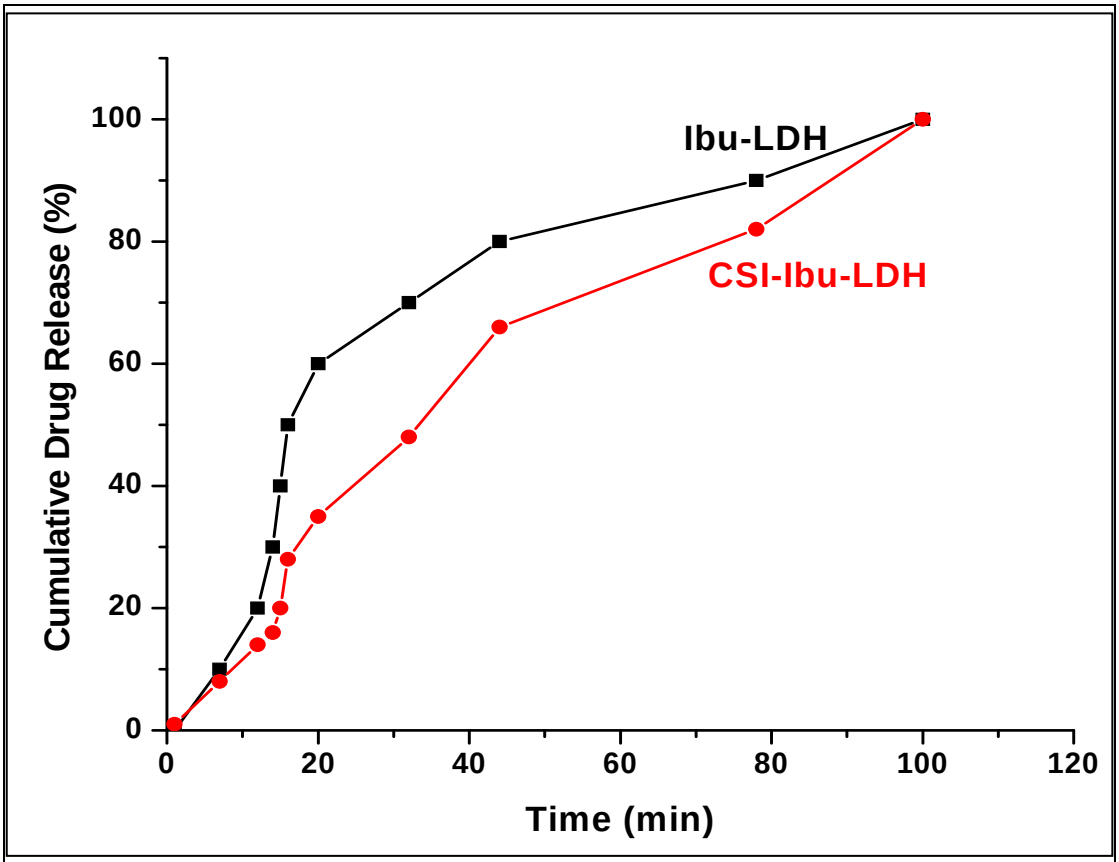

Figure 5.10 Drug release profile of Ibu-LDH and CSI-Ibu-LDH nanohybrids.

During initial stage of immersion (up to 25 min), the specimen is solvated, which facilitates the lateral diffusion of drugs. After 40-50 min, the rate of release is moderate and sustained over the time. This may be due to the interactions of LDH layers and biopolymer chains with the drug loaded. The interaction between the sodium salt of Ibuprofen and LDH surface is stable enough to exhibit the sustained release profile. In many pharmaceutical uses, drugs are exposed to various body fluids, such as blood, serum, and cytosol, which have a high concentration of salts and polyelectrolytes like proteins. In such conditions, the non-toxic minerals like LDH, which are ionic in nature, can flocculate with polyelectrolytes on the surface. The presence of CSI, results in the formation of the neutral biopolymer matrix on the surface, which is advantageous for the improvement of its dispersion stability and bioavailability. So, in the present study we have given a hypothesis of biosynthesis of LDH onto the surface of CSI and a novel approach of nanohybridization with Ibu drug molecules.

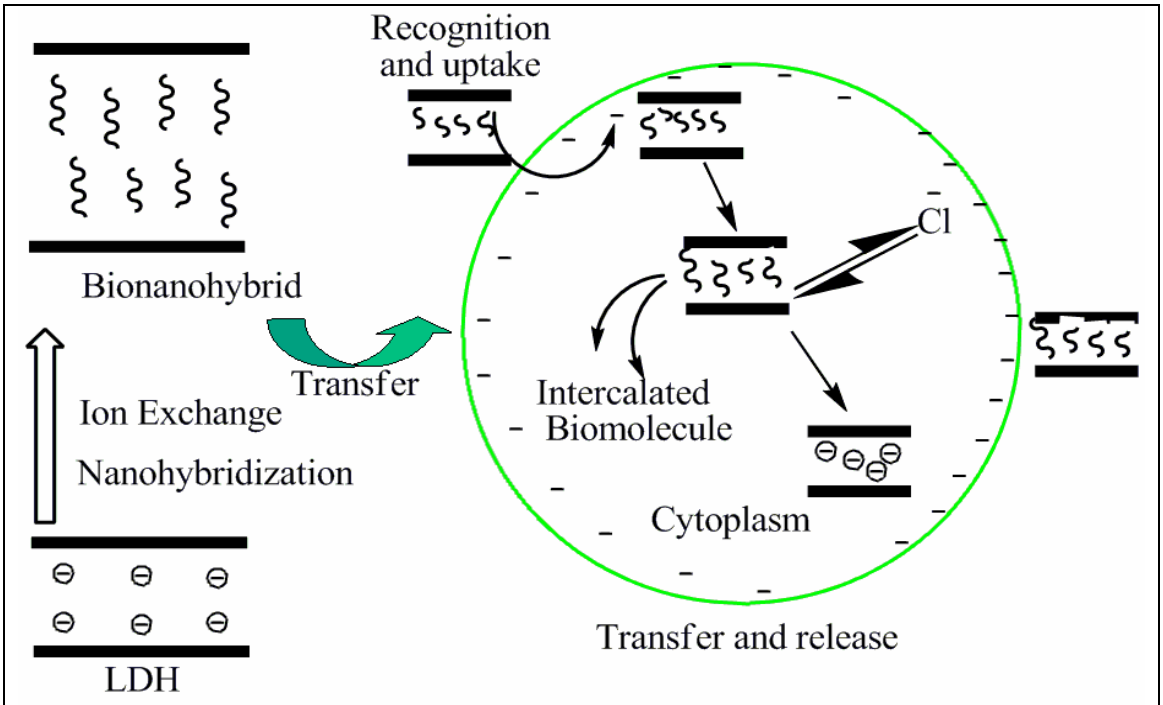

Scheme 5.1 Schematic illustration of preparation of nanohybrids and cellular uptake.

The prepared nanohybrids can be used as an effective nanocarrier of drugs and other bioactive molecules for site-specific drug delivery. Moreover, the prepared nanohybrids are cell-compatible and get dissolved in cellular environment to release the biomolecules as shown in **Scheme 5.1**.

5.5 CONCLUSIONS

In summary, this investigation provided evidence for the feasibility of template biomineralization of LDH onto CSI, with novel morphological and physiochemical properties, with an optimized route to avoid contamination by atmospheric carbon dioxide. XRD pattern indicates the formation of highly crystallized hydrotalcite-like phase. The buffer capability of the prepared nanohybrids in the pH range 3.6 seems to be ideal for the application as an antacid. The Ibu drug-release studies showed that the drug release was controlled for CSI-LDH. Our CSI-LDH nano hybrid approach represents a novel way to synthesize highly crystalline LDH, which can be used as inorganic carriers able to intercalate drugs and de-intercalation them in order to modify their release and to prepare a controlled release formulation.

5.6 REFERENCES

1. S. Mann, Oxford University Press, Biomineralization, Oxford, p. 198 (2001).
2. B. Smith, T. Schaffer, M. Viani, J. Thompson, N. Frederick, J. Kindt, A. Belcher, G. Stucky, D. Morse, and P. Hansma, *Nature*, **399,** 761 (1999).
3. P. Maiti, K. Yamada, M. Okamoto, K. Ueda, and K. Okamoto, *Chem. Mater.,* **14,** 4654 (2002).
4. T. Coradin, E. Mercey, L. Lisnard, and J. Lirage, *Chem. Comm.* **21**, 2496 (2001).
5. J.M. Didymus, P. Oliver, S. Mann and A.L. De Vries, *J. Chem. Soc., Faraday Trans*, **89,** 2891 (1993).
6. G. Falini, *Tissue Engineering*. **10,** 1 (2004).
7. M. Griffin, and M. Sheiman, *Am. J. Med*, **110,** S33 (2001).
8. A.C. Playle, S.R. gunning, and A.F. Llewwellyn, *Pharmac. Acta. Helvetiae.,* **49,** 298 (1974).
9. A. Ookubo, K. Ooi, and H. Hayashi, *J. Pharm. Sci.,* **84,** 1139 (1992).
10. A. Ookubo, K. Ooi, A. Ikawa, K. Kawashiro, and H. Hayashi, *Yakugaku Zashi,* **114,** 39 (1994).
11. V. Ambrogi, G. Fardella, G. Grandolini, and L. Perioli, *Int. J. Pharma.,* **220,** 23 (2001).
12. M.Z. bin-hussein, A.H. Yahaya, M. Shamsul, H.M. Salleh, T. Yap, and J. Kiu, *Mater. Lett.,* **58,** 329 (2004).
13. J.H. Choy, and Y.H. Son, *Bull. Korean Chem. Soc.,* **25,** 122 (2004).
14. M. del Arco, E. Cebadera, S. Gutierrez, C. Martin, M.J. Montero, V. Rives, J. Rocha, and M.A. Sevilla, *J. Phrama. Sci.,* **93,** 1649 (2004).
15. S.Y. Kwak, Y.J. Jeong, J.S. Park, and J.H. Choy, *Solid State Ionics.,* **151,** 229 (2002).
16. K.M. Tyner, M.S. Roberston, K.A. Berghorn, L. Li, R.F. Gilmour Jr, C.A. Batt, and E.P. Giannelis, *J. Control. Rel.,* **100,** 399 (2004).
17. N. Hirokazu, T. Kozi, and T. Mitsumoto, *J. Pharma. Sci.,* **92,** 2419 (2003).
18. H. Zhang, K. Zou, S. Guo, and X. Duan, *J. Solid State Chem*., **179,** 1792 (2006).
19. J-H. Choy, S-Y. Kwak, J-S. Park, and Y-J. Jeong, *J. Mater. Chem*., **11,** 1671 (2001).
20. F. Cavani, F. Trifiro, and A. Vaccari, *Catal. Today*, **11,** 173 (1991).
21. A. Goodman-Gilman, L.S. Goodman, and A. Goodman, 1975, The Pharmacological Basis of Therapeutics, VI. Macmillan Publishing Co. Inc. New York. p. 995.

22. A. de. Roy,C. Forano, M-El. Maiki, and J-P. Besse, 1992. Synthesis of Microporous Materials, Expanded Clays and other Microporous Solids, ed. M.L. Occelli and H. E. Robson, Van Nostrand Reinhold, NY, 108.
23. C.M. Adeyeye, and J.C. Price, **14,** 357 (1997).
24. M.O. Jae, P. Man, K. Sang-Tae, J. Jin-Young, K. Yong-Gu, and J.-H. Choy, *J. Phy. Chem. Sol.*, **67**, 1024 (2006).
25. S. Miyata, *Clays Clay Miner*, **23,** 369 **(**1975).
26. Y. Zhao, J. He, Q.Z. Jiao, D.G. Evans, and X. Duan, *Chinese J. Inorg. Chem*, **17,** 573 **(**2001).
27. T. Kwon, G.A. Tsigdinos, and T.J. Pinnavaia, *J. Am. Chem. Soc*. **110,** 3653 **(**1998).
28. F. Kooli, C. Depege, A. Ennaqadi, and J.P. Besse, *Clays Clay Miner*, **45,** 92 **(**1997),.
29. J.T. Kloprogge, and R.L. Frost, In Layered Double Hydroxides: Preset and Future; Rives*,* V., Ed.; Nova Science Publishers: New York, 2001, Chapter 5, p 139.
30. D. Depan, and R.P. Singh, *J. Biomed. Mater. Res, Part A,* **78,** 372 (2006).
31. B. Li, J. He, D.G. Evans, and X. Duan, *J. Phys. Chem. Solids*, **67,** 1067 (2006).
32. R.D. Piner, T.T. Xu, F.T. Fisher, Y. Csiao and R.S. Ruoff, *Langmuir*, **19**, 7995 (2003).
33. M.M. Malwitz, A. Dundigalla, V. Ferreiro, P. Butler, M.C. Henk and G. Schmidt, *Phys. Chem. Chem. Phys*., **6**, 2977 (2004).
34. S. Tanner, H. Chanzy, M. Vicendon, J.C. Roux, and F. Gaill, *Macromol*, **23,** 3576 (1990).
35. M.F. Cervera, J. Heinamaki, M. Rasanen, S.L. Maunu, M. Karjalainen, OMN. Acosta, A.I. Colarte, and J. Yliruusi, *Carbohyd. Polym*., **58,** 401 (2004).
36. P.B. Messermith, and S.I. Stupp, *Chem. Mater*., **7,** 454 (1995).
37. VRL. Constantino, and T.J. Pinnavaia, *Inorg. Chem*., **34,** 883 (1995).
38. W.M. Kriven, S.Y. Kwak, W.M. Kriven, M.A. Wallig, and J.H. Choy, *Biomater*., **25,** 5995 (2004).
39. V. Ambrogi, G. Fardella, G. Grandolini, and G. Perioli, *Int. J. Pharma*. **220,** 23 (2001).

CHAPTER VI

Enzymatic Synthesis of Nanosized Hydroxyapatite And it's Polymorphs

6.1 INTRODUCTION

Wheat bran, which has a substantial amount of bound phosphorous in the form of phytic acid, is a cheap agro-based waste material. However, surprsingly there have been no attempts at harnessing the enormous amount of phosphorous present in most of the agro wastes including wheat bran into nanosized hydroxyapatite particle and its polymorphs. Calcium phosphates are compounds of great interest in an interdisciplinary field of sciences involving chemistry, biology, medicine, and geology. The first attempts to determine their composition by chemical analysis began in the first half of the 19th century by Arnolds[1]. After that, Jones[2] introduced the idea of different calcium phosphate crystal phases; mixtures of them were called apatites until then. In aqueous solutions and at ambient temperatures the most important calcium phosphate salts may be seen in **Table 6.1**, in order of decreasing solubility. The so-called amorphous calcium phosphate (ACP) is absent from the list because it is not another phase but a microcrystalline mixture of other identified calcium phosphates.

Hydroxyapatite (HAP) [HAP, Ca_{10} $(PO_4)_6(OH)_2$], is the most stable calcium phosphate salt at normal temperatures and pH between 4 and 12. HAP has immense applications as artificial bone material, supportive media for drug delivery, purification of protein, nucleic acid, isolation of virus etc. Purification of biological molecules such as proteins and nucleic acids by HAP was first established by Tselius[3]. The calcium phosphate matrix is capable of various chemical interactions with DNA and proteins, including charge repulsion by crystal phosphates and metal affinity interactions with crystal calcium[4-8]. Indeed, human bone is a natural composite comprising of nano-apatite rods (which are <100 nm) arranged in lamellae and bound to collagen[9]. Thus, synthetic HAP is of interest as biocompatible phase reinforcement in biomedical composites, for filling bulk bone defects and for coatings on metal implants[10]. HA and other calcium phosphates (calcium deficient Hydroxyapatite, CDHA) are also of interest as components in injectable bone cements; controlling particle properties (*e.g.* size and shape) and is often used to modulate cement setting behavior[11].

It is a compound of great interest in catalysis, the industry of fertilizers and pharmaceutical products, protein chromatography applications; water treatment processes, preparation of biocompatible materials, and mostly because it is the main inorganic component in calcified hard tissues (e.g., bone and teeth) of vertebrates[12-15]. HAP is also formed pathologically as a result of functional irregularities resulting in cartilage arthritis, formation of renal, bladder, and bile stones, and calcification of

transplanted cardiac valves[16-18]. In this context, HAP is considered as a model compound to study biomineralization phenomena[19, 20]. For this reason there is a strong interest for synthetic, extra pure, well defined HAP crystals for use in detailed physicochemical *in vitro* and *in vivo* studies, bio-medical applications, and surgery (e.g., middle ear implants, reconstructive bone replacement, *etc.*)[21-23]. In literature, several methods to prepare HAP crystals have been reported, including solid state reactions, plasma techniques, crystal growth under hydrothermal conditions, layer hydrolysis of other calcium phosphate salts, and sol-gel crystallization[24–28]. Essentially, the synthesis of HAP crystals from supersaturated aqueous solutions is advantageous due to low cost and simplicity[29], but most of the synthetic procedures followed until now led to the formation of non-stoichiometric products[30]. Deviation from the stoichiometry of HAP is due to the presence in the crystal lattice of vacancies and ion substitutes such as carbonates, hydrogen phosphates, potassium, sodium, nitrates, and chloride, which are usually introduced into the precipitating system with the reactants. Contamination of HAP with these ions or formation of deficient hydroxyapatite suffer from significant changes in their crystallographic characteristics and have different crystal morphology as compared to the stoichiometric[31]. Difficulties encountered in preparing synthetic HAP crystals from aqueous solutions are mainly caused by the high chemical affinity of the material to some ions, the complex nature of the calcium phosphates system, and the role of kinetic parameters, which, depending on the experimental conditions, prevail over the thermodynamics. The formation of synthetic HAP crystals from highly supersaturated solutions proceeds via intermediate precursor phases, which have a transitory existence, such as tri-calcium phosphate and octa-calcium phosphate[32]. Traces of precursors can be detected even after prolonged times of hydrolysis, therefore affecting the quality of the final product.

Table 6.1 Various Calcium Phosphate salts and their composition.

Molecular Type	**Ca/P Ratio**	**Name**
$Ca_5 (PO_4)_3$. (OH)	1.67	Hydroxyapatite
α and β-$Ca_3 (PO_4)_2$	1.50	Tri-calcium phosphate
$Ca_4H (PO_4)_3$. 2.5 H2O	1.33	Octa-calcium Phosphate
Ca (HPO_4). 2 H2O	1.00	Di-calcium Phosphate Di-hydrate
Ca (H_2PO_4)2	0.50	Mono-calcium Phosphate
Ca (H_2PO_4)2. H2O	0.50	Monohydrate Calcium phosphate

The disadvantages of these methods include the following; they often require very precise control over reaction conditions, require expensive starting materials or large amounts of toxic organic solvents, or they are usually time consuming. For example, in wet chemical synthesis of HAP, a maturation step (>18 h), followed by a heat treatment of 650 °C, is required[33]. Failure to allow sufficient maturation, gives a phase-separated product upon heat treatment, which can adversely affect biological properties *in vivo*. Furthermore, the aforementioned synthesis approaches give little or no control over HAP particle characteristics (i.e. particle size, agglomeration surface area). To gain a better understanding of the factors that produce particles with the desired properties, current synthesis methods are essentially too slow and unpredictable. Thus, there is interest in developing faster synthesis techniques for synthetic apatite that allow a greater degree of control over particle properties. HAP powders for bioceramic applications have usually been chemically synthesized via aqueous solutions. However, there are several reports of synthesis of biomimetic HAP powders in the presence of simulated body fluid (SBF) by using calcium nitrate and diammonium hydrogen phosphate under the physiological conditions of 37°C and pH 7.4.

We have attempted to synthesize HAP powder by enzymatic hydrolysis of Sodium phytate, by using calcium chloride as a Ca precursor. In this study, we describe the rapid, single step synthesis of crystalline nano-particle of HAP by a wet biological method. Briefly, aqueous solution of calcium chloride was mixed with phytase and Phytic acid. Phytase are class of Phosphohydrolases that catalyzes the hydrolysis of myo-inositol hexakis phosphate (phytic acid, myo–inositol –p6) to inorganic mono-phosphate and lower phosphoric esters of myo-inositol, in some cases to free myo-inositols[34]. This is the first report, as per our knowledge of documentation, for the biomimetic synthesis of nanosized HAP.

6.2 EXPERIMENTAL

6.2.1 Materials

The wheat bran used in this study was obtained from an animal feed stuff outlet at Pune, Maharashtra, India. Phytic acid sodium salt from corn was purchased from Sigma Chemical Company, St Louis, MO, USA. Calcium chloride (purity>95 %), and NaOH was purchased from Aldrich Chemicals.

6.2.2 Synthesis of HAP and reaction conditions

Reaction was carried out strictly under inert environment and solutions were prepared in distilled deionized water (resistivity 18.2 MΩ. cm). Deionised water was obtained with a Millipore ultra pure water system, which was previously distilled and decarbonised by boiling and bubbling N_2. Reaction was carried out in acetate buffer (pH 5.5, 50mM) while keeping the constant temperature of 50 °C (optimum temperature for enzyme activity) with continuous stirring for 4 hours. Sodium phytate (3mM final concentration) and partially purified phytase (17.19 IU/ml) were added in a three neck round bottom (RB) flask. Calcium chloride (100mM) was dissolved in distilled water, under inert atmosphere and was added into this RB with an addition funnel. The whole assembly was kept nitrogen atmosphere, to avoid the CO_3^{2-} contamination. A white precipitate was obtained after reaction and aged in the mother liquid for 24h. The white solid products were isolated by repeated centrifuging and washing with decarbonated water and finally dried at 40 °C. During the centrifuging, sealed containers were used to avoid contact with air. The deionized-distilled water used for synthesis and washing, was decarbonated prior to use by boiling and subsequent cooling in the absence of CO_2 by means of a gas-washing bottle filled with KOH solution. During the washing process, some of the HAP particles that remained suspended in the supernatant after centrifuging were discarded. Dried Samples were calcined at 1000 ^{0}C for 2 hour.

Reaction was also carried out without enzyme as control experiment keeping all the conditions same.

6.3 CHARACTERIZATION OF MATERIAL

6.3.1 WXRD Analysis

The WAXD patterns of the sample powder were obtained using a Rigaku (Japan) Dmax 2500 X-ray diffractometer with Cu-Kα radiation. The system consists of a rotating anode generator with a Cu target and a wide angle powder goniometer having a diffracted beam graphite monochromator. The generator was operated at 40 kV and 150 mA. All the experiments were performed in the reflection mode. The samples were scanned between 2θ= 2° to 30 ° at a scan rate of 2°/minute. The d-spacing was calculated by Bragg's formula, where the λ was 0.154 nm.

6.3.2 FT-IR Spectral Analysis

Samples for Fourier transform infrared (FTIR) spectroscopy analysis analyzed on a Perkin-Elmer Spectrum One instrument. The samples were mixed with dry KBr, pelletized and then scanned in the range of 4000 cm-1 to 400 cm^{-1} at a resolution of 4 cm^{-1}. A total of 10 scans were used for signal averaging. Please note that the mass of materials used in the FTIR and XRD analysis were 2 mg and 10 mg respectively to obtain acceptable signal to noise ratios.

6.3.3 Microscopic Analysis

Samples for transmission electron microscopy (TEM) were prepared by drop coating films of nanosized HAP powder dispersed in water onto carbon-coated copper grids. TEM and selective area electron diffraction (SAED) patterns of synthesized products were obtained on a JEOL 1200 EX instrument operated at an accelerating voltage of 120 kV. For scanning electron microscopy (SEM) analysis, solution cast film of biogenic calcium phosphate was made on Si (111) substrates. SEM measurements were performed on a Leica Stereoscan-440 instrument equipped with a Phoenix energy dispersive analysis of X-rays (EDAX) attachment.

6.3.4 Thermal Analysis

The thermal gravimetric analysis (TGA) was conducted on a Perkin-Elmer TGA 7 – thermal analyzer from 50 °C to 900 °C with a heating rate of 10 °C min^{-1} under nitrogen with flow rate 20ml min^{-1}, in a platinum crucible.

6.3.5 ^{31}P-NMR Spectroscopy

Solid state ^{31}P nuclear magnetic resonance (NMR) spectra were obtained at 162 MHz on a Bruker spectrometer Avance 400 (rotor 4mm, spinning rate 2-12 kHz) using Magic Angle Spinning (MAS). Phosphoric acid (H_3PO_4) was used a reference sample. Samples were spun at 10 kHz. Spectrometer frequencies were set to 100.62 for ^{13}C. The numbers of scans were of 800. The cross polarization time was 0.5 ms.

6.3.6 Bioresorption Studies:

Bioresorption is one of the key characteristics of biomaterials, in particular, bone graft materials, as it controls their bioactivity and other biological functions.

Therefore, in this study, in-vitro bioresorbability of HAP nanoparticles was evaluated in a Hank's medium (a buffer solution used for cell/tissue cultures) of pH of 7.4 at a ratio of 1mg/ml in a thermostatic incubator at 37 ºC. The variations of buffer pH were recorded at predetermined time intervals using a pH meter according the reported procedure[35].

6.3.7 In vitro biocompatibility Studies:

The synthesized HAP was subjected to standard cell-growth tests to assess the biocompatibility. The in vitro cell-growth studies were done in direct contact method (ISO 10993–5, 1999), using L929 (mouse fibroblast subcutaneous connective tissue) cell line procured from National Center for Cell Sciences, Pune, India. The test samples were cleaned ultrasonically and sterilized by autoclaving. The cells were maintained in RPMI 1640 (Himedia, Pune, India) medium supplemented with 10% foetal bovine serum (Sigma, USA) and 100 IU/ml penicillin and 100 µg/ml streptomycin (medical grade). Cells were sub- cultured and $1x10^6$ cells/ ml seeded into 24 multi-well dishes to form a monolayer. After allowing 24 hours for cell adhesion, the cells were analyzed everyday (3 flasks per day) for 6 days. The samples (100µg-1000µg/ml) were placed gently under sterilized conditions onto the cells and incubated at 37 °C under 5% CO_2 and 95% Humidity for 72 h. The viability of the cells in the vicinity of the material was examined by MTT assay 34. Test was done in duplicate, along with control samples.

6.3.8 Gel Electrophoresis

The biomolecules occluded in the nanostructures were analyzed using 10% sodium dodecyl sulfate polyacrylamide gel electrophoresis (SDS-PAGE) according to the procedure published by Laemmli[36]. For protein analysis, the synthesized uncalcined particles of HAP, along-with occluded proteins were treated with β-mercapto ethanol (2-mercapto ethanol) for 5-10 min in boiling water bath. Free proteins were removed by repeated washing and centrifugation at 10000 rpm for 30 min in supernatant. Following dissolution, the protein sample was dialyzed against deionized water over 7 days, lyophilized, and analyzed using SDS-PAGE along with protein molecular weight markers.

6.4 RESULTS AND DISCUSSION

We are interested to know how the phytase enzyme and the substrate could affect the crystallization of HAP in the reaction mixture. The HAP powder obtained by the above biosynthetic route appears as white color and free-flowing bouncy particles.

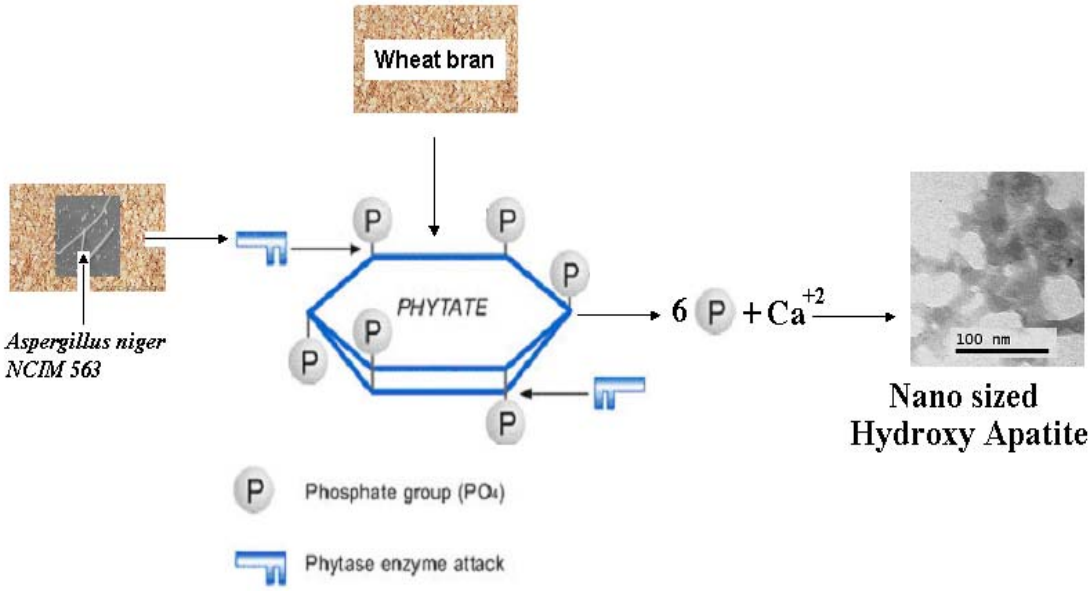

Scheme 6.1 Schematic illustration of preparation of HAP.

The white precipitate of calcium phosphate was formed by phytase and phytic acid at 50°C and pH 5.5, were found to be amorphous as shown in XRD pattern of uncalcined HAP (**Figure 6.1**).

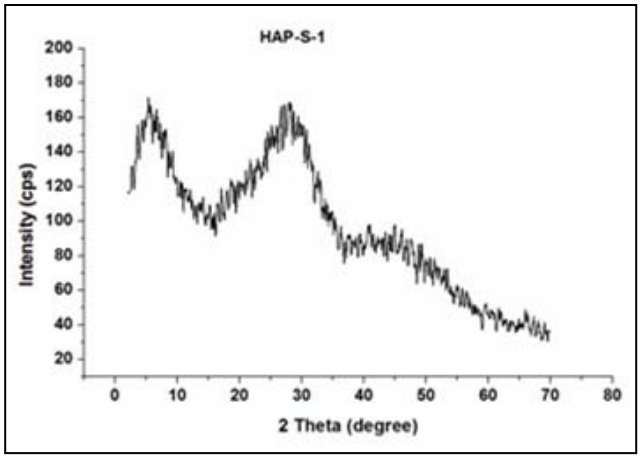

Figure 6.1 WXRD pattern of the uncalcined HAP.

XRD traces showed powders of low crystallinity, represented by broad diffraction peak at around 28.16 and at 5.32, and free of secondary phases owing to its low temperature

processing. However, the obtained results are comparable to the diffraction pattern of the biological apatite and are in good agreement with the previous results[37]. The possible reason for the poor crystalline nature of precipitated HA must be emerged from the preparation methodology owing to low temperature procedure. To prove this, a small amount of precipitated HA was calcined at 900 °C for 2 h in a muffle furnace under air atmospheric pressure and furnace cooled.

6.4.1 X-Ray Diffraction (XRD):

To further verify the crystallinity of particles, XRD analysis of as synthesized as well calcined HAP particles was performed. The results are shown in **Figure 6.2**. The room temperature XRD profile (2θ value) of the calcined material matches very well with HAP, β TCP (Tri calcium phosphate), DCP (Di calcium phosphate). The peaks of the resulting diffractogram were observed near 29.60 and 31.10 and are diagnostic for the presence of calcium hydroxyapatite (ICDD No. 9-432). In addition, the presence of organic molecules greatly influences the crystalline behavior of the HAP.

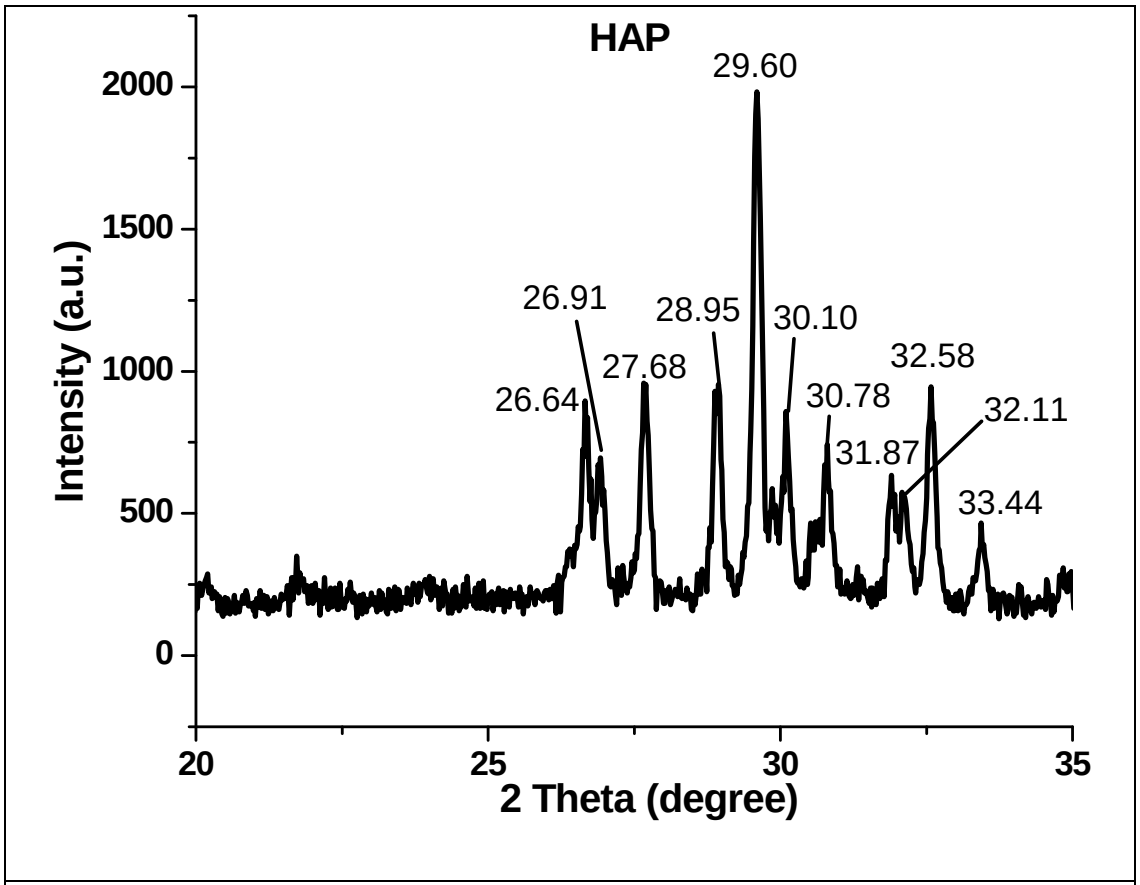

Figure 6.2 XRD pattern of prepared and calcined HAP.

We revealed the PC-PDF no. 34-0010, space group: $P6_3/m$, crystal structure: tetragonal, unit cell parameters a=b=9.414 A°, c=6.879 A°, α=β= γ=90^0 53, β-TCP, PC-PDF no. 40.0008, SG: $P2_1/n$, crystal structure: monoclinic, unit cell parameters a=9.332 A°, b=18.13 A°, c=7.841 A°, α= γ≠ β =106.69^0. ≠γ. DCP, PC-PDF no. 41.0483, SG: $P2_1/n$, crystal structure: monoclinic, unit cell parameters a=7.667A°, b=12.88 A°, c=7.144 A°, α= γ≠ β =107.0^0. ≠γ. The material is polyphasic in nature. The XRD pattern of the HAP powder resembles closely to the diffractogram of bone material. Hence, the prepared HAP in this investigation has more similarity with natural bone mineral in terms of degree of crystallinity and structural morphology. The calcined HAP exhibited all the characteristic diffracted peaks of stoichiometric HAP with higher degree of crystallinity. The obtained results did not show any peaks corresponding to calcium carbonate and calcium oxide and hence suggesting that the ingredients were reacted completely and produced a homogeneous HAP, without any atmospheric carbon di-oxide impurity.

6.4.2 Transmission Electron Microscopy and Selected Area Electron Diffraction:

Figure 6.3 (A-D) shows the transmission electron micrograph (TEM) of HAP and its polymorphs, demonstrating its nanosized regular structure. The as prepared uncalcined HAP was ~100 nm in size and formed a dense network.

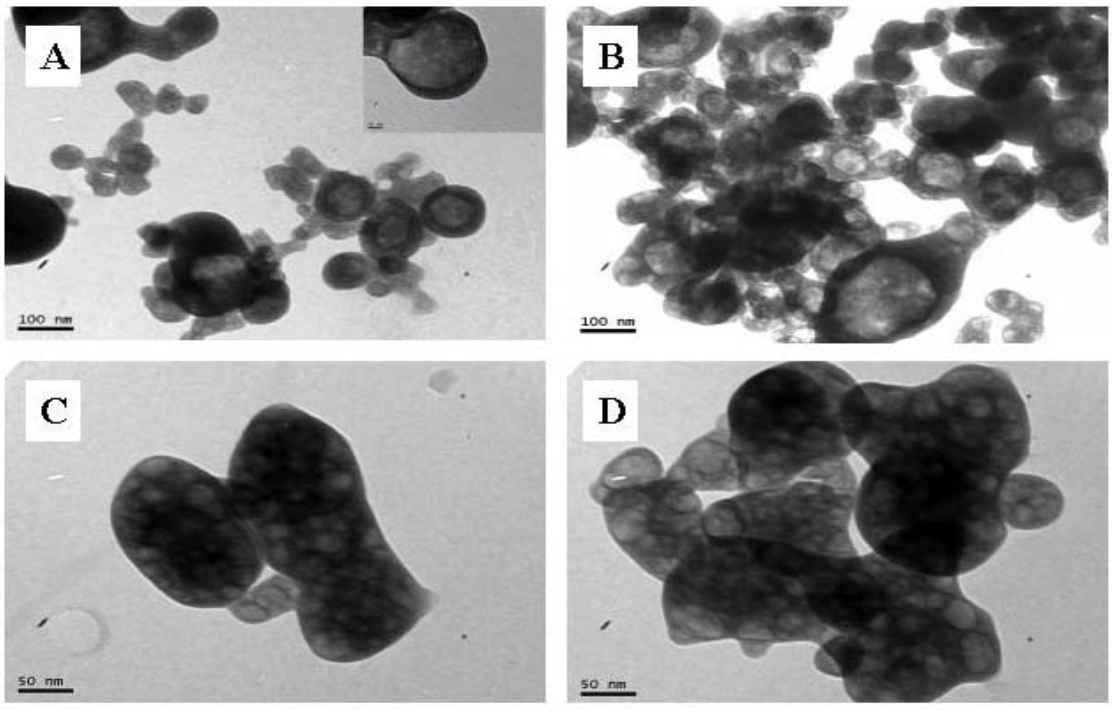

Figure 6.3 TEM images of HAP.

We observed interconnected hollow spheres like structures; those were having 3D, polyhedral or rounded and drop-like shape. The HR-TEM of calcined HAP (**Figure 6.4 A-D**) showed that after heat treatment, due to the loss of occluded proteins the morphology changed to an irregular interconnected lattice type structure. The smallest particles were ~100 nm in size, but in general, they were larger, up to tens of microns.

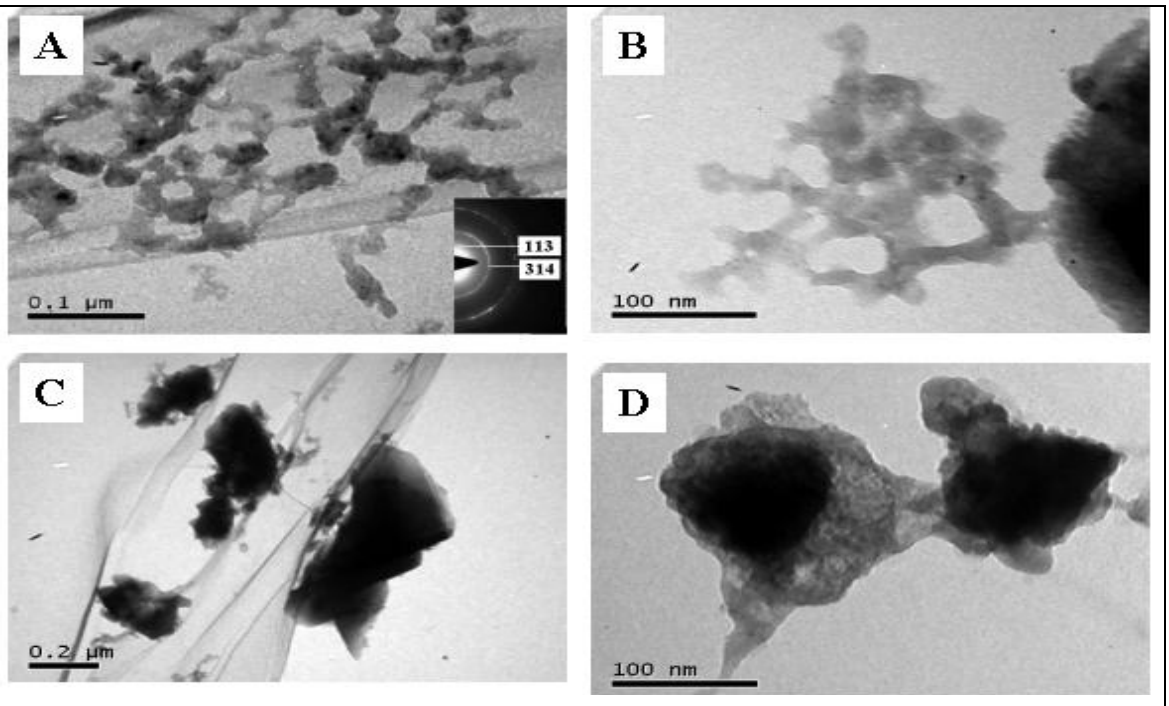

Figure 6.4 HR-TEM images of calcined HAP.

In **Figure 6.4** (INSET) selected area electron diffraction (SAED) analysis of calcined HAP particles shows sharp diffused ring patterns confirming the crystallinity of the calcined calcium phosphate, where the lattice planes exhibited spacing of ~ 2.077 Å and ~ 1.347 Å corresponding to the lattice planes (113) and (314) respectively. The as synthesized protein coated uncalcined HAP sample did not show any diffraction. SAED pattern for calcined HAP suggested that material was polycrystalline in nature.

6.4.3 Scanning Electron Microscopy:

In order to study the surface morphology, crystal orientation and growth of HAP, a scanning electron microscopy was done. The as prepared powder material was in the size of 100 nm to 200 nm, as shown in the SEM micrograph. A representative micrograph is shown in **Figure 6.5 (a)**, which provides a good evidence for the nucleation and bionic growth of HAP in the presence of enzyme. The calcined HAP

possesses large amount of ultrafine crystals embedded in the substrate along their axial direction with irregular shape and surface and irregular surface texture. Majority of the crystals are spread out on the substrate and few of them agglomerated with a broad size distribution, owing to their high surface area and thus occasionally appear to be in cluster like deposits. The mean aggregating size of the calcined grains was approximately 500 nm to 5 μm. The SEM micrograph of precipitated HAP exhibited nano sized crystals with almost uniform particles size. The HAP particles prepared were stoichiometric, mono-dispersive; roughly particles, and were not fused together with other crystals. It can be inferred that majority of the particles were of single crystals, regular shape and cleaner contours with no agglomeration. Eventually it becomes an advantage because these properties make these uniform particles highly beneficial for coating of nano HAP onto biomedical implants.

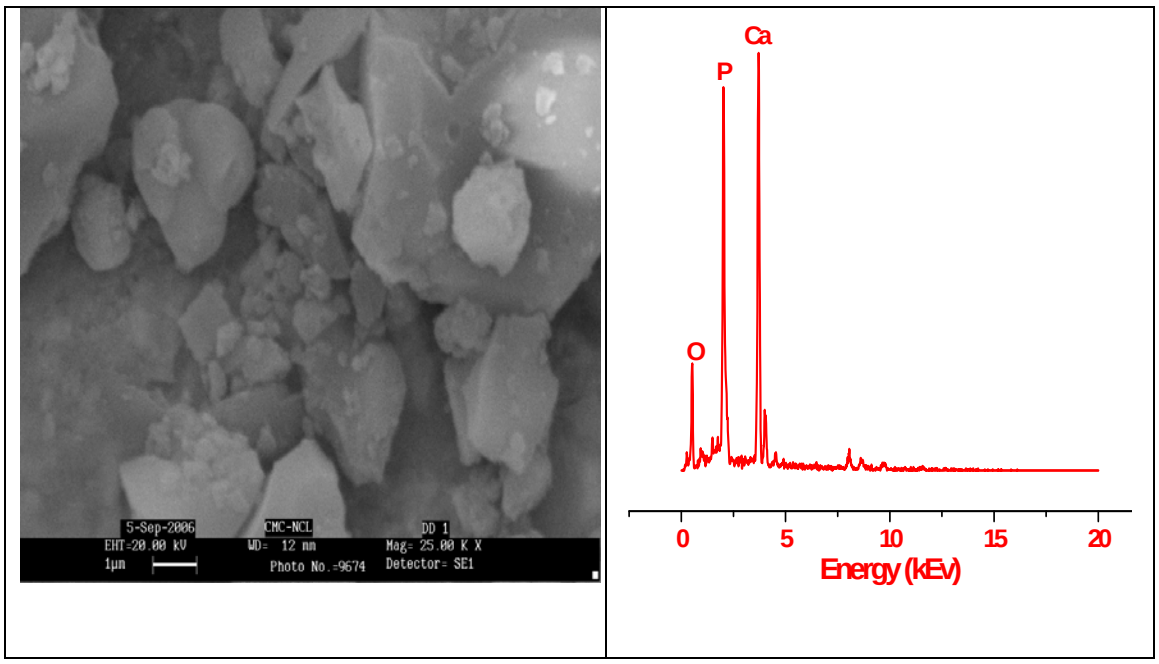

Figure 6.5 (a) SEM, and **(b)** EDAX result of the as prepared HAP.

These results suggest the feasibility of *in situ* nucleation of HAP crystals. The presence of Ca and P, with the Ca/P ratio of 1.55 is revealed by energy dispersive X-ray absorption (EDAX) analysis, which is shown in **Figure 6.5 (b)**. EDAX analysis showed strong peaks of calcium (Ca), Phosphorous (P) and oxygen (O), but Ca and P are primary elements in HAP, β TCP and DCP, confirming the presence of hydroxyapatite.

6.4.4 FT-IR- Spectroscopy:

The FT-IR spectrum of calcined and non-calcined HAP and its polymorphs (β TCP+DCP) is given in **Figure 6.6 (a-b),** respectively. An intense band observed at 3451 cm^{-1} corresponds to the combination of -OH group (HAP phase) and -NH group (Phytase phase). The apatitic PO_4^{3-} ν_4 modes, in the region of 600- 500 cm^{-1} and ν_1 and ν_3 modes at 1150-1000 cm^{-1}, which corresponds to the factor group splitting of PO_4^{3-} tetrahedral, were also detected[38]. The bands at ~953-961 cm^{-1} corresponds to ν_1 symmetric and ν_4 P-O stretching vibrations of the PO_4^{3-} ion, respectively. Samples have not been contaminated by atmospheric carbon dioxide, as no peak corresponding to a secondary carbonate is recorded. The presence of intense amide I and II bands at 1644 and 1547 cm^{-1} respectively are also observed in the FT-IR spectrum. This observation indicates that the particles in the hollow spherical/circular morphology are present with proteins that are possibly occluded into the particles or are bound to the surface of the particles, as shown in SEM image.

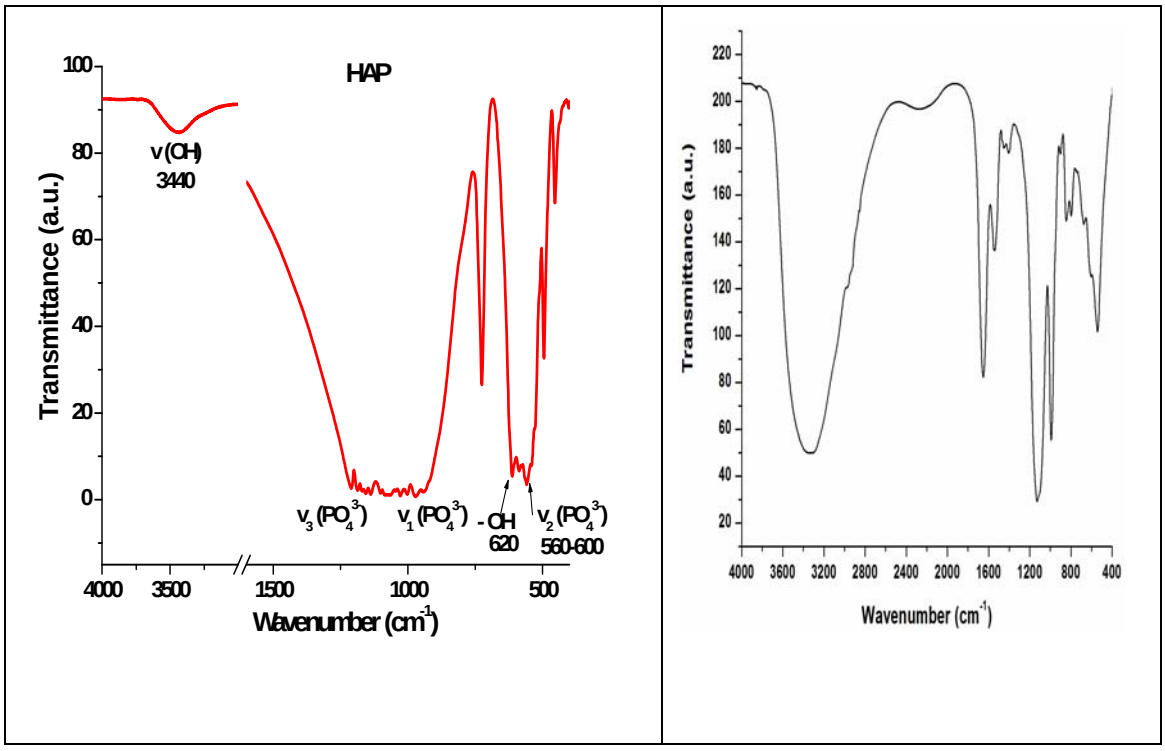

Figure 6.6 (a) FT-IR spectra of calcined and, **(b)** FT-IR spectra of uncalcined HAP.

When the HAP particles are calcined at 1100 ^{0}C for 2 h, the amide signatures as well as the signatures from organic molecules around 1400 cm^{-1} in FTIR spectra fade away, indicating the removal of most of the biomolecules during calcinations.

6.4.5 NMR Spectroscopy

To further confirm the synthesis of HAP and its polymorphs NMR analysis was done and the results are shown in **Figure 6.7**.

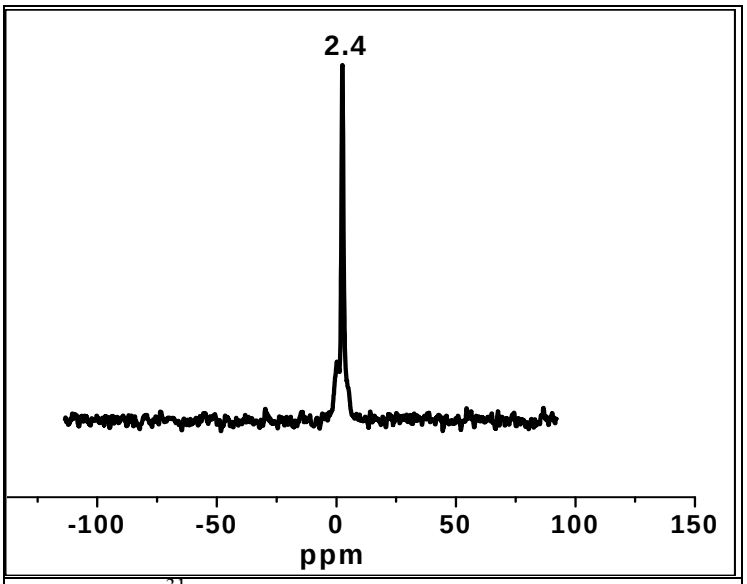

Figure 6.7 ^{31}P-NMR spectra of calcined HAP.

For HAP a sharp signal was observed at +2.65 ppm, corresponding to the phosphate (PO_4^{3-}) anion of nanocrystalline HAP[39].

6.4.6 TGA (Thermal Methods)

To understand better the nature of occluded protein onto the biogenic calcium phosphate particles, TGA measurements of the as prepared powder were done and the result is shown in **Figure 6.8 (a)**. It is observed that there are three prominent weight losses of material i.e. 15%, 7.39% and 8.57 % at 100-220 °C, 330-410 °C, and 620-830 °C, respectively. The first weight loss is clearly due to the release of water entrapped in protein-calcium phosphate biocomposite, whereas the second weight loss is attributed to the decomposition/desorption of proteins bound to the material. A third additional weight loss is ascribed to the further decomposition of HAP at higher temperature. The TGA curve shows an overall weight loss of 31%. Considering the above results, the thermal stability of the biogenic as prepared product seems to be not high. The calcined material (HAP, β TCP, DCP) was prepared at 1100°C, so it did not show any weight loss in the TGA measurements (**Figure 6.8 b**).

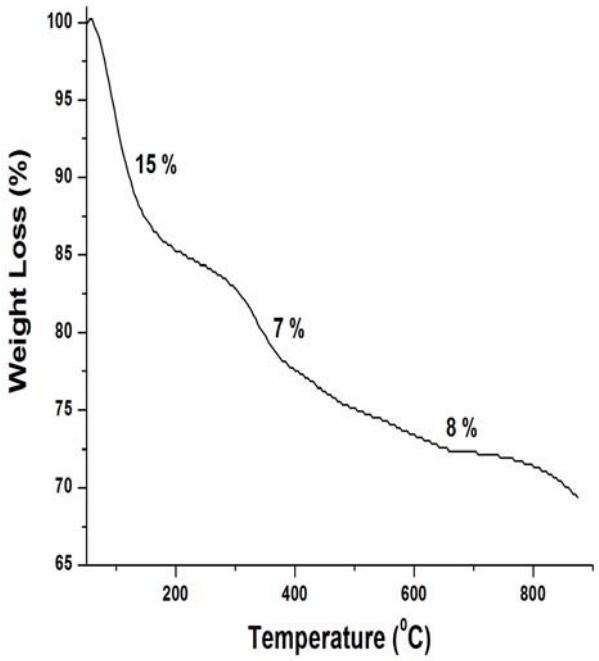

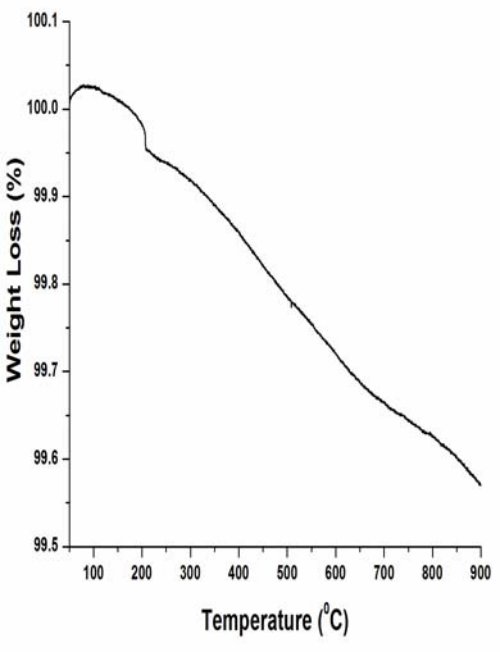

Figure 6.8 (a) TGA thermogram of uncalcined HAP. **(b)** TGA of calcined HAP.

It can be seen from the TGA thermogram of calcined HAP that there was no phase transformation taken place upon heating, which indicated its thermal stability even at high temperature. There was no notable occurrence of weight loss found for nano HAP. However, the observed weight loss at 120 °C can be due to the dehydroxylation of nano HAP.

6.4.7 Stability under physiological conditions

The stability of the Hank's solution with commercial available HAP, with and without the apatite samples were quantitatively measured *in-vitro* at predetermined time intervals (**Figure 6.9**). The pH of the buffer solution without the apatite sample was quite stable throughout the experimental period, while the addition of apatite has a more or less alkaline effect on the pH of the buffer medium. The pH of the buffer solution with enzymatically synthesized HAP was found to be stable indicating its physiological stability during the period of study. The commercial and synthesized HAP exhibited almost similar pH profile. However, the initial fluctuation of the pH may be due to the dissolution of trace carbonate ions of HAP.

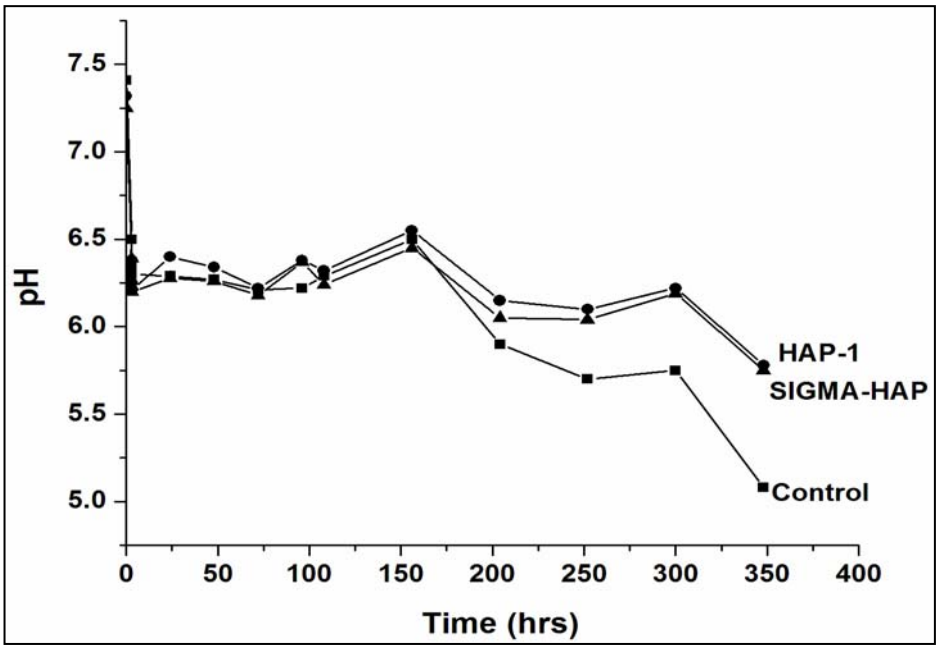

Figure 6.9 Results from the bio-resorption studies of HAP under Hanks Medium.

6.4.8 In vitro biocompatibility

The prepared HAP nanoparticles were subjected to *in-vitro* cell-culture tudies and the results are shown in **Figure 6.10 A-D**. The *in-vitro* biocompatibility screening showed highly promising results. The images were taken by light microscope for different time interval (0h-72h) during the direct contact cell-culture test.

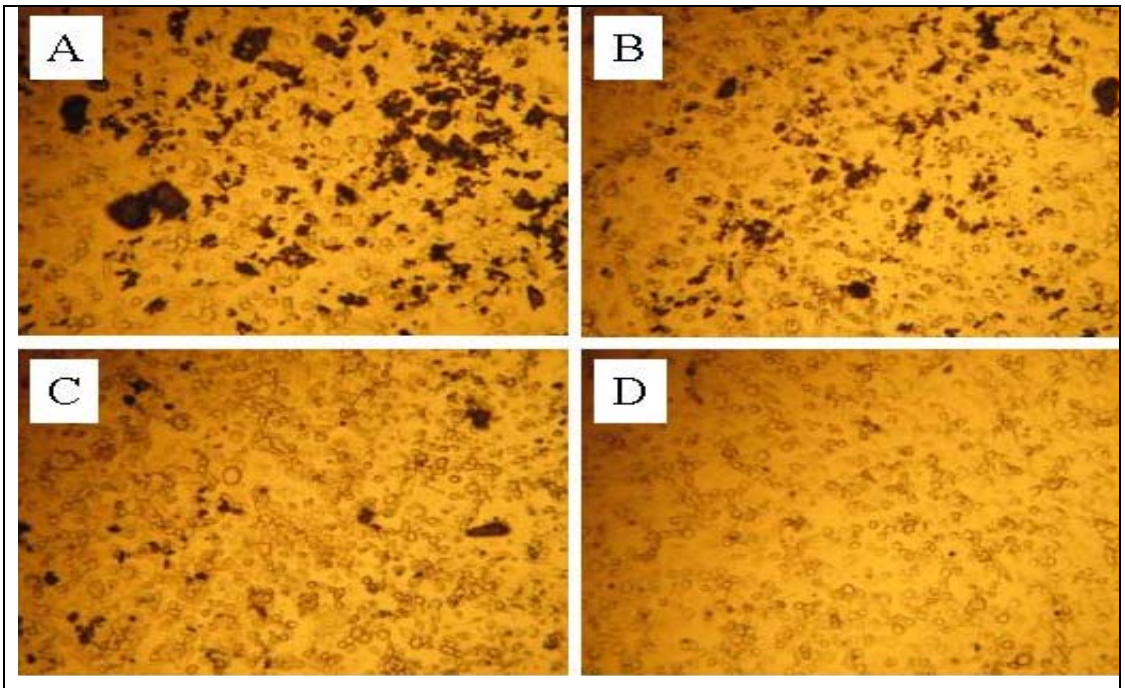

Figure 6.10 Results from the *in-vitro* cell-culture studies.

As observed in the **Figure 6.10** A-D, the mouse fibroblast cells with material grew well and remained in the same normal morphology like the cells cultured with sample at 0 hour (A), showing the non-toxic nature of the hydroxyapatite. Many investigators have exploited this asset of *in-vitro* biocompatibility testing and have reported their findings on biocompatibility of various biomaterials. It has been well known that cell behavior and interaction with a bioactive material surface are dependent on properties such as topography and chemistry. Results of the cell culture were expressed by area fraction of cell in the surface of materials. As shown in the optical images, the presence of bioactive HAP particles may have positive biological effects. Most of area of the test sample was covered by osteoblasts, which indicated that introducing of HAP can be of advantage to the cell adhesion and proliferation. This improving of cell adhesion and proliferation is largely due to the better surface provided by HAP for cell attachment and spreading.

To identify the biomolecules bound to the as- prepared HAP nanoparticles, the purified calcium phosphate particles were treated with β-mercapto ethanol (2-mercapto ethanol) for 5-10 min in boiling water bath which breaks the disulfide bond present in the quaternary structure of proteins, that leads to the conformational changes and finally detachment of occluded proteins from particles. Proteins when analyzed using 10% SDS-PAGE (**Figure 6.11**), four major proteins were identified (line P). Molecular weights of band 1-3 varied between 116 to 29 KDa (line M) and these proteins also present in the partial purified enzyme preparation (line A). The proposed role of these proteins may be to stabilize the size and shape of nanoparticles during synthesis[40]. Fourth broad band likely to be the mixture of low molecular weight peptide traces (3-5 KDa) of protein band 1-3, those may be produced during the detachment process.

These results suggest the possible application of synthesized bionic particles for purification of certain proteins. We also tried biological synthesis of calcium phosphate by the use of different phytase producing microorganisms (Fermentation media supplemented with phytic acid and salt of calcium) but as fungus grow in aerobic or micro aerobic conditions, we got calcium carbonate instead of calcium phosphate as major biosynthesis product. Pure synthesis of HAP nano particles by the direct use of fungus biomass and understanding of the role of fungal mechanism would definitely be an issue of great interest in future investigations.

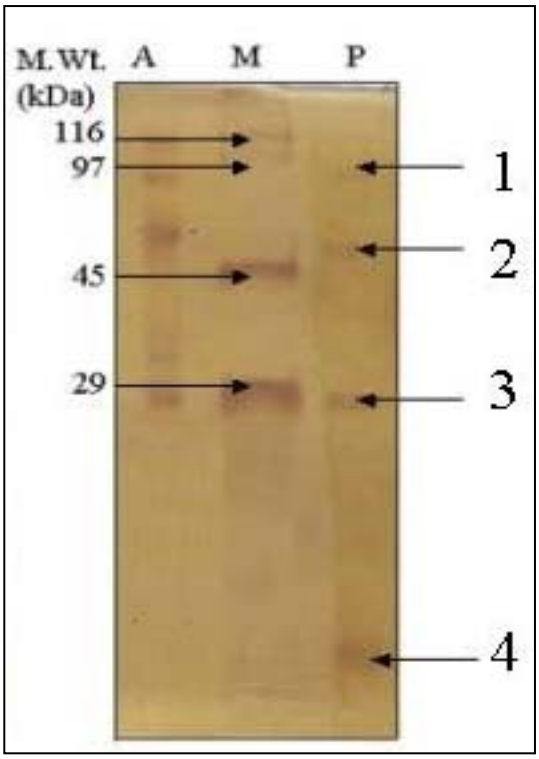

Figure 6.11 Result from a gel-run.

6.5 CONCLUSION

In summary, the experimental results of this investigation provided evidence for the feasibility of in situ formation of HAP nanospheres through bionic approach with the most desirable physiochemical and bioresorbable characteristics. The physiochemical characteristics confirmed the nucleation and crystal growth of HAP in the presence of phytase enzyme. The structural integrity and chemical interactions of these two phases are also evident wherein anionic functional groups of the substrate play a key role for the growth of HAP crystals. The in-vitro solubility evaluation of HAP performed under the physiological conditions has provided a proof for its resorbable nature. The overall results therefore, suggest that the HAP nanospheres may be a good choice for bone grafting applications.

6.6 REFERENCES

1. P.W. Arnold, *Trans. Faraday Soc.,* **46**, 133 (1950).
2. D.W. Jones, and J.A.S. Smith, *J. Chem. Soc., (Resumed)* 1414 (1962).
3. Tiselius, S. Hjerten and O. Levin, *Arch. Biochem. Biophys*., **65**, 132 (1956).
4. T. Kawasaki, *J. Chromatography*, **544**, 147 (1991).

5. H. Martinson, *Biochem*., **12**, 2731 (1973).
6. H. Martinson and E. Wagenaar, *Biochem*., **13** 1641 (1974).
7. G. Bernardi, *Biochim. Biophys. Acta*, **278**, 409 (1972).
8. G. Bernardi, *Met. Enzymol*., **21**, 95 (1971).
9. P. Fratzl, HS Gupta, E.P. Paschalis and P Roschger, *J. Mater. Chem.*, **14,** 2115 (2004).
10. L. L. Hench, *J. Am. Ceram. Soc.,* **81,** 705 (1998).
11. M.P. Ginebra, F.C.M. Driessens and J.A. Planell, *Biomaterials*, **25,** 3453 (2004).
12. A. Bigi, E. Boanini and K. Rubini, *J. Solid State Chem.*, **177,** 3092 (2004).
13. Y.X. Pang and X. Bao, *J. Eur. Ceram. Soc.*, **23,** 1697 (2003).
14. M.J. Philips, Ph. D. Thesis, Queen Mary University of London. (2005).
15. M.J. Philips, J.A. Darr, Z.B. Luklinska and I. Rehman, *J. Mater. Sci.: Mater. Med.*, **14,** 875 (2003).
16. G.K. Lim, J. Wang, S.C. Ng, C.H. Chew and L.M. Gan, *Biomater.*, **18**, 433 (1997).
17. Y. Wang, S. Zhang, K. Wei, N. Zhao, J. Chen, and X. Wang, *Mater. Lett*., **60,** 1484 (2006).
18. R. E. Riman, L. Suchanek, K. Byrappa, C. Chen, p. Shuk and C. S. Oakes, *Solid State Ionics*, **151,** 393 (2002).
19. S. Rhee, *Biomaterials*, **23,** 1147 (2002).
20. J.A. Darr, Z.X. Guo, V. Raman, M. Bououdina and I.U. Rehman, *Chem. Comm.*, **6,** 696 (2004).
21. S. Kim, H. Ryu, H. Shin, H.S. Jung and K.S. Hong, *Mater. Chem. Phys*., **91,** 500 (2005).
22. H. Arce, M.L. Montero, A. Saenz and V.M. Castano, *Polyhedron*, **23,** 1897 (2004).
23. L.Y. Cao, C.B. Zhang and J.F. Haung, *Mater. Lett*., **59,** 1902 (2005).
24. E.J. Mullaney, C. Daly and A.B. Ullah, *Adv. Phytase Res. Adv. Appl. Microbiol.,* **47,** 157 (2000).
25. R.L. Du, and J. Chang, *Biomed-Mater. Eng.,* **16,** 3488 (2006).
26. R. Murugan, K.P. Rao, and K. Sampath, *Bulletin of Materials Sci.,* **26,** 523 (2003).

27. U. K. Laemmli, *Nature,* **227,** 680 (1970).
28. M.I. Kay, R.A. Young, and A.S. Posner, *Nature*, **204**, 1050 (1964).
29. T.M.G. Chu, J.W. Halloran, S.J. Hollister, and S.E. Feinberg, *J. Mater. Sci.: Mater. Med.,* **12,** 471 (2001).
30. F. Miyaji, Y. Kono, and Y. Suyama, *Mater. Res. Bull*., **40,** 2, (2006).
31. W.P. Aue, A.H. Roufosse, M.J. Glimcher, and R.G. Griffin, *Biochem*., **23,** 6110 (1984).
32. I. Yamaguchi, T. Kogure, M. Sakane, S. Tanaka, A. Osaka, and J. Tanaka, *J. Mater. Sci. Mater. Med.,* **14,** 883 (2003).
33. S. Kim, H. Ryu, H. Shin, H.S. Jung, and K.S. Hong, *Mater. Chem. Phys.,* **91,** 500 (2005).
34. S.K. Soni, and J.M. Khire, *World J. Microb. Biotechnol.,* **23,** 1585 (2007).
35. R. Murugan, T.S. Sampath Kumar, F. Yang, and S. Ramakrishna, *J. Composite. Mater.,* **29,** 1159 (2005).
36. U. K. Laemmli, *Nature,* **227,** 680 (1970).
37. F. Wang, *Mater. Chem. Phy.,* **95,** 145 (2006).
38. T. -M.G. Chu, J.W. Halloran, S.J. Hollister, and S.E. Feinberg, *J. Mater. Sci.: Mater. Med*., **12,** 471 (2001).
39. R. M. Wilson, *Biomater.,* **26,** 1317 (2005).
40. V. Bansal, A. Ahmad, and M. Sastry, *J. Am. Chem. Soc.* **128,** 14059 (2006).

CHAPTER VII

Ultrasound-Triggered Smart Release of Ibuprofen from a CS-Mesoporous Silica Composite- a Novel Approach for Controlled Drug Release

7.1 INTRODUCTION

Chitosan (CS) is the deacetylated product of chitin, a pH dependent biopolymer found in the cell wall of fungi and microorganisms. Due to its biocompatibility, biodegradability, high mechanical strength, hydrophilicity, good adhesion, and non-toxicity, CS has been used in many biomedical applications[1] and is usually applied as a food additive and as an anticoagulant or wound healing accelerator. The ability of CS to form films permits its use in the formulation of film dosage forms or as a promising encapsulating agent in drug delivery systems[2-8].

Ibuprofen (Ibu) is a non-steroidal anti-inflammatory (NSAID) drug used for the relief of rheumatoid arthritis and osteoarthritis, and is frequently employed as a model drug for sustained release experiments due to its favorable molecular size, better pharmaceutical activity, and short biological half life. Due to frequent side effects, its therapeutic use is often limited[9]. This problem could be reduced by a formulation able to control the drug release. As matrices to prepare a controlled release formulation, we have taken into account the use of porous materials. The idea was to store the drug in the channels of a porous inorganic host and allow the drug release as a consequence of a de-intercalation and/or diffusion process.

Recently, there has been increased concern in Mesoporous silica (MS) materials for use as carriers in controlled drug release, to necessitate the prolonged and better control of drug administration[10]. Mesoporous silica have been investigated as a sustained release carrier agent because of biocompatibility, non-toxicity, adjustable pore diameter, and very high specific surface area with abundant Si-OH groups on the pore surface[11-16]. Previous studies pointed out that the drug release rate could be modulated by manipulating MS by varying pore size, or different pore inter-connectivity and pore geometry[17].

At present, most drug-delivery devices have release rates that are either constant or decay with time. However, there are a number of clinical situations where such an approach may not be therapeutically sufficient. These include the delivery of insulin for patients with diabetes mellitus, gastric acid inhibitors for ulcer control, birth control, general hormone replacement and immunization drugs, and cancer chemotherapy. So, it is highly desirable that drug-delivery patterns are optimized to a pulsatile fashion in which the molecules are naturally released from the implant body. The on/off or pulsatile control of drug release is especially important for diabetic patients requiring higher doses of insulin after meals. For a successful drug-delivery system, it is

desirable that drug-delivery pattern is optimized to a pulsatile behavior in which the drug molecules are naturally released at the targeted site from the implant body. Release systems that are susceptible to external impulses such as oscillating magnetic fields[18], thermal[19], ultrasound[20], or electric fields[21] at the target site have therefore been investigated to achieve on-demand drug regulation. In connection to this, ultrasound (US) is considered as the most potential technique of external trigger for pulsatile delivery in which the release rate of the incorporated drug can be modulated by applying US irradiation. Ultrasound is one of the most promising external triggers for pulsatile delivery in which the release rate of the incorporated drug can be altered by applying US irradiation from the outside surroundings. Ultrasound is defined as any sound which is of a frequency beyond 20 kHz. There are three distinctly different biomedical applications of ultrasound which can be identified in terms of their frequency ranges and applications:

1. High-frequency or diagnostic US (2-10MHz).
2. Medium-frequency or therapeutic US (0.7-3 MHz).
3. Low-frequency or power US (5-100 kHz).

Advantages of therapeutic US arise from the fact that it is relatively a noninvasive technique, broadly applicable to a variety of cells, can penetrate deep into the interior of the implant body, and it can be carefully controlled through a number of parameters including frequency, power density, duty cycles, and time of application.

Although US irradiation technique is at its early stage of development, still a high-intensity and focused US has found many biological applications[22]. Moreover, the ultrasonic irradiation enhances the release of the drug from both biodegradable and non-biodegradable polymer matrices. However, most research has focused on the application of US on the conventional constant release system to improve the release kinetics; on/off control has not been achieved. Although enhanced drug release has been observed, accurate and repeatable dosing of drugs is still difficult.

In general, mesoporous materials are derived from supra-molecular assemblies of surfactants, which template the inorganic component (commonly silica) during synthesis. After the surfactant is removed, commonly by pyrolysis or dissolution with the appropriated solvent, the silica mesoporous matrices are potential drug carriers with the following features:

a) An ordered porous network, which is very homogeneous in size and allows fine control of the drug load and release kinetics;

b) A high pore volume (>1cm^3/g), which accommodate the requisite amount of biomolecules;

c) A high surface area of the mesoporous lumen, which implies high potential for drug adsorption;

d) A Si-OH containing surface that can be functionalized to allow better control over drug loading and release. Such modifications can not only remain the ordered mesoporous channels, but also can strengthen the interaction force between functional groups and appropriate drug molecules.

e) Chemically and mechanically stable inorganic oxide framework of MS shelters the bio- molecules from exposure to harmful species, such as proteases and denaturation chemicals.

These unique features make mesoporous materials excellent candidates for controlled drug-delivery systems, and intensive research has been carried out on this topic during recent years.

Recently, several silica based mesoporous materials have attracted attention as an alternative controlled drug-delivery systems (DDS)[23]. However, most of the documented work is still focused on continuous, not pulsatile release of the drug. So in this work US was used as an external trigger for the smart release of the incorporated drug. In contrast with the unidirectional channels present in the most commonly used MS, SBA-15 have attracted much attention due to their unique penetrating and bi-continuous channel networks which are very useful for applications requiring easy molecular accessibility and fast molecular transport[24].

In an ideal case, DDSs have to interact with the physiological environment when performing their functions during oral intake or implantation. In the former situation, non-toxicity of the material is the key factor, while in the latter case the implants have to be considered as biomaterials. Therefore, the proper function of the implanted material is restricted by its long-term biocompatibility, which is a dynamic, two-way process that involves the time-dependent effects of the host on the material and of the material on the host. As already discussed in the Chapter 1 of this thesis, biocompatibility of any implanted material relies on several parameters regarding the site of implantation, the shape and size of the biomaterial, as well as its surface chemistry. A series of biological reactions occur when a material is exposed to blood begins with the rapid adsorption of certain proteins onto the surface of the material. This process is followed by platelet adhesion, and then immune and inflammatory cells

act to protect the body by isolating the foreign material in a fibrous capsule. Encapsulation in this context does not mean a non-biocompatible state and can be considered a normal response. However, the collagen capsule is a barrier for an encapsulated drug to diffuse into the surrounding tissue and for nutrients to supply the encapsulated cells. Also, the activation of adherent platelets leads to the formation of thrombus on the surface. Almost all biomaterials are known to cause surface-induced thrombosis, which, besides the medical complications related to thrombus formation, affects the drug-release profiles. Implantable DDS materials should provide an adequate combination of the desired biological response and the release of drugs against the inflammatory and encapsulation processes. Among the biomaterials that display biocompatibility are the silica-based systems. The biocompatibility of silica nanospheres that interact with cellular systems has been well documented[25]. Moreover, surface functionalization of MCM-41 nanoparticles has been shown to regulate the material endocytosis, an important factor for intracellular delivery[26]. This phenomenon, known as bioactivity, constitutes an advantage over currently used polymer-based devices. All these surface reactions affecting biocompatibility and bioactivity must be taken into account before application of a DDS.

Of particular relevance to this study, during the release process, the loaded drug diffuses subsequently through the channels of MS and the CS molecular chains into the release medium. That is, the drug release is doubly controlled by the mesoporous shell and the biopolymer matrix. For Ibu loaded MS, only the MS shells control drug diffusion, which results in the sustained-release behavior alone.

7.2 EXPERIMENTAL

7.2.1 Preparation of Mesoporous silica (SBA-15)

SBA-15 was prepared by the method already reported by Stucky et al[27]. In short, SBA-15 was prepared using tetraethyl orthosilicate (TEOS, Aldrich Co.) as silica source, Pluronic P123 (poly (ethylene glycol)-block-poly (propylene glycol)-block-poly (ethylene glycol), $EO_{20}PO_{70}EO_{20}$; average molecular weight = 5800, Aldrich Co.) as template and HCl as pH controlling agent. In a typical synthesis, 10 g of P123 was dispersed in 75 ml of water and 300 ml of 2 M HCl solution while stirring. To it, 22 g of TEOS was added over 45 min. The gel formed was continuously stirred at 40 °C for 24 h and aged at 100 °C, for 48 h. Then, the solid product was separated by filtration, washed with deionized water, and dried, first, at 25 °C, and then, at 80 °C. The material

was finally calcined in air at 550 °C for 6 h to decompose P123 and to obtain a white powder, SBA-15.

7.2.2 Preparation of Ibu loaded CS and CS-MS hybrids

For the preparation of drug loaded samples and release experiments, Ibu was used as the model drug. Ibu was completely dissolved in hexane (30 mg/ml). To prepare Ibu loaded MS (MI-1); MS was dispersed in Ibu solution and stirred for 24 h at room temperature. The drug-loaded powder was washed carefully with hexane to remove Ibu, which is physically adsorbed or bound on the exterior surface of the prepared MI-1, and finally dried at 60 °C in air oven. The amount of Ibu in the MI-1 was determined by thermogravimetry (TGA), and found to be around 20 weight %. Similar washing procedure of Ibu from hexane from the surface of MS was also followed by Zhu and coworkers[28]. However, from environmental concerns, pentane can also be used to wash the unadsorbed drug molecules.

For preparation of CS-MS composite (CMI-1), Ibu-loaded MS i.e. MI-1, was mixed with an aqueous solution of CS. The drug-loaded MS powder was dispersed and stirred vigorously in the CS solution with the ratio of 1:10 (MS/CS), for 24 h. The final solution was poured on a glass Petri plate, and vacuum dried at 37 °C for 48 h and cured at 60 °C for 24 h. Drug-loaded CS (CI-1) film sample was also prepared for control experiments. For this, Ibu was dispersed in a CS solution of 10:90 (Ibu/CS). The drying and curing procedures were the same as for the CMI-1 system.

7.3 CHARACTERIZATION METHODS

7.3.1 X-Ray Diffraction:

The WAXD patterns of the sample powder were obtained using a Rigaku (Japan) Dmax 2500 X-ray diffractometer with Cu-Kα radiation. The system consists of a rotating anode generator with a Cu target and a wide angle powder goniometer having a diffracted beam graphite monochromator. The generator was operated at 40 kV and 150 mA. All the experiments were performed in the reflection mode. The samples were scanned between 2θ= 2° to 30 ° at a scan rate of 2 °/minute. The d-spacing was calculated by Bragg's formula, where the λ was 0.154 nm. Small angle X-ray diffractograms (SXRD) were recorded on an X'Pert Pro (Philips) diffractometer using Cu Kα radiation and a proportional counter as detector at 0.01° step size and 2 s step-time over a $0.5<2\theta<3°$ range.

7.3.2 Transmission Electron Microscopy:

Transmission electron microscopy (TEM) was carried with a JEOL 2000 EX-II instrument (JEOL, Tokyo, Japan) operated at an accelerating voltage of 100 kV. TEM samples were prepared by dipping carbon coated copper TEM grids into dilute suspensions of the sample powder in ethanol, followed by sonication in a probe sonicator for 30 minutes.

7.3.3 FTIR- Spectroscopy:

The Fourier-transform infrared (FTIR) spectra were obtained from the sample on a Perkin-Elmer Spectrum GX. The samples were mixed with dry KBr, pelletized and then scanned in the range of 4000 cm-1 to 400 cm^{-1} at a resolution of 4 cm^{-1}. A total of 10 scans were used for signal averaging.

7.3.4 Adsorption Isotherms:

SBA-15 was characterized by type IV nitrogen adsorption-desorption isotherms. N2 adsorption/ desorption isotherms at -196 °C were measured using a Micromeritics Tristar 3000 sorptometer. Prior to the measurement, all samples were outgassed at 80 °C and 10^{-6} mm Hg overnight. The specific areas of the samples were calculated using the multiple-point Brunauer-Emmett-Teller (BET) method. The pore-size distribution was calculated from the adsorption branch of the isotherms using the Barrett-Joyner-Halenda (BJH) method.

7.3.4 Thermal Methods:

The thermal gravimetric analysis (TGA) was conducted on a Perkin-Elmer TGA 7 – thermal analyzer from 50 °C to 900 °C with a heating rate of 10 °C min^{-1} under nitrogen with flow rate 20ml min^{-1}, in a platinum crucible.

Thermograms of pristine CS powder and Ibu loaded CS-MS hybrid composite systems were obtained using a Mettler-Toledo DSC instrument equipped with an intra-cooler (Mettler-Toledo, Greifensee, Switzerland). Indium standards were used to calibrate the differential scanning calorimetry (DSC) temperature and enthalpy scale. The samples were hermetically sealed in aluminum pans and heated at a constant rate of 20 °C/min, over a temperature range of 0 to 550 °C. Inert atmosphere was maintained by purging nitrogen at the flow rate of 100 mL/min.

7.3.5 Cell-Growth Studies

To demonstrate the in-vitro biocompatibility of Ibu loaded CS-MS composites, growth studies were performed for HeLa and CHO cells. Two series of experiments were designed for both types of cells: one series studies the natural cells growth on pristine CS (control) and the other was studied on the prepared CS-MS composites. After allowing 24 hours for cell adhesion, the cells were analyzed everyday (3 flasks per day) for 6 days. The relative cell-growth compared to control cells containing cell culture medium without CS was calculated by $[A]_{test}/[A]_{control}$. For this, after every 24 h, 100 µl of the cell culture was incubated for MTT assay and the absorbance was taken at 490 nm wavelength in Spectrophotometer Plate Reader.

7.3.6 *In-vitro* Release Studies:

The in-vitro drug-release study was carried out by immersion of around 1.5 cm x 1.5 cm films of CMI-1 and CI-1 into 25 ml of simulated body fluid (SBF) (pH 7.4). For comparative studies, the release experiments were done in silent and ultrasound conditions. To study the effect of ultrasound on drug release and pulsatile release, the drug loaded sample flask was immersed in the ultrasound bath (frequency 33 kHz) and was continuously irradiated for ultrasound at 37 °C and the resultant release medium (5.0 ml) was removed for analysis at given time intervals, and replaced with fresh release media (SBF). The in-vitro medium thus collected was filtered through a 0.5-µm Millipore filter. The concentration of Ibu released was determined by UV-VIS spectrometer at λ 264 nm. Release studies were further performed by varying the temperature and pH of the release medium under silent conditions, i.e. without ultrasound. The temperature of the release media was kept constant by continuous addition of ice to the ultrasound bath. All the release experiments were run in a triplicate and the average values obtained are given.

7.4 RESULTS AND DISCUSSIONS

7.4.1 Characterization and General Features of CS-MS system

The TEM image of the MI-1 sample possesses an ordered mesoporous structure as shown in **Figure 7.1.** The small angle X-ray diffraction (SXRD) pattern of MS (SBA-15) and MI-1 is given in **Figure 7.2**. As compared with MS, there is a remarkable decrease in the intensity of the peaks of MI-1, which corresponds to (100),

(111) and (200) planes based on the hexagonal unidirectional structure. The peak positions were shifted to higher 2θ value because of the inclusion of drug molecules to the inter-pore region of MS.

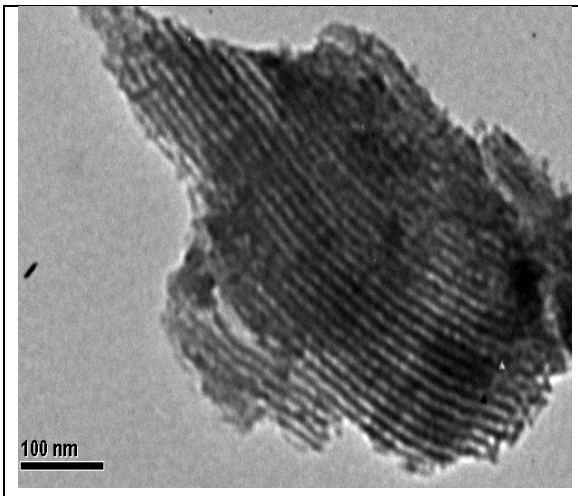

Figure 7.1 TEM image of MI-1

This observation is similar with the reported result[29], in which the authors demonstrated that this behavior is attributed to the filling of surfactant into MS pores. The d_{100} spacing and unit-cell size (a_0) for MI-1 measured to be 40.30 Å and 45.42 Å, respectively. As a_0 represents the repeated distance between two pore centers in the hexagonal array, the pore diameter can be calculated from a_0 by subtracting 10 Å, which is an approximate value of the pore-wall thickness[30]. Therefore, a pore diameter of 35.42 Å is obtained, which means that the pore size of MS is large enough to allow access to the large internal surface area to accommodate Ibu molecules[31]. The wide angle X-ray diffraction (WXRD) patterns of CMI-1 and CI-1 are given in the INSET of **Figure 7.2**. All the samples show a characteristic peak at around 21 °, which confirms the presence of crystalline CS in the composites. MS (SBA-15) and MI-1 were characterized by type IV nitrogen adsorption-desorption isotherms. MS has a Brumauer-Emmet-Teller (BET) surface area and pore volume of 900 m^2/g and 0.92 cm^3/g, respectively. On the other hand, MI-1 has a BET surface area of 335 m^2/g and pore volume of 0.31 cm^3/g. In addition, the pore size distributions of the MS and MI-1 are centered at 2.9 and 2.1 nm, respectively. The obtained results suggest that the impregnation of Ibu in the mesoporous channels leads to a decrease in the pore diameter, BET surface area, and pore volume. This observation confirms that Ibu molecules have been successfully retained inside the pore channels of mesoporous host.

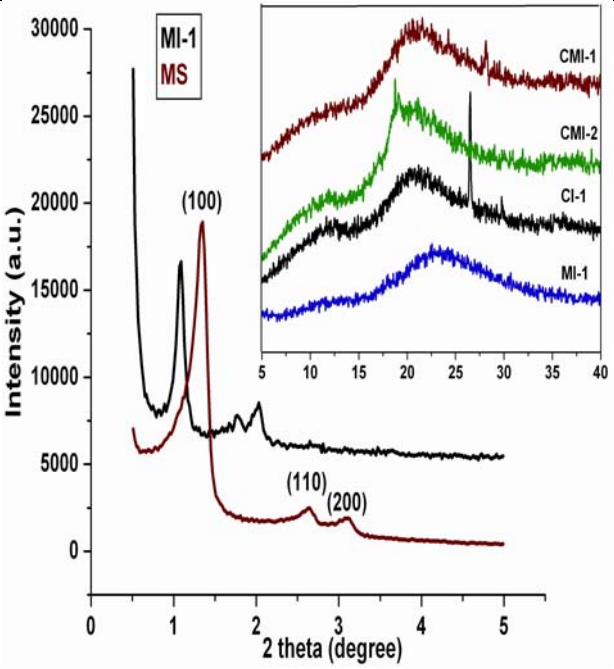

Figure 7.2 Low Angle and Wide Angle (INSET) patterns of composites.

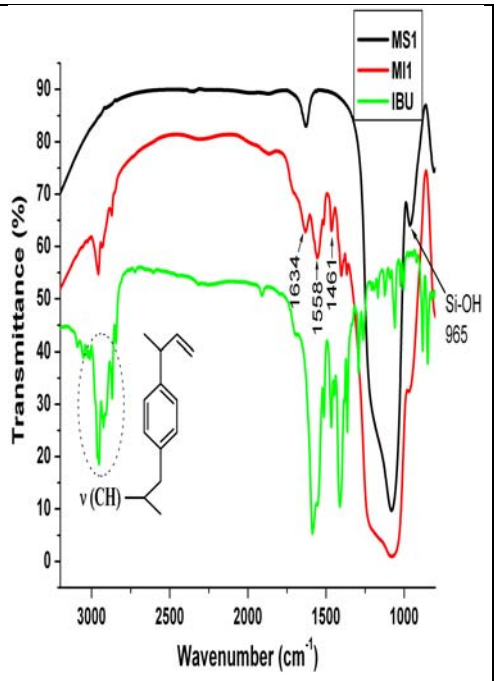

Figure 7.3 FT-IR spectral pattern of the Ibu loaded composites.

Figure 7.3 shows the FT-IR spectra of pristine Ibu and drug loaded MS samples. As compare to the pristine Ibu, the band corresponding to a free carboxylic acid (1718 cm^{-1}) in Ibu, has changed to a carboxylate one (1461 and 1634 cm^{-1}) in MI-1, which suggests the interactions between -COOH group of Ibu and Si-OH group of the MS host. Typical υ (CH) stretching vibrations of Ibu are observed at 2958, 2927, and 2871 cm^{-1} for pristine Ibu as well as for MI-1. In addition to that, Si-OH vibration band at 965 cm^{-1} present in MS[32], almost disappears after Ibu loading, which suggests that the –H bond has been formed between the –COOH group of Ibu and the Si-OH of the MS host[33]. Moreover, the FT-IR spectra of the prepared composites confirm that the structural integrity of the drug molecules is preserved upon intercalation with the MS pores with a structure and geometry similar to that of the drug molecule outside the MS pores. **Figure 7.4** shows a typical ^{13}C-MAS NMR spectrum for MI-1 sample. The peak of the carboxylic group of pristine Ibu at 182.85 ppm is shifted slightly to 184.02 in the MI-1 system due to the interaction between –COOH group of Ibu and Si-OH group of MS.

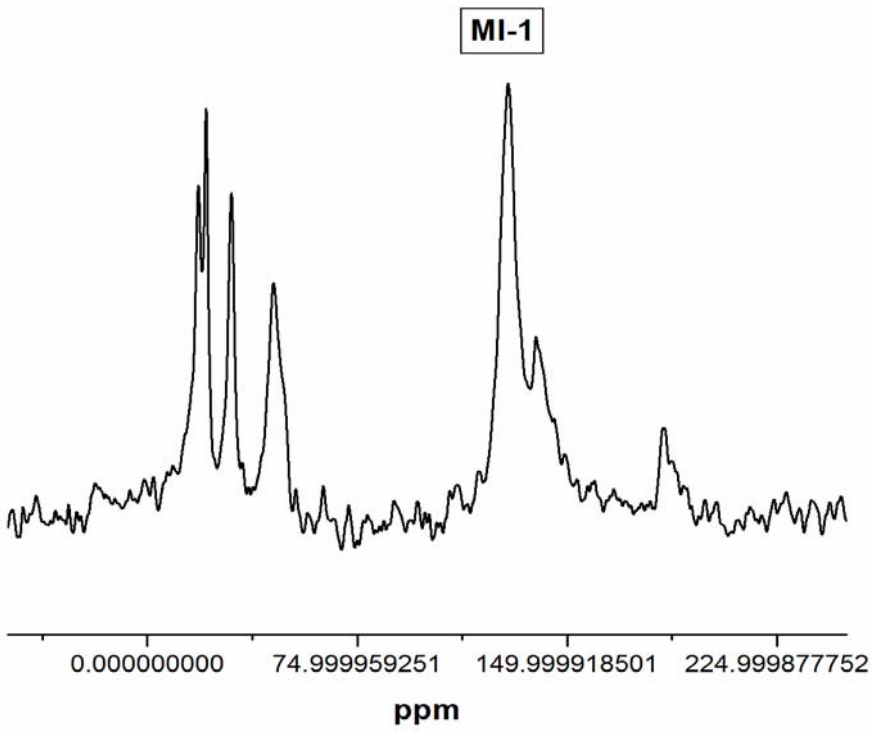

Figure 7.4 ^{13}-C-NMR spectrum for MI-1 sample.

7.4.2 Thermal Methods:

TGA curves of the pristine MS and the Ibu loaded CS-MS hybrid composites are shown in **Figure 7.5 (a)** and the results are summarized in **Table 7.1.** All the samples showed a weight loss below 180-200 ºC that resulted from the physical loss of water. For MI-1, another weight loss (about 18-20 %) occurred between 240-320 ºC, which demonstrates that the Ibu storage capacity of the MI-1 is ~20%.

Table 7.1 TGA results for the Ibu loaded MS and CS-MS composite systems.

	50-200ºC (wt %)	**240º-320 ºC (wt %)**	**320-480 ºC (wt %)**	**SiO_2 content (wt %)**	**Storage capacity (mg $_{Ibu}$/g $_{SiO2}$)**
MI-1	18.4	34.77	-	33.61	885.12
CMI-1	15.1	27.89	20.10	26.62	790.65

In the Ibu loaded CS-MS hybrid composite systems three weight losses were detected from 180-480 ºC. The loss of 15%, between 180-320 ºC is attributed to the removal of Ibu from the CS-MS systems, while the other two weight losses occur by the removal of the CS macromolecular chains. Here the Ibu storage capacity in the CS-MS

composites is little lower than MI-1, which may have resulted from the loss of some Ibu molecules during the composite preparation process. However, this drug storage capacity is almost two times higher than that of the conventional mesoporous material[34]. **Figure 7.5 (b)** shows the DSC curves of pristine CS and other CS-MS composite samples. Due to the melting of the ibuprofen confined to the pores, a broad endotherm in the DSC curve was observed before the sharp melting of bulk ibuprofen. DSC studies were performed to understand the thermal behavior of the CS-MS composites. Polysaccharides usually have a strong affinity for water and in solid state these macromolecules have disordered structures that can be easily hydrated. The hydration properties of polysaccharides depend on primary and supramolecular structures. The endotherm related to evaporation of water is expected to reflect the molecular changes brought in after the composite fabrication process. In CSI the bound water molecules are associated with hydrophilic hydroxyl groups. The thermogram of pristine CSI showed endotherm at 141.24 °C with the enthalpy of fusion (ΔH) 210 J/g. The hydrophilicity of CS-MS composite samples is higher, which might be responsible for its increase in the water-holding capacity. On the basis of these results it can be stated that increase in the polar groups from Si-OH groups and reduction in crystalline domains caused an increase in the water-holding capacity of CS-MS composites. The second thermal event observed was an exotherm due to the decomposition of the biopolymer. Owing to the differences in the chemical characteristics, changes in the exothermic peak of CSI and CS-MS samples were also observed.

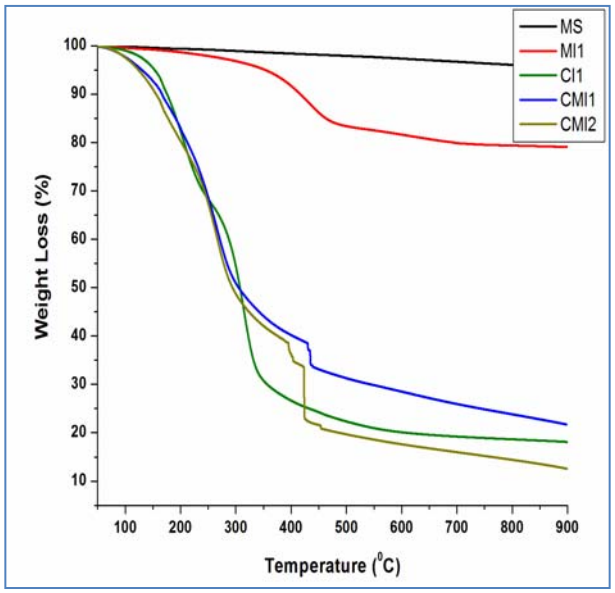

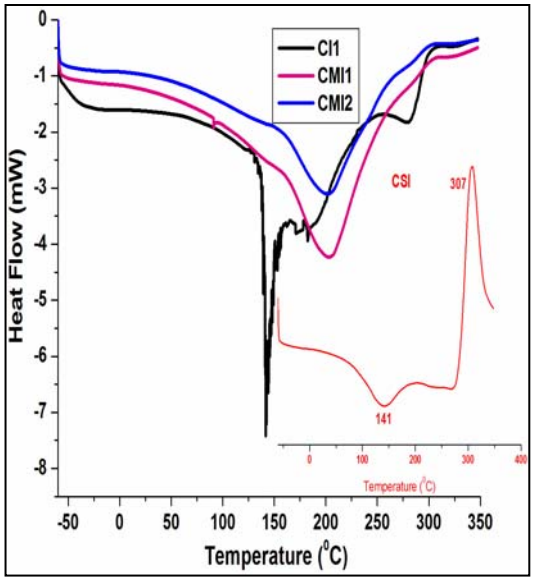

Figure 7.5 (a) TGA of composites | **(b)** DSC of the composites

7.4.3 Cell Growth studies

The prepared samples were subjected to the cell-growth studies and the results are shown in **Figure 7.6**. On the basis of the results, we predict that the incorporation of MS may significantly enhance the interactions between biopolymer matrix and cells. The results indicated that the cell growth for blank and CS-MS hybrid system were very similar indicating that the increase in numbers of cells was not hindered by the presence of either CS or MS. Also, the Si-OH groups of MS may develop London-Vander Valls forces and -H bonding with the cells. Suspended together with MS, the biopolymer matrix was surrounded and/ or adsorbed by the inorganic host, which acts as a bio-adhesive between the polymer and the cells.

The developed London- Vander Valls forces and H-bonding may be mainly responsible for the increased polymer-cells interactions. In addition to that the mesoporous structure of the inorganic silica host may allow enhanced cell invasion in the matrix. Although cell-growth studies shown that the samples does not affect the normal growth of cells, still in-vivo testing should be done to provide a better insight on its biological suitability.

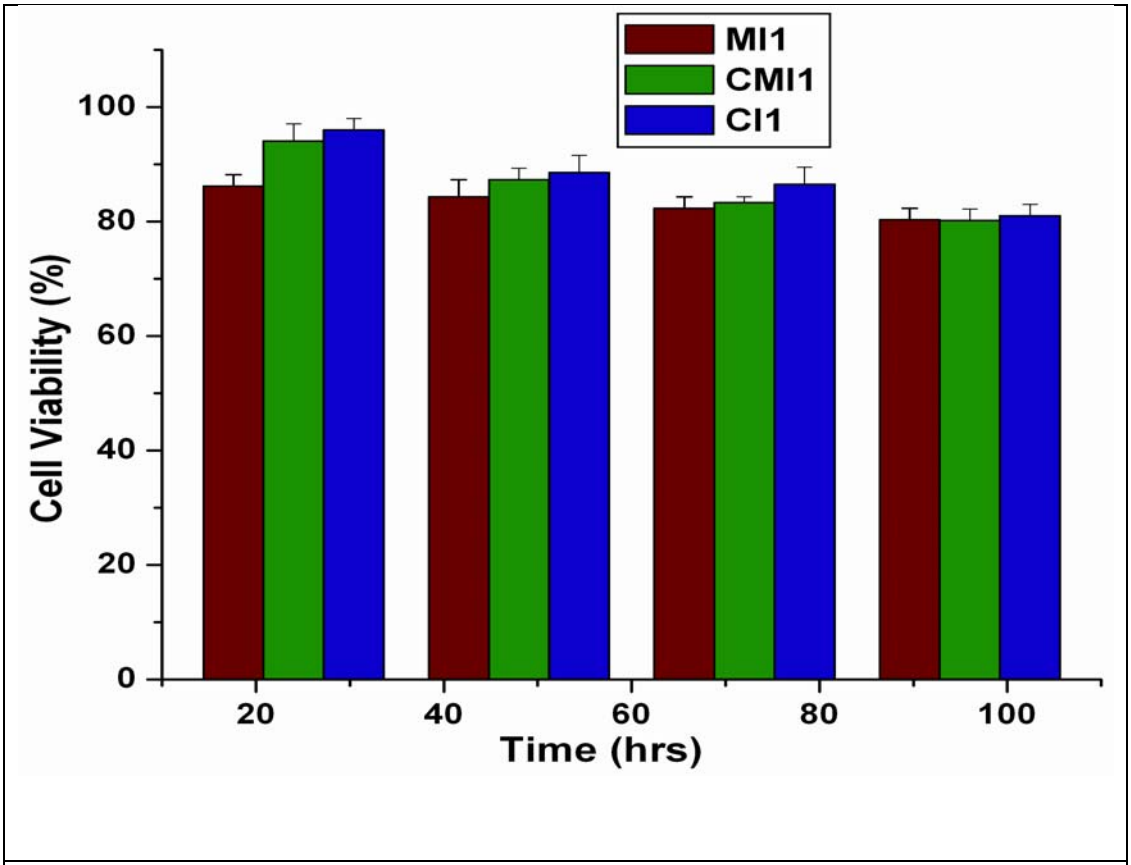

Figure 7.6 *In-vitro* cell-growth studies of the prepared composite samples.

7.4.4 In-Vitro Drug Release Studies:

7.4.4.1 Effect of temperature on drug release:

We have studied the stimuli-responsive investigation of the effect of temperature on the drug release of CS-MS system. The results are given in **Figure 7.7** (**a**) and it depicts that the range of temperature over which the transition takes place is quite broad (30-40 °C), which is due to the steric hindrance of CS chains with the silica host, and a transition is detected at 35 °C for CMI samples. In other words, CS inside CMI can respond to thermal stimulation of the release media. At low temperature, the drug molecules are restrained in the porous MS channels, and along with CS molecular chains, Ibu molecules takes part in the formation of -H bonding between CS and Ibu molecules. CS has a high water retention capacity, and it absorbs enormous amount of water. So, when the Ibu loaded CS-MS samples immersed in the aqueous release media, the films absorbs enough water, eventually taking the form of a hydrogel. However, at low temperature this water is in the form of a bound state, and as the temperature increases these bound-water molecules gains an enthalpy and changes from a bound state to a free state, with subsequent release of the incorporated drug molecules from the matrix. Moreover, MS is not a thermo-sensitive material, so we may predict that as the temperature increases, the biopolymer chains swells within the MS pore network resulting in the disruption of weak -H-bonds, accelerating the drug molecules from the pores.

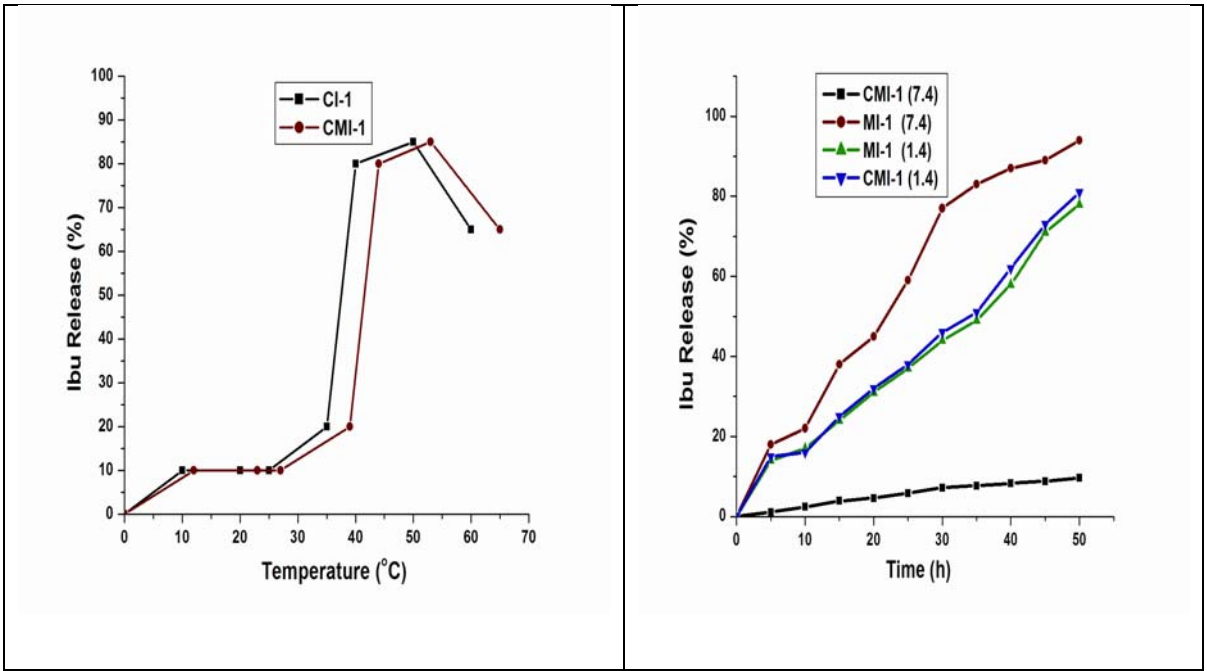

Figure 7.7 (a) Effect of temperature **(b)** Effect of pH of release media.

The obtained results reflect a situation similar to that obtained by Li et. al[35]. Consequently, this implies that the swelling of the polymer chains, as a consequence of temperature can be used for controlled and thermally-stimulated drug release.

7.4.4.2 Effect of pH on drug release

Since Ibu is mainly adsorbed in the stomach and proximal intestine, the release profiles of Ibu loaded samples were determined in simulated gastric fluid (pH 1.4) and simulated body fluid (pH 7.4). It is evident from **Figure 7.7** (**b**) that the release profile of both the systems (MI-1 and CMI-1) are very similar in the medium of pH 1.4, where the amount of drug released from the two systems reaches >75 % in 50 h. This behavior shows that both systems display sustained release, and the possible explanation is, at this low acidic pH, the $–NH_2$ groups of CS gets protonated, leading to the dissociation of the H-bonds involving the CS $–NH_2$ groups with the -COOH groups of the Ibu molecules. Hence, we can say that at this low pH, CS matrix could not cap the openings of the MS channels. Therefore, the drug molecules can easily diffuse out from the MS pores into the release medium. On the other hand, the release profile in the medium of pH 7.4 is apparently different. We observed that MI-1 also exhibits the sustained release property and the amount released reaches 90 % in 50 h, i.e. the release rate in the pH 7.4-release medium is higher than that in the pH 1.4 medium.

This dramatic difference in release rates should mainly be attributed to the unusual solubility of Ibu in release media of different pH values. Ibu is sparingly soluble in low-pH solutions (pH<7) but is readily soluble in high pH (>7) solutions. The obtained results find similarity with the findings of Donath and coworkers[36]. For CMI system, the release rate is very low, and the released amount reaches 12 % over a period of 50 h. This finding indicates the good storage space of MS and sealing effect of the CS chains at pH 7.4 solution; i.e. the CS chains are compact with MS, which leads in decreased permeability at the higher pH value, and the CS chains could easily cap the openings of the MS channels. It can be concluded that the CMI system has a much better controlled release than MI, and CMI can achieve a stimulated pH-responsive delivery profile by changing the pH value of the release medium. This kinetic profile offers a great interest for pharmaceutical applications in order to achieve better therapeutic efficacy and rapid delivery profile of poorly water-soluble drugs like Ibuprofen.

7.4.4.4 Effect of Ultrasound (US)

Figure 7.8 (**a-b**) shows the release profiles of Ibu from MI-1, CI-1, and CMI-1 under silent condition and subsequent release profile for CI-1 and CMI-1 samples under ultrasound irradiation, respectively. As shown in figure 5a, under silent condition, the release of Ibu stored in MS occurs only after the release medium has penetrated among the MS channels and subsequent dissolution of Ibu in the aqueous media.

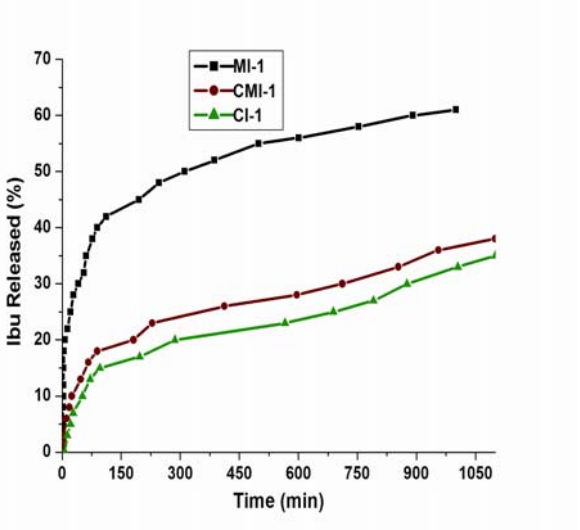

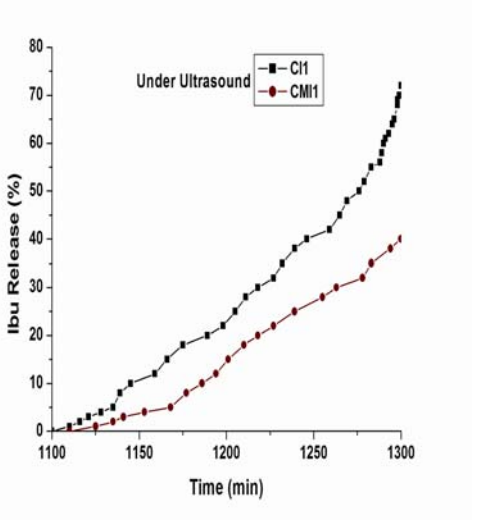

Figure 7.8 (a) Drug Release profile under silent condition.	**(b)** Release profile under Ultrasound.

Remarkably, MI-1 showed very fast release within first 100 min, while the subsequent release rate was quite low as compare to the initial rate. Similar release pattern was also observed by Linden et al[37], while according to Xue et al[38] this behavior of drug release could be ascribed to favorable physical hosting of the drug inside the inter-pore network of MS and ionic interactions of –Si-OH groups of MS and –COOH groups of Ibu molecules. For a successful controlled release of a drug, the initial burst from the inorganic host framework of MS should be controlled. As shown in **Figure 7.8** (a), the initial drug release rate of CMI-1 was substantially reduced. The Ibu release profile of CMI-1 was quite similar to that of CI-1. Conceivably, this similar release rate could be attributed to a strong dipolar interaction and H bonding between the abundant Si-OH groups of MS, -NH_2 of CS and –COOH groups of Ibu. The release profile was found to be a two step. In the initial stage a small amount of drug was continuously released for about the first 250 minutes, which may be due to the release of excessive drug

molecules which were weakly entrapped inside the pores or located at the external MS surface. The second stage shows extremely slow liberation of Ibu, which could be due to the physical blocking of the entrapped drug molecules inside the solvent filled channels of MS, along with CS chains. This demonstrates that the release of Ibu can be successfully controlled by the mixing of CS with MS. To understand the effect of US on the drug release profile of CI-1 and CMI-1, the samples were exposed to US for another 200 minutes to increases the release rates after 1100 minutes of release experiment under silent condition. For this the samples were immersed in the release media, and kept in an US bath, maintained at a constant temperature by continuous addition of ice. During the course of ultrasonic irradiation, it was observed that Ibu was continuously released from both CI-1 and CMI-1, while US was found to have an apparent effect to enhance the drug release kinetics of both the systems.

It has been well documented that US could increase the drug-release rate in polymeric systems[39] while, Kost[40] reported the enhanced release kinetics in a nondegradable polymer, exposed to ultrasound. In addition to that, US has already been used to alter polymer membrane permeability to stimulate the release of polymer encapsulated drugs[41]. This release effect can be ascribed to the enhancing effect of US irradiation which is capable of reversibly losing the rigid packing of the hydrocarbon chains[42] which results in increase the permeability of water and drug through the polymer. These effects can generally be explained by an important phenomenon called cavitation which is generated by ultrasonic irradiation.

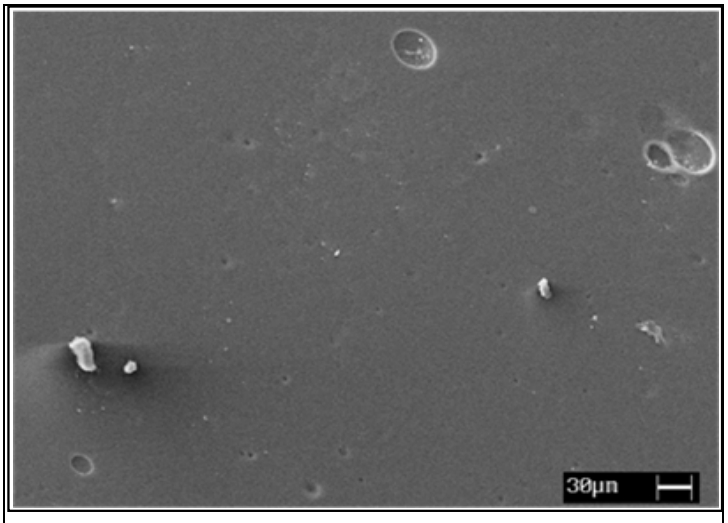

Figure 7.10 SEM image of CMI-1 after ultrasound irradiation for 48 h.

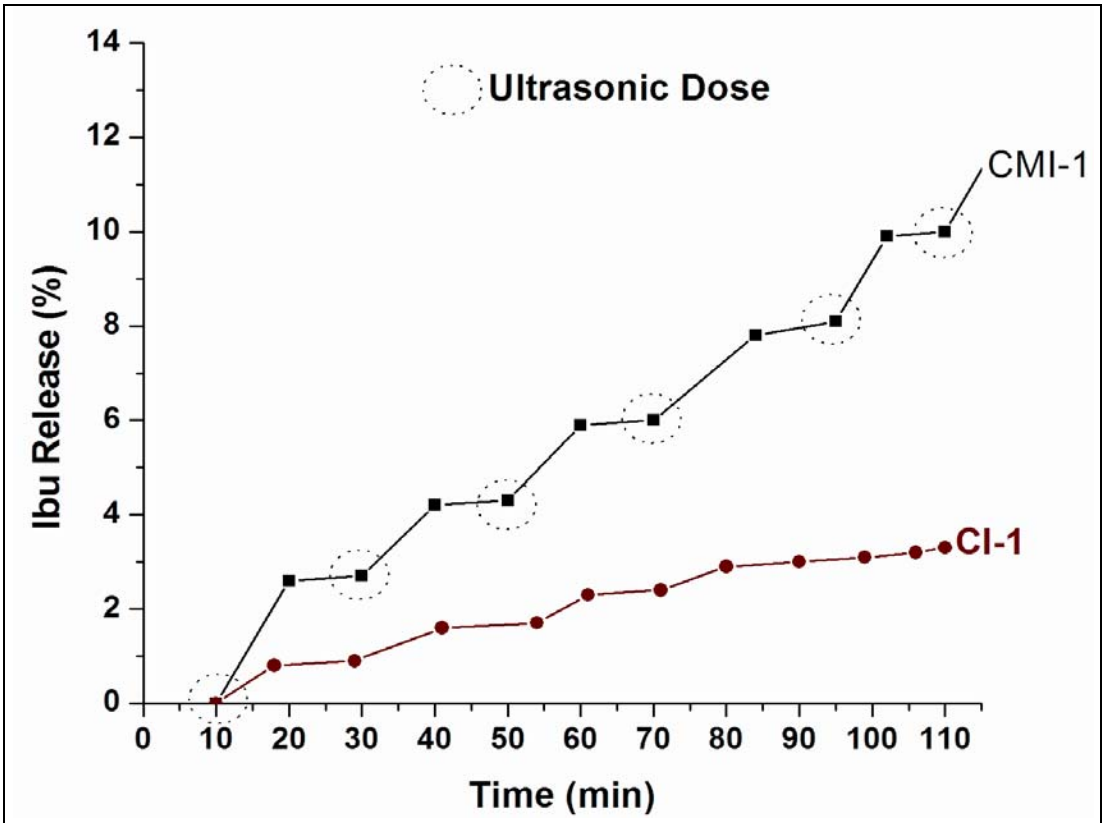

Figure 7.9 Effect of US on the pulsatile release of Ibu from the prepared composites.

Cavitation is a well-known effect of US[43] in which the burst of bubble takes place in an adiabatic fashion, which leads to concentrate the acoustic energy of the release system and creates conditions of temperature and pressure[44].

Moreover, the release effect of drug molecules from the CS-MS system is a combination of mechanical actions imposed by ultrasonically induced air pockets in the matrix, which may include (1) the disorganization of biopolymer film, and (2) subsequent formation of transport channels in the inter-pore network of MS (**Scheme 7.1**). To investigate the effect of US on the pulsatile release of the drug from CI-1 and CMI-1, the specimens were given an US dose of 10 minutes for around 120 min. The results were shown in **Figure 7.9**, where the release of Ibu was observed to start immediately for CMI-1, and sustained until the US irradiation was discontinued, while in the case of CI-1, the amount of released Ibu continuously decreased after a second irradiation. On the other hand, for CMI-1 regular pattern was displayed with repeated ultrasonic dose and the amount of Ibu released in each step was nearly the same each

time, and was higher than that of CI-1 release profile. Since, the extent of Ibu loading for both the systems was same at around 15 mg g^{-1}, this difference does not originate from the amount of Ibu present in the matrix. It suggests that CMI-1 released the Ibu more effectively than CI-1, and it is believed that the hydrophilicity, high permeability, and subsequent high ultrasonic susceptibility of CMI-1, makes it possible for ultrasound to be transferred deep into the biopolymer matrix, hence promoting the regularity of the pulsatile release of the drug from the CMI-1 system. This may allow repeated operation for a continuously controlled release of a drug into a patient's body to maintain a therapeutically effective dose for a longer period of time to efficiently treat the disease. Polymeric materials can be predicted to undergo mechanical damage or surface rupture after the release experiment due to the cavitation created by high-power ultrasound.

However, as expected, the sample films were intact and we could not observe any microholes or cracks on scanning electron microscope (SEM) images after the ultrasonic irradiation as shown in **Figure 7.10**. Consequently, US could be applied to enhance the drug-release kinetics in a nondestructive fashion. Apart from increasing the interaction with Ibu, the extended polymer chains of CS would act as a holder to retain the drugs inside the pores as verified by the nitrogen isotherms showing the complete filling of the pores after adsorption. When the release of drug is governed by diffusion through the matrix, the kinetics of release from the matrices is generally explained using the Higuchi model[45].

$$Mt/M = \sqrt{t}$$

Where, M_t and M_∞ denote the cumulative mass of drug released at time t and at infinite time, respectively, and K denotes the proportionality constant[46]. According to the model, for a purely diffusion-controlled process, the linear relationship is valid for the release of relatively small molecules distributed uniformly throughout the carrier. However, it was observed that all the releasing systems display a two-step release based on the Higuchi model, which is in good agreement with the Anderssons report[47]. The plot of the cumulative amount of Ibu released versus the square root of time resulted in a straight line as shown in **Figure 7.11 (a)**.

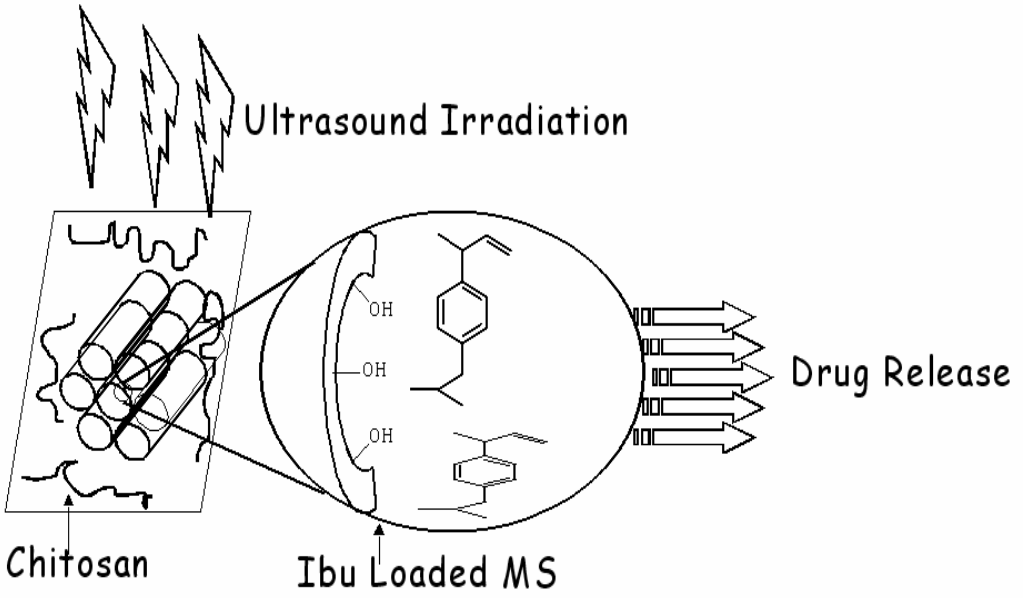

Scheme 7.1 Schematic illustration of release of drug under US.

Assuming that the diffusion coefficient is constant with respect to time and position in a plane sheet, the constant K is related to the diffusion coefficient by

$$K = \sqrt{4D/l^2\pi}$$

Where, D is the diffusion coefficient of the drug, and 2l is the thickness of the plate[48]. As shown in **Figure 7.11 (b)**, the diffusion coefficient of CS was 0.484×10^{-9} m^2/min, whereas that of CS-MS was 0.65×10^{-9} m^2/min, about 1.3 times higher. It is generally known that the polymer–SiO_2 hybrid membrane shows excellent permeability and hydrophilic properties when non-modified silica is mixed with a hydrophilic polymer. The enhanced diffusion coefficient might be because the MS is a highly porous material and CS is a dense and hydrophilic polymer. When ultrasound was applied to both systems, the diffusion coefficients of CS and CS- MS were enhanced by a factor of 3.4 (1.664×10^{-9} m^2/min) and 6.5 (4.232×10^{-9} m^2/min), respectively. US was found to be more influential on the CS-MS system than on the pristine CS.

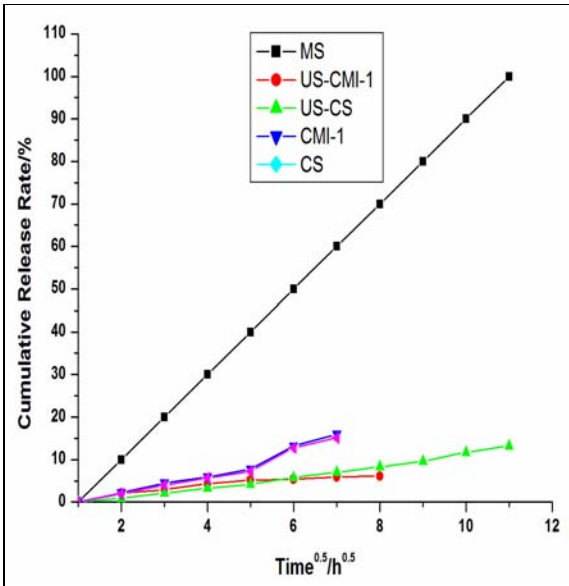

Figure 7.11 (a) Higuchi model for the release of Ibu from the composites.

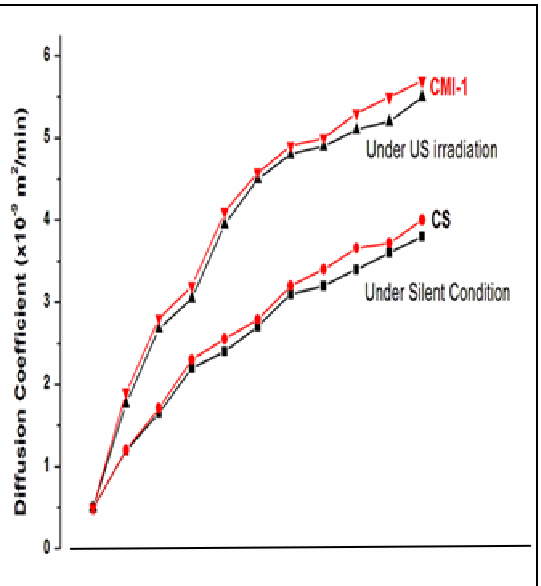

(b) Diffusion coefficient for CS and CS-MS composite systems.

Under ultrasonic irradiation, the hydrophilicity and high permeability of CS-MS should improve the penetration of water into the matrix body. Because water is a better contact medium for US than the organic solid CS, US energy could be more effectively transferred to the CS-MS matrix than to CS. As a result, the addition of MS into CS could enhance the ultrasonic susceptibility and subsequent high-diffusion rate of the drug.

We envision that CS-MS system could serve as a novel biocompatible sustained release drug carrier, and allows us to think about new potential applications in medical sciences, and more specifically, in biomaterials and tissue engineering applications.

7.5 CONCLUSIONS:

In conclusion, we have designed a novel stimuli-responsive controlled drug-release system where ultrasonic irradiation was used as an external trigger for smart drug release to obtain optimal therapeutic effects. The overall system was composed of MS as a drug storage device and CS as an implantable body. This system is efficient for storage and release of drug, further controlled by temperature and pH at will. CS successfully suppressed the initial burst of Ibu from the MS. Besides; the ultrasound was effective to improve the release kinetics of CS-MS system in a nondestructive manner. We envision that this novel system, which combines the advantages of both

high drug storage capacity and the property of stimuli-responsive controlled release, could play a significant role in the development of new generation, site specific, and smart drug release.

7.6 REFERENCES:

1. X. Qu, A. Wirsen, and A-C. Albertsson, *J. Appl. Polym. Sci*., **74,** 3193 (1999).
2. S.V. Madihally, and H.W. Matthew, *Biomater.,* **20,** 1133 (1999).
3. E. Khor, and L.Y. Lim, *Biomater.,* **24,** 2339 (2003).
4. K.Y. Lee, W.S. Ha, and W.H. Park, *Biomater.,* **16,** 1211 (1995).
5. S. Miyazaki, K. Ishii, and K. Nadai, *Chem. Pharam. Bull. (Tokyo*) **29,** 3067 (1981).
6. S. Roller, and N. Corill, *Intern. J. Food Microbiol*., **47,** 67 (1999).
7. N. Kubota, and K Ogha, *J. Appl. Polym. Sci*., **42,** 495 (1991).
8. S. Miyazaki, and H. Yamaguchi, *Acta. Pharm. Nord*., **2,** 401 (1990).
9. M.R. Griffin, *Am. J. Med.*,**104,** 23S (1998).
10. I, Izquierdo_Barba, L. Ruiz Gonzalez, J.C. Doadrio, J.M. Gonzalez-Calber, and M. Vallet-Regi, *Solid State Sci*., **7,** 983 (2005).
11. M. Vallet-Regi, A. Ramila, R.P. del Real, and J. Perez-Pariente, *Chem. Mater*., **13,** 308 (2001).
12. B. Munoz, A. Ramila, J. Perez-Pariente, and M. Vallet-Regi, *Chem. Mater*., **15,** 500 (2003).
13. S.S. Park, and C.S. Ha, *Chem. Rec*., **6**, 36 (2006).
14. A.L. Doadrio, E.M.B. Sousa, J.C. Doadrio, J. Perez-Pariente, I. Izquierdo-Barba, and M. Vellet-Regi, *J. Control Rel.,* **97,** 125 (2004).
15. K. A. Fisher, K.D. Huddersman, and M.J. Taylor, *Chem.- A Eur. J.,* **9,** 5873 (2003).
16. N.K. Mal, M. Fujiwara, and Y. Tanaka, *Nature*, **421,** 350 (2003).
17. P. Horcajada, A. Ramila, J. Perez-Pariente, and M. Vallet-Regi, *Microporous Mesoporous Mater*., **68,** 105 (2004).
18. J. Kost, J. Wolfrum, and R. Langer, *J. Biomed. Mater. Res.*, **21**A, 1367 (1987).
19. A.S. Huffman, A. Afrassiabi, and L.C. Dong, *J. Control. Rel.,* **4,** 213 (1986).
20. J. Kost, K. Leong, and R. Langer, *Proc. Natl. Acad. Sci, USA*, **86,** 7663 (1989).
21. S.R. Eisenberg, and A.J. Grodzinsky, J. *Membr. Sci*., **19,** 173 (1984).

22. P. Dietmar, *J. Mater. Chem*., **6,** 1605 (1996).
23. C. Charnay, S. Begu, C. Tourne-Peteilh, L. Nicole, P.A. Lerner, and J.M. Devoisselle, *Eur. J. Pharm. Biopharm*., **57,** 533 (2004).
24. C.Y. Lai, B.G. Trewyn, D.M. Jeftinija, K. Jeftinija, S. Xu, S. Jeftinija, and V.S.-Y. Lin, *J. Am. Chem. Soc.,* **125,** 4451 (2003).
25. I. Slowing, B.G. Trewyn, and V.S.-Y. Lin, *J. Am. Chem. Soc.,* **128,** 14792 (2006).
26. D. Zhao, J. Sun, Q. Li, and G.D. Stucky, *Chem. Mater*., **12,** 275 (2000).
27. D. Zhao, J. Feng, Q. Huo, N. Melosh, G.H. Fredrickson, B.F. Chmelka, and G.D. Stucky, *Science*, **279,** 548 (1998).
28. Y. Zhu, J. Shi, W. Shen, H. Chen, X. Dong, and M, Ruan, *Nanotechnol.,* **16,** 2633 (2005).
29. M.C. Burleigh, M.A. Markowitz, M.S. Spector, and B.P. Gaber, *J. Phys. Chem., B*, **105,** 9935 (2001).
30. C.Y. Chen, S.L. Burkett, H. X. Li, and M. E. Davis, *Microporous Mater*., **2,** 27 (1993).
31. M. Vallet-Regi, A. Ramila, R.P. del Real, and J. Perez-Pariente, *Chem. Mater*., **13,** 308 (2001).
32. M.S. Morey, S. O'Brien, S. Schwarz, and G.D. Stucky, *Chem. Mater*., **12,** 898 (2000).
33. Y.F. Zhu, J.L. Shi, Y. S. Li, H.R. Chen, W.S. Shen, and X.P. Dong, *Microp. Mesop. Mater.,* **85**, 75 (2005).
34. A. Ramila, B. Munoz, J. Perez-Pariente, and M. Vallet Regii, *J. Sol Gel Technol.,* **26,** 1199 (2003).
35. Z.Z. Li, L.X. Wen, L. Shao, and Z.F. Chen, *J. Control. Rel.,* **98,** 245 (2004).
36. X. Qui, S. Leporatti, E. Donath, and H. Mohwald, *Langmuir*, **17,** 5375 (2001).
37. J. Andersson, J. Rosenholm, S. Areva, and M. Linden, *Chem. Mater*., **16,** 4160 (2004).
38. J. M. Xue, and M. Shi, *J. Control. Rel.,* 98**,** 209 (2004).
39. N. Y. Rapoport, D.A. Christensen, H.D. Fain, L. Barrows, and Z. Gao, *Ultrasonics*, **42,** 943 (2004).
40. J. Kost, Ultrasound for controlled delivery of therapeutics, *Clin. Mater*. **13,** 155 (1993).

41. C.S. Kwok, P.D. Mourad, L.A. Crum, and B.D. Ratner, *J. Biomed. Mater. Res.*, **57,** 151 (2001).
42. E. B. Flint, and K. S. Suslick, *Science*, **253,** 1397 (1991).
43. C.E. Banks, and R.G. Compton, *Chem. Phys. Chem.,* **4,** 169 (2003).
44. I. Lavon, and J. Kost, *J Control. Rel.,* **54,** 1 (1998).
45. T. Higuchi, *J. Pharm. Sci.,* **52,** 1145 (1961).
46. S.S. Shah, M.G. Kulkarni, and R.A. Mashelkar, *J. Control. Rel.,* **15,** 121 (1991).
47. J. Andersson, J. Rosenholm, S. Areva, and M. Linden, *Chem. Mater.,* **16,** 4160 (2004).
48. N.K. Pandit, and D. Wang, *Int. J. Pharm. Sci.,* **167,** 183 (1998).

CHAPTER VIII

Conclusions

8.1 SUMMARY AND CONCLUSIONS:

The present study was investigated with a primary objective of intercalating Chitosan (CS) into Montmorillonite (MMT) clay and further modifies CS onto surface by chemical modification methods like grafting.

Although there are several reports on grafting of other synthetic polymers onto CS, but our study was mainly focused on the chemical grafting of poly-lactic acid (PLA) by a simple polycondensation method, and photo-grafting of poly dimethyl siloxane (PDMS) chains onto CS. The influence of intercalation of CS into MMT, and surface modifications on the properties was deduced from their physio-morphic analysis, cell-viability and protein adsorption studies, and the most important the controlled drug release experiments.

The **Chapter 1** portrays the literature background and main motivation for this study, and **Chapter 2** describes the objectives and approaches focused in the present study.

In **Chapter 3,** the intercalation chemistry of CS with MMT is described along with the grafting of PLA onto CS without any catalyst. The protonation of CS seems to be crucial for the intercalation into MMT by cation exchange process, assisted by H-bonding between CS and MMT. The grafting of PLA chains imparts hydrophilicity and desirable swelling properties to the CS based nanohybrids. Moreover, the increasing content of MMT decreases the water absorption and contact angle values, and imparts little branched crystalline structure in the films. Porous scaffolds and smooth films of the Ibuprofen (Ibu) drug loaded CS-g-LA/MMT nanohybrids were also prepared and are subjected to the controlled release studies. We found that the incorporation of MMT platelets controls the initial burst of the drug from the nanohybrids.

In **Chapter 4,** the photo-grafting of PDMS onto MMT intercalated CS is discussed. The grafted nanohybrids show interesting structural and bio-functional properties. The grafted PDMS chains acts as a plasticizer to give flexibility to CS films. Reduction in the amount of the single adsorbed protein on the CS-g-PDMS films was found to be around 40-50 %. It could be ascribed to the presence of highly hydrated thick layer around the grafted samples.

The use of CS was further extended to biomineralize anionic clay, Layered Double Hydroxide (LDH) onto the surface of CS by co-precipitation method, in **Chapter 5.** In this study, we have given a novel hypothesis of the biosynthesis of LDH with novel morphological and physio-chemical properties. The prepared nanohybrids were further studied for *in-vitro* controlled drug delivery and buffer capability. The release studies showed that the CS-LDH was a suitable candidate for site-specific release of a drug, and further it can be used as an effective antacid.

Chapter 6 describes an interesting and novel approach of Biomimetic synthesis of Hydroxyapatite (HAP), a natural bone mineral, by a cheap agricultural waste called as wheat bran. The physio-chemical characteristics confirmed the nucleation and crystal growth of HAP in the presence of phytase enzyme. The prepared HAP nanoparticles were further evaluated for Bioresorption and physiological stability experiments. The biosynthesized HAP was found to be cell-compatible by *in-vitro* cell-culture studies.

In an another interesting study, CS is used to prepare composites with Mesoporous silica (MS) and Ibuprofen (Ibu) drug is loaded to study the stimulated release by varying temperature, pH and by applying Ultrasound (US) to the prepared drug loaded composites in **Chapter 7.** Here, CS successfully suppressed the initial burst of Ibu from the MS and US can effectively improve the release kinetics of CS-MS system in a non-destructive manner. We envision that this novel system, which combines the advantages of high drug storage and the property of stimuli-responsive controlled release could play a significant role in the development of new-generation, site-specific, smart drug release.

8.2 FUTURE PERSPECTIVES:

On the basis of the above results of the present investigation, the further research can be extended to study the following aspects;

- ✓ In-situ polymerization of PLA into MMT, and grafting onto CS, could be more interesting, and better thermo-mechanical properties can be expected.

- ✓ The preparation of surface modified CS with various elastomers, to improve the bio-functional properties, and to study the adsorption studies of various properties.
- ✓ To study the biomineralization process of LDH on various biopolymers like cationic CS and anionic biopolymers like Alginate, Carrageenan etc, and to study the control over the LDH particle size, to get a better drug release.
- ✓ To prepare CS-MS composites and study release rates *in-vivo* under the influence of ultrasound.
- ✓ In-vitro and In-vivo sustained release studies of anti-cancer drugs like Taxol, under the pulsatile ultrasound effect from the prepared nanohybrids.

Publications

Research Articles:

1. A. P. Kumar**, D. Depan,** and R.P.Singh, Durability of Composites of natural fiber and EP Copolymers under accelerated weathering and composting conditions. *J. Thermoplast. Compos. Mater*, **18**, 489 (2005).
2. **D. Depan**, A.P. Kumar, and R.P.Singh, Preparation and characterization of novel hybrid of chitosan-g-lactic acid and montmorillonite, *J. Biomed. Mater. Res. Part A*, **78 A** (2); 372 (2006).
3. **D. Depan**, B. Kumar, and R.P.Singh, Preparation and characterization of novel hybrid of chitosan-g-PDMS and sodium montmorillonite, *J. Biomed. Mater. Res. Part B, Appl. Biomater.,* **84** (1); 184 (2008)**.**
4. **D. Depan**, and R.P. Singh, Preparation and characterization of novel hybrid of biomineralized Zn-Al layered double hydroxides using Chitosan as a template. *J. Appl. Polym. Sci*., (Under Peer Review).
5. **D. Depan**, A.P. Kumar, and R.P.Singh, Cell-proliferation and controlled drug release studies of nanohybrids based on Chitosan-g-LA and Montmorillonite. Acta Biomater., (Under Revision).
6. S.K. Soni, **D. Depan**, J.M. Khire, and R.P. Singh, Biomimetic synthesis of nanosized Hydroxyapatite by enzyme preparation of fungus *Asperigillus niger*., *Nature Nanotechnol*., (Under revision).
7. **D. Depan,** L. Saikia, and R.P. Singh, Ultrasound Triggered Release of Ibuprofen from a Chitosan-Mesoporous Silica Composite-A novel approach of controlled Drug Release. J. Control. Rel., (Under peer review).

Review Article:

A. Pratheep Kumar, **D. Depan**, and R.P. Singh, Nanoscale Materials for Polymer Degradation and Stabilization: Trends and Future Perspectives, Prog. Polym. Sci., (Communicated).

Book Chapter:

D. Depan, and R.P. Singh, A First Insight on Chitosan Based Nanocomposites for Biomedical Applications: Recent Trends and Applications. Editor: Dr. R. Jayakumar, Publisher-Research Sign Post, 2008.

Conferences/ Symposia

1. **D. Depan**, J.K. Pandey, **and** R.P.Singh, "On the durability of low-density polyethylene nanocomposites". Oral Presentation in International Seminar on Advances in Polymer Technology 2004 (APT-04) at CUSAT, **Kochin** on Jan 16-17th January 2004.
2. **D. Depan,** and R.P. Singh, Preparation and characterization of thermoplastic starch based nanocomposites. Poster Presentation in International Conference on Polymers - MACRO 2004 at **Trivandrum** on 14-17th Dec. 2004.
3. **D. Depan,** and R.P. Singh, Preparation and characterization of novel hybrid of CS and montmorillonite. Poster presentation at Euro Nano forum 2005- **Edinburgh, Scotland, UK,** September 5-9, 2005.
4. **D. Depan,** and R.P. Singh, Preparation and characterization of novel hybrid of Chitosan-g-LA and montmorillonite for drug release and biomedical applications. Poster Presentation in Nanotechnology in Advanced Drug Delivery at **NIPER**, Chandigarh on February 17-18, 2006.
5. **D. Depan,** and R.P. Singh, Preparation, drug release and cell-compatibility of Bionanohybrids of Layered Double Hydroxides using CS as a template. International conference on Polymers- MACRO-2006 at NCL, Pune on December 17-20, 2006.
6. **D. Depan,** A. Pratheep Kumar, and R.P. Singh, Bio-/Nanohybrids: From Degradation to Drug Delivery Applications, **Yonsie University, South Korea,** November 5-11, 2007.